CHEMICAL AND ELECTROCHEMICAL PROMOTION OF SUPPORTED RHODIUM CATALYST

THÈSE N^{O} 3245 (2005)

PRÉSENTÉE À LA FACULTÉ SCIENCES DE BASE

Institut des sciences et ingénierie chimiques

SECTION DE CHIMIE ET GÉNIE CHIMIQUE

ÉCOLE POLYTECHNIQUE FÉDÉRALE DE LAUSANNE

POUR L'OBTENTION DU GRADE DE DOCTEUR ÈS SCIENCES

PAR

Olena BARANOVA

M.Sc. in chemical technology and engineering, Ukrainian State Chemical Technology University, Ukraine
et de nationalité ukrainienne

acceptée sur proposition du jury:

Prof. C. Comninellis, directeur de thèse
Dr Y. Beaufils, rapporteur
Dr G. Foti, rapporteur
Prof. H. van den Bergh, rapporteur
Prof. C.G. Vayenas, rapporteur

Lausanne, EPFL
2005

Acknowledgements, Remerciements, Благодарность

Abstract

The chemical and electrochemical promotion of highly dispersed nanofilm Rh catalysts (dispersion: about 10 %, film thickness: 40 nm) has been investigated for the first time. To this end Rh metal was sputter-deposited, either on a purely ionic conductor (8 % Y_2O_3-stabilized ZrO_2) or on a mixed ionic-electronic conductor (TiO_2), the latter being a highly dispersed layer of TiO_2 (4 µm) deposited on YSZ. These catalysts are designated as Rh/YSZ and Rh/TiO_2/YSZ, respectively.

It was established analytically that both in the Rh/YSZ and in the Rh/TiO_2/YSZ system, the catalyst films have a nanoparticle-size grain structure. The Rh supported on titania is rather porous, exhibiting a higher dispersion and surface area than Rh on YSZ. Both after reduction (H_2, T=400 °C) and after oxidation (O_2, T=400 °C), Rh supported on TiO_2 was found to be in a more highly reduced state than Rh on YSZ. After reducing treatment, the Rh/TiO_2/YSZ samples contain a larger amount of weakly bonded oxygen, which can be attributed to oxygen "backspillover" from the TiO_2.

A major feature of this research was the electrochemical characterization of the oxygen/Rh/ solid electrolyte three-phase boundary by steady-state polarization measurements and by impedance spectroscopy. These are powerful techniques for extracting experimental trends and details that are useful for an understanding of the electrochemical promotion principles. It was shown that the exchange current densities at the Rh/solid electrolyte interface are lower on account of the TiO_2 layer. The exchange current densities are more than twice lower at Rh/TiO_2(4 µm)/YSZ than at Rh/YSZ, demonstrating that the former interface is much more polarizable.

The mechanism of oxygen exchange occurring close to equilibrium (O_2/O^{2-} couple) was investigated for the first time at Rh catalyst electrodes interfaced with solid electrolyte. The processes of cathodic oxygen reduction and anodic oxygen evolution are not symmetric, but they are similar in the two systems, Rh/YSZ and Rh/TiO_2(4 µm)/YSZ. The cathodic process consists of three steps: dissociative adsorption of oxygen at the gas-exposed Rh surface, atomic oxygen diffusion to the electrochemical reaction sites (ERS), and a two-electron transfer to this oxygen on the ERS. The cathodic process is limited by interfacial diffusion of oxygen atoms from the gas-exposed metal surface to the ERS. The anodic process includes two steps: two-electron transfer

reaction, which is the rate-determining step, and oxygen desorption to the gas phase. With data obtained from impedance spectroscopy at the equilibrium potential, it was possible to confirm the reaction scheme proposed.

It was demonstrated that Rh nanofilm catalysts interfaced with YSZ or TiO_2/YSZ can be electrochemically promoted for the reaction of ethylene oxidation. Small anodic currents cause periodic oscillations in catalytic rate and potential of the Rh/YSZ catalyst, while at Rh/TiO_2/YSZ they give rise to a stable and reversible rate enhancement by up to a factor 80. The increase in ethylene oxidation rate is up to 2000 times larger than the electrochemical rate, $I/2F$, of O^{2-} oxidation. The pronounced electrochemical promotion behavior that has been observed is due to the anodically controlled migration of O^{2-} species from the electrolyte to the Rh/gas interface. At the Rh surface, these species destabilize the formation of rhodium surface oxide (Rh_2O_3). The existence of backspillover oxygen species has been confirmed by impedance measurements under positive applied potential.

Another significant result for heterogeneous catalysis is the finding that thick as well as thin films of Rh/TiO_2/YSZ catalyst are open to chemical promotion of ethylene oxidation and partial methane oxidation, *ie*, they offer a higher catalytic activity and stability than the Rh/YSZ catalysts. The modification of catalytic activity observed for Rh/TiO_2/YSZ was attributed to either a "long-range" electronic-type SMSI mechanism or to a self-driven electrochemical promotion mechanism. In both cases, the ultimate cause of promotion are different work functions of catalyst and support. Equilibration of the work functions of two solids in contact induces surface charging, a migration of O^{2-} ions to the catalyst/gas interface, and a weakening of the Rh-O chemisorptive bonds. It facilitates reduction of oxidized surface sites.

Another important achievement of the present work was that of exploring and confirming the possibilities of current-assisted activation of Rh/TiO_2/YSZ catalysts. In partial methane oxidation using close to stoichiometric gas compositions ($CH_4 : O_2 = 2 : 1$) at 550 °C, the inactive (oxidized) Rh/TiO_2/YSZ catalyst was successfully activated by applied currents, either positive or negative. This phenomenon is an example of "permanent" electrochemical promotion furnishing a permanent rate enhancement ratio of $\gamma = 11$. The activation by negative currents is explained in terms of an electrochemical reduction of rhodium surface oxide, while the activation by positive currents can be explained by the mechanism of electrochemical promotion.

Version Abrégée

Pour la première fois, la promotion chimique et électrochimique des catalyseurs sous forme de nanocouche de Rh hautement dispersée (40 nm d'épaisseur, dispersion ~10%) a été étudiée. Dans le cadre de ce travail, des catalyseurs en Rh ont été déposés par sputtering soit sur un conducteur purement ionique (8%Y_2O_3-stabilizé-ZrO_2) soit sur un conducteur mixte ionique-électronique. Ce dernier est une couche de TiO_2 (4 μm) hautement dispersée sur du YSZ. Ces deux catalyseurs seront notés Rh/YSZ et Rh/TiO_2/YSZ, respectivement.

Nous avons montré que ces deux catalyseurs ont une structure en nanograins. De plus, il est apparu que l'intercouche de TiO_2 augmente la surface catalytique ainsi que la dispersion. En traitant les catalyseurs dans une atmosphère réductrice (H_2, T=400°C) puis oxydante (O_2, T=400°C), le Rh a été trouvé dans le Rh/TiO_2/YSZ à un état plus réduit, comparé au Rh dans Rh/YSZ. Plus particulièrement, la réduction en Rh de Rh/ TiO_2/YSZ contient plus d'oxygène faiblement lié qui peut être attribué à l'oxygène "backspillover" du support TiO_2.

La caractérisation électrochimique de l'interface triple O_2, Rh/électrolyte solide par des méthodes de polarisation stationnaire et de spectroscopie d'impédance, se révèle être l'un des axes majeurs de ce travail. C'est sans doute l'un des moyens d'investigation qui nous a permis de dégager le plus d'informations utiles à la compréhension du phénomène de promotion électrochimique. Il a été montré que l'intercouche de TiO_2 diminue la densité de courant d'échange à l'interface Rh/ électrolyte solide. Le courant d'échange trouvé est environ deux fois plus petit pour le catalyseur Rh/TiO_2/YSZ que celui du catalyseur Rh/YSZ. Cela indique donc que la première interface est plus polarisable.

Le mécanisme du processus d'échange d'oxygène proche de l'équilibre (couple O_2/O^{2-}) a été étudié sur une électrode en Rh en contact avec un électrolyte solide. Les processus de réduction cathodique et d'évolution anodique de l'oxygène ne sont pas symétriques. Par contre, ils sont identiques pour les deux systèmes. Plus précisément, il a été établi que le processus cathodique consiste en trois étapes: (*i*) adsorption dissociative de l'oxygène à la surface du Rh exposée au gaz, (*ii*) diffusion de l'oxygène sous forme atomique vers les sites électrochimique réactifs (SER) (*iii*) sur les SER, il apparaît finalement un transfert de deux électrons. L'étape (*ii*) est considérée

comme étant limitante. Le processus anodique est constitué de deux étapes: réaction de transfert électronique (étape limitante) puis désorption de l'oxygène formé vers la phase gazeuse. Nous avons pu confirmer ce mécanisme par la spectroscopie d'impédance sous un potentiel d'équilibre.

Nous avons montré que les catalyseurs sous forme de nanocouche de Rh peuvent être promu par l'application d'un potentiel positif pour la réaction d'oxydation de l'éthylène. Les faibles courants anodiques provoquent des oscillations périodiques de la vitesse de réaction et du potentiel du catalyseur Rh/YSZ, alors que le Rh/TiO$_2$/YSZ présente une augmentation de la vitesse de réaction stable et réversible d'un facteur ρ supérieur à 80. La vitesse de réaction d'oxydation est 2000 fois plus rapide que la vitesse électrochimique, $I/2F$, de l'oxydation de O^{2-}. La promotion électrochimique observée est due à la migration des espèces O^{2-} (*backspillover*) de l'électrolyte solide vers l'interface Rh/gaz sous polarisation anodique. Les espèces d'oxygène *backspillover* déstabilisent la formation d'oxyde Rh$_2$O$_3$ à la surface. L'existence de ces espèces, sous application d'un potentiel positif, a bien été confirmée grâce à la spectroscopie d'impédance.

L'autre fait expérimental important pour la catalyse mis en évidence est que le système Rh/TiO$_2$/YSZ présente une promotion chimique des réactions d'oxydation de l'éthylène et d'oxydation partielle du méthane, indépendamment des méthodes de préparation du catalyseur en Rh. Cela signifie une plus grande activité catalytique ainsi qu'une meilleure stabilité par rapport à Rh/YSZ. La modification observée de l'activité catalytique de Rh/TiO$_2$/YSZ est due soit à une forte interaction métal-support (de nature électronique, se manifestant à longue distance) soit au mécanisme de promotion électrochimique automotrice (*self-driven electrochemical promotion)*. Dans ces deux cas, la promotion est due principalement à la différence de travail d'extraction entre le catalyseur et le support. L'équilibre du travail d'extraction des deux solides affaiblit la force avec laquelle l'oxygène s'adsorbe à la surface du catalyseur et facilite ainsi la réduction de l'oxyde à la surface.

L'autre resultat important de ce travail est l'exploration de la possibilité d'activation du catalyseur Rh/TiO$_2$/YSZ par un courant. Lors de la réaction d'oxydation partielle de méthane proche de la composition gazeuse stœchiométrique (CH$_4$:O$_2$=2:1), l'activation du Rh/TiO$_2$/YSZ oxydé a été effectué. Cette activation a été réalisée par l'application d'un courant aussi bien positif que négatif. Le phénomène observé est un exemple de promotion électrochimique "permanent", que nous avons caractérisée par le facteur d'augmentation "permanent", γ. Des valeurs de γ

supérieures à 11 ont été determinées. L'activation par un courant négatif s'explique par une réduction électrochimique d'oxyde de Rh à la surface, alors que sous l'application d'un courant positif, l'oxyde de Rh réduit par le mécanisme de la promotion électrochimique.

Table of Contents

CHAPTER 1 **Introduction**

The electrochemical promotion of catalysis (EPOC) or nonfaradaic electrochemical modification of catalytic activity (NEMCA) that was discovered toward the end of the 1980s by Vayenas and co-workers is an interdisciplinary phenomenon observed at the interface of catalysis and electrochemistry. Today, several research groups all over the world are studying this effect, and it has been demonstrated that it is not limited to any particular electrolyte, conductive catalyst, or type of reaction.

Apart from good prospects for a commercial utilization of electrochemical promotion, investigations into the mechanism and origin of EPOC have already made an enormous contribution to the understanding of related phenomena in heterogeneous catalysis, such as promotion and metal-support interactions (MSI). It has been established more recently [1], that promotion, electrochemical promotion, and metal-support interactions are all linked via the phenomena of spillover and backspillover, the catalytic reaction occurring in the presence of a double layer which for electrochemical promotion can be controlled *in situ*.

1.1 Motivation and Objectives

The mechanistic equivalence between electrochemical promotion and metal-support inter-actions was first demonstrated by Nicole et al. [2] in studies of ethylene oxidation on an IrO_2 film catalyst supported on YSZ and on IrO_2-TiO_2 mixtures. It was demonstrated that the IrO_2 electrode can be promoted electrochemically, but for the two oxides present in intimate contact, this is not possible, as they are already promoted via O^{2-} spillover [2]. The mechanistic equivalence of EPOC with YSZ and of MSI with ZrO_2, TiO_2 and CeO_2-based supports was established by this important experiment as well as by several others [1].

Despite the many studies of the two phenomena: EPOC and MSI, several key questions still remain: (i) Is a catalyst promoted by metal-support interactions in its "best" electrochemi-cally promoted state? (ii) Do metal-support interactions occur only at highly dispersed catalysts? (iii) Is it possible to induce electrochemical promotion at such a catalyst? Further investigations of the interfaces between catalyst and support (solid electrolyte), of the interfaces between catalyst and gas phase, and of the three-phase boundary (catalyst/solid electrolyte/gas interface) are required to answer these questions.

The present work constitutes part of the complex investigations that have been conducted in our laboratory over the last decade [3-7]. Its objective are the first studies ever of an electro-chemical modification of catalytic activity and of metal-support interactions at nanofilm rhodium catalysts (thickness 40 nm) characterized by high dispersion (about 10 %). These catalysts were supported, either on a purely ionic conductor (8 % Y_2O_3-stabilized ZrO_2) or on a mixed ionic-electronic conductor (TiO_2) present as a highly dispersed (80 %) layer of TiO_2 (4 μm) deposited on YSZ (TiO_2/YSZ). The electrochemical promotion of highly dispersed catalysts, that is, cata-lysts with low metal loading, is an important achievement, both from theoretical and from practi-cal points of view. On one hand, at catalysts having such a design (which is similar to that of the catalytic systems exhibiting the effects of metal-support interactions), the phenomena of EPOC and MSI can be studied in parallel. On the other hand, efficient electrochemical promotion of highly dispersed catalysts virtually eliminates the major economic obstacle to the commercial uti-lization of EPOC that existed in the poorly dispersed metal catalysts (typically 10^{-3}-10^{-5}) employed in the form of thick porous films (0.2 - 10 μm) in all prior electrochemical promotion studies [1].

Toward these objectives, the following investigations have been performed:

1. Investigations of Rh/solid electrolyte systems by surface science (SEM, AFM, XPS) (Chapter 4) and electrochemical techniques (steady-state polarization and impedance spectroscopy) (Chapters 5, 6). Particular attention was paid to the kinetics of electron transfer and to the mechanism of oxygen reduction and evolution (the O_2/O^{2-} couple) at the O_2, Rh/solid electrolyte interface (Chapters 4, 5).

2. Studies of the effect of different supports (solid electrolytes) on the catalytic performance of the Rh catalyst in model reactions under open-circuit conditions, development of a macroscopic model for catalyst deactivation (Chapters 7 and 9).

3. Investigations of electrochemical promotion of Rh catalysts interfaced with YSZ and TiO_2/YSZ supports in the oxidation of ethylene and methane as model reactions (Chapters 8 and 9).

4. Establishment of the relationship between EPOC and MSI on the basis of partial methane oxidation over Rh/TiO_2/YSZ catalysts as a model reaction (Chapter 9).

1.2 References

1. C. G. Vayenas, S. Bebelis, C. Pliangos, S. Brosda, and D. Tsiplakides, *Electrochemical activation of catalysis. Promotion, Electrochemical promotion, and metal-support interaction.* Kluwer Academic/Plenum Publishers, New York (2001).

2. J. Nicole, D. Tsiplakides, C. Pliangos, X. E. Verykios, C. Comninellis, and C. G. Vayenas, *J. Catal.,* **204** (2001) 23.

3. E. Varkaraki, *Electrochemical promotion of an IrO$_2$ catalyst for the gas phase oxidation of ethylene.* Thesis No 1455, EPFL, Lausanne, (1996).

4. J. Nicole, *Etude de la Promotion Electrochimique de l'Oxydation Catalytique de l'Ethylène sur des Oxydes Métalliques.* Thesis No 1933, EPFL, Lausanne, (1999).

5. S. Wodiunig, *Electrochemical promotion of RuO$_2$ catalysts for the gas phase combustion of ethylene.* Thesis No 3138, EPFL, Lausanne, (2000).

6. I. Bolzonella, *Electrochemical promotion of rhodium catalyst. Application to nitrogen monoxide reduction.* Thesis No 2743, EPFL, Lausanne, (2003).

7. J. Eaves, *Promotion électrochimique des catalyseurs à base de rhodium et d'iridium.* Thesis No 2883, EPFL, Lausanne, (2004).

CHAPTER 2 Review of relevant basic work (bibliography)

In this chapter, the current state of the art in the electrochemical promotion of catalysis (EPOC) and related fields is presented. Particular attention is paid to the origin of EPOC and to the mechanism of the phenomenon (Section 2.1.2). In subsequent sections, metal-support interactions (MSI) are discussed. Plausible mechanisms of this phenomenon and its connection with EPOC are demonstrated. The main properties of the $ZrO_2(8 \% Y_2O_3)$ and TiO_2 solid electrolytes used as substrates (supports) are described.

2.1 Electrochemical promotion

2.1.1 Definitions and basic quantities involved

The electrochemical promotion of catalysis (EPOC), also known as nonfaradaic electrochemical modification of catalytic activity (NEMCA), is a rather general phenomenon observed in heterogeneous catalysis that was discovered relatively recently and made a strong impact on modern electrochemistry and surface science [1-9].

The basic setup used to observe this effect on O^{2-}-conducting solid electrolytes is shown in Fig 2.1 A in the instance of the combustion of ethylene. The porous, electropromoted catalyst film also serves as the working electrode in the solid-electrolyte cell (Fig. 2.1 A). The catalytic rate can be altered dramatically by an applied current or potential (Fig. 1.1 B). Under open-circuit conditions ($I = 0$, no electrochemical rate contribution) a catalytic rate r_0 is measured. Application of an electrical current, I, or potential difference between the catalyst and a counterelectrode gives rise to very pronounced, nonfaradaic changes (*ie.,* $\Delta r \gg I/2F$) in the catalytic rate, r, and quite often in product selectivity [5]. The rate of the catalytic reaction, r, can become up to 200 times larger than the open-circuit rate, r_0, and up to 3×10^5 times larger than the faradaic rate ($I/2F$ for O^{2-}) of ion supply to (or removal from) the catalyst electrode [4, 5, 10]. The dramatic, and often highly nonfaradaic increase in the catalytic reaction rate as well as the enhancement of product selectivity that are induced when applying a very low electric current are entirely reversible in most cases, the steady-state open-circuit catalytic reaction rate after current interruption typically relaxing within 10 to 30 minutes to the value observed prior to application of the current.

The phenomenon of electrochemical promotion can be described by three parameters:

(a) The rate enhancement ratio, ρ, defined as [5]:

$$\rho = \frac{r}{r_0} \tag{2.1}$$

where r_0 is the catalytic rate at open circuit, and r is the catalytic rate observed under polarization by an applied current or potential difference.

(b) The apparent faradaic efficiency, Λ, is defined as the ratio of the observed rate increase to the highest possible electrochemical rate [5]:

$$\Lambda = \frac{r - r_0}{I/2F} = \frac{\Delta r}{r_{\mathrm{F}}} \tag{2.2}$$

where I is the applied current, F is the Faraday constant, and $r_{\mathrm{F}} = I/2F$ is the rate of O^{2-} supply to the catalyst.

T=350°C

A

Gas mixture $C_2H_4 + O_2$

Catalytic Oxidation

Electrochemical Oxidation

$C_2H_4 + 3O_2 \rightarrow 2CO_2 + 2H_2O$

$C_2H_4 + 6O^{2-} \rightarrow 12e^- + 2CO_2 + 2H_2O$

catalyst

U_{WR}

I **e⁻**

YSZ $O^{2-}\uparrow$ $O^{2-}\uparrow$ $O^{2-}\uparrow$

U

e⁻

gold

$O_2 \rightarrow 2O^{2-} + 2e^-$

Gas mixture $C_2H_4 + O_2$

current

B

I

0

reaction rate

r

r_F

r_0

0

0 t_1 t_2 time
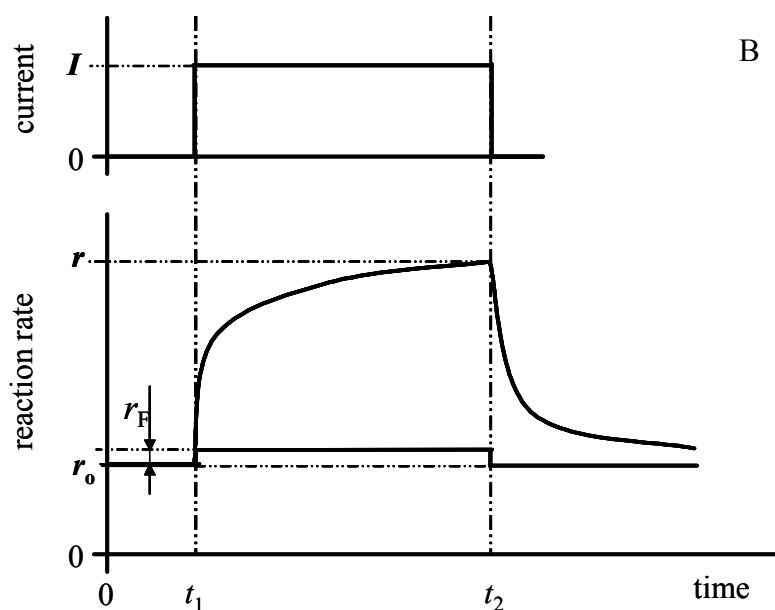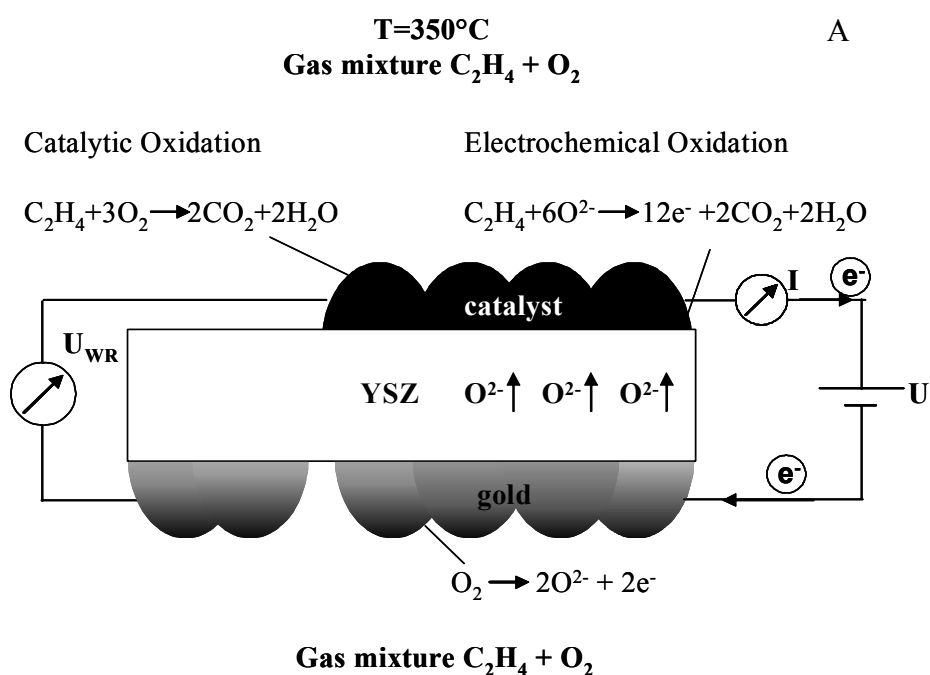
FIGURE 2.1. Electrochemical cell (A) and galvanostatic transient (B) of electrochemical promotion with O^{2-}-conducting support; r_0 is the catalytic oxidation rate, r_F is the electrochemical oxidation rate, r *is* the observed reaction rate. The catalytic rate increase largely exceeds the rate of O^{2-} supply to the catalyst electrode: $r - r_0 >> I/2F.$

(c) The promotion index, PI_j, defined as:

$$PI_j = (\Delta r/r_0)/\Delta\theta_j \qquad (2.3)$$

where θ_j is the coverage of the catalyst surface by the promoting ion j (eg., O^{2-}).

The effect has been studied for more than seventy catalytic reactions [5, 10] at porous metal films deposited on a variety of solid electrolytes, including O^{2-} conductors such as yttria-stabilized zirconia (YSZ) [2], Na^+ conductors such as β"-Al_2O_3 [11], F^- conductors such as CaF_2 [12], H^+-conducting solid electrolytes such as $CaZr_{0.9}In_{0.1}O_{3-\alpha}$, $CsHSO_4$, and Nafion [13-15], as well as on mixed ionic-electronic conductors [16, 17]. Work in this area has been reviewed repeatedly [5, 18-20].

In the current theory of electrochemical promotion, the effect is attributed to specific promoting species [5, 18]. These are generated electrochemically at the three-phase boundaries (tpb) between solid electrolyte, catalyst, and gas phase, and then spread out over the gas-exposed catalyst surface.

The overall parameters of the complex phenomenon of electrochemical promotion are readily investigated by phenomenological techniques such as catalytic rate measurements [3-5], solid-state cyclic voltammetry [5, 21, 22], catalyst work function measurements [3, 23, 24], and AC impedance spectroscopy [25, 26], while more sophisticated techniques such as XPS [5, 27-30], UPS, TPD [21, 31-37], PEEM [38], or STM [23] are needed to identify and monitor particular promoting species.

Apart from its obvious scientific interest, the phenomenon of electrochemical promotion may be of great importance in present [39-41] and future industrial applications. The first step in the development of reactors for reactions to be promoted electrochemically is that of realizing bipolar cell configurations [19, 42], the second step was recently realized in terms of a monolithic electropromoted reactor through a collaboration between EPFL, the University of Patras, and Bosch, Stuttgart [43].

In the following, a mechanistic interpretation of electrochemical promotion will be outlined while demonstrating more particularly the connection between the catalyst's surface work function and the catalyst's potential under electrochemical promotion conditions.

2.1.2 The mechanism of electrochemical promotion

The electrochemical promotion of catalysis, similarly to the usual (chemical) promotion and to metal-support interactions in heterogeneous catalysis, is related to spillover-backspillover phenomena. The latter can be described as the mobility of adsorbed species from one phase on which they easily adsorb (donor) to another phase where they do not directly adsorb (acceptor). By this mechanism a seemingly inert material can acquire catalytic activity. Spillover may lead to an improvement of catalytic activity or selectivity and also to an increase in lifetime of the catalyst.

In the presence of spillover in heterogeneous catalysis, the usual kinetic models can no longer be applied in a direct way. The generation of new surface sites or changes in surface concentrations lead to new terms in the rate equations. A general reaction scheme of oxygen spillover in a purely catalytic (that is, not electrocatalytic) system [44] may be formulated as follows, see also Figure 2.2:

$$O_2 + 2D \leftrightarrows 2O \cdot D \tag{2.4}$$

$$A + O \cdot D \rightarrow D + O \cdot A \tag{2.5}$$

$$O \cdot A + B \rightarrow C \tag{2.6}$$

$$R + C \rightarrow P + B \tag{2.7}$$

Equation (2.4) describes the dissociative adsorption and recombination of oxygen on a donor D. The transfer of O from donor D to acceptor A is described by equation (2.5). The spillover oxygen (O) is a mobile species present on the acceptor surface without being associated with a particular surface site. The mobile spillover species may interact with a particular surface site B (Equation (2.6)) forming an active site C. Equation (2.7) represents the deactivation of the active site C by interaction with a reactant R and the formation of product P. Kinetic models based on this mechanism are well supported by experiment [45].
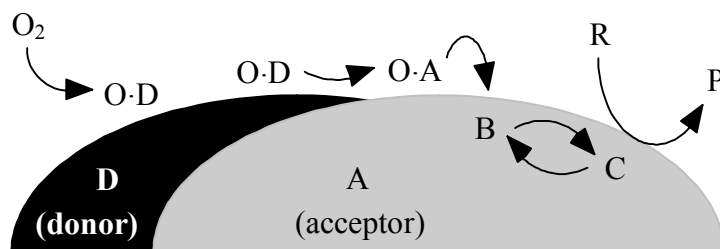
FIGURE 2.2. Schematic representation of the mechanism of oxygen spillover in a purely catalytic system. Symbols as in Equations (2.4) to (2.7).

The most plausible mechanism of electrochemical promotion illustrated in Figure 2.3 is based on analogous donor-acceptor interactions [4, 5]. Consider the example of anodic polarization of the catalyst. In this case the solid electrolyte functions as donor supplying O^{2-} ions to the catalyst functioning as acceptor. (This migration from the support to the catalyst may be termed backspillover, in order to distinguish it from the migration in the opposite direction, which is quite common in catalysis and known as spillover.) The O^{2-} ions are released from the solid electrolyte at the three-phase boundaries. By a thermodynamic analysis of electrochemical promotion involving O^{2-} conductors, it was demonstrated that two types of adsorbed oxygen species exist [46]: one type is the catalytically active species adsorbed from the gas phase; the other is backspillover oxygen from the solid electrolyte, which acts as a sacrificial promoter [4, 5, 20, 47]. The rate of consumption of the promoter is slow relative to the kinetics of migration (backspillover) from the electrolyte to the metal/gas interface.
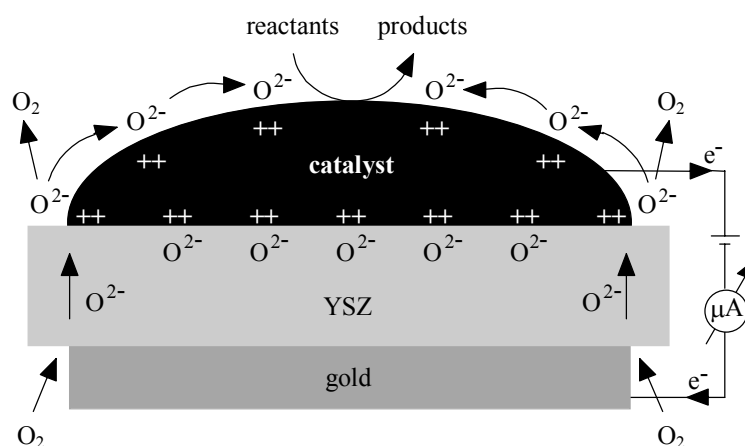
FIGURE 2.3. Schematic representation of the mechanism of electrochemical promotion by an applied anodic current *via* backspillover of charged promoting species (O^{2-}).

Backspillover species may either be consumed in electrochemical reactions (oxygen evolution and/or oxidation of adsorbed reactants) occurring along (or close to) the tpb, and obviously obeying Faraday's law, or they may migrate over the gas-exposed catalyst surface. The existence of backspillover oxygen ions at a gas-exposed catalyst surface was demonstrated by XPS measurements [30]. No charged oxygen species could be detected under open-circuit conditions, but they were found in abundance after anodic polarization of the catalyst/solid electrolyte interface. Charged backspillover oxygen and neutral chemisorbed oxygen may be clearly distinguished also by temperature-programmed desorption (TPD) [31]. It was shown that oxygen adsorbed from the gas phase desorbs at a lower temperature, hence is more reactive, than the oxygen species generated electrochemically. During their migration, the oxygen ions are accompanied by their compensating image charges in the catalyst, with which they form surface dipoles. When these dipoles spread out, an overall neutral, effective double layer is built up at the gas-exposed catalyst surface. The concomitant change in the catalyst's work function acts so as to modify the binding strength of chemisorbed reactants and intermediates, and thus gives rise to changes in catalytic activity and/or selectivity. A more detailed explanation of the underlying phenomena is presented below.

Consider a metal (or metal oxide) catalyst (c) supported by an O^{2-}-conducting solid electrolyte (s), both in contact with a gas phase (g) containing oxygen. For oxygen species, the reaction scheme is shown in Figure 2.4 [48]. In the charge transfer reaction, O^{2-} is oxidized to O. The catalyst/solid electrolyte (c/s) interface is not accessible to O or O_2, therefore, direct charge transfer between O^{2-}(s) and O(c) may occur only at the three-phase boundaries (tpb). Considering the possibility of backspillover of O^{2-} from the tpb to the gas-exposed catalyst surface, however, charge transfer will no longer be restricted to the tpb but may take place through O^{2-}(c) species over the entire catalyst/gas (c/g) interface. Under open-circuit conditions all reactions of the scheme will come to equilibrium, and one may write:

$$\mu_{O^{2-}}(s) = \bar{\mu}_{O^{2-}}(c) = 2\bar{\mu}_{e^-}(c) + \mu_O(c) = 2\bar{\mu}_{e^-}(c) + \frac{1}{2}\mu_{O_2}(g) \qquad (2.8)$$
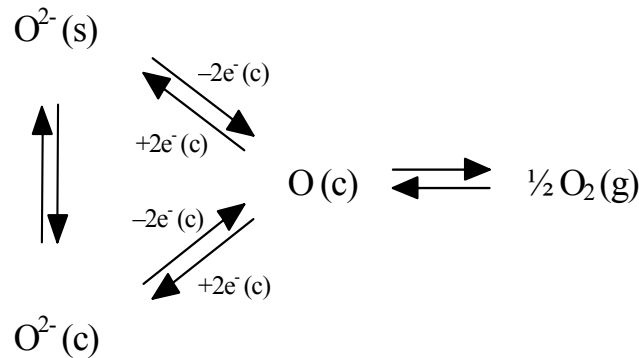
FIGURE 2.4. Reaction network for oxygen species associated with an electron conductor catalyst (c) on an oxygen-ion (O^{2-})-conducting solid-electrolyte support (s) in contact with an oxygen (O_2)-containing gas phase (g).

where μ_i is the chemical potential and $\bar{\mu}_i$ ($\equiv \mu_i + z_i F\phi$) is the electrochemical potential of species i, z_i is its charge number, and ϕ is the inner (*Galvani*) potential.

Obviously, the driving force for O^{2-} backspillover from the solid electrolyte to the catalytically active surface (c/g) is given by $\bar{\mu}_{O^{2-}}(s) - \bar{\mu}_{O^{2-}}(c)$. This difference vanishes at equilibrium

(see the left-hand side of Equation ()) when an effective double layer has been established at the c/g interface, by analogy to the case of an emersed electrode in aqueous electrochemistry [49].

In a typical electrochemical promotion experiment, a potential step is applied to the electrochemical cell. In the ideal case of a perfect reference electrode having invariant potential, the induced change in the ohmic-drop-free potential difference between the catalyst (working electrode) and the reference electrode, U_{WR}, is equal to the change in the inner (*Galvani*) potential of the catalyst, ϕ:

$$\Delta U_{WR} = \Delta \phi \tag{2.9}$$

This difference is measurable. By changing the potential of the catalyst one modifies its Fermi level, E_F, or - in other terms - the electrochemical potential of the electrons in the catalyst ($\bar{\mu}_e = E_F$). This latter quantity is defined as the difference between the zero-energy state of the electrons (taken in the ground state at infinite distance from the solid) and the energy of a conduction electron in the bulk of the catalyst. It is common practice to count this energy difference in two conceptually different ways. One of them is common in electrochemistry, the other is common in surface science.

In electrochemistry, one considers the electrochemical potential of electrons as the sum of their chemical potential in the solid, μ_e, and the contribution due to the electrostatic (inner) potential:

$$\bar{\mu}_e = \mu_e + (-e\phi) \tag{2.10}$$

Under polarization, the chemical potential of electrons in the bulk solid remains invariant, and one may write:

$$\Delta \bar{\mu}_e = -e\Delta\phi = (-e\Delta U_{WR}) \tag{2.11}$$

Hence, in the electrochemical approach formulated in terms of the bulk properties $\bar{\mu}_e$, μ_e, and ϕ, the change in electrochemical potential of the electrons can be related, directly to the applied potential difference.

Yet, since heterogeneous catalysis is a surface phenomenon, it is preferable to express the change in electrochemical potential, $\Delta\bar{\mu}_e$, in terms of the surface science approach:

$$\bar{\mu}_e = -\Phi + (-e\Psi) \tag{2.12}$$

where Φ is the work function of the solid surface, and Ψ is the outer (*Volta*) potential. This approach has the distinct advantage that both Φ and Ψ are surface properties, and both are measurable quantities.

The work function, Φ, is defined as the minimum energy required to extract an electron from the bulk of the solid (*ie.,* from the *Fermi* level) and to eject it with zero kinetic energy to a point just outside the solid surface where the image force interactions are negligible (typically 0.1 to 1 μm). This is schematically represented in Fig. 2.5.

The *Volta* potential at this point defines the energy, $e\Psi$, required to bring the electron from there to its zero energy level (to infinite distance from the solid). When the surface is electrically neutral (zero *Volta* potential), the work function alone measures the electrochemical potential of the electrons in the bulk solid. Two quantities contribute to the work function:

$$\Phi = -\mu_e + e\chi \tag{2.13}$$

the chemical potential, μ_e, of the electron in the solid, and the surface potential, χ, which accounts for the potential barrier that the electron must overcome in order to cross the surface of the solid. Since the chemical potential, μ_e, is an invariant bulk property, any change in the work function due to application of a potential difference will be equal to the change in surface potential. Population of the surface with dipoles *via* O^{2-} backspillover, *ie,* the formation of an electric double layer, will increase the surface potential, and the concomitant increase in work function will affect the binding strength of chemisorbed reactants. It follows that the adsorption energy of electron acceptors (*eg,* atomic O) will be weakened while that of electron donors (*eg,* C_2H_4) will be strengthened. This results in a variation of the adsorption equilibrium constants, hence also in coverage of the adsorbed species [5, 50, 51]. A corresponding change in catalytic reaction rate must then be expected.
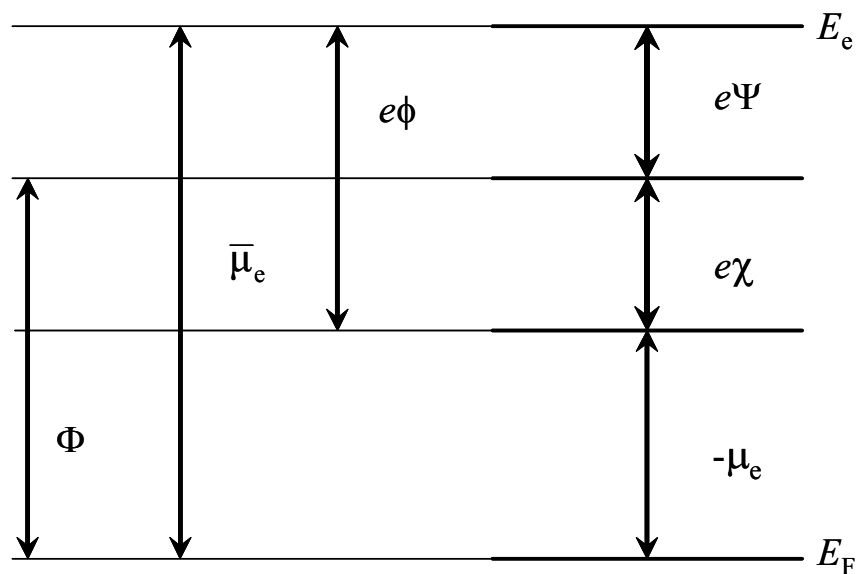
FIGURE 2.5. Energy levels at a metal surface relative to the energy of a free electron, E_e. Symbols as in Equations (2.10), (2.12), (2.13).

The catalyst's work function is a quantity directly measurable, either by the Kelvin probe technique or by the electron cut-off energy technique. It was found experimentally [52] that for steady-state electrochemical promotion, the following relationship holds over a wide range of conditions (*ie,* as long as ion backspillover from the solid electrolyte forms a double layer at the metal/gas interface) [23, 53-55]:

$$e\Delta U_{WR} = \Delta \Phi \qquad (2.14)$$

It follows that solid-electrolyte cells may be used as work function probes. Comparing this experimental relationship with Equations (2.11) and (2.12), one may conclude that the *Volta* potential difference at the catalyst surface remains invariant, provided the electric double layer has been built up at the catalyst/gas interface. Based on electrodynamic arguments, it was also concluded [5] that in an overall neutral electrochemical cell, this invariant *Volta* potential difference is zero, since the double layer formed via ion backspillover is overall neutral.

The validity of Eq. (2.14) has been demonstrated, both with the Kelvin probe technique [30, 52, 56, 57] and with the UPS technique [58] (use of electron cutoff energy in UPS experi-

ments), for work function measurements at gas-exposed electrode surfaces (Pt [30, 52], Ag [58], IrO$_2$ [56, 57]) and for catalysts in contact with YSZ [30, 52, 56-58] and β"-Al$_2$O$_3$ (a Na$^+$ conductor) [30, 52] at temperatures of 200 to 550 °C.

Although changes in catalyst work function with catalyst potential were widely studied and understood, Eq. (2.14) has been the subject of vivid controversy and discussions in recent years [54, 59, 60].

New important points concerning the validity of Eq. (2.14) were brought up recently by Leiva and Sánchez [61]. These authors elucidated the physical conditions that lead to the validity of Eq. (2.14), by putting forward a physical model based on electrostatic considerations. The authors performed the integration of the Poisson equations across the catalyst/solid electrolyte and catalyst/gas interphases, and emphasised the role of charge distribution at the interfaces.

2.1.3 Rationalization of the potential-work function equivalence

Like every experimental "law", Eq. (2.14) has its limitations. These limitations are considered below.

The key experimental observation is [5]:

$$e\Delta U_{WR} = \Delta\Phi_W \tag{2.15}$$

where Φ_W denotes work function of the working electrode (catalyst).

Using an arrangement with two-Kelvin probes [32] for monitoring *in situ* the work functions of both the working and the reference electrode, Φ_W and Φ_R, the following simple relationships were found:

$$eU_{WR} = \Phi_W - \Phi_R \tag{2.16}$$

$$\Psi_W = \Psi_R = 0 \tag{2.17}$$

and attributed to ion backspillover onto the electrode surface and to the formation of an effective electrochemical double layer on the electrode surface. This double layer neutralizes any net electrostatic charge residing on the gas-exposed electrode surface in the simple cell Po$_2$/Pt/ YSZ/Pt/P'o$_2$. The partial pressures of O$_2$ on the two sides of the cell are Po$_2$ and P'o$_2$. Oxygen

may chemisorb on the metal surfaces, so that the work functions Φ_W and Φ_R of the two gas-exposed electrode surfaces are $\Phi_W(Po_2)$ and $\Phi_R(P'o_2)$. In such a cell the following situations are possible:

1. The temperature is low, so that ionic mobility on the electrode surface is negligible, *ie,* there is no spillover. One always has, by definition:

$$eU_{WR} \;=\; -(\bar{\mu}_W - \bar{\mu}_R) \;=\; \Phi_W - \Phi_R + e\Psi_W - e\Psi_R \tag{2.18}$$

Also, due to establishment of the equilibrium:

$$O_{2(g)} + 4e^- \;\leftrightarrow\; 2O^{2-} \tag{2.19}$$

at the metal-gas-solid electrolyte three-phase-boundaries, one has:

$$\mu_{O_2} + 4\bar{\mu}_W \;=\; 2\bar{\mu}_{O^{2-}} \;=\; \mu'_{O_2} + 4\bar{\mu}_R \tag{2.20}$$

and from Eq. (2.18):

$$eU_{WR} \;=\; \frac{1}{4F}(\mu_{O_2} - \bar{\mu}_{O^{2-}}) \;=\; \left(R\frac{T}{4F}\right)\ln\left(\frac{P_{O_2}}{P'_{O_2}}\right) \tag{2.21}$$

Then, comparing Eqs. (2.18) and (2.21) one has:

$$e\Psi_W + e\Psi_R \;=\; eU_{WR} + \Phi_R(p'_{O_2}) - \Phi_W(p_{O_2}) \tag{2.22}$$

Since Po_2 and $P'o_2$ are fixed, U_{WR} is fixed, and since there is no spillover, $\Phi_W(Po_2)$ and $\Phi_R(P'o_2)$ are also fixed. Thus, in situation 1 (no ion spillover) $e\Psi_W$ - $e\Psi_R$ is fixed to a nonzero value.

In fact, as an application of Eq. (2.22), consider the case of $Po_2 = P'o_2$ and, thus, of $U_{WR} = 0$. Then one has:

$$e\Psi_W + e\Psi_R \;=\; \Phi_{R(P'_{O_2})} - \Phi_{W(P_{O_2})} \neq 0 \tag{2.23}$$

The nonzero value of $e\Psi_W$ - $e\Psi_R$ in Eq. (2.22) implies that net surface charges exist on the gas-exposed electrode surface. These charges (q^+, q^-) have to be opposite and equal, as the cell

overall is electrochemically neutral and all other charges are located at the metal-solid electrolyte interfaces to maintain their electroneutrality. The charges $q^+ = q^-$ are quite small relative to the charges, Q, stored at the metal-electrolyte interface, yet due to their presence the system has excess electrostatic energy:

$$E_C = (\Psi_W - \Psi_R)q^+ \qquad (2.24)$$

2. The temperature is increased to the point where the ionic mobility on the electrode surface is high, so ion spillover occurs.

Oxygen ions are now attracted to the electrode having positive charge, or to the electrode that has been made positive by anodic polarization. Backspillover will continue until the charge is neutralized. Similarly, oxygen anions will be repelled from the electrode that is negatively charged or cathodically polarized. The charges q^+ and q^- thus disappear, Ψ_W and Ψ_R vanish.

In this situation Eq. (2.22) becomes

$$e\Psi_W + e\Psi_R = eU_{WR} + \Phi_R - \Phi_W \qquad (2.25)$$

where eU_{WR} is still fixed by Eq. (2.21) but Φ_W and Φ_R are variables. They can change due to the spillover of ions. They will change in such a way as to minimize the excess electrostatic energy of the system:

$$E_C = (\Psi_W - \Psi_R)q_+ = 0 \qquad (2.26)$$

This is possible when $\Psi_W = \Psi_R$, which implies that $q^+ = q^- = 0$ for an overall neutral system, *ie,* $\Psi_W = \Psi_R = 0$. But note that even for an overall charged system, *ie,* a system where a net charge q has been introduced, the excess electrostatic energy is given by:

$$E_C = (\Psi_W - \Psi_R)q \qquad (2.27)$$

and minimized by

$$\Psi_W = \Psi_R \qquad (2.28)$$

It thus follows from Eqs. (2.25) and (2.28) that:

$$e\,U_{\mathrm{WR}} \;=\; \Phi_{\mathrm{W}} - \Phi_{\mathrm{R}} \tag{2.29}$$

$$\Psi_{\mathrm{W}} \;=\; \Psi_{\mathrm{R}} \;=\; 0 \;\;\text{(overall neutral cell)} \tag{2.30}$$

$$\Psi_{\mathrm{W}} \;=\; \Psi_{\mathrm{R}} \;\;\text{(overall charged cell)} \tag{2.31}$$

The reasons for deviations from potential-work function equivalence showing up as a nonzero *Volta* potential difference can be summarized as [55]: (*i*) slow or negligible ion backspill-over; (*ii*) excessively high or excessively low applied voltage; (*iii*) high and low temperature.

In summary, electrochemical promotion may be regarded as catalysis occurring in an electric double layer controlled by application of a current or a potential difference [5]. The condition required to achieve electrochemical promotion is formation of a double layer at the catalyst/gas interface by the mechanism of ion backspillover from the solid electrolyte support. This may occur over a wide range of conditions. The most important experimental parameters that are favorable for electrochemical promotion are the following: an extensive tpb (porous catalyst), moderate diffusion lengths (thin catalyst films), an adequate temperature range, *eg,* 250 to 500 °C for YSZ (a temperature not too low, so as to have sufficient ionic mobility, and not too high, so as to avoid a high reactivity of backspillover ions).

2.1.4 Work function measurements

The technique most commonly used for work function measurements in a reacting atmosphere is known as *the Kelvin* or vibrating-capacitor method [62-64]. Its principle is as follows. By placing a conductor, the *Kelvin* probe, into the immediate proximity of the catalyst surface and connecting the probe to the catalyst *via* an external circuit, a capacitor is formed. The contact potential difference between the two conductors arising from their work function difference results in a charge separation between the opposing surfaces. Vibration of the *Kelvin* probe then generates an alternative current *via* periodic variation of the capacitance. The external potential difference that must be applied to make the current vanish is the measure of the work function difference between the two conductors. By using a *Kelvin* probe made of an inert material, which has an invariant work function, any variation of the response due to varying experimental conditions may be attributed to the changes in work function of the catalyst alone. For an illustration of the usefulness of work function studies in electrochemical promotion, a dynamic approach was

selected where the time dependence of work function changes due to polarization steps is investigated. The model reaction is ethylene combustion over RuO_2 catalyst [65]. Such experiments should provide insight into the migration of promoting species towards the gas-exposed catalyst surface. Figure 2.6 shows the time dependence of the work function change ($\Delta\Phi$) and of the corresponding reaction rate (r) and catalyst potential (U_{WR}) following galvanostatic steps of 50 μA.

The work function transients observed during anodic polarization of the catalyst were composed of two main steps: a sharp increase just after application of the current, and a subsequent slow increase leading to a new steady-state value under polarization. Between these two steps, a sharp peak is observed in certain cases, as exemplified in Figure 2.6 A. The initial jump in work function is associated with the surface region easily accessible to promoting species. This region is supposed to be close to the three-phase boundary (tpb) where the promoting species are generated. The adsorption of charged oxygen on sites next to the tpb leads to the observed increase in work function. The final step, where the work function exhibits a slow increase, is due to migration of the promoting species from the tpb towards the entire gas-exposed catalyst surface. The work function continues to change until steady-state coverage by the promoting species is reached and, in parallel, the catalytic reaction rate reaches its new promoted steady-state value. The sharp peak preceding the final step might only appear when the relative positions of the catalyst and the *Kelvin* probe are properly adjusted. In principle, the probe must be placed into a region next to the catalyst where the tpb is accessible for the work function measurements. If the *Kelvin* probe is too far away from the tpb, no sharp peak but only a smooth transition between initial jump and final slow increase might be observed. Further investigations are required for a verification and satisfactory interpretation of the sharp peak appearing in some work function transients.
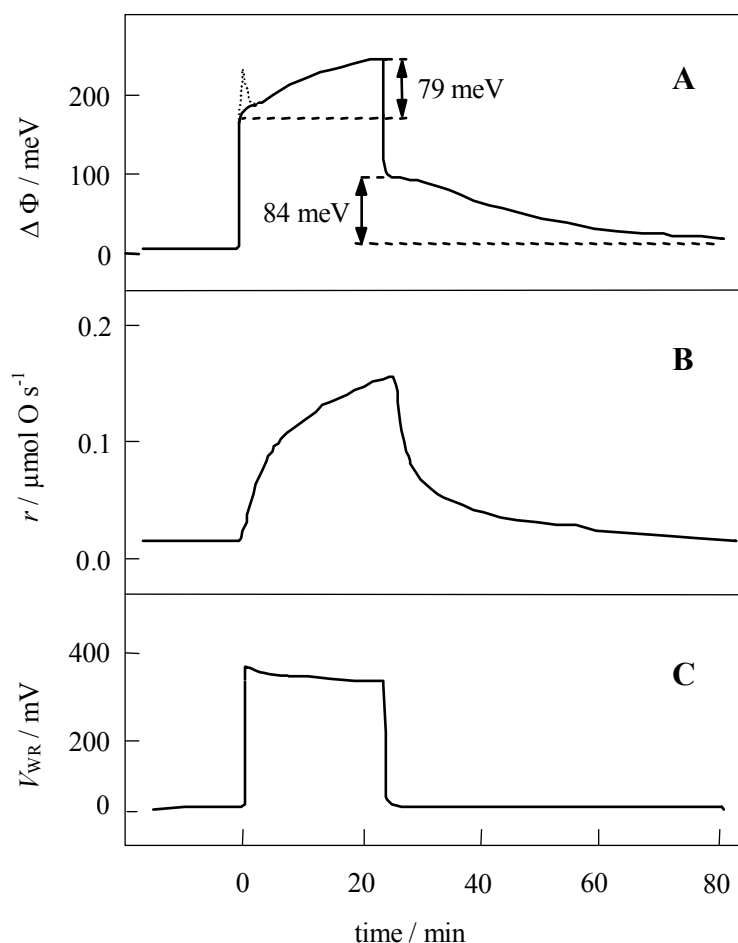
FIGURE 2.6. Time dependence of the work function change (A), the reaction rate (B), and the catalyst potential (C) following galvanostatic steps. Catalyst: RuO_2 (m = 0.4 mg; S = 0.5 cm^2), I = 50 µA during 23 min, P_{C2H4} = 114 Pa, P_{O2} = 17.7 kPa, flow rate: 175 mL/min STP, T = 380 °C.

2.1.5 Permanent electrochemical promotion

In rare cases, presumably when the particular catalyst can exist in several oxidation states of different catalytic activity, the effect of EPOC may appear to be irreversible. This phenomenon, known as "permanent electrochemical promotion" or "permanent NEMCA effect", was first observed with an IrO_2/YSZ catalyst in ethylene combustion [66], and explained by the formation of higher iridium oxide sites generated electrochemically. In order to quantitatively describe the

irreversible nature of electrochemical promotion, a "permanent" rate enhancement ratio, γ, defined as the ratio of two open-circuit catalytic reaction rates, one after current interruption, r', and the other prior to application of the current, r_0, has been proposed:

$$\gamma = \frac{r'}{r_o} \tag{2.32}$$

Figure 2.7 shows the results of a galvanostatic transient experiment in terms of the rate response to an applied current step (+300 μA for 120 min) during ethylene oxidation on an IrO_2 catalyst [56]. Initially the circuit is open ($I = 0$), the unpromoted catalytic rate is very low. At $t = 0$ a constant current ($I = +300$ μA) is applied between the catalyst (working electrode) and the counterelectrode. This current corresponds to an O^{2-} supply to the catalyst through the solid electrolyte at a rate of $I/2F = 1.55 \times 10^{-9}$ mol O/s.

The reaction rate increases rapidly at the beginning, and within the first few minutes of current flow reaches a value about eight times higher than the initial rate. After this rapid increase, the rate increases much more slowly to a steady-state value 13 times higher than the initial open-circuit rate. The final increase in catalytic rate is strongly nonfaradaic, *ie,* it is two orders of magnitude higher than the rate $I/2F$ of O^{2-} supply to the IrO_2 catalyst.

Upon current interruption, the rate decreases rapidly at first, and this rapid decrease is followed by a slow decrease to a new steady-state value. This new value is about three times higher than the initial rate measured prior to application of the current. It follows that the open-circuit enhancement factor, γ, defined by Equation (2.32) has a value of three. Thus, the steady-state open-circuit catalytic activity of the IrO_2 catalyst for ethylene combustion has been enhanced by the electrochemical (pre)treatment. This phenomenon has been called a permanent electrochemical promotion or permanent NEMCA effect.
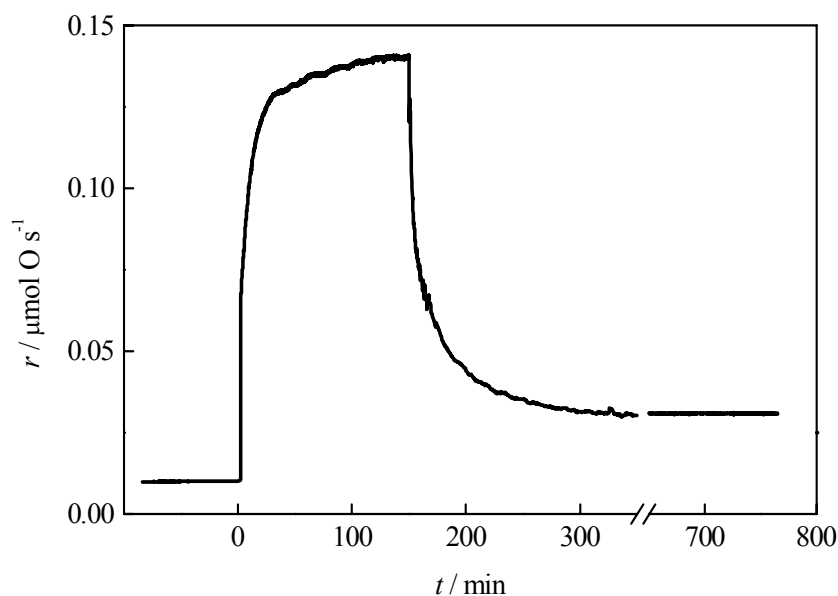
FIGURE 2.7. Permanent EP: polarization and relaxation transient of the rate of ethylene combustion on IrO$_2$/YSZ catalyst due to galvanostatic polarization with +300 µA. Conditions: P_{C2H4} = 0.14 kPa, P_{O2} = 17 kPa, T = 380 °C.

The regions of rate increase and decrease are similar, indicating that similar mechanisms are involved in the processes occurring after application and interruption of the current, but the permanent enhancement of the open-circuit rate indicates that the electrochemical promotion of the IrO$_2$ catalyst is not reversible. This behavior of an oxide catalyst is different from that of typical metal catalysts for which the electrochemical promotion usually is reversible [4, 5].

The extent of permanent promotion depends on the length of time of application of the current. As shown in Figure 2.8, the open-circuit rate enhancement factor, γ, increases with the duration of the galvanostatic step, t, reaching a plateau for polarization times of about 90 min. For very short polarization times corresponding to the region of fast rate increase, γ is very close to unity, *ie,* the effect of the current is reversible.

These results suggest that the electrochemical activation of IrO$_2$ is a two-stage process. It consists of a rapid reversible stage, where the initial catalytic activity of the catalyst would be restored after interruption of the current ($\gamma = 1$), followed by a slow irreversible stage, where the increase in catalytic activity acquired by the IrO$_2$ catalyst persists after interruption of the current ($\gamma > 1$). It is evident that the slow step is responsible for the permanent effect.
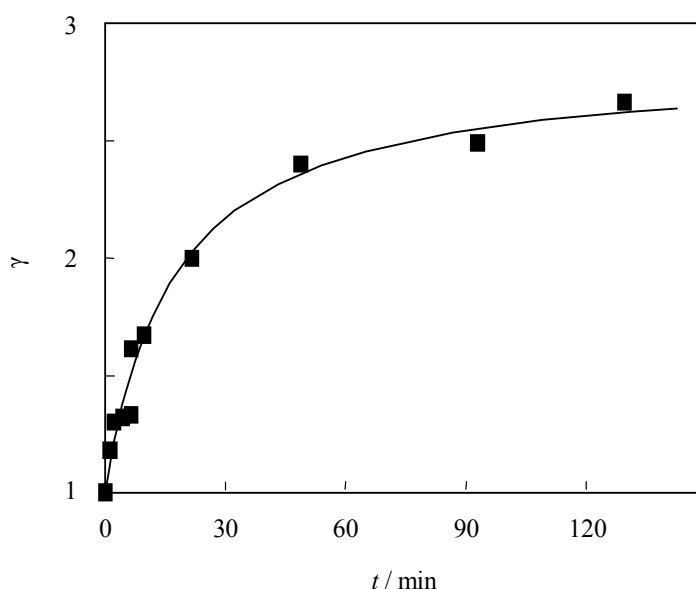
FIGURE 2.8. Influence of the duration, *t*, of the galvanostatic step on the open-circuit enhancement factor, γ, defined by Equation (1.32). Experimental conditions as in Figure 2.7.

The phenomenon of permanent electrochemical promotion has also been observed with rhodium catalysts supported on YSZ. Reduction of NO by propene in excess O_2 has been studied at 300 °C, a temperature that is low enough to avoid spontaneous open-circuit activation of a deactivated (oxidized) rhodium by the highly reactive gas mixture [67]. Activation of the catalyst has been achieved via application of a very low electric current (a few μA), the level of permanent activation being a function of the time of polarization (Section 2.1.7).

At 380 °C, "permanent" rate enhancement ratios of up to six have been obtained for the same reaction by Pliangos *et al* [68], while for NO reduction by CO in the presence of O_2 at 270 °C, γ–values as high as 14 have been reported [69].

2.1.6 Electrochemical promotion on rhodium catalysts

The oxidation of ethylene to CO_2 on rhodium-based catalysts has been investigated at temperatures between 300 and 400 °C [70-72]. The reaction exhibits a very strongly electrophobic

behavior, and the values obtained for ρ (Eq. (2.1)) and Λ (Eq. (2.2)) are among the highest found thus far in EP experiments (100 and 10000, respectively).

In these recent publications, the extremely effective electrochemical promotion of rhodium catalysts has been explained in terms of a dependence of the reaction rate on the oxidation state of the rhodium-based catalyst. Measurements of the catalyst's potential actually revealed the changes in oxidation state of the rhodium-based catalyst that were caused by variations in composition of the reactive gas mixture. In fact, when increasing the oxygen partial pressure Pliangos *et al* [70] observed, first an increase in reaction rate and then, at a certain critical gas composition, an abrupt drop in reaction rate that was accompanied by a significant change (increase) in catalyst potential (by up to 150 mV). This increase was evidence for catalyst oxidation.

Moreover, the drop in reaction rate was displaced to higher oxygen concentrations when positive potentials were applied to the catalyst, implying that the stability of the surface oxides decreases with an increase in catalyst potential. It has been suggested that oxygen back-spillover is responsible for this effect. The presence of these species at the catalyst surface causes a weakening of the chemisorptive bond strength of electron acceptor adsorbates (oxygen) and, hence, an easier formation of metallic rhodium. Electrochemical promotion was most effective on a fairly highly oxidized rhodium catalyst surface having sufficient opportunity for reduction of this surface.

Recently, the reactions of propylene oxidation and NO reduction by propylene on rhodium-based catalysts were studied in detail [73]. The primary goal was that of modelling the reaction of propylene combustion on rhodium oxide and on metallic rhodium while revealing the different catalytic properties in the two oxidation states. This modelling was able to explain why the rhodium metal is a far better catalyst for propylene combustion. In fact, the catalytic reaction rate on Rh strongly depended on feed composition, which could be divided into three domains (Fig. 2.9).

In the first domain, the gas mixture is sufficiently oxidative to prevent reduction of the rhodium-based catalyst surface. The catalyst surface is in the oxide form. The combustion of propylene over the rhodium oxide is a reaction of pseudofirst order in propylene. In the second domain, the surface of the catalyst is between its oxidized and reduced state. Progressive reduction of the catalyst induces an abrupt increase in reaction rate over that of the first domain. The third domain begins where this abrupt increase in the reaction rate ends. In this domain the rhodium catalyst surface is completely reduced. The rhodium metal proved to be a far better catalyst than the rhodium oxide. In terms of the ratio between propylene and oxygen partial pressures

(C_3H_6/O_2), the three composition domains into which the catalyst's behavior was divided become identical for all oxygen or propylene partial pressures.
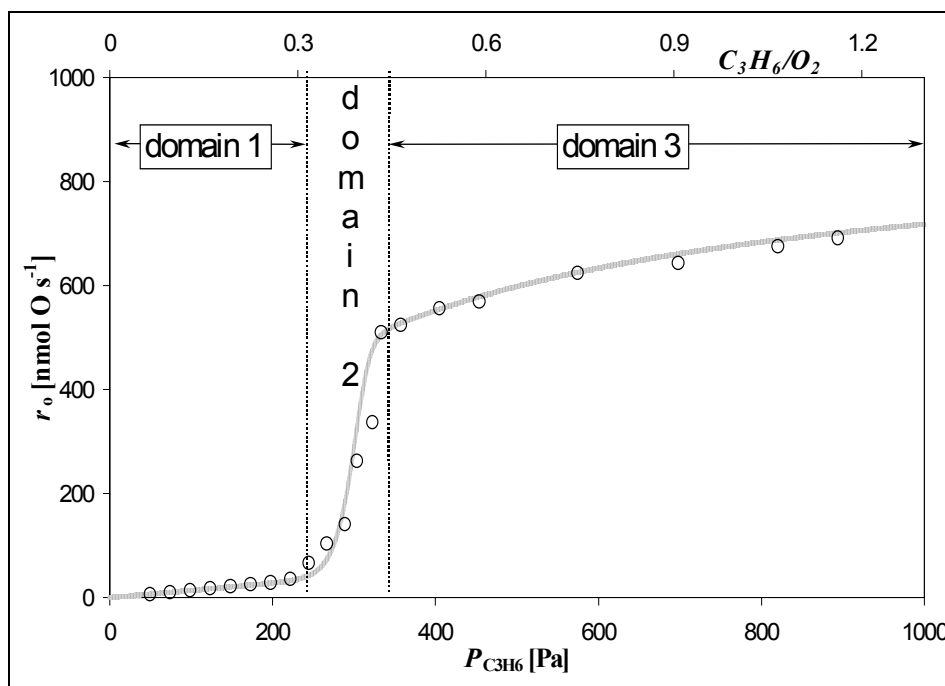
FIGURE 2.9. Complete combustion of propylene with oxygen over Rh catalyst. Reaction rate as a function of propylene pressure for the rhodium-based catalyst. Reaction conditions: 375 °C, 1000 Pa oxygen, and 200 mL/min. The ratios C_3H_6/O_2 are provided as a second *x*-axis. The plot is divided arbitrarily into three regions called: domain 1, domain 2, domain 3. Rhodium loading: 2.5 g/m^2. Geometric surface area: 0.5 cm^2.

On the basis of these observations, a reaction model was proposed (Fig. 2.10). The core of the model are the reversible changes between rhodium oxidation states. Two different reaction pathways leading to the formation of CO_2 and H_2O are possible, and depend on the rhodium oxidation state. On rhodium oxide, only propylene is adsorbed. The adsorbed propylene reacts with the rhodium oxide forming CO_2 and H_2O as the final reaction products. On metallic rhodium, to the contrary, only oxygen is adsorbed. Propylene from the gas phase reacts with the adsorbed oxygen, again to CO_2 and H_2O. According to this reaction pathway, the reaction rate of propylene oxidation on metallic rhodium follows the Eley-Rideal mechanism. By open-circuit steady-state measurements on the Rh catalyst, it was possible to verify both models. The kinetic rate constant

on metallic rhodium was found to be 25 times higher than that on rhodium oxide, in agreement with the difference in reactivities between the two oxidation states of the same rhodium catalyst. The Eley-Rideal model also provided ways to estimate the surface coverage by oxygen. Oxidation of the surface of the rhodium catalyst to rhodium oxide begins at a coverage by adsorbed atomic oxygen of about 45 %.
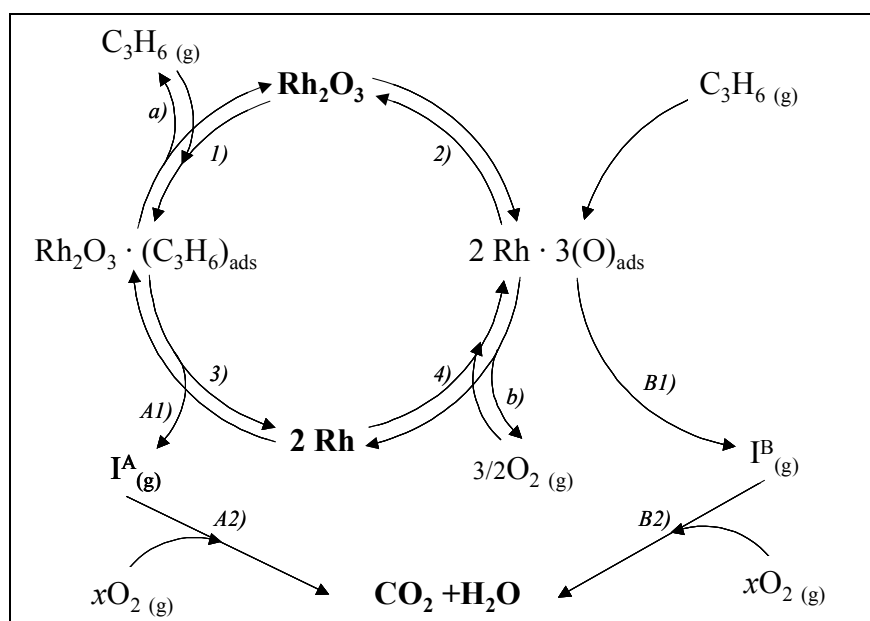
FIGURE 2.10. Reaction scheme for the reaction between oxygen and propylene on a rhodium-based catalyst. $I^A_{(g)}$ and $I^B_{(g)}$: reaction intermediates.

Measurements of catalyst potential were used as a potentiometric titration giving the amount of rhodium oxide relative to rhodium metal. Combining this information with the proposed model, a complete simulation that was valid over the entire gas composition range was possible. By combining the catalyst potential measurements with work function measurements, it was possible to satisfactorily confirm the one-to-one relationship proposed by Vayenas and coworkers (Eq. (1.17)). Finally, XPS analyses coupled with the electrochemical promotion experiments proved that spillover oxygen assisted in the reduction of the surface of the rhodium-based catalyst (reduction of Rh_2O_3 to Rh).

The rhodium-based catalyst was further tested in the reduction of NO by propylene, first in the absence of oxygen and then at different partial pressures of oxygen. It was found that the reaction between NO and propylene was very similar to that between oxygen and propylene. Addi-

tionally, it was found that NO oxidizes the catalyst surface in the same manner as oxygen does. As a consequence, in the presence of oxygen a strong competition between oxygen and NO for propylene combustion was observed. The selectivity of NO reduction to N_2 (S_{N2}) was found to be rather independent of the gas composition (S_{N2} ˜ 65 %). Electrochemical promotion induces a distinct nonfaradaic enhancement of the reaction rate, but it hardly affects the N_2 selectivity. The selectivity of NO reduction by propylene, to the contrary, is strongly affected (decreased) by increasing oxygen content at a fixed partial pressure of propylene.

On the basis of these results, the model proposed for the combustion of propylene with oxygen (Fig. 2.10) was adapted to propylene combustion with NO. This reaction mechanism took into account the oxidation state of the rhodium-based catalyst. Here again, on rhodium oxide the adsorbed propylene reacts directly with the oxidized catalyst following the Mars-van Krevelen model (redox catalysis). The role of NO, like that of O_2, is that of furnishing the adsorbed oxygen for catalyst oxidation. The kinetics is found to be zero order in the O_2 and NO partial pressure. On the reduced surface, the Eley-Rideal mechanism was supposed to be valid. The reaction occurs between the atomic oxygen adsorbed on the rhodium catalyst surface and propylene from the gas phase. Now the role of NO, similarly to that of O_2, is that of furnishing the adsorbed atomic oxygen at the catalyst surface. From experimental data, it was found that in this respect, $2.3P_{NO}$ is equivalent to Po_2.

At the rhodium oxide surface, EPOC induces an increase in reaction rate. The role of oxygen backspillover is that of favoring the adsorption of propylene at the oxidized surface. At the metallic rhodium surface, EP induces an increase in the kinetic constant of the reaction, which is more than doubled. To the contrary, EPOC does not increase the kinetic constant of oxygen adsorption. The role of the oxygen backspillover is that of lowering the strength of oxygen adsorption, thus increasing the rate of the reaction. Relative to the reduced rhodium surface, on rhodium oxide the reaction rate is lower but more sensitive to EP, which can give rise to a 300-% increase in the rate constant.

2.1.7 Electrochemical activation of a catalyst

The concept of a nonfaradaic electrochemical modification of catalysts may also be applied to an *in-situ* control of catalytic activity. This phenomenon was studied using YSZ-interfaced Rh

film catalysts for the reduction of NO by C_3H_6 in the presence of excess oxygen [67]. The measurements were performed in a slightly oxidizing gas mixture (0.1 kPa C_3H_6; 0.1 kPa NO; 0.5 kPa O_2) at $T = 300\ °C$. At this composition, a temporary heating (one hour) to 400 °C resulted in a strong deactivation of the catalyst due to partial oxidation of the rhodium surface; the new steady-state catalytic activity at 300 °C was ~90 % smaller than prior to heat treatment, see Figure 2.11. Under open-circuit conditions, no spontaneous reactivation occurred at 300 °C, so that the catalyst's performance could be investigated systematically in both the active (*a*) and the deactivated (*d*) state.
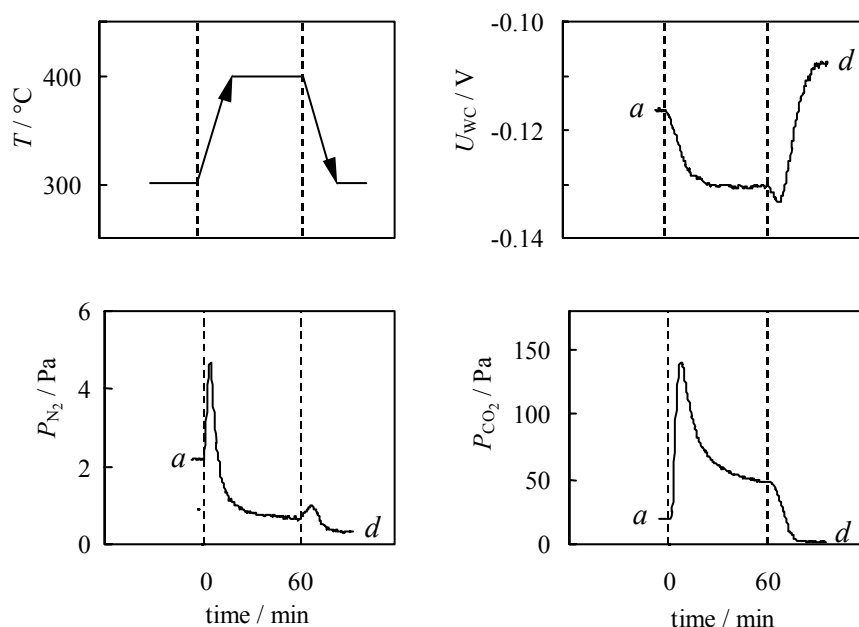
FIGURE 2.11. Deactivation of a Rh/YSZ film catalyst by temporary heating (one hour) to 400 °C. Transients of cell potential (U_{WC}), N$_2$ production (P_{N2}), and CO$_2$ production (P_{CO2}). (*a*): active state; (*d*): deactivated state. Feed composition: C$_3$H$_6$: NO : O$_2$ = 0.1 : 0.1 : 0.5 kPa. $T = 300\ °C$.

In both states, application of a low positive current (+5 µA) gave rise to an enhancement of N_2 and CO_2 production, the latter exceeding several hundred times the faradaic rate. While active rhodium exhibited a fairly reversible behavior, electrochemical promotion on the deactivated catalyst was quite unusual. On one hand, no apparent steady-state was reached within reasonable times of polarization and, on the other hand, the promotion was highly irreversible, as seen in Figure 2.12.
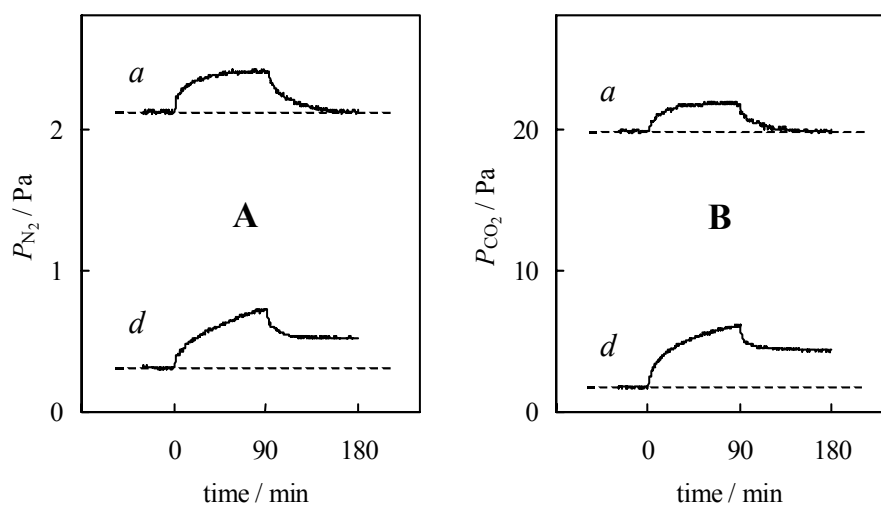
FIGURE 2.12. Electrochemical promotion of the production of N_2 (A) and CO_2 (B) over the active (*a*) and the deactivated (*d*) Rh/YSZ catalyst during a galvanostatic polarization cycle. Anodic current applied (+5 µA) at *t* = 0 min; current interrupted at *t* = 90 min. Feed composition as in Figure 2.11, *T* = 300 °C.

The effect seen at the deactivated catalyst could be split into two parts: a reversible electro-chemical promotion (EP$_r$) being rather independent of the time of polarization, and an irreversible electrochemical promotion (EP$_i$) increasing with longer polarization times. The reversible electro-chemical promotion (EP$_r$) vanishing after an interruption of the current is related to the steady-state accumulation of promoting species at the gas-exposed catalyst surface.

The irreversible effect (EP$_i$) persisting after interruption of the current is due to the pro-gressive reduction of oxidized (hence, deactivated) surface sites. It is believed that the applied positive current raises the rate of rhodium oxide reduction *via* weakening the Rh-O bond in a way similar to the case of platinum oxides [21]. As a practical consequence, a current applied with practically negligible power consumption may efficiently assist the recovery of accidentally lost catalytic activity at rhodium.

2.2 Metal-support interaction

Metal-support interactions are a phenomenon responsible for changes which occur in the catalytic activity or selectivity of catalytically active phases when varying the catalyst support [74-76]. In commercial catalysts, the catalytically active phase usually is dispersed on a highly porous, high-surface-area (>100 m^2/g) support. Such a support, frequently termed carrier, has pores as small as 0.1 nm and can serve as a substrate for the active phases in a highly dispersed form. In the early days of catalysis, this porous, high-surface-area support usually was regarded as inert. It soon became obvious, though, that the catalytic activity in a reaction on a given active phase often was strongly influenced by crystallite size and by the material of the support. Geometry ("structure effects") did not yield a satisfactory explanation.

Thus, metal-support interactions have been a focal point of extensive research during recent decades. Typical examples are:

1. the phenomenon of strong metal-support interactions (SMSI) discovered by Tauster *et al* [77];

2. the effect of dopant-induced-metal support interactions (DIMSI) studied by Verykios and coworkers [78];

3. the discovery of highly active Au/SnO$_2$ oxidation catalysts by Haruta and coworkers [79, 80].

An explanation frequently offered for the nature of MSI are electronic-type interactions between support and catalyst particles. A concept of electronic interactions associated with the bulk electronic properties of the two phases in contact (metal crystallites and support materials) was first proposed by Schwab ([81] and references therein) and Solymosi ([82] and references therein). This concept is based on metal-semiconductor boundary-layer theory, according to which thermodynamic equilibrium develops at a metal-semiconductor contact (in the present case, the interface between the metal crystillites and the support). The equilibrium condition requires that the Fermi energy levels of the electrons in the two solids be the same. In order for this to be achieved, charge must be transported from one material to the other. For instance, in cases where the electron work function of the metal is higher than that of the semiconductor, charge will flow from the semiconductor to the metal until the Fermi levels at the interface are equilibrated. The charge transfer process causes significant alterations in the catalytic properties

and selectivity of the dispersed metal particles. The driving force for charge transfer is the difference in electrochemical potentials.

2.2.1 Metal-semiconductor boundary layer theory

The condition of thermodynamic equilibrium at a metal-semiconductor contact implies that the electrochemical potential should be uniform throughout the system. If, prior to contact, the metal and the semiconductor have different electrochemical potentials, then upon contact, charge will flow to the material with the smaller potential until the potentials are equalized. When the two materials carry no net charge, then $\bar{\mu}_e^M = \Phi_M$ and $\bar{\mu}_e^S = \Phi_S$, where M and S denote the metal and the semiconductor, respectively. For $\Phi_M > \Phi_S$ the electron flux will be toward the metal. At equilibrium, the common electrochemical potential will be (similarly to Eq. (2.12):

$$\bar{\mu}_e^{eq} = -\Phi_M - e\Psi_M = -\Phi_S - e\Psi_S \tag{2.33}$$

and

$$\Delta\Phi = e(\Delta\Psi) \tag{2.34}$$

that is, a contact potential difference equal to the work function difference has developed. Quantities Ψ_M and Ψ_S are the outer potential of the metal and the semiconductor, respectively. For instance, in a situation where $\Phi_M > \Phi_S$, charge is transferred from the semiconductor to the metal. Electrons transferred to the metal are associated with the interface atoms, while the more extended region in the semiconductor that is depleted of electrons is characterized by a bending of the valence and conduction bands [83, 84]. The Schottky barrier, Φ_{SB}, at the interface is given by

$$\Phi_{SB} = (\Phi_M - \Phi_S)/e \tag{2.35}$$

It could be shown that for strongly ionic semiconductors, the barrier height will be equal or proportional to the work function difference [83, 84], just as indicated by Eq. (2.35). It was also shown that the ideal Schottky theory can be used to describe a metal-TiO_2 contact [85]. Experimentally, the barrier height in contacts of TiO_2 with metals such as Pd, Pt, or Au in air was found to be equal to the work function difference [86].

2.2.2 Strong metal-support interactions

In more recent years, the concept of strong metal-support interactions (SMSI) was introduced by Tauster *et al* [77, 87]. It was observed that Group VIII-metal particles supported on titania and other reducible oxides lose their ability to chemisorb H_2 and CO when they are subjected to reduction at temperatures higher than 773 K. A number of models have been proposed to explain the mechanism of this phenomenon, which include formation of intermetallic bonds with localized charge transfer from the reduced titania support to the metal crystallites [88, 89]. Another model is diffusion of a suboxide species to the surface of the metal crystallites, rendering them partially inaccessible to chemisorption and catalytic action [76, 90]. A model involving geometric decoration has been shown by many investigators to be most often responsible for the SMSI state. Direct experimental evidence for the occurrence of metal decoration by TiO_x species has been provided by HREM and XPS [91-93]. In some cases, electronic effects may also be playing an important role in the phenomenon [93, 94]. Certain similarities with the M/TiO_2 catalytic system, but also significant differences are observed for the M/CeO_2 system [95].

Recently an alternative interpretation of metal-support interactions was proposed [5, 85, 96] (Section 2.2.3).

2.2.3 Electrochemical promotion and metal-support interactions

Recent experiments in our laboratory have provided evidence that electrochemical promotion and metal-support interactions are phenomena which are functionally identical, and differ only operationally [96].

For studies of the relation between EPOC and MSI, it was proposed to prepare mixed IrO_2-TiO_2 catalysts consisting of micro and nanoparticles of IrO_2 (as an active phase) and TiO_2 (as an inert support) in intimate contact. A series of catalyst films of varying composition was prepared in which the IrO_2 loading was kept constant (130 μg/cm^2) [96].

A decrease in the effect of electrochemical promotion with increasing TiO_2 content is clearly manifest in Fig. 2.13, which shows plots of the open-circuit ($I = 0$) and electrochemically promoted ($I = 200$ μA) steady-state catalytic rates against film composition. It is worth noting that:

1. pure TiO$_2$ (x_{IrO_2} = 0) is catalytically inactive;

2. pure IrO$_2$ (x_{IrO_2} = 1) has a moderate catalytic activity;

3. addition of TiO$_2$ to the IrO$_2$ catalyst causes a pronounced increase in catalytic rate;
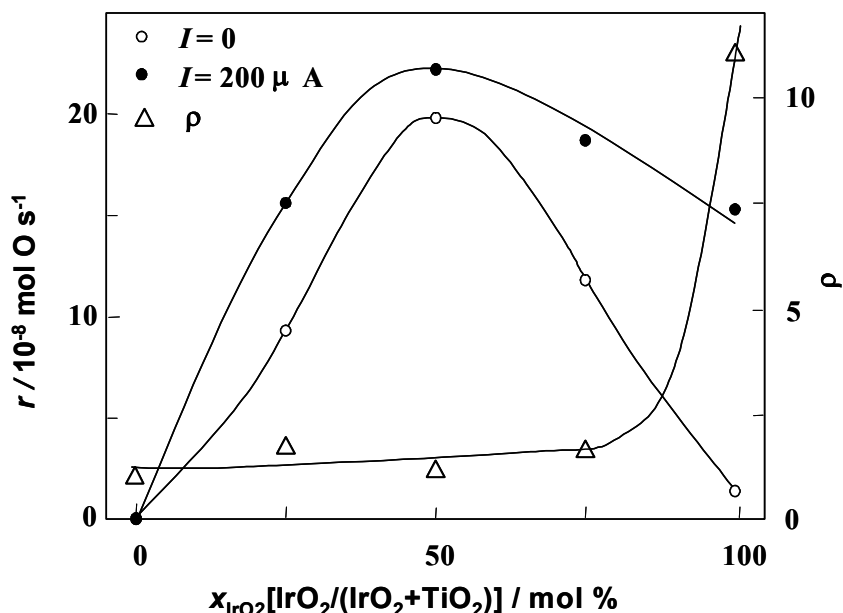
FIGURE 2.13. Effect of composition of the IrO$_2$-TiO$_2$/YSZ catalyst films on the rate of C$_2$H$_4$ oxidation under open-circuit (open circles) and electrochemical promotion (full circles) conditions. Triangles indicate the corresponding rate enhancement ratio (r) value. Applied anodic current: I = 200 μA during 60 min. Feed composition: $P_{C_2H_4}$ = 0.15 kPa, P_{O_2} = 20 kPa. T = 380 °C.

for the promotional (metal-support interaction) rate enhancement ratio ρ_{MSI} defined as:

$$\rho_{MSI} = \frac{r}{r_u} \tag{2.36}$$

where r_u is the unpromoted catalytic rate per unit mass of the active catalyst, values of up to 13 were obtained for x_{IrO_2} = 0.5;

4. electrochemical promotion of the pure IrO$_2$ catalyst (x_{IrO_2} = 1) leads to a pronounced electrochemical promotion with ρ-values of up to 12;

5. EPOC of the IrO$_2$-TiO$_2$ catalyst is negligible, with ρ-values below two.

Observations 3 and 5 strongly suggest that for the TiO_2-IrO_2 catalyst, the same type of promoting mechanism is operative as for the electrochemically promoted IrO_2 catalyst. One may consider the IrO_2-TiO_2 metal-support interactions as a remote-control mechanism [97] or as a "wireless"-type NEMCA configuration [42, 98] where TiO_2 continuously provides promoting O^{2-} species to the IrO_2 catalyst surface and gaseous O_2 continuously replenishes spent O^{2-} in the TiO_2.

The same reaction of ethylene oxidation was investigated over Rh nanoparticles dispersed on pure and doped TiO_2 and other porous supports [96]. It was established that under conditions under which the change in work function of the catalyst is the same, regardless of the means by which the alteration in the work function is achieved, the influence of electrochemical promotion on the kinetic parameters of the model reaction is identical to the influence of metal-support interactions [96].

These results indicate that at least under certain conditions, the mechanism of metal-support interactions may be identical to that of electrochemical promotion, *ie,* the charge exchanged between the metal particles and the support material owing to the difference in electrochemical potentials between the two solids may consist of oxygen ions, just as in cases of electrochemical promotion.

The concept of electronic-type metal-support interactions is still valid: the thermodynamic driving force for charge transport is due to equilibration of the Fermi levels of the two solids in contact. This is true for the electrochemically promoted catalysts and for the dispersed metal particles on an ion-conducting support. This interpretation of metal-support interactions involving oxygen ion backspillover from the support to the metal crystallites is shown schematically in Fig. 2.14. In the same figure, the concept of electrochemical promotion induced by application of a current or potential is also ilustrated. The difference between electrochemical promotion and metal-support interactions is the driving force for the transport of oxygen ions from the carrier to the metal particles.

At the three-phase boundary (metal-support-gas), the following charge-transfer equilibrium is established:

$$O_2(g) + 4\ e^-(M) \leftrightarrows 2\ O^{2-}(S) \tag{2.37}$$

where M denotes the metal particles and S denotes the support. Then the electrochemical potentials of the electrons, $\bar{\mu}_e$, oxygen ions, $\bar{\mu}_{O^{2-}}$, and gaseous oxygen, μ_{O_2}, are related as follows [96]:

$$\bar{\mu}_{O^{2-}}(S) = 2\bar{\mu}_e(M) + (1/2)\mu_{O_2}(g) \qquad (2.38)$$
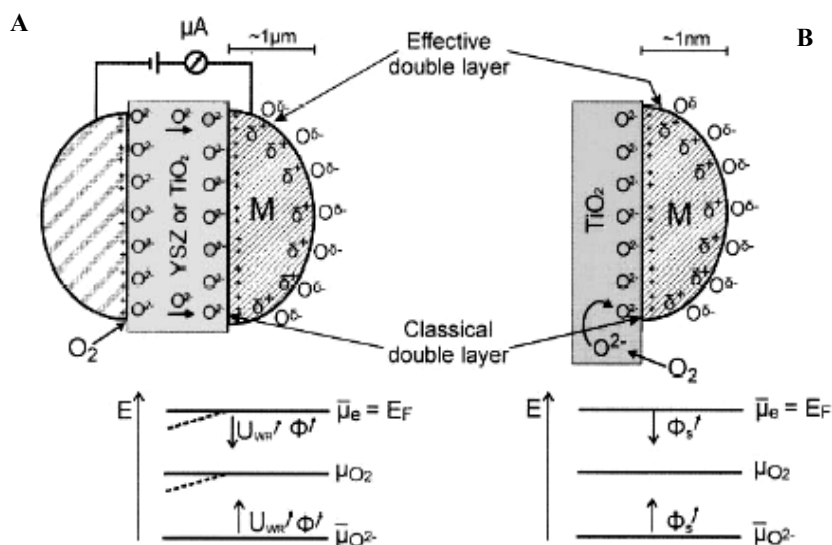
FIGURE 2.14. (A) Electrochemical promotion, (B) Metal-support interactions. Alternative approach to metal-support interactions involving backspillover of oxygen ions from the TiO$_2$ carrier to the metal nanoparticles. The locations of the classical double layers formed at the metal–support interface and of the effective double layers formed at the metal–gas interface are shown. The energy diagrams (bottom) schematically indicate the Fermi level, E$_F$ (or electrochemical potential, $\bar{\mu}_e$, of electrons), the chemical potential of oxygen, and the electrochemical potential of O$_2$ (from Ref. [96]).

If one assumes that the oxygen ions are mobile on the metal surface and do not rapidly desorb nor participate in fast catalytic reactions, then the equilibrium described by Eq. (2.37) is also established at the catalyst surface, in which case

$$\bar{\mu}_{O^{2-}}(M) = 2\bar{\mu}_e(M) + (1/2)\mu_{O_2}(g) \qquad (2.39)$$

Thus, in the metal-support system the thermodynamic driving force for O^{2-} backspillover from the support to the metal surface is the difference in electrochemical potentials of the oxygen ions, $\bar{\mu}_{O^{2-}}$ (S)$-\bar{\mu}_{O^{2-}}$ (M) [5, 54]. Alternatively, the Fermi levels of the two solids in contact are equalized by transport of charged carriers, such as oxygen ions. This could occur simultaneously with the transport of electrons or positive holes, depending on the relative values of electronic and ionic conductivities of the semiconducting support.

2.2.4 Solid electrolytes

Solid electrolyte should have high ionic conductivity and low electronic conductivity. Known electrolyte materials mainly differ in the nature of their conductivity, either having pure ionic or mixed ionic-electronic conductivity. The preparation, properties, and some applications of solid electrolytes have been discussed in a number of books [99-101] and reviews [102, 103]. The major commercial application of solid electrolytes is in gas sensors [104, 105] and solid-oxide fuel cells [106, 107]. Solid electrolytes play an increasingly important role in heterogeneous catalysis, both as nanodispersed catalyst carriers and as supports of thick or thin, electrochemically promoted films [4, 5, 18-20, 85]. The lowest acceptable ionic conductivity of a solid electrolyte in practical fuel cell applications is 0.1 to 1 ohm^{-1}cm^{-1}. This places severe restrictions on the choice of materials and operating temperatures. For catalytic (promotional) and sensor applications, however, much lower conductivities (10^{-4} ohm^{-1}cm^{-1}) usually are sufficient. This implies that a great variety of solid electrolytes can be used over a very wide temperature range. In published electrochemical promotion studies, the following solid electrolytes were used:

(i) Yttria-stabilized-zirconia (YSZ), an O^{2-} conductor at temperatures higher than 280 °C.

(ii) β"-Al_2O_2 and $Na_3Zr_2Si_2PO_{12}$ (NASICON), which are Na^+ conductors at temperatures between 180 °C and 400 °C.

(iii) $CsHSO_4$, Ca $Zr_{0.9}In_{0.1}O_{3-\alpha}$, and Nafion, which are proton conductors at temperatures between 150 and 25 °C, respectively.

(iv) CaF_2, a F^- conductor at temperatures between 550 and 700 °C.

(v) Mixed ionic-electronic conductors such as TiO_2 and CeO_2.

Other solid electrolytes were also reported [5].

In this section, a short description is provided of some important properties of YSZ and TiO_2 oxide materials that are of interest within the scope of the present thesis.

2.2.4.1 Properties of yttria-stabilized-zirconia

The majority defects in pure ZrO_2 are oxygen vacancies Vö and electrons e⁻, both at very low concentrations. Lower-valent oxides such as Y_2O_3 or CaO when added to ZrO_2 raise its oxygen vacancy concentration, and thus lead to a much higher ionic conductivity.

For ZrO_2 doped with Y_2O_3, the oxide conductivity is plotted schematically as a function of the oxygen partial pressure in Fig. 2.15.

The "partial pressure window", that is, the range of partial pressures over which a compound is an ionic conductor, is relatively wide for the stabilized zirconias, covering about 20 to 30 orders of magnitude around the minimum of electronic conductivity.

The cubic fluorite structure is one of the most important crystal structures in the field of ionically conducting oxides. It is the structure of the high-temperature form of ZrO_2 and of the so-called stabilized zirconias. At room temperature, ZrO_2 has a deformed structure derived from the fluorite (CaF_2) structure. Pure ZrO_2 when cooled down from high temperatures undergoes several phase transitions accompanied by relatively large volume changes.
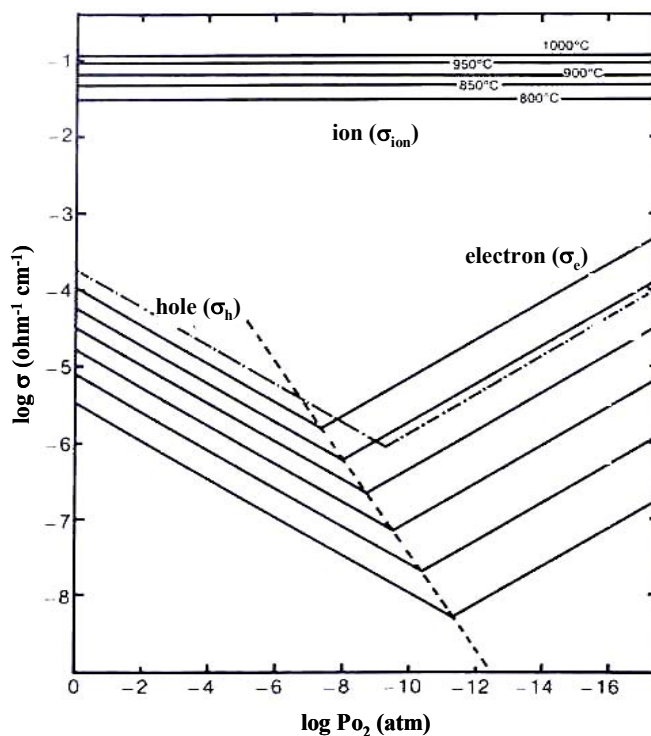
FIGURE 2.15. Electron, hole, and ion conductivities in yttria-stabilized zirconia [108] .

By doping ZrO_2 with lower-valent ions such as calcium or yttrium, the cubic structure is stabilized and remains viable down to room temperature. Some properties of ZrO_2 + 8 % Y_2O_3 are given in Table 2.1.

TABLE 2.1. The main properties of yttria-stabilized-zirconia (ZrO_2 + 8 % Y_2O_3)

Property	Value
Melting point, °C	2680
Density, g cm^{-3}	5.9
Conductivity (1000 °C), ohm^{-1}m^{-1}	12.0
Thermal conductivity, Wcm^{-1}K^{-1}	0.02
Standard enthalpy, kJ/mol (25 °C)	1097.5
Standard entropy, J/mol.K (25 °C)	50.4

2.2.4.2 Properties of titanium dioxide

Nanocristalline titanium dioxide has been investigated extensively in recent years because of its uses in photocatalysis [109, 110], photovoltaics [111, 112], catalysis [76, 77, 85, 87]. Titania is an important support material in catalysis. It has been studied in the context of metal-support interactions, and more particularly of strong metal-support interactions (SMSI). In addition to its importance as a metal support material, TiO_2 is a highly valued material in sensor technology [104, 113-115], which is due to its predominantly n-type semiconductivity and concomitant, marked variation in electronic conductivity with the chemical potential of oxygen. The Pt/TiO_2 interface, and particularly its electrical properties, have been studied in detail for sensor applications using a variety of surface spectroscopic techniques [104, 113-115].

Titania exists in a number of crystalline forms, the most important ones being anatase and rutile. Some physical properties of sintered titania are summarised in Table 2.2 [116].

TABLE 2.2. The physical and mechanical properties of titania

Property	Value
Density, $g\ cm^{-3}$	4
Resistivity (25 °C), ohm·cm	10^{12}
Resistivity (700 °C), ohm·cm	2.5×10^4
Dielectric Constant (1 MHz)	85
Thermal Conductivity (25 °C), $Wm^{-1}K^{-1}$	11.7

One important materials property of TiO_2 is mixed conduction, *ie,* in addition to n-type semiconductivity at low Po_2 values and p-type semiconductivity at high Po_2 values, it also exhibits some ionic conductivity due to the migration of O^{2-} ions or vacancies [103]. Figure 2.16 shows that the relative importance of ionic conductivity can be high at intermediate or high Po_2 values, while at low Po_2 the n-type semiconductivity is predominant [103].
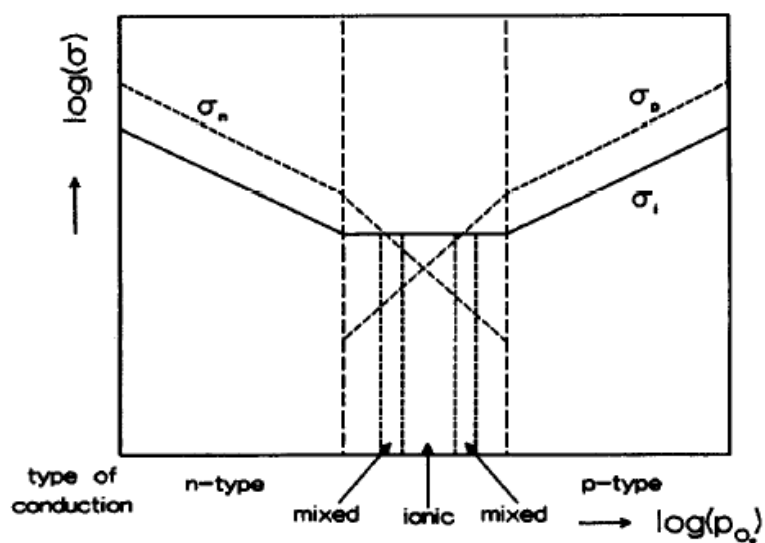
FIGURE 2.16. Effect of oxygen partial pressure on the electrical conductivity of mixed-conducting MO$_2$ oxides, and the relative contributions of *n*- and *p*-type semiconductivity and of ionic conductivity.

Literature reports on the electrical properties of TiO$_2$ are not free of speculation and conflicting conclusions concerning the contribution of ionic conductivity to the overall conduction process [117-122].

It has been generally assumed that the electrical properties of TiO$_2$ are determined by the electronic conduction while the ionic component assumes negligibly small values. Popov *et al* [117] reported that below 1273 K, undoped TiO$_2$ is mainly an ionic semiconductor. On the other hand, Cronemeyer [118] argued that the electrical conductivity is determined by the transport of electronic charge carriers while the contribution of the ionic component is negligible. Also, Baumard and Tani [119] claimed that the contribution of the ionic component at 1273 K is limited to 0.1 % of the total conductivity value. Carpentier *et al* [120] concluded that TiO$_2$ at 1000 °C under Po$_2$ = 10^5 Pa exhibits mixed conductivity with an ionic component smaller than 5 %. Singheiser and Auer [121] reported that the ionic component plays a significant role in conduction in reduced TiO$_2$ (10^{-14} - 10^{-19} Pa) at 1125-1255 K; however, they did not specify the absolute value of this component. Nowotny *et al* [122] have evaluated the ionic conductivity component in undoped TiO$_2$ within the *n-p* transition region over the temperature range from 985 to 1387 K and at Po$_2$ of 1 to 10^5 Pa. It was found that the ionic transport number for TiO$_2$ at the *n-p* transition is approxi-

mately 0.5. Another indirect confirmation concerning an ionic component of TiO_2 conductivity was reported by Pliangos *et al* [16] who studied the Pt/TiO_2 system in electrochemical promotion experiments at 773 K. These authors have shown by work function and XPS measurements in UHV that under oxidizing conditions, TiO_2 partly behaves as a solid electrolyte due to O^{2-} conduction, and can be electropromoted. Under reducing conditions in UHV, the *n*-type conductivity of TiO_2 is predominant, and hence the $Pt-TiO_2$ contact is totally ohmic. Under these conditions electrochemistry is inoperative.

It is well known that TiO_2 conductivity depends on the oxidation state of Ti, and the series $TiO_2-Ti_2O_3-TiO-Ti$ is an interesting oxide system in which the progressive transition from insulator to metal is accomplished by reduction [116]. In fact, TiO_2 is readily reduced by hydrogen at relatively moderate temperatures (T > 400 °C). TiO_x is a degenerate semiconductor with a very high carrier concentration, and the high electrical resistivity of TiO_2 (10^{10} ohm·cm) dramatically decreases upon partial reduction, see Fig. 2.17 [116, 123, 124].
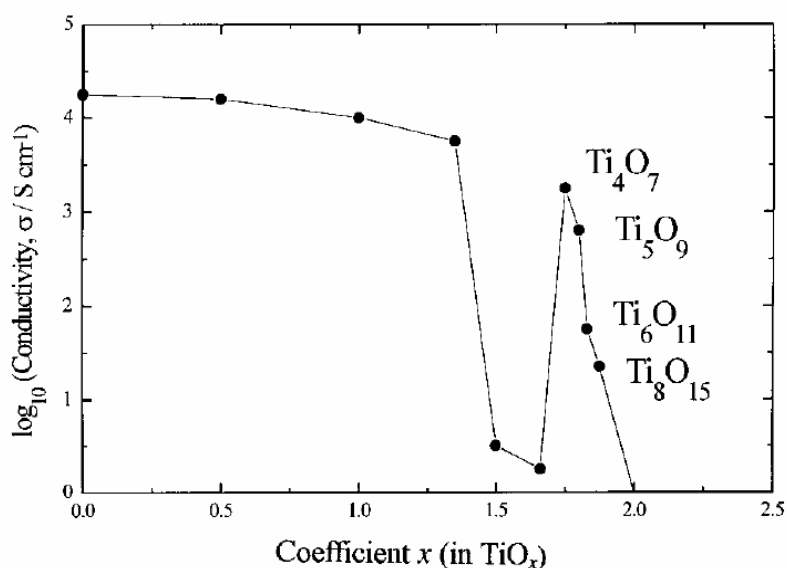
FIGURE 2.17. Conductivity of TiO_x as a function of *x* [116].

It was seen that available reports offer a variety of conflicting views on the transport mechanism in TiO_2, which so far remains unresolved. Opinion is unanimous, however, that TiO_2 conductivity depends on the extent of nonstoichiometry and the defect concentrations in TiO_2, which in turn are functions of the temperature and of oxygen partial pressure.

2.3 Electrode reactions at gas/metal/YSZ interfaces

In reactions at gas electrodes, the reactants exist in three different phases: the uncharged reactants are associated with a gas phase, ions as charged reactants are present as a solid electrolyte, and the electrons are associated with a metal. The geometric line representing the three-phase boundary has zero width, hence some of the steps of the electrode reaction have to take place at the two-phase boundaries, and for practical purposes one can speak about an extension of the three-phase boundary towards two-phase boundaries (Fig. 2.18).
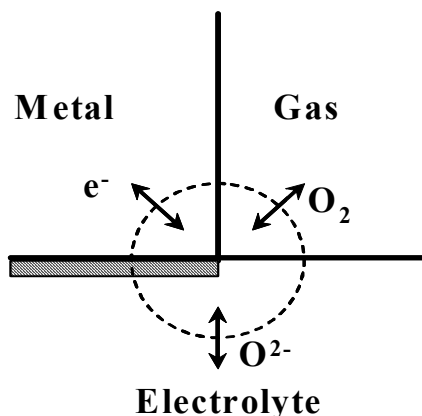
FIGURE 2.18. Schematic representation of the three-phase boundary metal/electrolyte/gas.

An electrode process involving a gas phase can thus proceed at different surface boundaries: metal-electrolyte (ME); electrolyte-gas (EG); and metal-gas (MG) [99, 100].

1. Electrochemical reactions at the metal-electrolyte (ME) phase boundary. The ME surface boundary is the most favorable place for the electrochemical step of a process. This boundary is an unlimited sink or source for electrons, and the electrochemical reaction basically may occur

over the entire surface of the electrolyte, which serves to decrease the electrode's polarization and contact resistance.

The higher the diffusion rate of electrochemically active species and the smaller the rate of discharge process, the longer will be the distance over which the reaction is spread out along the ME boundary from the three-phase boundary (MEG). Electrochemically active species are supplied to the boundary of electrolyte and metal or withdrawn in the three-phase boundary through the EG and MG surfaces. At these boundaries, active species are exchanged with a gas phase through adsorption and desorption processes. This process scheme can be realized on an anode as well as on a cathode.

It must be asked whether gas atoms can diffuse into the interface region between electrode and electrolyte and, if so, whether the diffusivity is the same as that measured for a gas over the free and clean surface of a metal crystal. It appears reasonable to expect that, as long as there is no strong chemical bonding between the metal electrode and the electrolyte, gas atoms should have no difficulty in diffusing along the interface, and do so with a diffusivity that is similar (at least in order of magnitude) to that at the free surface [125].

2. Electrochemical reactions at the electrolyte-gas (EG) surface boundary. For an electrochemical reaction to occur at the EG interface, diffusion of electrons along the boundary is required. The electrochemically active species can be supplied, either directly from the gas phase or from an adsorbed layer at the MG boundary. Typically, solid electrolytes have very low electronic conductivity, and thus a very low electronic surface conductivity. Therefore, this process is hampered by a lack of electrons at the EG interface.

3. Electrochemical reactions at the metal-gas (MG) surface boundary. For an electrode reaction to occur at the MG interface, ions must be supplied to it by diffusion. This implies an extension of the reaction zone toward the gas-exposed electrode surface. Mechanisms of this type have often been described in the literature on electrochemical promotion [5]. This extension of the reaction zone means that an effective double layer is developed along the gas-exposed electrode surface. Once this effective double layer is formed, the reaction can take place at the metal-gas interface.

2.3.1 Oxygen electrode O$_2$, M/YSZ

Solid-electrolyte electrochemical cells are widely used as high-temperature oxygen sensors, as solid-oxide fuel cells and, as shown before, in electrochemical promotion experiments. Interest in these devices has motivated a large number of investigations into the kinetics and mechanism of the most common electrochemical reaction, *viz*, oxygen oxidation/reduction at O$_2$, M/solid electrolyte interfaces. The overall reaction in an O$_2$, M/YSZ cell can be written as:

$$1/2 \; O_{2(g)} + 2 \; e^- \leftrightarrows O^{2-} \tag{2.40}$$

or, using Kröger-Vink notation, as:

$$1/2 \; O_{2(g)} + 2 \; e^- + V_ö \leftrightarrows O_o{}^x \tag{2.41}$$

where $V_ö$ and $O_o{}^x$ are a doubly charged oxygen vacancy and an oxygen atom, respectively, both located at a normal oxygen site in the electrolyte.

A variety of kinetic studies have been performed over the last three decades, and many kinetic models have been proposed in the literature to explain the mechanism of this electrode reaction at O$_2$, M/solid electrolyte interfaces between Pt, Au, Ag, and Pd as the metal and YSZ and doped ceria as the electrolyte [99, 100, 125-135]. The geometric complexity of the various metal electrodes complicates the kinetics of the oxygen reactions, and to date no consensus has emerged as to the details of the reaction mechanism.

One of the systems most thoroughly studied in solid-state electrochemistry is the O$_2$/Pt/solid-electrolyte electrochemical cell. It is generally accepted that oxygen reduction at Pt occurs in several steps of which any one may be rate determining:

(i) Gas-phase diffusion from the bulk gas into a Pt pore (Eq. (2.42)) as well as gas-phase diffusion within the open Pt pore system (Eq. (2.43)):

$$O_{2(g)} \leftrightarrows O_{2(Pt\text{-}pores)} \tag{2.42}$$

$$O_{2(Pt\text{-}pores,1)} \leftrightarrows O_{2(Pt\text{-}pores,2)} \tag{2.43}$$

Gas-phase diffusion has been suggested to be rate-limiting in references [136, 137].

(ii) Oxygen may then dissociatively adsorb on the electrode:

$$O_{2(\text{Pt-pores})} \leftrightarrows 2\,O_{(\text{MG})} \qquad\qquad (2.44)$$

Dissociative adsorption is known to be the common mode of adsorption for oxygen on most transition metals at high temperatures [138], and was suggested to contribute to the rate-determining step in reference [139].

(iii) The adsorbed oxygen atoms may diffuse to a three-phase boundary $O_{(\text{MEG})}$:

$$O_{(\text{MG})} \leftrightarrows O_{(\text{MEG})} \qquad\qquad (2.45)$$

$$O_{(\text{MEG})} \leftrightarrows O_{(\text{ERS})} \qquad\qquad (2.46)$$

and, further, along the electrode/electrolyte interface ("laterally") to an electrochemical reaction site (O_{ERS}). Surface diffusion of atomic oxygen has been suggested as being rate-determining in [131, 137, 140], lateral diffusion has been suggested as being rate-determining in [99, 125, 129].

At the electrochemical reaction site (ERS), adsorbed oxygen atoms pick up charge and enter the electrolyte:

$$O_{(\text{ERS})} + 2\,e^- \leftrightarrows O^{2-} \qquad\qquad (2.47)$$

Equation (2.47) represents an overall charge transfer reaction that may itself consist of several elementary reactions. It represents a cathodic current in the forward direction, and an anodic current in the reverse direction.

Disagreement exists as to the location of the ERS; they might be located in the three-phase boundary (MEG) or in the more extensive two-phase boundary (ME). Two distinct models have in fact been proposed for the electrode reaction, one which places the ERS at the three-phase boundary MEG, and one that places the ERS into the two-dimensional interface between the electrode and the electrolyte. They are shown schematically in Fig. 2.19 as models I and II, respectively [132].
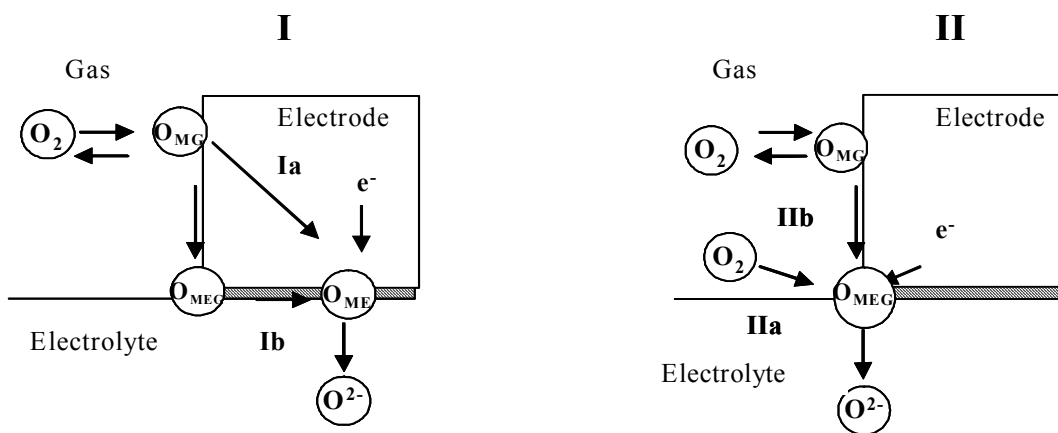
FIGURE 2.19. Schematic of the oxygen exchange reaction mechanism. Ia and b: the charge-transfer reaction at (in) the electrode-electrolyte interface. IIa and b: the charge transfer reaction at the three-phase boundary (MEG). The arrows are drawn so as to correspond to the cathodic reaction.

For the supply of oxygen to the electrode-electrolyte interface, two diffusive steps have been proposed. In mechanism Ia, oxygen atoms are transported by bulk diffusion through the metal electrode. This process can occur in the case of electrode metals in which oxygen is soluble (for instance, silver). Given the low solubility and diffusivity of oxygen in bulk Pt, Rh, Pd, and Au, the applicability of this mechanism is strongly limited. In mechanism Ib, oxygen atoms are supplied by surface diffusion through the tpb into the electrode-electrolyte interface [125, 130, 131].

In the kinetic models of type II, it is assumed that the reduction and incorporation of oxygen occur at the tpb. Here again, two diffusive steps have been proposed, which are shown in Fig. 2.19 as mechanisms IIa and IIb. In mechanism IIa, oxygen diffuses through a gas phase boundary layer or through pores of the electrode. In mechanism IIb, it is assumed that oxygen is supplied to the tpb by surface diffusion of dissociatively adsorbed oxygen [130, 131].

In oxygen electrode reactions taking place in the two-phase region, oxygen atoms must diffuse laterally inward along the metal-electrolyte interface from the three-phase region. This is particularly true for Pt, Au, etc. since the solubility and diffusivity of oxygen in the bulk metals are extremely small. The concentration of oxygen at (in) the ME interface will then depend on the

interfacial diffusion rate as well as on the local charge transfer rate. The ratio of these two rates can be modified by varying the particle size of the electrode.

Along these lines, Wang and Nowick [125] proposed a model to describe the electrode process at thick Ag and Au electrodes and thin Pt electrodes (foil) interfaced with doped ceria electrolyte, where the reaction occurs in the two-phase region consuming oxygen arriving by diffusion along the electrode from the three-phase region. They assumed that the electrode/electrolyte interface has a simple rectangular geometry (Fig. 2.20 A)

According to Nguyen *et al* [128], the electrode/electrolyte interface of a porous Au electrode sitting on YSZ has a more complex structure (Fig. 2.20 B). In their model, a simplified pore structure with cylindrical geometry is considered.

A   **B**
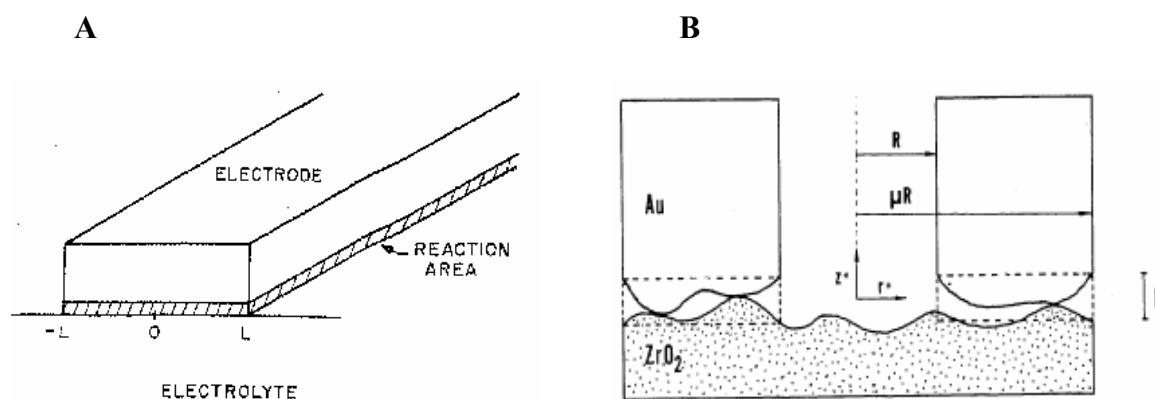
FIGURE 2.20. Representation of electrode/electrolyte interfaces. A: Schematic diagram of an electrode particle of simple rectangular geometry on an electrolyte [125]. B: Simplified pore geometry (*R* is the radius of the electrode pore) [128].

Different electrode morphologies should give rise to different overall polarization behavior. At porous electrodes of small particle size, the electrode reaction predomenantly proceeds at the three-phase boundary (MEG), while at compact and thick electrodes it occurs at (in) the ME boundary [125-127]

Information about the mechanism of an electrode process, and thus about the rate-determining step, can be derived from a knowledge of the relationship between the exchange current, I_0, at the metal/electrolyte interface and the oxygen partial pressure. It was established experimentally [125-127, 133, 141] that quite generally:

$$I_0 \infty (P_{O_2})^m \tag{2.48}$$

This equation follows for Langmuir-type adsorption of oxygen at the electrode surface:

$$\theta_O = K_O P_{O_2}^{1/2} / (1 + K_O P_{O_2}^{1/2}) \tag{2.49}$$

where θ_O is the oxygen coverage. It can be shown [125-127] that:

$$I_0 \sim [\theta(1 - \theta_O)]^{1/2} \tag{2.50}$$

or, equivalently:

$$I_0 \sim K_O P_{O_2}^{1/4} / (1 + K_O P_{O_2})^{1/2} \tag{2.51}$$

Depending on whether atomic or molecular oxygen is involved in the rds, m is related to the transfer coefficients of the cathodic (α_c) and anodic (α_a) process through the following relations:

$$m = \frac{\alpha}{2(\alpha_a + \alpha_c)} \tag{2.52}$$

for atomic oxygen and

$$m = \frac{\alpha}{(\alpha_a + \alpha_c)} \tag{2.53}$$

for molecular oxygen, where α in the denominator will be, either α_a or α_c, depending on which exponential term does not vanish.

The relationship between oxygen partial pressure and I_0 depends on whether electrons are transferred in the rate-determining step to atomic oxygen or molecular oxygen. Thus, for a purely charge-transfer-limited reaction (when the coefficients $\alpha_c = \alpha_a = 1$), the m-values are 1/4 and 1/2 for atomic and molecular oxygen, respectively. The competition between mass transport and charge transfer leads to "apparent" transfer coefficients different from unity, and also to a different oxygen partial-pressure dependence of the equilibrium exchange current density. When atomic oxygen is the diffusing species, it changes from $I_0 \infty (P_{O_2})^{1/4}$ to $I_0 \infty (P_{O_2})^{3/8}$, but with

molecular oxygen as the diffusing species, it changes from $I_0 \propto (P_{O_2})^{1/2}$ to $I_0 \propto (P_{O_2})^{5/8}$ [133, 141].

Wang and Nowick have studied the exchange current as a function of Po_2, and could show that at the Pt electrode, oxygen for the charge transfer process is supplied from oxygen atoms adsorbed on the Pt surface where a Langmuir isoterm is obeyed. The proportionality of $I_0 \propto Po_2^{1/4}$ was found for the Pt electrode when the process occurred under charge-transfer control. The rate of charge transfer can switch from a $Po_2^{-1/4}$ dependence at high surface coverage (θ) and low temperature to a $Po_2^{+1/4}$ dependence at small θ and high temperature. The same authors found for an electrode process controlled by interfacial diffusion of adsorbed oxygen atoms from the gas-exposed metal surface to the electrochemical reaction sites that the proportionality of $I_0 \propto Po_2^{3/8}$ is applicable [125-127].

2.4 Aim of the work

Considering prior work as outlined in Sections 2.1 through 2.3, it was decided that in the present work, the investigations should for a first time be targeted at the electrochemical modification of catalytic activity and at metal-support interactions in the instance of highly dispersed (about 10 %) nanofilm rhodium catalysts (film thickness 40 nm). As supports for this catalyst, a pure ionic conductor (8 % Y_2O_3-stabilized ZrO_2) and a mixed ionic-electronic conductor (TiO_2) were used, the latter support being a highly dispersed (80 %) layer of TiO_2 (4 μm) deposited on YSZ (TiO_2/YSZ). Successful electrochemical promotion of such a highly dispersed catalyst having low metal loadings would be a most valuable achievement from theoretical and practical points of view, since one of the factors holding back a commercial utilization of EPOC is the low metal-catalyst dispersion (typically 10^{-3} to 10^{-5}) typically found in the thick porous films (0.2 - 10 μm) used in all prior electrochemical promotion studies [5]. With such a catalyst design, which is similar to that of catalytic systems exhibiting effects of metal-support interactions, parallel investigations of EPOC and MSI phenomena can be performed.

2.5 References

1.   M. Stoukides and C. G. Vayenas, *J. Catal.,* **70** (1981) 137.

2.   C. G. Vayenas, S. Bebelis, and S. G. Neophytides, *J. Phys. Chem.,* **92** (1988) 5083.

3.   C. G. Vayenas, S. Bebelis, S. G. Neophytides, and I. V. Yentekakis, *Nature,* **343** (1990) 625.

4.   C. G. Vayenas, M. M. Jaksic, S. I. Bebelis, and S. G. Neophytides, in *Modern aspects of Electrochemistry* J. O. M. Bockris, B. E. Conway, and R. E. White, eds., Plenum Press, New York, (1996), p. 57.

5.   C. G. Vayenas, S. Bebelis, C. Pliangos, S. Brosda, and D. Tsiplakides, *Electro-chemical activation of catalysis. Promotion, Electrochemical promotion, and metal-support interaction.* Kluwer Academic/Plenum Publishers, New York (2001).

6.   J. O. M. Bockris, A. K. N. Reddy, and M. Gamboa-Aldecco, Kluwer Academic/ Plenum, New York (2000).

7.   K. Juttner, U. Galla, and H. Schmieder, *Elecrochim. Acta,* **45** (2000) 2575.

8.   G. Ertl, H. Knötzinger, and J. Weitkamp, *Hand Book of Catalysis* VCH, Weinheim (1997).

9.   J. Pritchard, *Nature,* **343** (1990) 592.

10.   C. G. Vayenas, S. Brosda, and C. Pliangos, *J. Catal.,* **216** (2003) 487.

11.   C. G. Vayenas, S. Bebelis, and S. Despotopoulou, *J. Catal.,* **128** (1991) 415.

12.   I. V. Yentekakis and C. G. Vayenas, *J. Catal.,* **149** (1994) 238.

13.   M. Makri, A. Buekenhoudt, J. Luyten, and C. G. Vayenas, *Ionics,* **2** (1996) 282.

14.   T. I. Politova, V. A. Sobyanin, and V. D. Belyaev, *React. Kinet. Catal. Lett,* **41** (1990) 321.

15.   D. Tsiplakides, S. G. Neophytides, O. Enea, M. M. Jaksic, and C. G. Vayenas, *J. Electrochem. Soc,* **144** (1997) 2072.

16.   C. Pliangos, I. V. Yentekakis, S. Ladas, and C. G. Vayenas, *J. Catal.,* **1996** (1996) 189.

17.   P. D. Petrolekas, S. Balamenou, and C. G. Vayenas, *J. Electrochem. Soc,* **145** (1998) 1202.

18.   C. G. Vayenas, S. Bebelis, C. Pliangos, and S. G. Neophytides, *The electrochemical activation of catalysis* Kluwer Acadenic/Plenum Publishers, New York (1996).

19.   G. Fóti, I. Bolzonella, and C. Comninellis, in *Modern Aspects of electrochemistry*, Vol. 36 C. G. Vayenas, B. E. Conway, R. E. White, and M. E. Gamboa-Adelco, eds., Kluwer Academic / Plenum Publisher, New York, Boston, Dordrecht, London, Moscow, (2003), p. 310.

20.   R. M. Lambert, F. Williams, A. Palermo, and M. S. Tikhov, *Topics in Catalysis,* **13** (2000) 91.

21.   S. G. Neophytides and C. G. Vayenas, *J. Phys. Chem.,* **99** (1995) 1763.

22.   J. Nicole and C. Comninellis, *Solid State Ionics,* **136-137** (2000) 687.

23.   D. Tsiplakides and C. G. Vayenas, *J. Electrochem. Soc,* **148** (2001) E189.

24.   S. Wodiunig, *Electrochemical promotion of RuO_2 catalysts for the gas phase combustion of ethylene.* Thesis No 3138, EPFL, Lausanne, (2000).

25.   D. Kek, N. Bonanos, M. Mogensen, and S. Pejovnik, *Solid State Ionics,* **131** (2000) 249.

26.   A. D. Frantzis, S. Bebelis, and C. G. Vayenas, *Solid State Ionics,* **136-137** (2000) 863.

27.   I. R. Harkness and R. M. Lambert, *J. Catal.,* **152** (1995) 211.

28.   T. Arakawa, A. Saito, and J. Shiokawa, *Appl. Surf. Sci,* **16** (1983) 365.

29.   T. Arakawa, A. Saito, and J. Shiokawa, *Chem. Phys. Lett,* **94** (1983) 250.

30.   S. Ladas, S. Bebelis, and C. G. Vayenas, *Surf. Sci.,* **251-252** (1991) 1062.

31.   S. G. Neophytides, D. Tsiplakides, and C. G. Vayenas, *J. Catal.,* **1998** (1998) 414.

32.   D. Tsiplakides and C. G. Vayenas, *J. Catal.,* **185** (1999) 237.

33.   D. Tsiplakides, S. G. Neophytides, and C. G. Vayenas, *Solid State Ionics,* **136-137** (2000) 839.

34.   S. Wodiunig and C. Comninellis, *J. Eur. Ceram. Soc.,* **19** (1999) 931.

35.   A. Katsaounis, Z. Nikopoulou, X. E. Verykios, and C. G. Vayenas, *J. Catal.,* **222** (2004) 192.

36.   A. Katsaounis, Z. Nikopoulou, X. E. Verykios, and C. G. Vayenas, *J. Catal.,* **226** (2004) 197.

37.   F. Tietz, C. Papadelis, D. Tsiplakides, A. Katsaounis, and C. G. Vayenas, *Ionics,* **7** (2001) 101.

38.   J. Poppe, S. Völkening, A. Schaak, J. Janek, and R. Imbihl, *Phys. Chem. Chem. Phys.,* **1** (1999) 5241.

References

39. H. Chritensen, J. Dinesen, H. H. Engell, and K. K. Hansen, *SAE,* **SP-1414** (1999) 225.

40. J. Dinesen, S. S. Nissen, and H. Chritensen, *SAE,* **SP-1313** (1998) 197.

41. H. Chritensen, J. Dinesen, H. H. Engell, L. C. Larsen, K. K. Hansen, and E. M. Skou, *SAE,* **SP-1497** (2000) 141.

42. S. Wodiunig, F. Bokeloh, J. Nicole, and C. Comninellis, *Elecrochem. Solid-State Lett.,* **2** (1999) 281.

43. S. Balamenou, D. Tsiplakides, A. Katsaounis, S. Thiemann-Handler, B. Cramer, G. Fóti, C. Comninellis, and C. G. Vayenas, *Applied Catalysis B: Environmental,* **52** (2004) 181.

44. T. Rebitzki, B. Delmon, and J. H. Block, *AIShE J,* **41** (1995) 1543.

45. F. M. Faus, B. Zhou, H. Matralis, and B. Delmon, *J. Catal.,* **132** (1991) 200.

46. C. G. Vayenas, *Solid State Ionics,* **168** (2004) 321.

47. G. Fóti, S. Wodiunig, and C. Comninellis, *Current topics in Electrochemistry,* **7** (2000) 1.

48. I. S. Metcalfe, *J. Catal.,* **199** (2001) 247.

49. S. Trasatti, *Electrochim. Acta,* **36** (1991) 1659.

50. C. G. Vayenas, S. Brosda, and C. Pliangos, *J. Catal.,* **203** (2001) 329.

51. S. Brosda and C. G. Vayenas, *J. Catal.,* **208** (2002) 38.

52. C. G. Vayenas, S. Bebelis, and S. Ladas, *Nature,* **323** (1990) 625.

53. C. G. Vayenas and D. Tsiplakides, *Surf. Sci.,* **467** (2000) 23.

54. C. G. Vayenas, *J. Electroanal. Chem.,* **486** (2000) 85.

55. I. Riess and C. G. Vayenas, *Solid State Ionics,* **159** (2003) 313.

56. J. Nicole, D. Tsiplakides, S. Wodiunig, and C. Comninellis, *J. Electrochem. Soc,* **144** (1997) L312.

57. J. Nicole, *Etude de la Promotion Electrochimique de l'Oxydation Catalytique de l'Ethylène sur des Oxydes Métalliques.* Thesis No 1933, EPFL, Lausanne, (1999).

58. W. Zipprich, H.-D. Wiemhöfer, U. Vohrer, and W. Göpel, *Ber. Bunsenges. Phys. Chem.,* **99** (1998) 1406.

59. F. J. Williams and C. M. Aldao, *Surf. Sci.,* **425** (1999) L387.

60. R. Parsons, *J. Electroanal. Chem.,* **486** (2000) 91.

61. P. M. Leiva and C. G. Sánchez, *J. Solid State Electrochem,* **7** (2003) 588.

62.   J. C. Rivière, *Solid State Surface Science* Marcel Dekker, New York (1969).

63.   K. Besocke and S. Berger, *Rev. Sci. Instrum.,* **47** (1976) 840.

64.   N. A. Surplice and R. J. D'Arcy, *J. Phys. E.,* **3** (1970) 477.

65.   S. Wodiunig, C. Comninellis, and C. Mousty, in *Energy and Electrochemical Processing for a Cleaner Environment.*, The Electrochemical Society Proceedings Series: PV 97 28 E. J. Rudd and C. W. Walton, eds., Pennington, (1997), p. 147.

66.   J. Nicole and C. Comninellis, *J. Appl. Electrochem.,* **28** (1998) 223.

67.   G. Fóti, O. Lavanchy, and C. Comninellis, *J. Appl. Electrochem.,* **30** (2000) 1223.

68.   C. Pliangos, C. Raptis, T. Badas, and C. G. Vayenas, *Solid State Ionics,* **136-137** (2000) 767.

69.   C. Pliangos, C. Raptis, T. Badas, and C. G. Vayenas, *Ionics,* **6** (2000) 119.

70.   C. Pliangos, I. V. Yentekakis, X. E. Verykios, and C. G. Vayenas, *J. Catal.,* **154** (1995) 124.

71.   C. Pliangos, I. V. Yentekakis, V. G. Papadakis, C. G. Vayenas, and X. E. Verykios, *Applied Catalysis B: Environmental,* **14** (1997) 161.

72.   T. Ioannides and X. E. Verykios, *J. Catal.,* **161** (1996) 560

73.   I. Bolzonella, *Electrochemical promotion of rhodium catalyst. Application to nitrogen monoxide reduction.* Thesis No 2743, EPFL, Lausanne, (2003).

74.   L. L. Hegedus, R. Aris, A. T. Bell, M. Boudart, N. Y. Chen, B. C. Gates, W. O. Haag, G. A. Somorjari, and J. Wei, *Catalyst design: Progress and Perspectives.* John & sons, New York (1987).

75.   A. Wieckowski, E. R. Savinova, and C. G. Vayenas, *Catalysis and Electrocatalysis at Nanoparticles* Marcel Dekker, Inc., New York (2003).

76.   G. L. Haller and D. E. Resasco, *Advances in Catalysis,* **36** (1989) 173.

77.   S. J. Tauster, S. C. Fung, and R. L. Garten, *JACS,* **100** (1978) 170.

78.   E. C. Akubuiro and X. E. Verykios, *J. Catal.,* **113** (1988) 106.

79.   M. Haruta, A. Ueda, S. Tsubota, and R. M. T. Sanchez, *Catal. Today,* **29** (1996) 443.

80.   Y. Iizuka, H. Fujiki, N. Yamauchi, T. Chijiiwa, S. Arai, S. Tsubota, and M. Haruta, *Catal. Today,* **36** (1997) 115.

81.   G. M. Schwab, in *Advances in Catalysis*, Vol. 27 D. D. Eley, H. Pines, and P. B. Weisz, eds., Academic Press, New York, (1978).

82. F. Solymosi, I. Tombacz, and M. Kocsis, *J. Catal.,* **75** (1982) 78.

83. H. K. Henisch, in *Electrode processes in solid state ionics* M. Kleitz and J. Dupay, eds., Reidel, Dordrecht, Holland, (1976).

84. M. S. Tyagi, in *Metal-semiconductor schottky barrier junctions and their applications* B. L. Sharma, ed.), Plenum, New York, (1984).

85. X. E. Verykios, in *Catalysis and Electrocatalysis at nanoparticle surface* A. Wieckowski, E. R. Savinova, and C. G. Vayenas, eds., Marcel Dekker, Inc., New York - Basel, (2003), p. 745

86. N. Yamamoto, S. Tonomura, and H. Tsubomura, *J. Electrochem. Soc,* **129** (1982) 444.

87. S. J. Tauster, S. C. Fung, R. T. K. Baker, and J. A. Horsley, *Science,* **211** (1981) 1121.

88. P. Meriaudeau, O. H. Ellestad, M. Dufax, and C.Naccache, *J. Catal.,* **75** (1982) 243.

89. P. Meriaudeau, O. H. Ellestad, M. Dufaux, and C. Naccache, *J. Catal.,* **75** (1982) 243.

90. R. Burch, in *Hydrogen Effects in Catalysis* Z. Paal and P. G. Menon, eds., Marcel Dekker, New York, (1988), p. 347.

91. A. D. Logan, A. K. Datye, and J. E. Houston, *Surface Sci.,* **245** (1991) 280.

92. A. K. Datye, D. Kalakkad, M. H. Yao, and D. J. Smith, *J. Catal.,* **155** (1995) 148.

93. V. Andera, *Applied Surf. Sci.,* **51** (1991) 1.

94. J. P. Belzunegui, J. M. Rojo, and J. Sanz, *J. Phys. Chem.,* **95** (1991) 3464.

95. P. Meriaudeau, J. F. Dutel, M. Dufax, and C. Naccache, *Stud. Surf. Sci. Catal,* **11** (1982) 95.

96. J. Nicole, D. Tsiplakides, C. Pliangos, X. E. Verykios, C. Comninellis, and C. G. Vayenas, *J. Catal.,* **204** (2001) 23.

97. B. Delmon and G. F. Froment, *Catal. Rev.-Sci. Eng.,* **38** (1996) 69.

98. M. Marwood and C. G. Vayenas, *J. Catal.,* **168** (1997) 538.

99. V. N. Chebotin and M. V. Perfilev, *Electrochemistry of solid electrolytes* Khimiia Publ. House, Moscou (1978).

100. C. Deportes, M. Duclot, P. Fabry, J. Fouletier, A. Hammou, M. Kleitz, E. Siebert, and J.-L. Souquet, *Electrochimie des solides* Press Universitair de Grenoble, Grenoble (1994).

101. H. Rickert, in *Electrochemistry of Solids*, Springer-Verlag, Berlin, (1982).

102. E. C. Subbarao and H. S. Maiti, *Solid State Ionics,* **11** (1984) 317.

103. P. J. Gellings and H. J. M. Bouwmeester, *Catalysis Today,* **12** (1992) 1.

104. W. Göpel, *Sensor and Actuators B,* **18-19** (1994) 1.

105. A. Mandelis and C. Christofides, *Solid State Gas Sensor Devices* John Wiley & Sons, New York (1993).

106. P. J. Gellings and H. J. M. Bouwmeester, *The CRC handbook of solid state electrochemistry* CRC Press, Boca Raton (1997).

107. W. Vielstich, H. A. Gasteiger, and A. Lamm, *Handbook of Fuel Cells - Fundamentals, Thechnology and Applications* John Wiley & Sons, Ltd (2003).

108. J. H. Park and R. N. Blumenthal, *J. Electrochem. Soc,* **136** (1989) 2867.

109. M. F. Fox and M. T. Dulay, *Chem. Rev.,* **93** (1993) 341.

110. A. L. Linsebigler, G. Lu, and J. T. Yates, *Chem. Rev.,* **95** (1995) 735.

111. C. J. Barbé, F. Arendsen, P. Comte, M. Jirousek, F. Lenzmann, V. Shklover, and M. Grätzel, *J. Am. Ceram. Soc.,* **80** (1997) 3157

112. M. Grätzel, *Nature,* **414** (2001) 338.

113. K. D. Schierbaum, U. K. Kirner, J. F. Geiger, and W. Göpel, *Sensor and Actuators B,* **4** (1991) 87.

114. W. Göpel, U. K. Kirner, H. D. Wiemhöfer, and G. Rocker, *Solid State Ionics,* **28-30** (1988) 1423.

115. U. K. Kirner, K. D. Schierbaum, W. Göpel, B. Leibold, N. Nicoloso, W. Weppner, D. Fischer, and W. F. Chu, *Sensor and Actuators B1,* (1990) 103.

116. *Gmelin's Handbook Part 24* Weinheim (1951).

117. V. P. Popov and V. E. Svaiko-Svaikovski, *Fiz. Tverd. Tiela (Russ. Solid State Phys.),* **21** (1979) 383.

118. D. C. Cronemeyer, *Phys. Rev.,* **87** (1952) 876.

119. J. F. Baumard and E. Tani, *Phys. Stat. Sol.,* **39** (1977) 373.

120. J. L. Carpentier, A. Lebrun, F. Perdu, and P. Tellier, *C. R. Acad. Sci.,* **304 serie II** (1987) 1489.

References

121.   L. Singheiser and W. Auer, *Ber. Bunsen. Gessellschaft Phys. Chem.,* **81** (1977) 1167.

122.   J. Novotny, M. Radecka, M. Rekas, S. Sugihara, E. R. Vance, and W. Weppner, *Ceramics International,* **24** (1997) 571

123.   J. F. Marucco, J. Gautron, and P. Lemasson, *J. Phys. Chem. Solids,* **42** (1981) 363

124.   F. Millot, M.-G. Blanchin, R. Tétot, J. F. Marucco, B. Poumellec, C. Picard, and B. Touzelin, *Prog. Solid St. Chem.,* **17** (1987) 263.

125.   D. Y. Wang and A. S. Nowick, *J. Electrochem. Soc,* **128** (1981) 55.

126.   D. Y. Wang and A. S. Nowick, *J. Electrochem. Soc.,* **126** (1979) 1155.

127.   D. Y. Wang and A. S. Nowick, *J. Electrochem. Soc.,* **126** (1979) 1166

128.   B. C. Nguyen, L. M. Rinco-Rubio, and D. M. Mason, *J. Electrochem. Soc,* **133** (1986) 1860.

129.   M. V. Perfilev, *Solid State Ionics,* **9 & 10** (1983) 765.

130.   J. Mizusaki, K. Amano, S. Yamauchi, and K. Fueki, *Solid State Ionics,* **22** (1987) 313.

131.   J. Mizusaki, K. Amano, S. Yamauchi, and K. Fueki, *Solid State Ionics,* **22** (1987) 323.

132.   N. L. Robertson and J. N. Michaels, *J. Electrochem. Soc,* **137** (1990) 129.

133.   B. A. v. Hassel, B. A. Boukamp, and A. J. Burggraaf, *Solid State Ionics,* **48** (1991) 155.

134.   O. J. Velle, T. Norby, and P. Kofstad, *Solid State Ionics,* **47** (1991) 161

135.   C. Athanasiou, G. Karagiannakis, S. Zisekas, and M. Stoukides, *Solid State Ionics,* **136-137** (2000) 873.

136.   T. H. Etsell and S. N. Flengas, *J. Electrochem. Soc,* **11** (1971) 1890.

137.   T. M. Gur, I. D. Raistrick, and R. A. Huggins, *J. Electrochem. Soc,* **127** (1980) 2620.

138.   J. R. Anderson, *Structure of metallic catalysts* Academic Press, New York (1975).

139.   J. E. Bauerle, *J. Phys. Chem. Solids,* **30** (1969) 2657.

140.   S. Pizzini, in *Fast ion transport in solids* W. v. Gool, ed.), North-Holland, Amsterdam, (1973), p. 461.

141.   B. A. v. Hassel, B. A. Boukamp, and A. J. Burggraaf, *Solid State Ionics,* **48** (1991) 139.

CHAPTER 3 **Experimental**

In this chapter the experimental setup and protocols used for preparing the-catalyst electrodes and the electrochemical cells used in this work are presented. The most important experimental techniques are listed but details concerning each technique will be provided at the beginning of each chapter reporting experimental results.

3.1 Electrochemical cells

3.1.1 Single-pellet cells

Two single-pellet cell configurations have been used in the present work. One of the configurations is the cell presented in Figure 3.1, where the rhodium catalyst used as the working electrode was deposited on one side of a pellet of yttria-stabilized zirconia (YSZ 8 mol%, Technox 802 from Dynamic Ceramic), while the Au counterelectrode and reference electrodes were deposited on the other side (Fig. 3.1) [1].
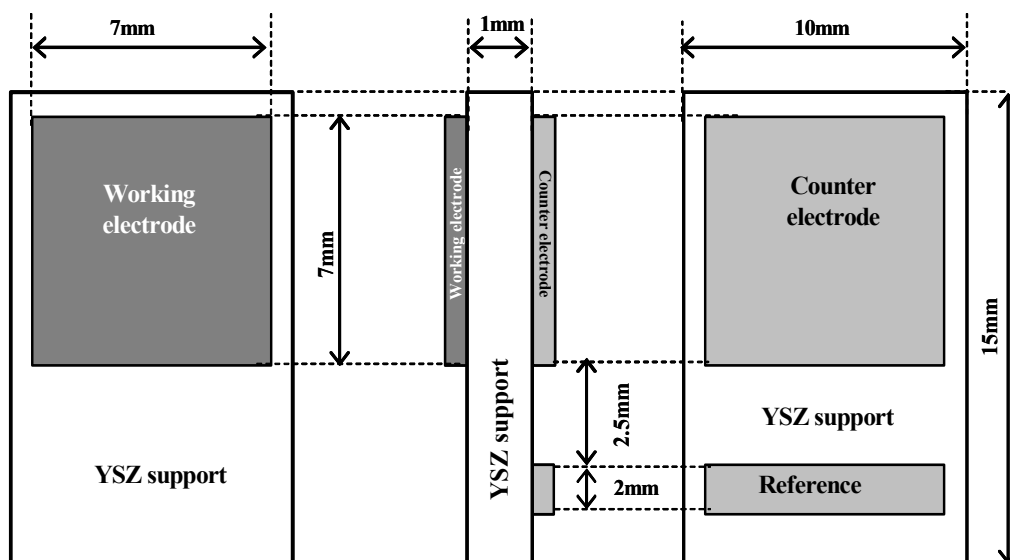
FIGURE 3.1. Schematic representation of a single-pellet cell for steady-state polarization measurements and electrochemical promotion studies.
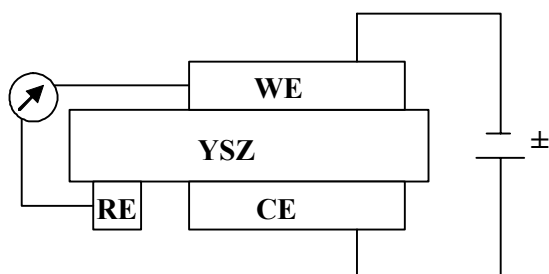
FIGURE 3.2. Polarization mode of the electrochemical cell shown in Figure 3.1.

Such three-electrode cells were used for electrochemical measurements, for example steady-state polarization experiments. The same type of cell was used for catalytic measurements and experiments under conditions of electrochemical promotion.

The cell configuration used for impedance measurements is shown in Fig. 3.3, where two Rh electrodes ($S = 0.18$ cm^2) were deposited on one side, a counterelectrode was deposited on the other side of the YSZ pellet. A schematic representation of the polarization mode is shown in Fig.

3.4. Alternative current was applied between two Rh electrodes, one of them serving as the working electrode and the other as the auxiliary electrode. Direct polarization of the working electrode was accomplished by using a gold counterelectrode.
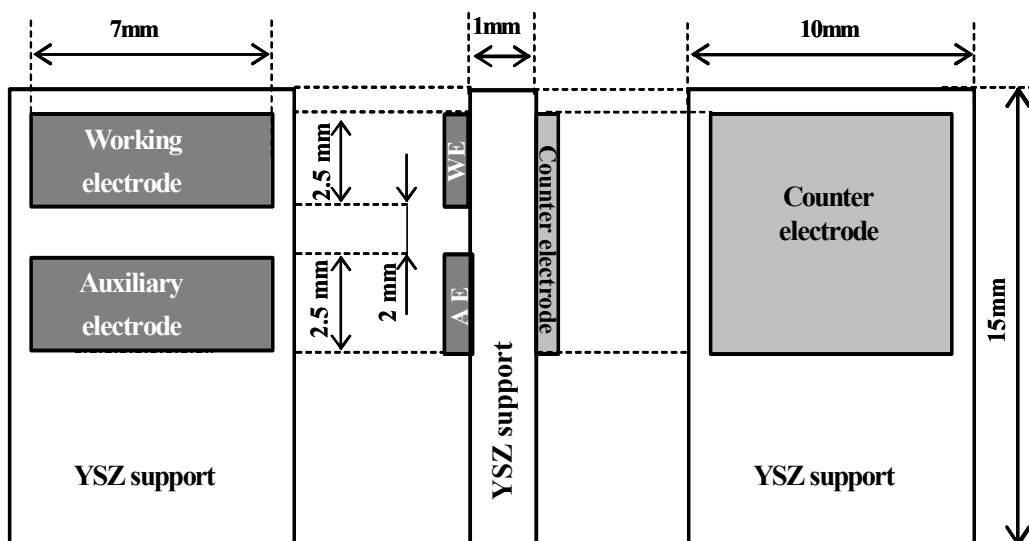
FIGURE 3.3. Schematic representation of a single-pellet cell for impedance spectroscopy studies.
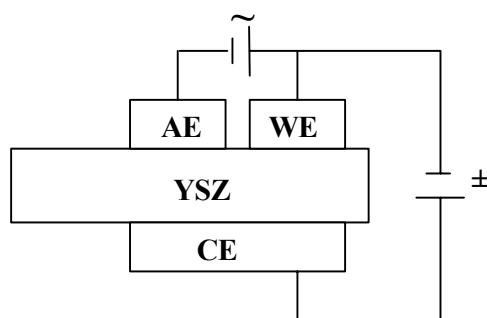
FIGURE 3.4. Polarization mode of the electrochemical cell shown in Figure 3.3.

3.1.2 Ring-shaped cells

Ring-shaped electrochemical cells were used in the partial methane oxidation experiments, and are shown schematically in Fig. 3.5 [2, 3]. The catalyst film was deposited on the inner surface using the procedure described in section 3.2.3, while the gold reference electrode was deposited on the outer surface of a ring (OD 20 mm, ID 17 mm, height 10 mm) of yttria-stabilized zirconia (YSZ 8 mol%, Technox 802 from Dynamic Ceramic), which provided a geometrical catalyst surface area of about 5 cm^2.
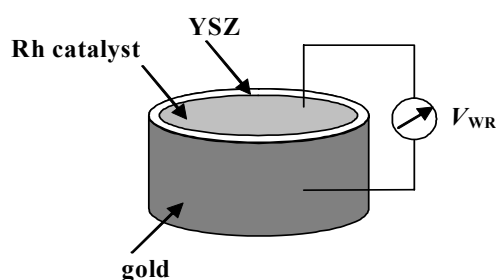
FIGURE 3.5. Schematic representation of the ring-type electrochemical cell for partial methane oxidation studies.

3.2 Electrode preparation

The following catalyst electrodes were investigated: (a) a sputtered Rh catalyst electrode on YSZ and TiO$_2$/YSZ supports, (b) a Rh catalyst electrode prepared with commercial paste.

3.2.1 YSZ pretreatment

Prior to Rh and TiO$_2$ deposition, the YSZ plates were pretreated by sandblasting in order to increase the roughness of the surface and, hence, the adhesion of Rh and TiO$_2$ to YSZ. The increase in support roughness was accompanied by changes in surface morphology, as will be shown below by SEM. From the point of view of electrochemistry, any increase in roughness will

influence the surface of contact between catalyst and support, and with it the length of the three-phase boundary.

The surface roughness was estimated using a UBM profilometer (*Hommel Tester T800, Hommelwerke GmbH*, Schwenningen, Germany).

Figure 3.6 shows the surface roughness of YSZ before sandblasting and after 20 seconds of this treatment (the pressure of sandblasting was 2 kg/m^2).
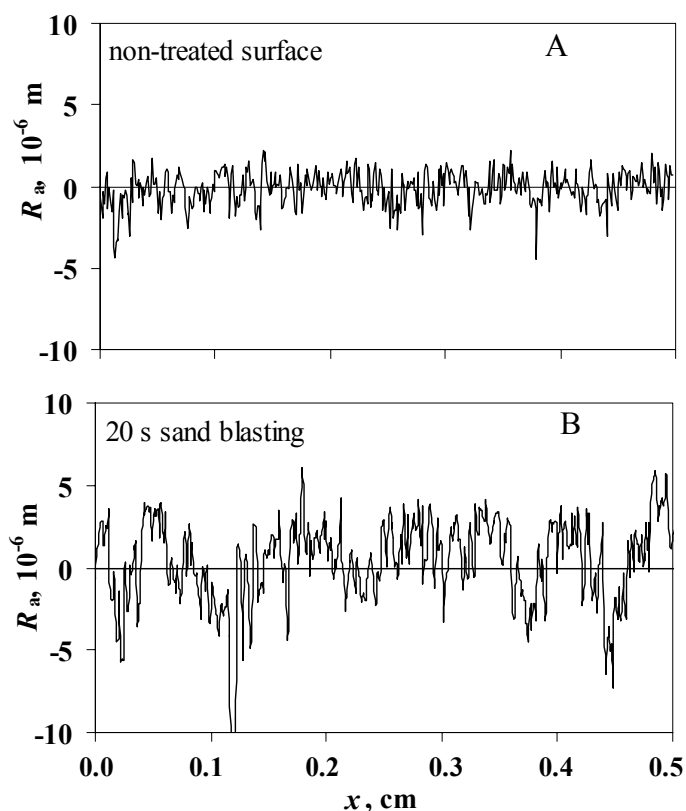
FIGURE 3.6. Profile of YSZ surface. A) untreated surface, B) after 20 s of sandblasting at 2 kg/m^2.

The surface roughness parameter is given by R_a, which is the arithmetic average of the absolute values of all points of the profile:

$$R_a = \frac{1}{n} \sum_{1=1}^{n} |y_i| \tag{3.1}$$

The roughness parameters were compared between samples at which the roughness was measured over equal lengths (3 cm) and at the same scan density. It can be seen from Fig. 3.6 that

20 s of sandblasting lead to a twofold increase in surface roughness. The roughness parameters, R_a, are 0.82 μm and 2.1 μm for the untreated and the sandblasted surface, respectively.

After the sandblasting procedure, the support was carefully cleaned in order to avoid the presence of impurities on the support surface that would interfere with film growth. The cleaning procedure was the following:

1. The support was cleaned for 10 min in acetone in an ultrasonic bath (*1200, Branson*);

2. After sonication, the support was rinsed for 10 min with demineralized water.

3. Then the support was immersed into 2-propanol and cleaned for 30 min in the ultrasonic bath.

3.2.2 Preparation of Rh catalyst electrodes by sputtering

The technique of sputtering is often used to deposit thin films. Deposition by sputtering offers many unique characteristics as compared to other thin-film deposition methods. These characteristics include a very simple control of thickness of the deposited film and a good adhesion to the support due to the high energy of sputtered atoms. When a solid is heated to a sufficiently high temperature, it is possible for individual atoms to acquire enough energy to escape from the surface. This effect is known as evaporation. Sputtering is similar to evaporation, though energy is transferred to the solid, not by heating but by bombardment of the solid via collisions. As it is more convenient to accelerate ions, sputtering normally is obtained by ion bombardment [4]. The pressure inside the deposition chamber has to be as low as possible in order to avoid the back-diffusion of sputtered atoms and collisions between the ions and the gas during the acceleration phase. The growth process will influence the morphological characteristics of the thin film. These depend, not only on the parameters of the sputtering process but also on the surface roughness of the support and on the nature of the material deposited.

The sputtering was performed in Prof. F. Lévy's laboratory (*Laboratoire de physique des couches minces, EPFL*) by H. Jotterand; their contribution is gratefully acknowledged.

After cleaning, the support was introduced into the sputtering chamber that was filled with pure argon. Then rhodium (Rh 99.8, Lesker) was deposited onto the substrate (YSZ support) at 50 °C. The sputtering conditions were the following: direct-current (dc) mode with a discharge of 305 V, argon pressure 0.5 Pa. Under these conditions the deposition rate was 0.25 nm/s. The film

thickness was measured by calibration with smooth silicon samples processed simultaneously. The thickness of the sputter-deposited rhodium film was 40 nm.

The Rh/TiO$_2$/YSZ samples were prepared by the same method of deposition but on YSZ supports previously covered with a thin film of TiO$_2$ (see below, section 3.2.4)

The geometric surface area of the rhodium catalyst was 0.5 cm^2.

The surface area and dispersion of the metal in the Rh film catalysts was estimated with the transient galvanostatic catalytic rate response technique [5]. This is based on measuring the time, τ, required for the rate increase to reach 63 % of its final steady-state value in galvanostatic electropromotion experiments. It is well established that τ, which expresses the time required to form a monolayer of O^{2-} on the catalytically active gas-exposed catalyst electrode surface, is given by:

$$\tau \approx \frac{2FN_G}{I} \qquad (3.2)$$

where N_G is the surface area (in mol) of the gas-exposed catalyst electrode, and I is the applied current. From this expression, and taking into account that (see Chapter 8) τ is approximately 1 min for I = 50 μA, one can estimate that N_G = 1.6 x 10^{-8} mol.

The catalyst dispersion is defined as:

D_C = (number of catalyst surface atoms/total number of catalyst atoms) x 100 $\qquad$ (3.3)

Assuming 10 % porosity for the Rh film, one finds that the 40-nm film having a geometric surface area of 0.5 cm^2 contains 2 x 10^{-7} mol Rh. These numbers yield an estimate for the metal's dispersion of 8 % ($\pm$3 %).

The counterelectrode and the reference electrode consisted of porous gold deposited onto the YSZ by thermal decomposition of a gold paste (Gwent C70219R4); the calcining temperature was 550 °C. It should be noted that the Au reference electrode is a pseudoreference electrode, since it is exposed to a gas of varying composition. It has been shown [5] that Au/YSZ is a satisfactory pseudoreference electrode in oxygen atmosphere.

3.2.3 Preparation of Rh catalyst electrodes using commercial paste

Two types of catalyst electrode were prepared: Rh/YSZ and Rh/TiO$_2$/YSZ.

Rh/YSZ: prepared by depositing 30 µL/cm^2 of Rh paste (Engelhard Rh8826; 10 % Rh) diluted three times (by mass) with THF on the YSZ support. Three consecutive layers were deposited. Each layer was fired at 400 °C/10 min; the final heat treatment occurred at 550 °C/1 hour (estimated loading: 0.54 mg Rh /cm^2).

Rh/TiO$_2$/YSZ: This differed from the Rh/YSZ catalyst, only in that the YSZ support was covered with a thin film of TiO$_2$ (see section 3.2.4)

A gold film serving as the counterelectrode was deposited onto the outer surface of the YSZ ring (Fig. 3.5) using gold paste (Gwent C70219R4); the deposition temperature was 550 °C.

3.2.4 Preparation of the TiO$_2$ layer

A micropipette was used to deposit 2.5 µL of a slurry of 20 % TiO$_2$ (1 g TiO$_2$ Degussa P25 in 20 mL EtOH : H$_2$O = 1 : 1) on YSZ of 0.6 cm^2 surface area, which was then evaporated for 10 min at 60 °C and heat-treated for 30 min at 450 °C in air. The loading of the TiO$_2$ layer was 1 mg/cm^2. The apparent density of the TiO$_2$ was 2 g/cm^3, the estimated layer thickness was about 4 μm. For preparation of TiO$_2$ with a thickness 20 µm and 40 µm the ammount of a slurry was deposited 5 and 10 times higher than for 4 µm, subsecuently. Following by the same procedure of evaporation and heat treatment.

For preparation of the ring-type cells (Fig. 3.5), the same slurry of 20 % TiO$_2$ was applied onto the inner surface of the YSZ ring. Several layers were applied until reaching the desired loading (1.7 mg TiO$_2$/cm^2).

The thicknesses were estimated with a *KLA-Tencor Profile,* Model P15 profilometer.

3.3 Catalyst characterization

3.4. Scanning electron microscopy (SEM)

The measurements were carried out with a scanning electron microscope (*JSM-6300F, JEOL*).

Catalyst characterization

The thin (40 nm) Rh films sputtered on YSZ and TiO$_2$/YSZ were analyzed twice, first as prepared and again after 200 hours spent working under reaction conditions.

3.5. Atomic force microscopy

Atomic force microscopic (AFM) studies were carried out in air under ambient conditions (25 °C) using an Atomic Force Microscope (Topometrix Model Explorer). Topographic (3D, height) images were recorded in the tapping mode using an etched silicon probe. The scan area was 20 μm × 20 μm, the image contained 300×300 data points.

For the acquisition of topographical information, a probe tip traverses the surface and senses the force of interaction between itself and the investigated surface. The measurements were performed with the naked YSZ support, with a YSZ surface covered by a thin layer of TiO$_2$ (4 μm), and with the Rh/YSZ and Rh/TiO$_2$/YSZ samples having a Rh film thickness of 40 nm.

3.6. X-ray photoelectron spectroscopy (XPS)

The measurements were carried out with an XPS system (*PHI 5500 ESCA, Perkin Elmer*) using the Kα radiation of Mg. The energy was varied between 0 eV and 1100 eV.

The 40-nm Rh films sputtered on YSZ and TiO$_2$/YSZ were investigated twice, first after reduction (H$_2$/400 °C/1 h) and again after oxidation (O$_2$/400 °C/1 h).

Deconvolution of the XPS spectra and element quantification were performed using the *CasaXPS program* (*Version 2.1.34*).

3.7. Electrochemical measurements

The following electrochemical methods have been used in the present work: steady-state polarization measurements and impedance spectroscopy.

Steady-state polarization measurements have been performed with a computer-controlled *Autolab PGstat30* in a single-pellet cell (Fig. 3.1, polarization mode as shown in Fig. 3.2) using 40-nm Rh working electrodes deposited on YSZ and on TiO$_2$/YSZ. The temperature was varied from 450 °C to 600 °C; the oxygen partial pressure from 0.5 kPa to 20 kPa. The gas flow rate was kept constant at 200 mL/min.

Current-potential curves in the low catalyst potential window between -0.025 V and 0.025V were recorded at stationary currents.

Impedance measurements were performed with an *Autolab PGstat30* using Frequency Response Analyser software (version 4.9). Measurements were made at the equilibrium potential and under polarization (0 to 0.2 V), always sweeping from high to low frequencies over the range from 50 kHz to 0.1 Hz. The three-electrode single-pellet cell configuration was used for the impedance measurements (Fig. 3.3). Impedance measurements at Rh electrodes at the equilibrium potential were performed between two Rh electrodes having equal geometric surface areas ($S =$ 0.18 cm^2). In this case the total measured impedance is given by:

$$Z_t = 2Z_{Rh} + R_{el} \qquad (3.4)$$

where Z_t is the total impedance of the electrochemical cell;

Z_{Rh} is the impedance of one Rh electrode; and

R_{el} is the electrolyte resistance.

In this way one can obtain very precise values of impedance of the Rh electrode alone, and investigate the electrode process only including the reactions occurring at the Rh electrode.

The temperature dependence was investigated over the range of T from 450 to 600 °C. The impedance measurements were always made at constant oxygen partial pressure ($P_{O_2} = 0.5$ kPa) and proceeding in the direction from lower to higher temperature.

3.7.1 Kinetic measurements

The kinetic measurements were made with the single-pellet cell configuration for ethylene oxidation and with the ring-type cell for the experiments concerning partial CH_4 oxidation. These studies were performed under open-circuit and electrochemical promotion conditions at Rh/YSZ and Rh/TiO$_2$/YSZ catalysts.

The experimental setup used in these studies consisted of a gas flow system (*F/201C* and *E-5514-FA, Bronkhost*) (Fig. 3.7). Reactants and products were continuously monitored using on-line infrared (NDIR) analyzers (*Ultramat 5E-2R* for C_2H_4 and CO_2; *Siemens*). Gases O$_2$ and H$_2$ were analyzed with an off-line gas chromatograph (*GC-8A, Shimadzu,* detector TCD, column packed with molecular sieves 13X).

An atmospheric-pressure single-chamber quartz reactor (30 cm^3) was used. The gas flow rate was typically 200 mL/min STP, the temperature range investigated was 350 to 600 °C. The temperature in the reactor was measured with a K-type (NiCr-Ni) thermocouple placed close to the catalyst surface. Reactants were *Carbagas* certified standards of CH$_4$ (99.95%) and O$_2$ (99.95%) supplied as 20-% mixtures; and C$_2$H$_4$ (99.95%) as a 12.5-% or 1-% mixture in He (99.996%) constituting the balance.

Electrochemical promotion measurements were carried out by applying a constant current between the working and counterelectrode (galvanostatic operation) using a scanning potentiostat (*Model 362, EG&G Princeton Applied Research*). For on-line acquisition of current, potential, and outlet gas concentration data the *LabTech Note Book* system was used.
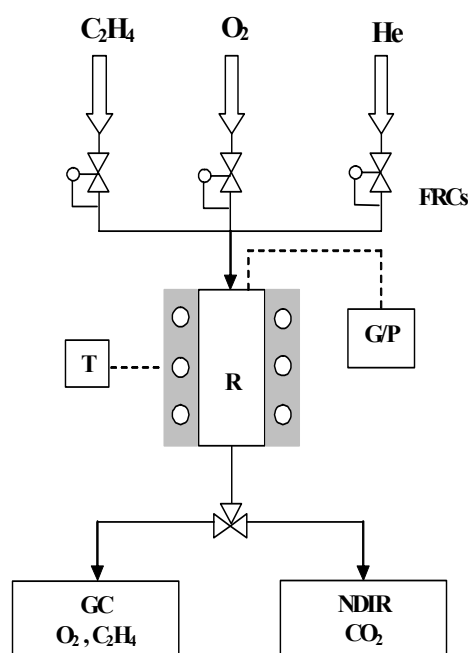
FIGURE 3.7. Schematic representation of the experimental setup. FRCs: flow rate controllers; R: reactor; T: temperature controller; G/P: galvanostat-potentiostat; GC: gas chromatograph; NDIR: non-dispersive infrared analyzer.

3.8 References

1.   E. A. Baranova, A. Thursfield, S. Brosda, G. Fóti, C. Comninellis, and C. G. Vayenas, *J. Catal.,* **152** (2005) E40.

2.   G. Fóti, I. Bolzonella, J. Eaves, and C. Comninellis, *CHIMIA,* **56** (2002) 137.

3.   G. Fóti, S. Wodiunig, and C. Comninellis, *Current topics in Electrochemistry,* **7** (2000) 1.

4.   R. V. Stuart, *Vacuum Technology, thin films, and Sputtering: An introduction* Academic press (1983).

5.   C. G. Vayenas, S. Bebelis, C. Pliangos, S. Brosda, and D. Tsiplakides, *Electrochemical activation of catalysis. Promotion, Electrochemical promotion, and metal-support interaction.* Kluwer Academic/Plenum Publishers, New York (2001).

CHAPTER 4 **Characterization of Rh catalyst electrodes**

In this chapter the characterization of sputtered Rh catalyst electrodes on YSZ (Rh/YSZ) and on thin layers of TiO_2 deposited on YSZ supports (Rh/ TiO_2/YSZ) is presented. Several types of analysis were performed with the aim of investigating the morphological properties (SEM, AFM) and chemical surface composition (XPS) of the Rh catalysts. Both Rh/YSZ and Rh/ TiO_2/YSZ have a nanoparticle structure that remains stable over a period of 200 hours when the catalyst electrodes are exposed to working conditions. The Rh film interfaced with TiO_2 has a higher surface area and catalyst dispersion than Rh/YSZ. It was found that TiO_2 is able to keep Rh in a more highly reduced state, probably due to strong electronic metal-support interactions between Rh and TiO_2.

4.1 Introduction

In the present PhD work, Rh catalysts supported on YSZ and TiO_2/YSZ were investigated. Due to a strong public interest in environmental problems and to more stringent automobile exhaust standards, Rh catalysts have attracted much attention during recent years. At present, Rh

is a major constituent of the three-way catalysts (TWC) used for the catalytic treatment of motor vehicle exhaust gases. Rhodium catalysts have also been examined for a possible use in the reforming reaction of methane with carbon dioxide to carbon monoxide and hydrogen. This reaction is a very attractive route for the production of energy and chemicals [1-3].

The Rh catalysts offer many advantages, such as a high activity in NO_x reduction, low NH_3 formation, and high resistance against poisoning [4, 5]. The major disadvantages of rhodium catalysts are their high price and their ease of deactivation in excess oxygen. For this reason it is highly desirable to design more efficient catalysts which are promoted and work at lower loadings.

Rhodium is a noble metal; it belongs to group VIII. Relative to other group-VIII metals, rhodium behaves quite differently, because it can more easily form surface oxides, and its oxidation state dramatically influences its catalytic activity [6]. In an overall oxidizing environment, the surface of rhodium-based catalysts is populated primarily by Rh_2O_3 (the most common rhodium oxide), while exposure to an overall reducing gas stream predominantly yields metallic rhodium at the surface [6, 7]. Reversible changes in oxidation state occur in response to a change in stoichiometry of the gaseous environment at temperatures between 200 and 500 °C. In the reduced state, rhodium-based catalysts were found to be much more active catalytically than in the oxidized state.

The Rh/TiO_2 system is one of the systems exhibiting effects of strong metal-support interactions (SMSI), where catalytic and selective properties of the catalyst are significantly altered by its reduction by H_2 at elevated temperatures (T > 350 °C) (Chapter 2, section 2.2). Studies of this system by several surface techniques such as XPS, XAES, and HREM were reported [8, 9].

It is the aim of the present chapter to study the morphological and surface properties of the Rh catalyst films interfaced with YSZ and TiO_2/YSZ supports by SEM, AFM, and XPS techniques. More particularly, it will be attempted to elucidate the changes in morphology between as-prepared and "spent" catalysts as well as the changes in the XPS spectra of Rh/YSZ and Rh/TiO_2 accompanying the transition between two distinct states: 1) after heating in H_2/400 °C/1 h, and 2) after oxidation in O_2/400 °C/1 h. According to literature data, the former state would correspond to metallic rhodium, and in the case of Rh/TiO_2 to SMSI, while the latter state would correspond to Rh oxide lacking SMSI.

4.2 Scanning electron microscopy (SEM)

The morphology and surface properties of the Rh/YSZ and Rh/TiO$_2$/YSZ catalysts have been studied by scanning electron microscopy (SEM).

Prior to catalyst electrode deposition, the morphology of the bare YSZ solid electrolyte was investigated. The SEM analysis is able to provide important information about surface topography, crystal size, and surface roughness. Figure 4.1 A shows SEM photographs of an as-prepared (sandblasted for 20 seconds) YSZ surface prior to Rh film deposition. Each image subsequently recorded for the Rh catalysts was first compared with Fig. 4.1 A in order to differentiate the characteristics of the catalyst itself. It can be seen that the YSZ surface is amorphous and very rough. The estimated surface roughness is about 2 μm, in good accord with the profilometric data reported in the Experimental part (Chapter 3, section 3.2.1).

Figure 4.1 B shows the same surface of the yttria-stabilized zirconia sample, but now covered with a TiO$_2$ layer. The estimated thickness of the TiO$_2$ layer is about 4 μm. One can see that TiO$_2$ covers the YSZ substrate forming a continuous layer. This layer is highly porous and consists of individual nanosize particles and particle agglomerates.

A   B
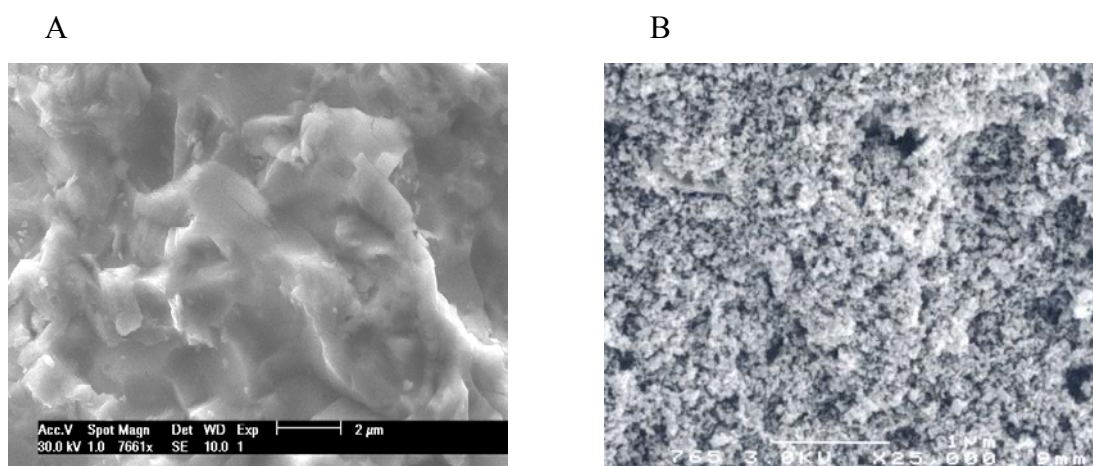
FIGURE 4.1. SEM images of the YSZ surface (A) and of a TiO$_2$ layer deposited on the YSZ surface (B). Thickness of TiO$_2$: 4 μm.

4.2.1 SEM of Rh/YSZ catalysts

Figure 4.2 A shows scanning electron microscopy images of freshly sputtered Rh film catalysts on YSZ. The images of the Rh deposits do not look conspicuously different from those of the bare YSZ, they reflect the topography of YSZ. It is interesting to note that the layer formed is quite porous, and at higher magnification (Fig. 4.2 B) individual crystals and holes with a size of 20 to 200 nm can be distinguished on the Rh surface. The size of holes exceeds that of the crystals, and the YSZ support can be discerned through these holes. This demonstrates the high dispersion of the Rh layer, and at the same time its continuity was confirmed by electrochemical characterization of the Rh/YSZ system (Chapters 5 and 6).

The same sample of Rh/YSZ was analysed by SEM after its exposure to working conditions (T > 300 °C, $C_2H_4 + O_2$ gas mixture, polarization; for details see Chapter 8) over a period of 200 hours. The corresponding images are shown in Figs. 4.2 C, D. Figure 4.2 C shows a photograph similar to Fig. 4.2 A taken at lower magnification. After 200 hours of work the layer of Rh is still present on the surface, but large holes and cracks have appeared. The image recorded at higher magnification gives information about the morphology of the Rh film itself. It can be seen that it changes dramatically under working conditions: it becomes amorphous, and the size of the holes decreases. This may be related to effects of sintering occurring at high temperature, and in part to the effects of electrochemical polarization.

A

B

C

D
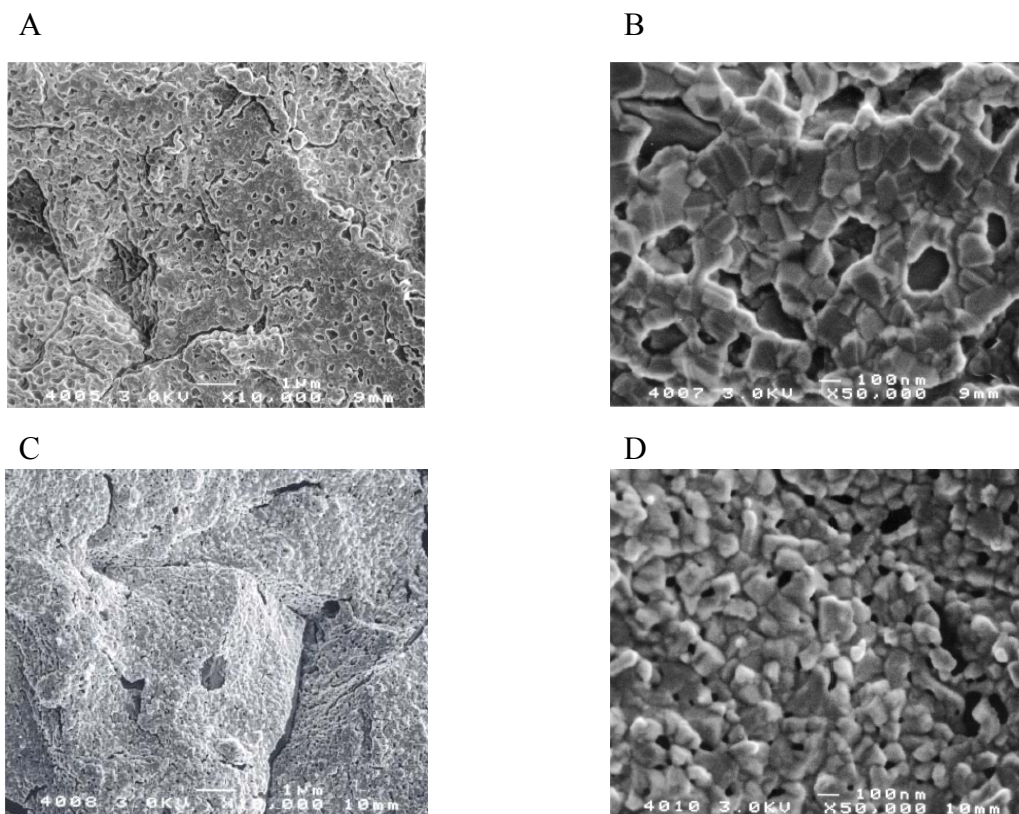
FIGURE 4.2. SEM images of Rh/YSZ catalyst freshly deposited (A, B) and spent (C, D) under reactive conditions during a period of 200 hours (T > 300 °C, C_2H_4 + O_2 gas mixtures, polarization).

4.2.2 SEM of Rh/TiO$_2$/YSZ catalysts

The SEM images of freshly prepared Rh(40 nm)/TiO$_2$/YSZ catalysts are shown in Figure 4.3 A, B at low and high magnification, respectively. It is seen first of all that the Rh film structure is completely different from that of Rh deposited on YSZ. The Rh film again replicates the morphology of the substrate, which now is titania. At low magnification, the image is similar to that recorded at the bare support (Fig. 4.1 B). The porous nanostructure of the TiO$_2$ support remains unchanged, since the Rh film is thin. At high magnification nanoparticle-size agglomerates and holes are readily distinguished on the catalyst surface. The SEM images recorded at the Rh/TiO$_2$/YSZ catalyst after its exposure to working conditions (see Chapter 8) during a period of 200 hours

are shown in Figs. 4.3 C, D. Here the Rh catalysts exhibit a morphology very similar to that of a freshly deposited catalyst (Figs. 4.3 A, B).

The structure has become more compact, but in general it was scarcely altered after catalyst utilization under working conditions. The SEM images of as-prepared and "spent" samples generally indicate that the adhesion of Rh to the support is quite good, and that the layer remains continuous even if some morphological modifications occur during utilization.

A

B

C

D
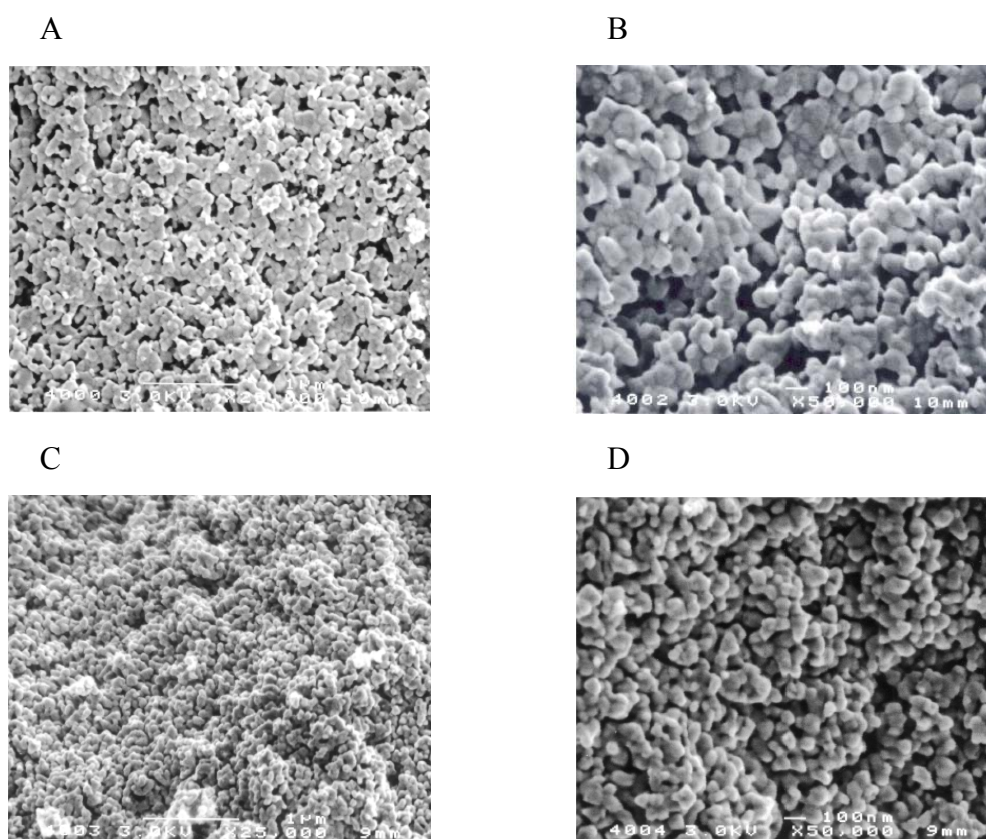
FIGURE 4.3. SEM images of Rh/TiO$_2$/YSZ catalyst freshly deposited (A, B) and spent (C, D) under reactive conditions during a period of 200 hours (T > 300 °C, C$_2$H$_4$ + O$_2$ gas mixtures, polarization).

4.3 Atomic Force Microscopy

The surface topography of bare YSZ and of YSZ covered with a thin (4 μm) layer of TiO$_2$ was investigated by Atomic force microscopy. Figures 4.4 A, B show 3D images of the YSZ and TiO$_2$/YSZ surfaces.
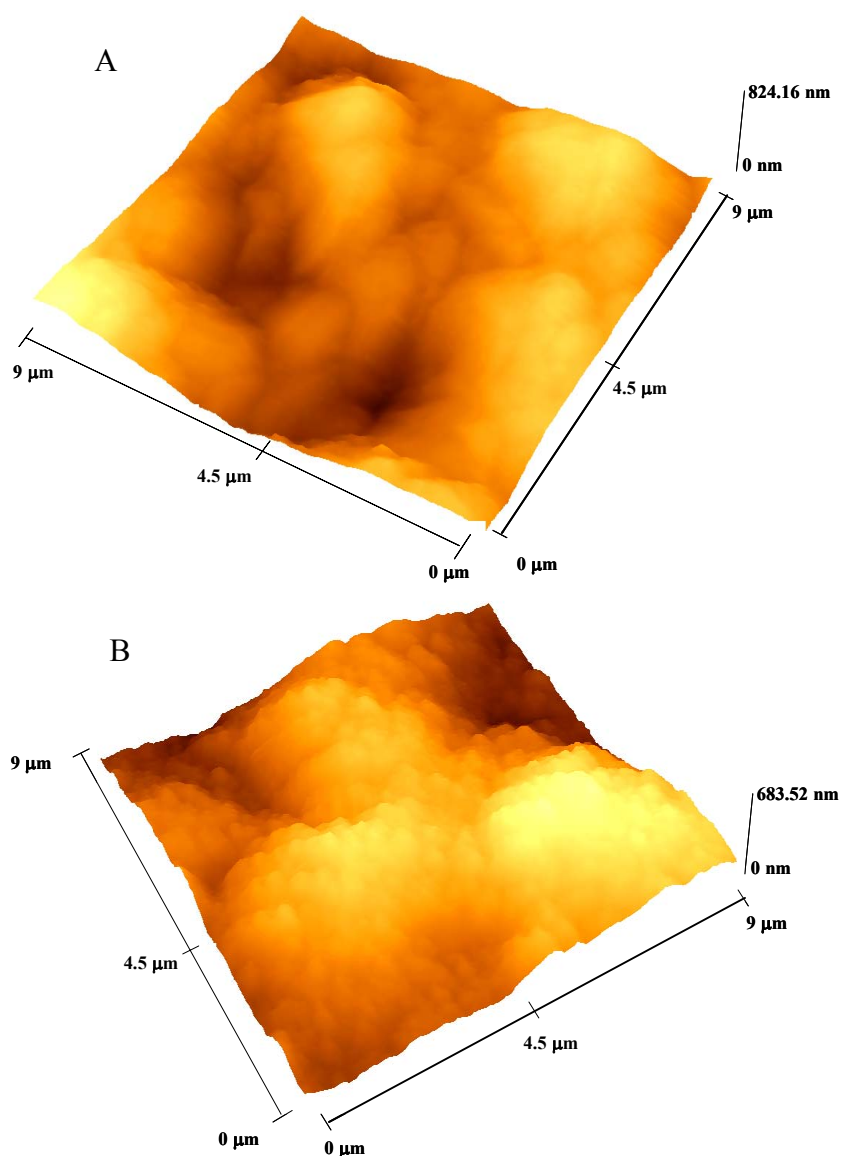
FIGURE 4.4. AFM images of the YSZ (A) and TiO$_2$/YSZ (B) surfaces.

As expected, the surface morphology of the TiO$_2$/YSZ sample is very different from that of the YSZ sample. The surface of YSZ is smooth, while TiO$_2$ exhibits a microstructured topography. The relief of YSZ is clearly seen beneath the titania layer, since TiO$_2$ layer thickness is of the same order of magnitude as YSZ roughness. These results are in a good agreement with the SEM images.

For the aims of the present work, it will be very important to know whether the YSZ substrate is entirely covered by the thin oxide layer or not, since for the behaviour of the catalyst, the

Rh/support interface is of key importance for the kinetics of electrochemical and catalytic processes. Complete coverage of the YSZ surface by TiO_2 is solidly confirmed, both by SEM and by AFM, implying that a good direct contact between Rh and YSZ cannot exist.

Topographic images of the sputtered Rh catalyst electrodes (40 nm film thickness) on YSZ and on TiO_2/YSZ are presented in Figs. 4.5 A, B.
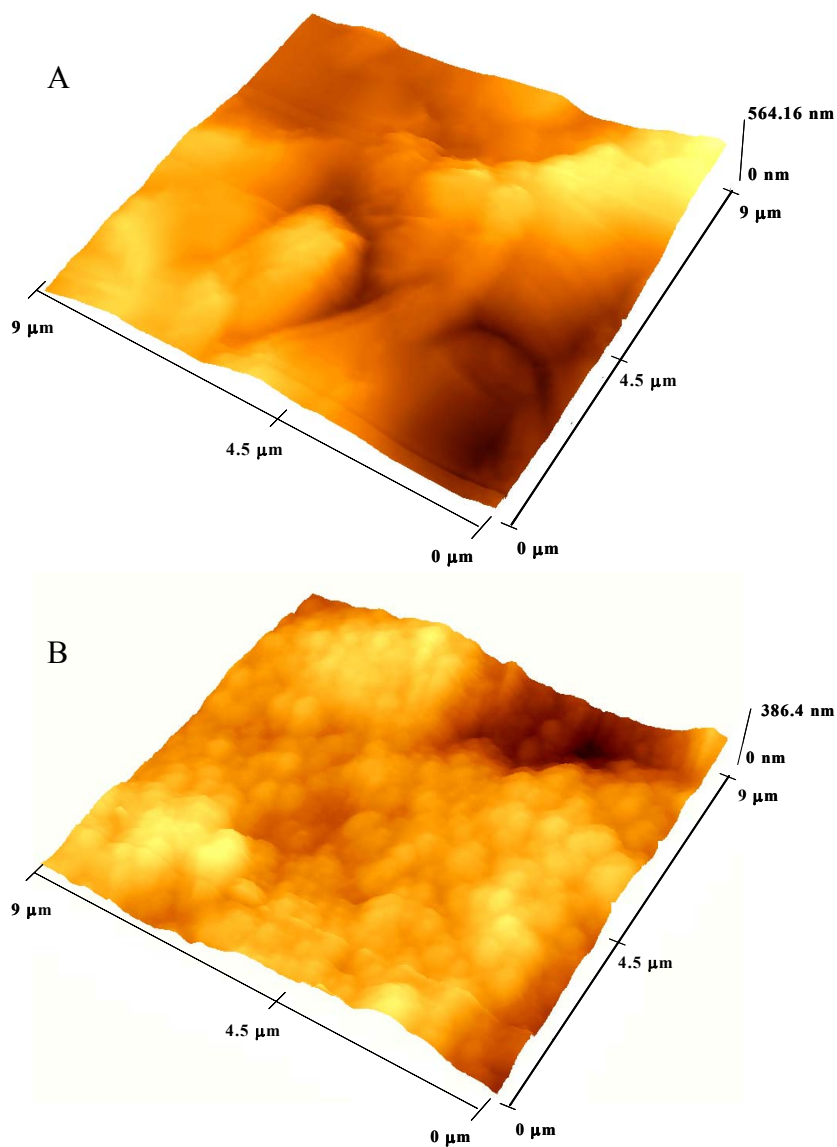
FIGURE 4.5. AFM images of the Rh/YSZ (A) and Rh/TiO$_2$/YSZ (B) surface. Thickness of the Rh film: 40 nm; thickness of TiO$_2$: 4 μm.

4.4 X-ray photoelectron spectroscopy (XPS)

Using X-ray photoelectron spectroscopy one can quantify the atomic composition of surfaces. This analysis was performed on the same catalysts as the SEM and AFM analyses, namely Rh/YSZ and Rh/TiO$_2$/YSZ; the thickness of the Rh film was 40 nm, that of TiO$_2$ was 4 μm. The samples were analysed after treatment in oxygen (20 kPa O$_2$/400 °C/1 hour) and after reduction in hydrogen (H$_2$/400 °C/1 hour). In XPS analysis, particular interest was paid to the oxidation state of rhodium and to the amounts of oxygen present at the surface due either to oxide formation and/or to oxygen adsorption. In the analyses of the Rh/TiO$_2$/YSZ samples, attention was focused on the presence of Ti at the rhodium surface after oxidation/reduction procedures.

Prior to starting quantification of the atomic composition, survey spectra were recorded. An example is presented in Fig. 4.6. for an as-prepared Rh film deposited on YSZ. This is a spectrum recorded with a wide binding energy window. Similar surveys were obtained for the Rh films deposited on TiO$_2$/YSZ.
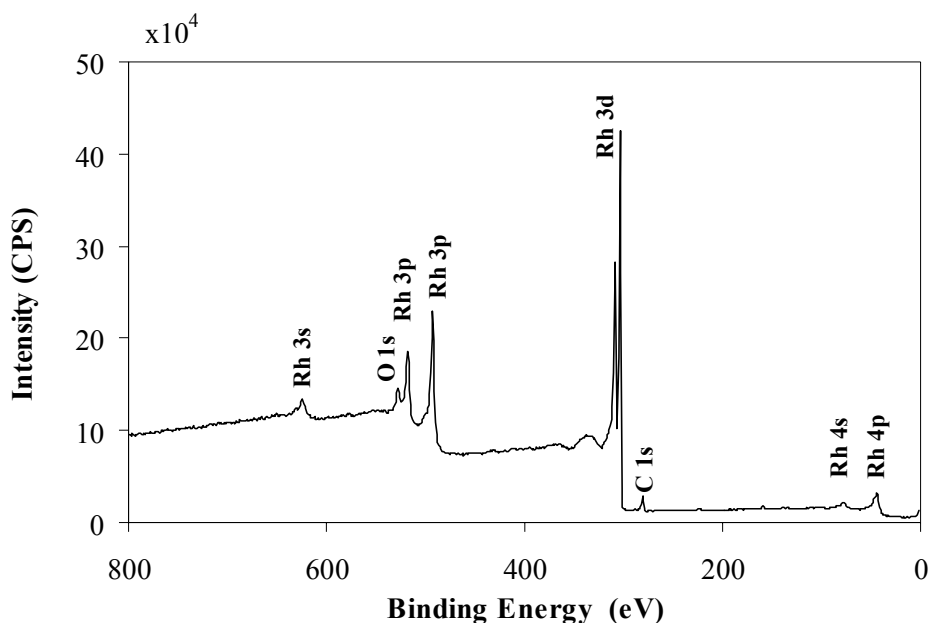
FIGURE 4.6. XPS survey spectrum for Rh film catalyst deposited on YSZ.

The elements expected on the surface of the rhodium catalysts deposited on YSZ supports and exposed to the gas are the following:

- Rhodium;

- Oxygen due to oxide formation or to oxygen adsorption from the air or to backspillover of oxygen from the support;

- Carbon, from CO_2 adsorbed from air;

- Zirconium and yttrium from the YSZ support.

The elements expected on the surface of the rhodium catalysts deposited on TiO_2/YSZ support are the same as those on Rh/YSZ, but they also include Ti from the titania interlayer support.

None of the samples analysed by XPS revealed traces of zirconium or yttrium at the rhodium catalyst surface exposed to the gas. It is worth noting that no trace of the titanium was found in the XPS survey spectrum for as-prepared Rh supported on TiO_2. These results indicate that as-prepared Rh films are uniform and do not have microcracks or holes through which the TiO_2 or YSZ surfaces are visible.

After recording the survey spectra, further analyses were performed within the narrow binding energy ranges of the atoms of interest. For each element one has at least one specific analytical region (in terms of electron binding energies). These binding energies yield important information as to whether and how the chosen atom is bonded to other atoms. The carbon peak was used as an internal standard to correct for any shift in binding energies that could occur, mainly due to surface charging during the XPS measurements.

4.4.1 XPS spectra of Rh $3d_{5/2}$ and $3d_{3/2}$

Figure 4.7 compares the samples in their reduced form. Two major peaks are present in each spectrum in this region of binding energies: the $3d_{5/2}$ peak (between 307 and 308 eV) and the $3d_{3/2}$ peak (between 312 and 315 eV). For each of the narrow spectra, the atomic abundance at the catalyst surface was determined by peak deconvolution. According to the XPS data base [10] the $3d_{5/2}$ electrons of metallic rhodium should be found at 307.2 eV, the $3d_{5/2}$ electrons of rhodium oxide at 308.1 eV. For Rh/TiO_2/YSZ, the position of the maximum of the $3d_{5/2}$ peak was shifted by 0.2 eV toward lower binding energies (307.0 eV), while for Rh/YSZ this peak was shifted by about 1 eV towards higher binding energies. This means that Rh supported on YSZ is in more highly oxidized state than in Rh/TiO_2. Another feature that can be analyzed in the spectra is the width of the peaks. It is well known that for metals, the XPS peaks are narrow, for oxides they are

much broader. It can be seen from Fig. 4.7 that each peak in the spectra can be deconvoluted into two peaks. Narrow, high-intensity peaks are found at lower binding energies, while broader, low-intensity peaks are found at higher binding energies, the former corresponding to Rh metal and the latter to Rh oxide. This indicates that even after reduction, the surface of rhodium is partially covered by oxygen species; their quantity is higher on the Rh/YSZ samples. Deconvolution of the peaks yields the ratio between metallic and oxidized surface species in the Rh film. For Rh/YSZ, this ratio was Rh : Rh_xO_y = 72 : 28 %, for Rh/TiO_2/YSZ it was Rh : Rh_xO_y = 80 : 20 %.
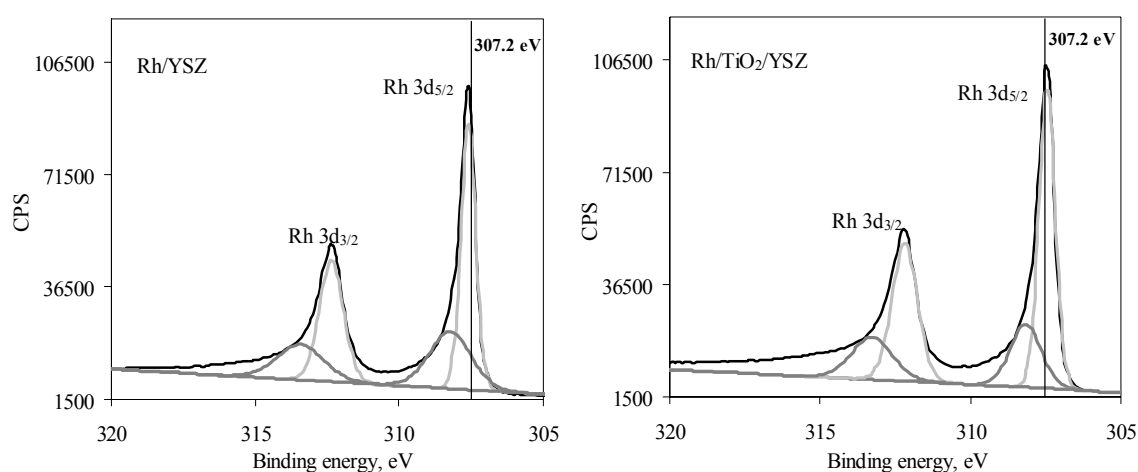
FIGURE 4.7. XPS spectra recorded in the rhodium window at reduced (H$_2$/400 °C/1 h) Rh catalysts supported on YSZ and TiO$_2$/YSZ. Black lines correspond to the experimental spectra, gray lines to the deconvoluted spectra.

Additional information about particle size and dispersion can be drawn from the XPS spectra. Smaller particles with high dispersion would give narrower peaks with a higher intensity. Narrower peaks with slightly higher intensity ($3d_{5/2}$ and $3d_{3/2}$) were obtained for the Rh catalyst supported on TiO$_2$/YSZ. This sample has high dispersion and a smaller particle size than Rh/ YSZ. This is in good agreement with the SEM images, which reveal higher dispersion for Rh/ TiO$_2$ than for Rh on YSZ (Figs. 4.2 and 4.3). In additional to particle size, effects of the support may be relevant to keeping Rh in a reduced state. It is well known that TiO$_2$ is a reducible oxide, i.e., it is readily reduced to TiO$_{2-x}$, a process leading to changes in oxide conductivity and to shifts in Fermi level of the electrons in TiO$_2$. Varying the Fermi level of the electrons in the support will

alter the surface properties of Rh, in accordance with metal-semiconductor boundary-layer theory (Chapter 2, section 2.2.1).

After an oxidizing treatment (20 kPa O_2/400 °C/1 hour), the same samples display a less intense peak for the $3d_{5/2}$ and $3d_{3/2}$ electrons, and these peaks are split (Fig. 4.8). The new part of the peak corresponds to Rh_2O_3. For the Rh/YSZ sample, the peak of $3d_{5/2}$ is shifted to binding energies higher than 307.2 eV (Rh metal). The new parts of the $3d_{5/2}$ and $3d_{3/2}$ peaks are less intense than the peaks of reduced Rh.

For Rh/TiO_2, the peak of the $3d_{5/2}$ electrons was found at binding energies corresponding to Rh metal (307.2 eV). From spectra deconvolution, the ratio Rh : Rh_2O_3 was extracted and found as: Rh : Rh_2O_3 = 45 : 55 % for Rh/YSZ, and Rh : Rh_2O_3 = 55 : 48 % for Rh/TiO_2/YSZ.

The spectra obtained after further reduction of both catalysts were identical with those of the reduced catalysts (Fig. 4.7), demonstrating reversibility of the redox system.
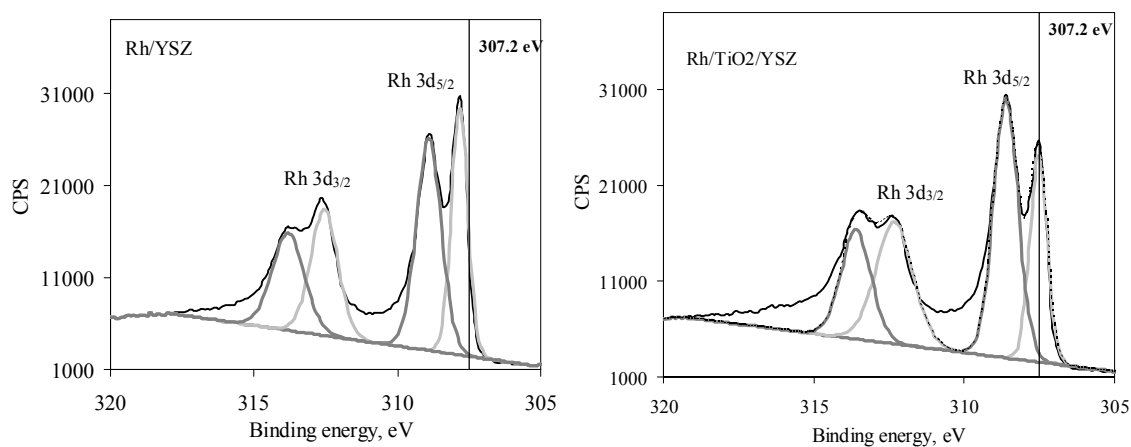
FIGURE 4.8. XPS spectra recorded in the rhodium window at the oxidized (20 kPa O_2/400 °C/1 h) Rh catalysts supported on YSZ and TiO_2/YSZ. Black lines correspond to the experimental spectra, gray lines to the deconvolution data.

4.4.2 XPS spectra of O 1s

Figure 4.9 shows the O1s spectra of Rh/YSZ and Rh/TiO$_2$/YSZ samples in their reduced state (H$_2$/400 °C/1 hour). The binding energy of 530.4 eV corresponds to strongly bonded oxygen (in the form of Rh$_2$O$_3$). Neither of the two samples yields evidence for strongly bonded oxygen. This means that oxygen present on the Rh surface after reduction (Fig. 4.7) is weakly bonded oxygen originating, either from air (during transfer of the samples from the reactor to the XPS vacuum chamber) or from the YSZ or TiO$_2$ support. Strongly bonded oxygen in the form of Rh$_2$O$_3$ oxide is not present on the Rh surface after reduction. Moreover, two kinds of weakly bonded oxygen species are detected on the Rh surface, one at a binding energy of 531 eV and the other at 532.8 eV. The first one may be oxygen from the solid electrolyte, the second one probably is air oxygen bonded to carbon.

FIGURE 4.9. XPS spectra recorded in the oxygen window at reduced (H$_2$/400 °C/1 h) Rh catalysts supported on YSZ and TiO$_2$/YSZ. Black lines correspond to the experimental spectra, gray lines to the deconvoluted spectra.

The amount of oxygen present on the Rh surface changes strongly upon oxidation (1 h/O$_2$/ 400 °C) (Fig. 4.10) and is indicative of Rh$_2$O$_3$ formation. Weakly bonded oxygen remains on the surface but produces a less intense peak than found for the reduced Rh surface.

The XPS analyses were used to quantify the atomic surface compositions of the rhodium-based catalysts supported on YSZ and TiO$_2$/YSZ. The atomic abundance of the two catalysts was

determined twice: first after reduction, then after oxidation. The atomic concentrations of the main elements are presented in Table 4.1. The atomic abundances of yttrium and zirconium on the catalyst surface were negligibly small, therefore, they are not displayed in Table 4.1. After reduction, both catalysts have high rhodium surface concentrations and a low oxygen surface concentration. It is interesting to note that after reduction, a small quantity of Ti was observed on the Rh surface supported on TiO_2. A plausible explanation would be that TiO_x suboxide migrates to the Rh surface simultaneously with O^{2-} from the TiO_2 support. It is well known that Rh/TiO_2 is one of the metal/oxide systems exhibiting the effect of strong metal-support interactions (SMSI) [11 , 12] (Chapter 2, section 2.2.2).
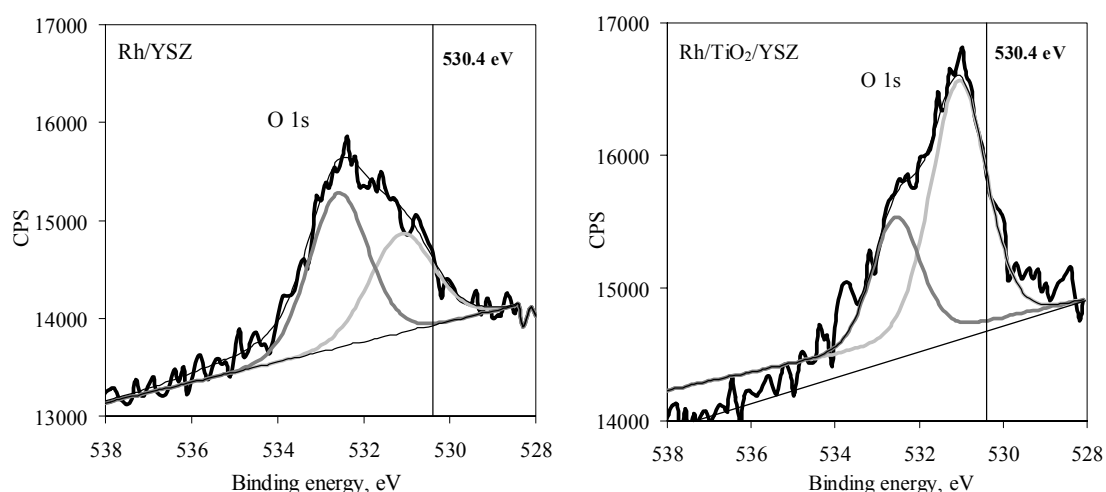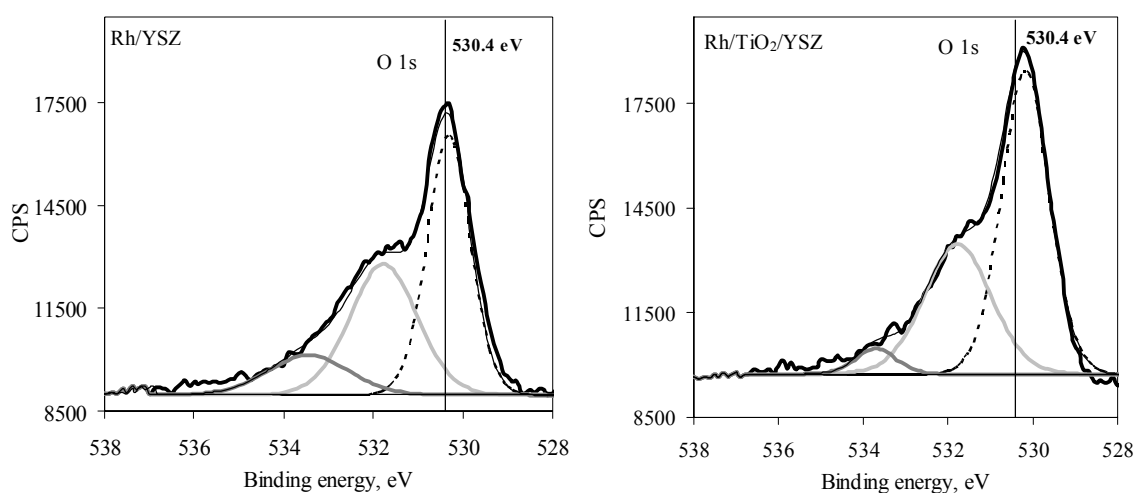

FIGURE 4.10. XPS spectra recorded in the oxygen window at oxidized (20 kPa O_2/400 °C/1 h) Rh catalysts supported on YSZ and TiO_2/YSZ. Black lines correspond to the experimental spectra, gray lines to the deconvoluted spectra.

TABLE 4.1. XPS atomic abundance in % for Rh/YSZ and Rh/TiO_2/YSZ catalysts

XPS peak	Rh/YSZ H_2/400 °C/1 h	Rh/YSZ O_2/400 °C/1 h	Rh/TiO_2/YSZ H_2/400 °C/1 h	Rh/TiO_2/YSZ O_2/400 °C/1 h
O 1s	3.02	19.27	2.61	17.73
Rh 3d	91.75	76.76	93.52	79.44
C 1s	5.23	3.97	2.97	2.83
Ti 2p	0.00	0.00	0.91	0.00

One interpretation of SMSI effects is oxides covering the metal clusters, which is also known as "decoration model", where the catalyst surface is being encapsulated by partially reduced TiO_x from the titanium dioxide support. However, the amount of TiO_2 that is found is not large enough to serve as a basis for explaining the SMSI effect. Obviously, in the system $Rh/TiO_2/YSZ$ the presence of Ti at the Rh surface probably is a result of the electronic influence exerted by the support (TiO_2) on the rhodium catalyst, and the two interpretations of the SMSI effect, electronic or decoration effects, may yield a plausible explanation. Specifically, treatment in hydrogen at elevated temperature leads to TiO_2 reduction, and thus to changes in its work function. The change in TiO_2 work function affects the Rh work function, requiring the transfer of charge in form of either O^{2-} or TiO_x from TiO_2 to Rh.

After oxidation, the amount of rhodium decreases while that of oxygen increases, suggesting Rh oxide formation. No trace of Ti was observed at the oxidized Rh surface.

4.5 Conclusions

It was seen from SEM and AFM analyses that TiO_2 forms a nanostructured layer totally covering the YSZ substrate. The thin sputtered layers of Rh catalyst on YSZ and TiO_2 are continuous and reproduce the support's morphology. For both the Rh/YSZ and the $Rh/TiO_2/YSZ$ system, the catalyst films show a nanoparticle-size grain structure. Rh supported on titania is rather porous, exhibiting a higher dispersion and surface area than Rh on YSZ. After exposure of the systems to working conditions (high temperature, current/potential application, gas mixture) for a period of 200 hour, the catalyst films exhibit different behaviour. Thus, the morphology of the Rh/YSZ catalyst changes dramatically under working conditions: it becomes amorphous, and the size of the holes decreases. While, the $Rh/TiO_2/YSZ$ catalyst film exhibits good stability and adhesion to the substrate surface. The catalyst-film structure is scarcely altered after utilization.

According to XPS analyses, the oxidation state of the Rh surface may change considerably by exposure to oxidizing or reducing gas compositions. These changes were found to be completely reversible for the samples investigated. Both after reduction and after oxidation, Rh supported on TiO_2 was found to be in a more highly reduced state than Rh on YSZ. The $Rh/TiO_2/YSZ$ sample after reducing treatment contains a larger amount of weakly bonded oxygen, which can be attributed to oxygen "backspillover" from the TiO_2. This oxygen may migrate in the form

of TiO$_x$, since after reduction some quantity of Ti was found on the Rh surface but disappeared after oxidation of the catalyst. The driving force for this migration is the difference in the work functions of Rh and TiO$_2$, especially after reducing treatment leading to electronic-type SMSI.

4.6 References

1. V. A. Tsipouriari, A. M. Efstathiou, and X. E. Verykios, *J. Catal.,* **161** (1996) 31.

2. A. M. Efstathiou, A. Kladi, V. A. Tsipouriari, and X. E. Verykios, *J. Catal.,* **158** (1996) 64.

3. Z. L. Zhang, V. A. Tsipouriari, A. M. Efstathiou, and X. E. Verykios, *J. Catal.,* **158** (1996) 51.

4. R. J. H. Voorhoeve, in *Advanced materials in catalysis* J. J. Burton and R. L. Garten, eds., Academic Press, New York, (1977).

5. V. P. Zhdanov and B. Kasemo, *Surface Science Reports,* **29** (1997) 31.

6. S. H. Oh and J. E. Carpenter, *J. Catal.,* **80** (1983) 472.

7. G. L. Kellog, *Surface Sci.,* **171** (1986) 359.

8. V. Andera, *Applied Surf. Sci.,* **51** (1991) 1.

9. S. Bernal, J. J. Calvino, M. A. Cauqui, J. M. Gatica, C. L. Cartes, J. A. P. Omil, and J. M. Pintado, *Catal. Today,* **77** (2003) 385.

10. C. Wagner, W. Riggs, L. Davis, and J. Moulder, *Handbook of x-ray photoelectron spectroscopy* Perkin Elmer Corporation, Physical Electronics Division, Eden Prairie, Minnesota (1979).

11. S. J. Tauster, S. C. Fung, and R. L. Garten, *JACS,* **100** (1978) 170.

12. S. J. Tauster, S. C. Fung, R. T. K. Baker, and J. A. Horsley, *Science,* **211** (1981) 1121.

CHAPTER 5 **Electrochemical characterization of the Rh catalysts:** Polarization measurements

In the present chapter, the first studies ever conducted are reported, of the kinetics of the oxygen couple O_2/O^{2-} at Rh thin-film electrodes interfaced with the pure ionic conductor, YSZ (ZrO_2 + Y_2O_3 solid oxide electrolyte), and with the mixed electronic-ionic conductor, TiO_2 supported on YSZ. These studies were performed over a range of oxygen partial pressures from 0.5 to 20 kPa at temperatures of 450 to 600 °C. The exchange current densities determined at different temperatures and oxygen partial pressures (P_{O_2}) provide important information about the kinetics and mechanism of the O_2/O^{2-} electrode reaction at the interface. At Rh/YSZ, the exchange current densities are less than half those at Rh/TiO$_2$(4 μm)/YSZ, and decrease further with increasing titania thickness. At the Rh electrode supported on YSZ, an activation energy of 126 kJ/mol was estimated for the oxygen evolution and oxygen reduction reaction close to equilibrium. At Rh/TiO$_2$/YSZ, the activation energy decreases with increasing TiO_2 layer thickness, and has values of 132.5, 101.4, and 83.4 kJ/mol for layer thicknesses of 4, 20, and 40 μm. On the basis of the polarization measurements, a mechanism of the oxygen evolution and oxygen reduction was proposed.

5.1 Introduction

Electrochemical cells with solid oxide electrolytes have attracted much attention for use in high temperature fuel cells [1] and sensor technology [2, 3]. The O^{2-} conductors such as Y_2O_3-stabilized ZrO_2 (YSZ) play an increasingly important role in heterogeneous catalysis, both as nanodispersed catalyst carriers and as supports of thick or thin, electrochemically promoted films [4-8]. Interest in these devices has been the motivation for a large number of investigations on the kinetics and mechanism of the reduction and oxidation of oxygen (the O_2/O^{2-} couple), which is a very fundamental electrochemical reaction:

$$1/2 \ O_{2(g)} + 2 \ e^- \leftrightarrows O^{2-} \tag{5.1}$$

or, using Kröger-Vink notation:

$$1/2 \ O_{2(g)} + 2 \ e^- + V_{\ddot{o}} \leftrightarrows O_o{}^x \tag{5.2}$$

where $V_{\ddot{o}}$ and $O_o{}^x$ are a doubly charged oxygen vacancy and an oxygen atom, respectively, occurring at normal oxygen sites in the electrolyte.

Oxygen exchange is a three-phase reaction between oxygen in the gas phase, electrons in the electrode, and oxygen vacancies in the electrolyte. In solid electrolyte cells, the electrodes typically are thin and porous, conductive metal films adhering to the smooth electrolyte surface. These metal electrodes have complex geometric and physical properties complicating the kinetics of the oxygen reaction. To date no consensus has in fact been reached as to details of the reaction mechanism and location of the electrochemical reaction sites in the system O_2/metal/electrolyte (see Chapter 2, section 2.3).

No investigations at Rh electrodes were found in the literature. The present chapter reports the first studies ever conducted of the kinetics of the oxygen couple O_2/O^2 at Rh thin-film electrodes interfaced with the pure ionic conductor, YSZ (ZrO_2 + Y_2O_3 solid oxide electrolyte), and with the mixed electronic-ionic conductor, TiO_2 supported on YSZ. These studies were performed over a range of oxygen partial pressures from 0.5 to 20 kPa at temperatures of 450 to 600 °C. The exchange current densities, i_0, and the influence of different parameters on i_0 were investigated for both systems (Rh/YSZ and Rh/TiO_2/YSZ). On the basis of these data, an attempt was

made to identify the mechanism of the process of Eq. (5.1) at rhodium film electrodes interfaced with YSZ and TiO$_2$/YSZ.

5.2 Results

5.2.1 Basic relations relevant to the work

The simplest possible electrode process is one where species A and B engage in a one-electron transfer or exchange at the interface without being involved in any other chemical step:

$$A + e^- \leftrightarrows B \tag{5.3}$$

The Butler-Volmer equation can be written for a one-step, one-electron process as [9]:

$$i = FSk^0[C_A(0, t)e^{-\alpha f\eta} - C_B(0, t)e^{(1-\alpha)f\eta}] \tag{5.4}$$

where α and $1-\alpha$ are the transfer coefficients; F is the Faraday constant; $f = F/RT$; k^0 is the standard rate constant; C_A and C_B are the concentrations of the reactants and products, respectively; η is the overpotential; and S is the electrode's surface area.

The oxygen exchange reaction (formulated above as an overall reaction Eq. (5.1)) is a multistep reaction. In chemical kinetic studies, one often can simplify the prediction and analysis of behavior by recognizing that a single step of a process is much more sluggish than all the others, and hence controls the rate of the overall reaction. If the process is an electrode process, this rate-determining step (rds) can be a heterogeneous electron transfer reaction. In developing a kinetic equation for a process consisting of several steps, one may consider that an overall process in which A and B are coupled by an overall multielectron process [9]:

$$A + ne^- \leftrightarrows B \tag{5.5}$$

proceeds by a mechanism having the following general character:

$$A + n'e^- \leftrightarrows A' \text{ (net result of steps preceding the rds)}$$

$$A' + e^- \leftrightarrows B' \text{ (rds)} \tag{5.6}$$

$$R' + n''e^- \leftrightarrows B \text{ (net result of steps following the rds)}$$
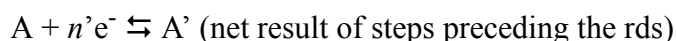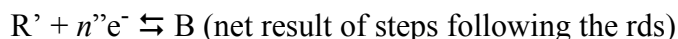
where n, the total number of electrons, may be written as $n' + n'' + 1 = n$. This equation remains valid when either or both of n' or n'' are zero.

The current- potential characteristic for a multistep reaction can then be written as

$$i = nFSk_{rds}^0 \ [C_A(0, t)e^{-\alpha f\eta} - C_R(0, t)e^{(1-\alpha)f\eta}] \tag{5.7}$$

where k_{rds}^0 and α apply to the rds. This relation is obtained from Eq. (5.4) written for the rds, and multiplied by n, because each net conversion of A to B results in the flow, not just of one electron but of n electrons across the interface.

The Butler-Volmer equation is of special interest in two limiting cases. At overpotentials much lower than RT/F (low-field approximation) both exponential terms in the Butler-Volmer equation can be linearized, and Eq. (5.7) becomes:

$$i = i_0\left(\frac{nF\eta}{RT}\right) \tag{5.8}$$

The second limiting case is that found at very high overpotentials ($\eta \gg RT/F$), where the high-field approximation of the Butler-Volmer equation is obtained:

$$\ln i = \ln i_0 + \alpha\left(\frac{nF}{RT}\right)\eta \tag{5.9}$$

where α is the transfer coefficient of either the cathodic or the anodic process, depending on which exponential term does not vanish. According to Eq. (5.9) (the Tafel equation), the apparent values of the exchange current density and the corresponding charge transfer coefficient can be obtained from the slope and intercept of the linear relationship between ln i and η.

Polarization measurements have been performed at Rh/YSZ and Rh/TiO$_2$/YSZ electrodes in the low-polarization region, where the low-field approximation of the Butler-Volmer equation is valid. At high overpotentials, precise measurements are difficult due to a significant contribution of ohmic resistance of the solid electrolyte to the current-potential characteristics. Therefore, most of the polarization measurements in Rh/YSZ and Rh/TiO$_2$/YSZ electrochemical cells were made in the region of low overpotentials, where the influence of the ohmic resistance is negligible. These measurements were carried out at different T and P_{O_2}, and used to estimate the

exchange current density, the electron transfer resistance, and the apparent activation energy. On the basis of the polarization results, a mechanism was proposed for the oxygen exchange process.

5.2.2 Low-field polarization of the O_2(g), Rh/YSZ interface

Figure 5.1 shows typical current-potential relations presented as plots of the current density against the electrode potential (potential of the working electrode, W, referred to the potential of the reference electrode, R, denoted hereafter as U_{WR}). The polarization characteristics were measured over a narrow range of potentials within which the resulting i-U_{WR} relation is linear. The slope of the straight-line plots increases with temperature, which implies a decrease of the electron transfer resistance. According to the linear low-field approximation (Eq. (5.8)) of the Butler-Volmer equation, the interfacial resistance, R_F, and the exchange current density, i_0, can be calculated from the slopes of the straight lines that fit the experimental data of Fig. 5.1.
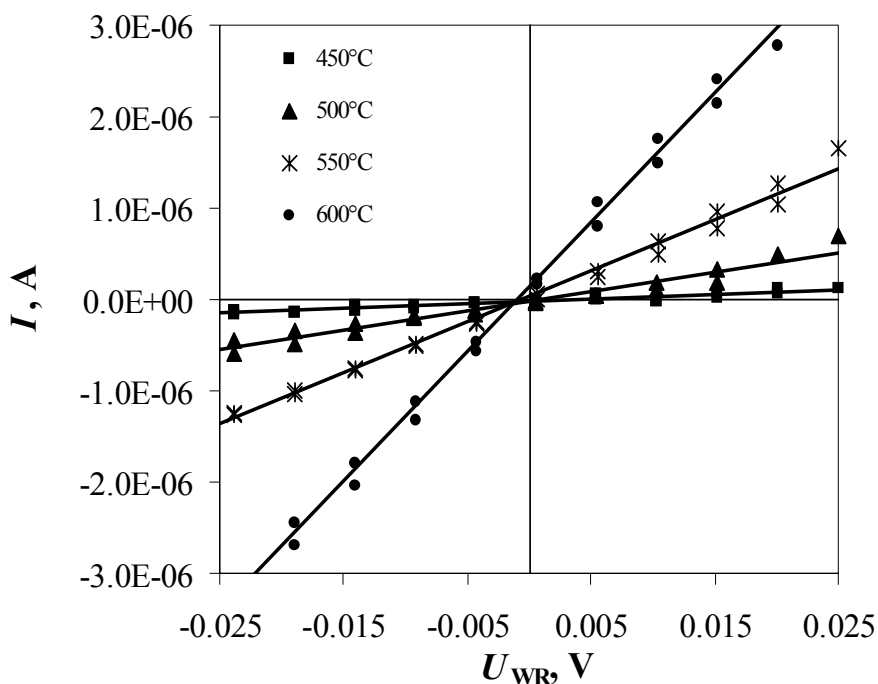
FIGURE 5.1. Stationary current-potential curves recorded at Rh/YSZ with Po_2 = 0.5 kPa, T = 450 - 600 °C.

The values found for R_F and i_0 are presented in Table 5.1. The exchange current density was calculated with respect to the electrode's geometric surface area. It increases with temperature, as expected, which implies an increase in reaction rate of the electrode process.

TABLE 5.1. Charge transfer resistance and exchange current density at Rh/YSZ obtained in the low-field approximation of the Butler-Volmer equation, Eq. (5.8)

T, °C	R_F, kohm/cm^2 *	i_0, µA/cm^2 *
450°	448.6	0.28
500	94.93	1.40
550	35.72	3.96
600	14.09	10.67

*geometric surface area of the electrode

Figure 5.2 shows an Arrhenius plot of the exchange current density extracted from the low-field approximation. The apparent activation energy calculated from the slopes of the plots was 126 kJ/mol. Similar values of E_a were found in the literature for Pt and Au electrodes [10] under charge transfer control of the process Eq (5.1). The apparent activation energy was much lower when the process was limited by mass transport [10].
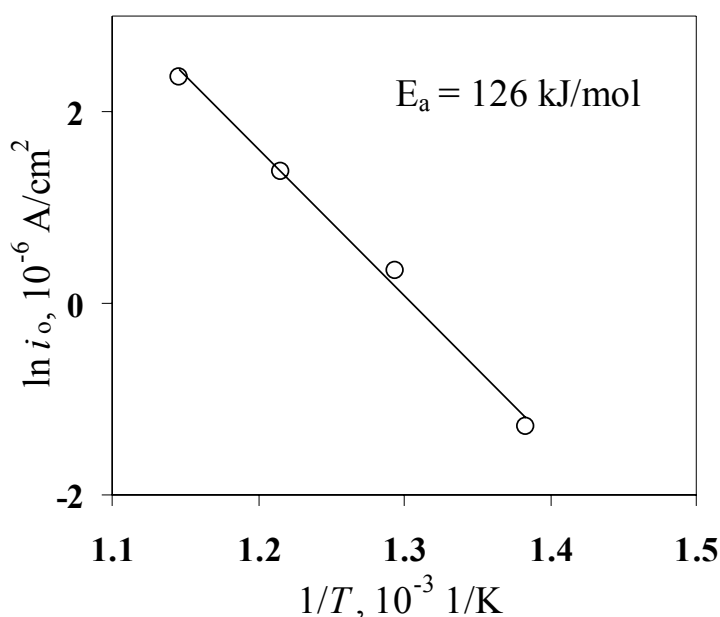
FIGURE 5.2. Arrhenius plot of the exchange currents for Rh/YSZ, Po_2 = 0.5 kPa.

The effect of oxygen partial pressure on the polarization behavior of Rh/YSZ electrodes at a constant temperature of $T = 600$ °C is shown in Fig. 5.3. The slope of the plots increases with increasing oxygen partial pressure. For the cathodic process of oxygen reduction, such a relation between oxygen partial pressure and charge transfer resistance can be expected. It indicates once more that oxygen is electrochemically active and participates in an electrode process.

The values of i_0 at different oxygen partial pressures extracted from low-polarization experiments using Equation (5.8) are presented in Table 5.2.
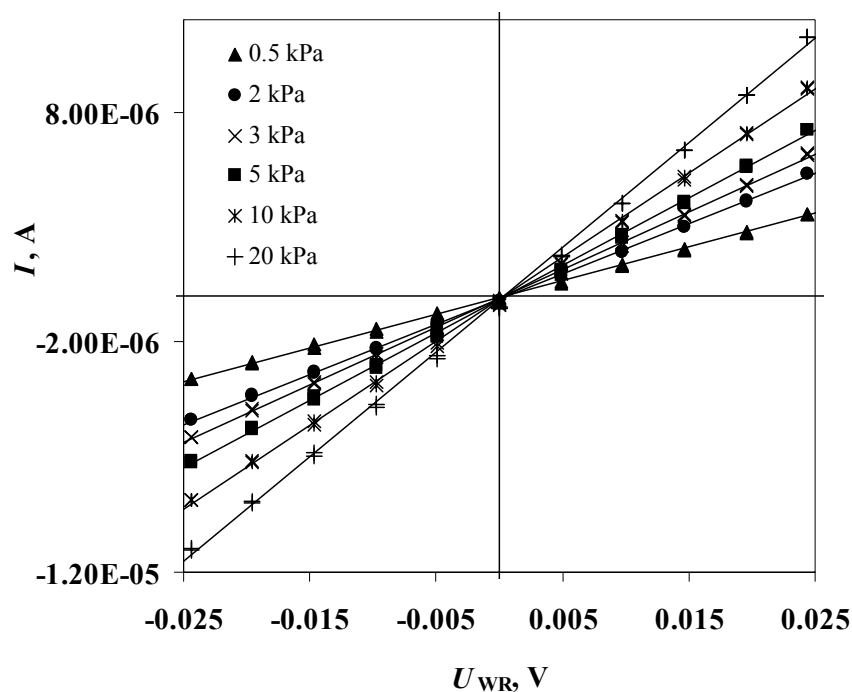
FIGURE 5.3. Stationary current-potential curves of Rh/YSZ at different oxygen partial pressures. T = 600 °C.

TABLE 5.2. Oxygen pressure dependence of the exchange current density at Rh/YSZ obtained in the low-field approximation of the Butler-Volmer equation (Eq. (5.8))

P_{O_2}, kPa	i_0, μA/cm^2 *
0.5	10.67
2	16.42
3	18.87
5	22.10
10	27.51
20	34.20

*geometric surface area of the electrode

A log i_0-log P_{O_2} plot for the Rh/YSZ system under isothermal conditions is given in Fig. 5.4. It appears that i_0 is proportional to $P_{O_2}{}^m$ (Chapter 2, section 2.3) and, by linear regression, the exponent m was found to be 0.32. The value of m can provide important information about the mechanism of the electrode process at the given temperature and oxygen partial pressure. Thus, if the process is controlled by charge transfer to/from oxygen atoms, an exponent of 0.25 should be observed (Chapter 2, section 2.3.1). For a process that is controlled by interfacial diffusion of atomic oxygen, an exponent of 0.375 was proposed in the literature [11]. The observed value of 0.32 possibly represents a combination of the two processes.
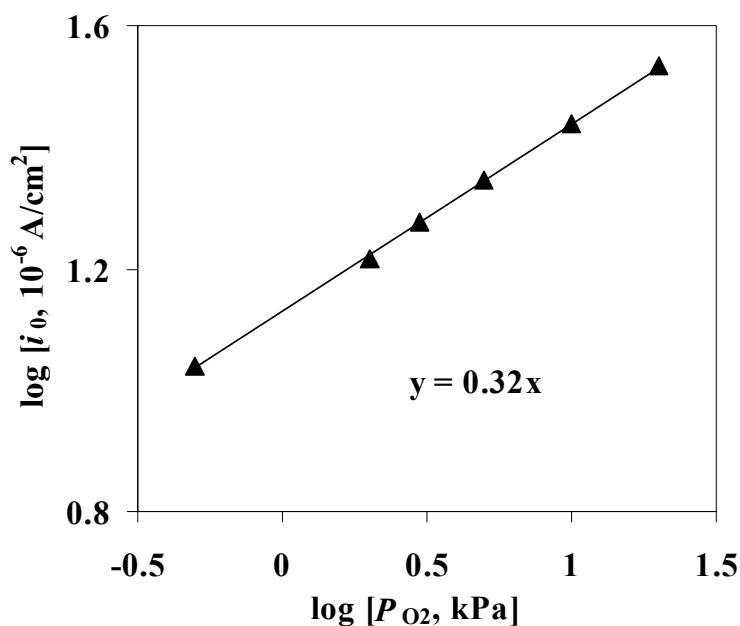
FIGURE 5.4. Plots of log i_0 against log P_{O_2} for the Rh electrode on YSZ at T = 600 °C.

5.2.3 Low field polarization of the O_2(g), Rh/TiO_2/YSZ interface

In this part of the present work the oxygen electrode reaction was investigated in a Rh/TiO_2/YSZ electrochemical cell. This cell is very similar to that used in the Rh/YSZ system, *ie*, cell geometry, thickness of the Rh electrode (40 nm), and the properties of the YSZ solid electrolyte remain unchanged, the main difference being the presence of a thin TiO_2 layer between the electrode and the YSZ electrolyte. This highly porous layer completely covers the YSZ surface in such a way that the porous Rh electrode is in contact exclusively with TiO_2. The morphological and chemical characterization of the Rh/TiO_2/YSZ cell has been reported in Chapter 1, section 2.4.2

Titania (TiO_2) is well known as an important support material, both from a practical and from a fundamental point of view. It has been studied extensively in the context of metal-support interactions, and in particular that of strong metal-support interactions (SMSI) [12, 13]. In addition to its importance as a support material for metals, TiO_2 is a very significant material in sensor

technology [2] due to its predominantly *n*-type semiconductivity and concomitant variation in electronic conductivity with oxygen pressure. One important materials property is the mixed conduction found in TiO_2, *ie,* in addition to *n*-type semiconductivity at low Po_2 values and *p*-type semiconductivity at high Po_2 values, it also exhibits some ionic conductivity due to the migration of O^{2-} ions or vacancies [14]. Recent investigations of electrochemical promotion of catalysis (EPOC) on Pt catalysts using TiO_2 supports have shown that at moderate temperatures and oxygen partial pressures, TiO_2 has some ionic conductivity and can act as a solid electrolyte [15].

Therefore, studies of polarizability of the metal/TiO_2 interface and of the electrode processes at it are of great interest from both a theoretical and a practical point of view.

5.2.3.1 Effect of TiO_2 thickness

As mentioned above, TiO_2 was applied as a thin layer between YSZ and the Rh catalyst. The thickness of the TiO_2 interlayer was chosen large enough to obtain a continuous TiO_2 film. In this case YSZ serves as a support and does not affect electrode properties such as morphology and catalyst dispersion, nor probably the mechanism of the electrode process. Several thicknesses of TiO_2 were investigated: 2, 4, 20, and 40 μm. In the case of 2 μm, the TiO_2 film was not continuous allowing direct contact to exist between the YSZ surface and Rh.

Figure 5.5 shows typical current-potential plots obtained for the low-polarization region of the Rh electrode (40 nm) on TiO_2 interlayers of different thickness supported by YSZ. The partial pressure of oxygen was maintained constant while varying the temperature. The electrode potential varies linearly with the applied current, and Eq. (5.8) can be used to determine the exchange current density.

Values of i_0 and the corresponding apparent activation energies for three cells with different TiO_2 thicknesses are given in Table 5.3. Higher temperatures lead to decreasing electron transfer resistance and increasing exchange current density for all Rh/TiO_2/YSZ cells investigated, similar to the Rh/YSZ cell. However, the effect of TiO_2 thickness on i_0 is noteworthy. Larger TiO_2 thicknesses lead to a considerable decrease in exchange current density. Since the experimental conditions and electrode material have remained constant, this decrease in i_0 might be related to transport limitations in the titania.
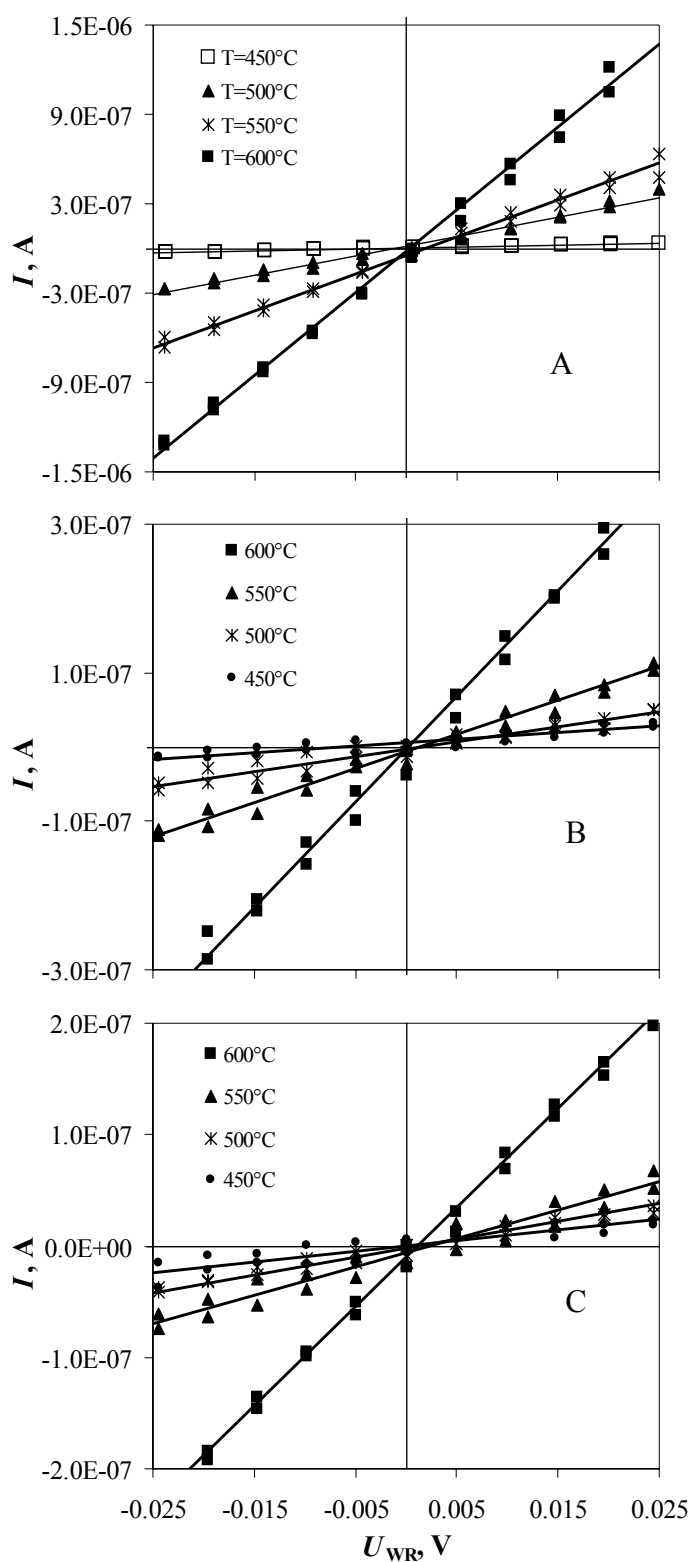
FIGURE 5.5. Stationary current-potential curves recorded at Rh on TiO$_2$/YSZ at Po$_2$= 0.5 kPa and T = 450 to 600 °C. Different thicknesses of TiO$_2$: A) 4 μm; B) 20 μm; C) 40 μm.

TABLE 5.3. Exchange current densities determined for a Rh film electrode (40 nm) on TiO$_2$ (different thicknesses)/YSZ solid electrolyte in the low-field approximation of the Butler-Volmer equation (Eq. (5.8))

T, °C	4 μm TiO$_2$ $i_{0,}$ μA/cm^2 *	20 μm TiO$_2$ $i_{0,}$ μA/cm^2 *	40 μm TiO$_2$ $i_{0,}$ μA/cm^2 *
450°	0.083	0.056	0.054
500	0.87	0.135	0.098
550	1.79	0.327	0.181
600	4.18	1.07	0.653
E_a, kJ/mol	132.5	101.4	83.4

*geometric surface area of the electrode

The Rh/TiO$_2$/YSZ system is much more complex than the Rh/YSZ system and, depending on TiO$_2$ conductivity, the electron transfer process can take place at different interfaces. Three main possibilities may exist depending on the type of TiO$_2$ conductivity:

1. The electronic conductivity of TiO$_2$ layer predominates (TiO$_x$, where $x < 2$, $x \neq 1.5$ and $x \neq 1.65$, Chapter 2, Fig. 2.17). Titania serves as an electrode similar to rhodium, and charge transfer occurs at the O$_2$, TiO$_2$/YSZ interface. Titania supplies electrons, YSZ supplies oxygen ions. In this case, one would expect no influence of TiO$_2$ thickness on the exchange current density. Decreasing i_0 with increasing TiO$_2$ thickness clearly indicates that under working conditions the conductivity of TiO$_2$ is not purely electronic.

2. The ionic conductivity of TiO$_2$ predominates (TiO$_x$, where $x = 2$; 1.5; 1.65, Chapter 2, Fig. 2.17). Titania serves as an electrolyte similar to YSZ, and charge transfer occurs at the O$_2$, Rh/TiO$_2$ interface. In this case, no influence of TiO$_2$ thickness on the exchange current density should be expected. Under working conditions, the likelihood of having pure ionic conduction in TiO$_2$ is rather low.

3. TiO$_2$ is a mixed electronic-ionic conductor (O^{2-} conductivity in addition to electronic conductivity). In this case titania will also be able to play the role of a solid electrolyte by supplying oxygen ions, and the oxygen exchange process may take place at the O$_2$, Rh/TiO$_2$ interface, similar to the Rh/YSZ interface.

Results

Under the working conditions adopted in the present work, the ionic conductivity of TiO_2 is rather low [14], and this may be one of the reasons why the exchange current density decreases with increasing TiO_2 thickness. Hence, in the anodic process O^{2-} ions supplied from YSZ will be able to cross the TiO_2 layer and reach the reaction zone situated at the O_2, Rh/TiO_2 interface.

Evidence in favor of the third case is the finding that the general polarization behavior of the Rh electrode is similar for Rh/YSZ and Rh/TiO_2/YSZ electrochemical cells, the only difference being in the rate of the electrode process (quantified by the i_0 value), which may be due to the low ionic conductivity of TiO_2. Besides, it has been shown by Pliangos et *al* [15] while studying electrochemical promotion of ethylene oxidation over Pt catalysts supported on TiO_2 that titania can act as a supplier of oxygen ions (backspillover) to the Pt catalyst. The conclusion of ionic character of the conductivity of titania is also supported by the efficient electrochemical promotion of ethylene oxidation in the Rh/TiO_2/YSZ system (see below in Chapter 8).

At first sight, the difference between the values of i_0 at the Rh/YSZ (Table 5.1) and Rh/TiO_2 (Table 5.3) interfaces is insignificant but it worth remembering that the exchange current densities refer, not to real but to geometric surface areas of the electrode. According to scanning electron microscopic analysis (Figs. 4.2 - 4.3, Chapter 4), the surface areas of Rh catalysts supported on TiO_2 are higher than those of Rh on YSZ, which implies that the real exchange current densities are much lower.

Figure 5.6 shows plots of the exchange current densities against the reciprocal temperature for three catalysts with 40-nm Rh catalysts. These Arrhenius plots have different slopes, and the highest apparent activation energy, E_a, obtained for Rh/TiO_2(4 μm) is close to E_a at Rh/YSZ. The lowest apparent activation energy obtained for Rh/TiO_2(40 μm) suggests a change in reaction mechanism, and specifically a change in the rate-determining step. Obviously, the reaction becomes mass-transfer controlled.
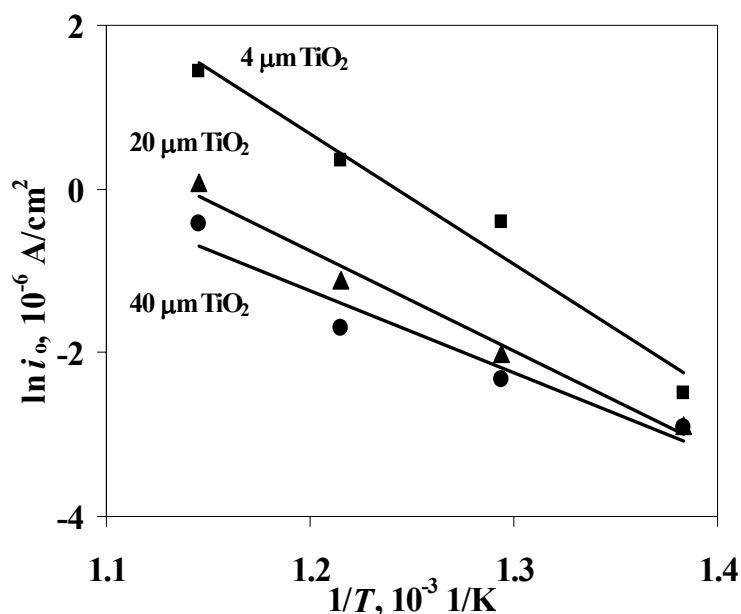
FIGURE 5.6. Arrhenius plot of exchange current ensity against reciprocal temperature for Rh/TiO$_2$/ YSZ, Po_2 = 0.5 kPa and T = 600 °C.

On the basis of the effect of TiO$_2$ thickness on the steady-state polarization behavior, and more particularly on i_0 and on the apparent activation energy, a value of 4 μm was selected for the thickness of TiO$_2$ in the further electrochemical characterization (impedance measurements, see Chapter 6) and catalytic studies of Rh/TiO$_2$/YSZ (see Chapters 7 and 8).

The TiO$_2$ layers having a thickness of 4 μm are thick enough to completely cover the YSZ surface and form a continuous porous layer of titanium oxide (see Chapter 4). At Rh interfaced with TiO$_2$ (4 μm thickness), the exchange current density is less than half that at Rh/YSZ.

5.2.3.2 Effect of oxygen partial pressure

The effect of oxygen partial pressure on the electrode process was studied using steady-state polarization measurements performed at a constant temperature of T = 600 °C. Typical results obtained at low values of polarization are given in Fig. 5.7. Higher Po_2 lead to a larger slope of I-U_{WR} plots, as in Rh/YSZ electrochemical cells. Again, the exchange current densities

calculated with Eq. 5.8 are lower than at the Rh/YSZ catalyst (Table 5.4). This indicates that the electrode kinetics of oxygen reduction and oxygen evolution (O_2/O^{2-} couple) at the Rh electrode in contact with TiO_2 is slower than at Rh/YSZ.
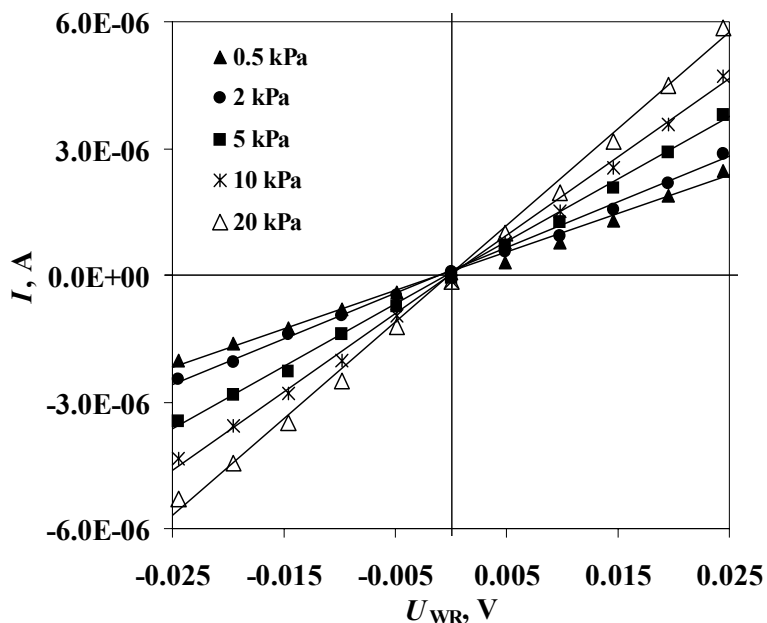
FIGURE 5.7. Stationary current-potential curves of Rh/TiO$_2$/YSZ at different oxygen partial pressures, T = 600 °C.

TABLE 5.4. Oxygen pressure dependence of the exchange current density at a Rh electrode on TiO$_2$/YSZ solid electrolyte calculated with the low-field approximation of the Butler-Volmer equation

Po_2, kPa	i_0, $\mu A/cm^2$
0.5	4.18
2	8.14
5	11.11
10	13.93
20	17.22

Over the range of P_{O_2} investigated, the relationship between oxygen partial pressure and exchange current density (Fig. 5.8) at constant temperature yields an exponent, $m = 0,31$ that is similar to the value obtained for Rh/YSZ. This indicates that the electrode process is not purely charge-transfer-controlled and may include some control by the mass-transfer step of atomic oxygen.
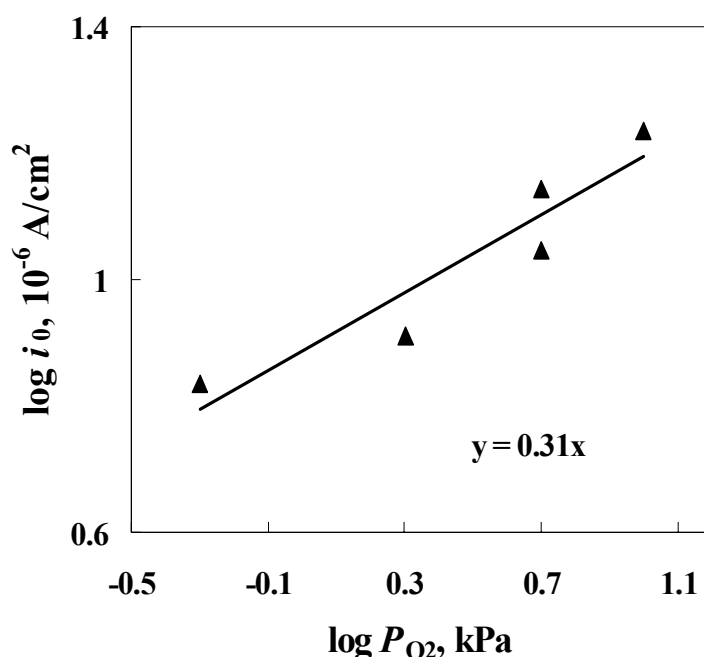
FIGURE 5.8. Dependence of i_0 on P_{O_2} at the Rh electrode on TiO$_2$/YSZ at T = 600 °C.

5.2.4 High-field polarization of the O$_2$(g), Rh/YSZ and O$_2$(g), Rh/TiO$_2$/YSZ interfaces

With the aim of obtaining additional information about the electrode process at the Rh/ solid electrolyte interface, steady-state polarization measurements were performed at high over-potentials. The I - η measurements with strong cathodic and anodic polarization were performed over a broad range of overpotentials, -0.75 V to 0.75 V, at Rh/YSZ (Fig. 5.9, A) and at Rh/TiO$_2$/ YSZ (Fig. 5.9, B) at constant temperature and several oxygen partial pressures.
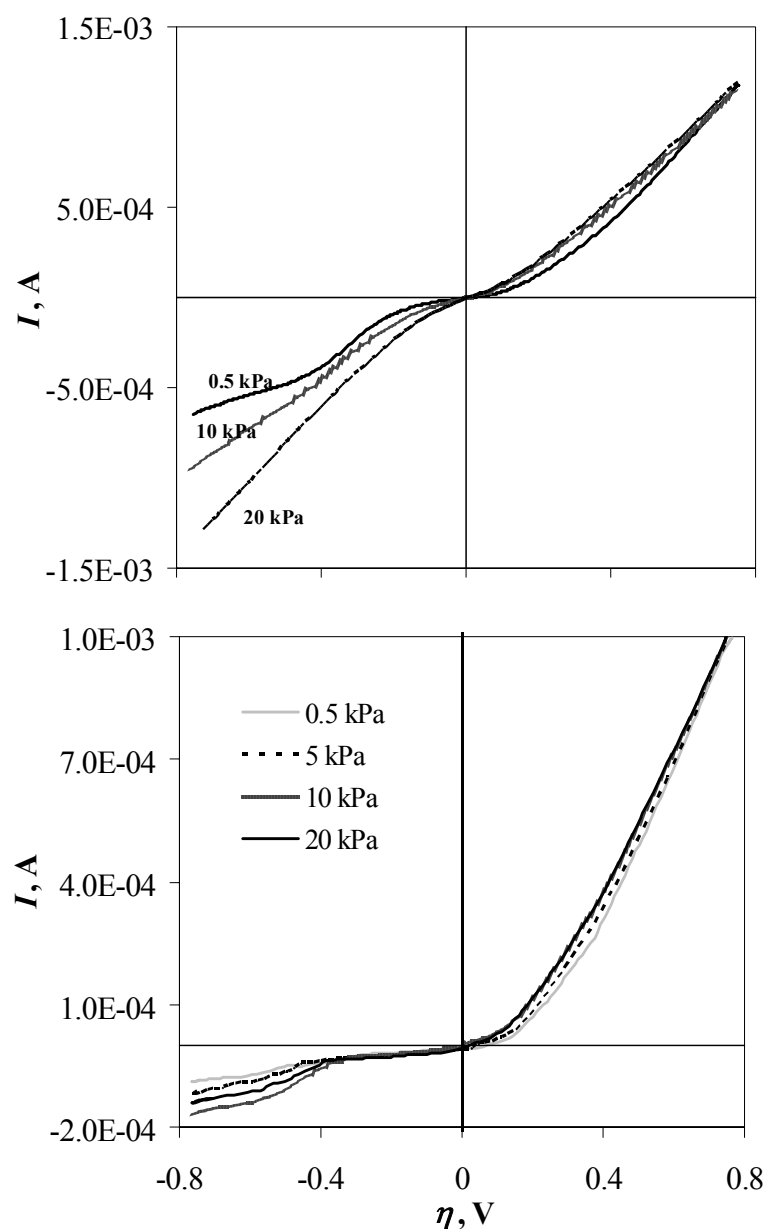
FIGURE 5.9. *I-η* **curves recorded at Rh/YSZ (A) and Rh/TiO$_2$/YSZ (B) at different oxygen partial pressures and T = 600 °C**

Contrary to the case of low polarization, at high potentials the contribution of the ohmic component to the current-potential dependence is significant. The ohmic drop correction was introduced by using the electrolyte resistance (R_{el}). This parameter was found from impedance measurements at the given temperature and gas composition. These results will be reported in Chapter 6.

Much higher current flow in the Rh/YSZ than in the Rh/TiO$_2$/YSZ cell, which is similar to the results obtained at low polarisation. The anodic and cathodic processes are no longer symmetrical under strong polarization. At a given absolute value of the applied potential difference, at both electrodes much higher anodic than cathodic currents are recorded, which shows the asymmetry of the electrode processes. This asymmetry is higher for the Rh/TiO$_2$/YSZ electrode, and is certainly related to the TiO$_2$ interlayer. For example, cathodic oxygen reduction requires an overpotential of almost -0.4 V, while oxygen evolution needs only 0.1 V.

Another interesting feature observed for both electrodes is that the anodic process is slightly Po$_2$-dependent, and this only at low overpotentials where the anodic current increases with increasing Po$_2$. The cathodic process at Rh/YSZ and Rh/TiO$_2$/YSZ strongly depends on the oxygen partial pressure, especially at high overpotentials. At Po$_2$ = 0.5 kPa the cathodic currents at both electrodes exhibit a limiting value, I_{lim}. This limiting current disappears with increasing Po$_2$ at Rh/YSZ, while at Rh/TiO$_2$/YSZ, values of I_{lim} that increase with increasing Po$_2$ are seen over the full range of oxygen partial pressures.

5.3 Discussion

The general polarization behavior of the Rh/YSZ and Rh/TiO$_2$/YSZ catalysts is the same. The observed effects of applied potential, temperature, and oxygen partial pressure are similar for the Rh/YSZ and Rh/TiO$_2$/YSZ systems. The main difference resides in the rate of the electrode process in the two cells, as given by the exchange current densities. The exchange current densities at the Rh/TiO$_2$ interface are less than half (for the case of 4 μm thick titania layers; the difference is even more pronounced at large TiO$_2$ thicknesses) those at Rh/YSZ, indicating a significant polarizability of the Rh/TiO$_2$ interface. It is likely that despite its low ionic conductivity [14, 15], TiO$_2$ acts as a solid electrolyte [16].

The exponents found for the relationship between i_0 and Po$_2{}^m$ clearly indicate that atomic rather than molecular oxygen is involved in the electrode process. Thus, m was found to have values between 1/4 (rds is charge transfer) and 3/8 (rds is interfacial diffusion of atomic oxygen to the electrochemical reaction sites) [11], the actual rds depending on the operating conditions such as applied potential and oxygen partial pressure. Values of m between 1/2 and 5/8 would be

expected for the relationship between the exchange current density and oxygen partial pressure [17, 18] if molecular oxygen was involved in the charge transfer process and in diffusion. The exponents, m, obtained for Rh/YSZ and Rh/TiO$_2$/YSZ also show that oxygen may dissociatively adsorb on the electrode surface. The overall electrode process contains a charge transfer step and a diffusion step competing as the slow steps.

The polarization behavior observed at Rh electrodes interfaced with YSZ and TiO$_2$/YSZ indicates that the mechanisms that are possible for the anodic and cathodic processes are different. This becomes particularly obvious at high overpotentials (Fig. 5.9) where asymmetry appears. This implies that the rate-determining step is not the same for the anodic and cathodic process. The anodic process of oxygen evolution is independent of oxygen partial pressure, as should be expected. The cathodic process depends on P_{O_2} and, as indicated by I_{lim}, includes a slow diffusion stage. Several authors have reported a similar polarization dependence and similar limiting cathodic currents [19, 20].

According to the experimental results obtained at low and high polarization and after an analysis of literature data, the equilibrium processes of cathodic oxygen reduction and anodic oxygen evolution (O_2/O^{2-}) at Rh electrodes, both interfaced with YSZ and with TiO$_2$, may be described by the same reaction scheme. The reaction mechanisms at cathode and anode include different rate determining steps.

The mechanism of the cathodic process can be written as follows:

$$O_2 \leftrightarrows 2\,O_{(MG)} \text{ fast step} \tag{5.10}$$

$$O_{(MG)} \xrightarrow{\textit{diffusion}} O_{(ERS)} \text{ slow step} \tag{5.11}$$

$$O_{(ERS)} + 2e^- \rightarrow O^{2-} \qquad \text{fast step} \tag{5.12}$$
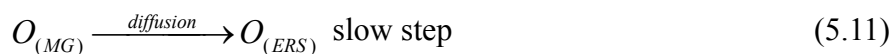
In the cathodic processs the first step is a fast step of dissociative oxygen adsorption on the gas-exposed Rh surface (Eq. (5.10)). The next step (Eq. (5.11)) is atomic oxygen diffusion to the electrochemical reaction sites (ERS). The third step (Eq. (5.12)) is a two-electron transfer process.

It is worth noting that the mechanism (5.10) - (5.12) was many times described in the literature for O$_2$ reduction at Pt electrodes (see Chapter 1, section 3) [10, 11, 19, 21-26].

The mechanism of the anodic process can be represented as follows:

$$O^{2-} - 2e^- \rightarrow O_{(ERS)} \quad \text{slow step} \tag{5.13}$$

$$2\, O_{(ERS)} \leftrightarrows O_{2(G)} \text{ fast step} \tag{5.14}$$

The first step is the electrochemical step of oxygen formation at the electrochemical reaction sites (Eq. (1.13)), the second step is its desorption in molecular form to the gas phase (Eq. (5.14)).

It is worth emphasizing that in mechanisms (5.10) - (5.12) and (5.13), (5.14) the nature of the rate-determining step of the cathodic and anodic process will considerably depend on several factors, and first of all on the electrode potential and also on oxygen partial pressure. The above mechanisms are able to describe the cathodic and anodic processes under certain conditions, namely in the region of low electrode polarization (close to equilibrium) and in an excess of gaseous oxygen.

The location of the electrochemical reaction sites for the cathodic and anodic processes is not trivial. In the literature no consensus exists as to the location of the ERS; to a large extent, it depends on the geometry of the electrode, the shape of the gas/metal/electrolyte contact and also on the electrode and electrolyte materials. In both processes, the electrochemical step may occur at the three-phase boundary or at the two-phase metal/electrolyte boundary. If there is no strong chemical bonding between rhodium and the electrolyte or/and formation of a new phase is inhibited, oxygen will diffuse along the interface. In the cathodic reaction, if the surface diffusion rate of atomic oxygen is slower than the rate of charge transfer, current will flow predominantly close to the three-phase boundary (MEG). In this case the central area of the electrode initially becomes blocking. The relationship between the rates of mass transfer and charge transfer will be determining for the spread of the three-phase boundary across the two-phase boundary (ME). The anodic process can take place at the ME boundary. This interface is fully accessible to O^{2-} from the solid electrolyte and to electrons from the metal. Because it requires oxygen exchange with a gas phase, the electrochemical reaction will occur predominantly at the MEG boundary or in its close vicinity. Therefore, the location of the electrochemical reaction sites merits further investigations.

In order to confirm and validate the oxygen exchange mechanism proposed, impedance spectroscopic analysis will be performed and reported in Chapter 6.

5.4 Conclusions

In the present chapter, the electrochemical characterization of Rh electrodes in the systems with yttria-stabilized zirconia solid electrolyte and with titanium dioxide was performed using the steady-state polarization technique. The following conclusions may be drawn from the results presented above:

1. Both the Rh/YSZ and the Rh/TiO$_2$/YSZ interfaces are polarizable, and reproducible polarization results were obtained in the present chapter. The general features of the kinetic process of oxygen reduction/oxidation at the Rh catalyst electrode are similar for Rh/YSZ and Rh/TiO$_2$/YSZ electrochemical cells. The electrode kinetics depends on applied potential, working temperature, and oxygen partial pressure.

2. The exchange current densities provide important information about the rate of the O$_2$/O^{2-} electrode reaction at the interface. The exchange current densities at Rh/TiO$_2$ (4 μm) are less than half those at Rh/YSZ, and decrease further with increasing titania thickness.

3. The thickness of TiO$_2$ strongly influences the exchange current density of the reaction. Increasing TiO$_2$ thickness leads to decreasing i_0. The observed dependence of i_0 on TiO$_2$ thickness shows that under working conditions, the conductivity of titania is not purely electronic. It was suggested that at the given oxygen atmospheres and temperatures, the conductivity of TiO$_2$ is mixed ionic-electronic with a strong ionic constituent. For further investigations, a layer thickness of TiO$_2$ of 4 μm was chosen at which the ohmic contribution is the lowest.

4. At high values of polarization of Rh/YSZ and Rh/TiO$_2$/YSZ, the cathodic and anodic curves are not symmetrical. It was found that the anodic process of oxygen evolution is independent of oxygen partial pressure, while the cathodic process depends on P_{O_2} and shows I_{lim} at low oxygen partial pressures.

5. A mechanism was proposed for the oxygen exchange process (O$_2$/O^{2-}). The processes of cathodic oxygen reduction and anodic oxygen evolution are not symmetrical. The cathodic process consists of three steps: dissociative adsorption of oxygen at the gas-exposed Rh surface, atomic oxygen diffusion to the electrochemical reaction sites, and two-electron transfer reaction at the electrochemical reaction sites. The cathodic process is limited by interfacial diffusion of oxygen atoms from the gas-exposed metal surface to the ERS. The anodic process includes two steps: a two-electron transfer reaction, which is the rds, and oxygen desorption to the gas phase.

5.5 References

1. A. Wieckowski, E. R. Savinova, and C. G. Vayenas, *Catalysis and Electrocatalysis at Nanoparticles* Marcel Dekker, Inc., New York (2003).

2. W. Göpel, *Sensor and Actuators B,* 18-19 (1994) 1.

3. A. Mandelis and C. Christofides, *Solid State Gas Sensor Devices* John Wiley & Sons, New York (1993).

4. C. G. Vayenas, S. Brosda, and C. Pliangos, *J. Catal.,* 216 (2003) 487.

5. C. G. Vayenas, S. Brosda, and C. Pliangos, *J. Catal.,* 203 (2001) 329.

6. C. G. Vayenas, S. Bebelis, C. Pliangos, S. Brosda, and D. Tsiplakides, *Electro-chemical activation of catalysis. Promotion, Electrochemical promotion, and metal-support interaction.* Kluwer Academic/Plenum Publishers, New York (2001).

7. C. G. Vayenas, M. M. Jaksic, S. I. Bebelis, and S. G. Neophytides, in *Modern aspects of Electrochemistry* J. O. M. Bockris, B. E. Conway, and R. E. White, eds., Plenum Press, New York, (1996), p. 57.

8. G. Fóti, I. Bolzonella, and C. Comninellis, in *Modern Aspects of electrochemistry*, Vol. 36 C. G. Vayenas, B. E. Conway, R. E. White, and M. E. Gamboa-Adelco, eds., Kluwer Academic / Plenum Publisher, New York, Boston, Dordrecht, London, Moscow, (2003), p. 310.

9. J. O. M. Bockris and A. K. N. Reddy, *Modern electrochemistry* Plenum Press, New York (1977).

10. O. J. Velle, T. Norby, and P. Kofstad, *Solid State Ionics,* 47 (1991) 161

11. D. Y. Wang and A. S. Nowick, *J. Electrochem. Soc,* 128 (1981) 55.

12. S. J. Tauster, S. C. Fung, and R. L. Garten, *JACS,* 100 (1978) 170.

13. S. J. Tauster, S. C. Fung, R. T. K. Baker, and J. A. Horsley, *Science,* 211 (1981) 1121.

14. P. J. Gellings and H. J. M. Bouwmeester, *Catalysis Today,* 12 (1992) 1.

15. C. Pliangos, I. V. Yentekakis, S. Ladas, and C. G. Vayenas, *J. Catal.,* 1996 (1996) 189.

16. J. Nicole, D. Tsiplakides, C. Pliangos, X. E. Verykios, C. Comninellis, and C. G. Vayenas, *J. Catal.,* 204 (2001) 23.

References

17. B. A. v. Hassel, B. A. Boukamp, and A. J. Burggraaf, *Solid State Ionics,* 48 (1991) 139.

18. B. A. v. Hassel, B. A. Boukamp, and A. J. Burggraaf, *Solid State Ionics,* 48 (1991) 155.

19. N. L. Robertson and J. N. Michaels, *J. Electrochem. Soc,* 137 (1990) 129.

20. M. V. Perfilev, *Solid State Ionics,* 9 & 10 (1983) 765.

21. D. Y. Wang and A. S. Nowick, *J. Electrochem. Soc.,* 126 (1979) 1155.

22. D. Y. Wang and A. S. Nowick, *J. Electrochem. Soc.,* 126 (1979) 1166

23. J. Mizusaki, K. Amano, S. Yamauchi, and K. Fueki, *Solid State Ionics,* 22 (1987) 313.

24. J. Mizusaki, K. Amano, S. Yamauchi, and K. Fueki, *Solid State Ionics,* 22 (1987) 323.

25. A. Mitterdorfer and L. J. Gauckler, *Solid State Ionics,* 117 (1999) 187.

26. A. Mitterdorfer and L. J. Gauckler, *Solid State Ionics,* 117 (1999) 203.

CHAPTER 6 **Electrochemical characterization of Rh catalysts:** Impedance measurements

On the basis of the oxygen exchange mechanism, an impedance model was set up for the Rh/oxygen electrode in contact with a solid electrolyte. Electrochemical impedance spectra were recorded at T = 450 - 600 °C and Po_2 = 0.5 kPa at open circuit and under polarization in order to confirm the impedance model for the processes occurring at Rh electrodes interfaced with YSZ and TiO_2/YSZ. Good agreement was found to exist between the model (theory) and experiments (the impedance spectra). This agreement constitutes support for validity of the reaction mechanism proposed in the preceding chapter. The validity of the mechanism was confirmed in an indirect way by the values obtained for the exchange current density, i_0, since the values obtained from the impedance measurements are very close to those obtained from low-field polarization experiments.

Impedance data recorded under polarization provide information as to the origin of electrochemical promotion. Under positive polarization the adsorption capacitance of the Rh/YSZ electrode increases dramatically, which is understood as reflecting the creation of an effective double layer across the entire gas-exposed electrode surface. The second semicircle

appearing in the impedance spectra of the Rh/TiO$_2$/YSZ electrode indicates that the system has additional complexity.

6.1 Introduction

The technique where the cell's or electrode's impedance is studied as a function of frequency of the ac signal source is called electrochemical impedance spectroscopy (EIS) [1]. The equivalent resistance and capacitance values can be interpreted theoretically in terms of interfacial phenomena. The mean (dc) potential of the working electrode is the equilibrium potential determined by the ratio of oxidized and reduced forms of the redox couple. This technique is very precise, and is frequently used in electrochemistry to evaluate heterogeneous charge-transfer parameters and study double-layer structure.

The impedance, Z, is a kind of generalized resistance that links voltage E and current I in phasor notation:

$$\dot{E} = \dot{I}Z \tag{6.1}$$

where $\dot{E}$ is the phasor of the electrode potential, and $\dot{I}$ is the phasor of applied current.

This equation is a generalized Ohm's law. It is convenient to represent phasors in complex notation. Components along the ordinate are regarded as imaginary, and are multiplied by $j = \sqrt{-1}$, while components along the abscissa are regarded as real. In this case, Ohm's law can be represented as

$$Z(\omega) = Z_{Re} - jZ_{Im} \tag{6.2}$$

where Z_{Re} and Z_{Im} are the real and imaginary parts of impedance. For example: $Z_{Re} = R$ and $Z_{Im} = 1/\omega C$.

Interesting information can be derived from the variation of impedance with frequency, which can be displayed in different ways. In one of the common representations, the Nyquist plots, values of Z_{Im} are displayed as functions of Z_{Re} for different values of ω. The plot that is obtained for a parallel R-C circuit is shown in Fig. 6.1. The first intersection of the semicircle with the abscissa gives the electrolyte resistance (R_{el}), the second intersection gives the sum of electro-

lyte resistance and charge-transfer resistance ($R_{el} + R_F$). The capacitance of the electric double layer (C_{dl}) can be computed from Z and the frequency value at the top of the semicircle.

In a general sense, an electrochemical cell when excited or perturbed by a sinusoidal voltage signal will behave as an impedance. It should be possible then to represent its behavior by an equivalent circuit of resistors and capacitors that pass a current having the same amplitude and phase angle as the real cell subjected to the same excitation. A very simple circuit known as the Randles equivalent circuit which corresponds to the impedance spectrum of Fig. 6.1 is shown in Fig. 6.2. All current passes through the solution resistance, thus R_{el} is present as a series element. The parallel elements of impedance represent the total current through the working interface as the sum of distinct contributions from a faradaic process, i_f, and from double-layer charging, i_c, at the working electrode. The counterelectrode in the cell would contribute similar impedance elements in series, but their values are made negligibly small by experimental design, so that the working electrode alone can be studied.
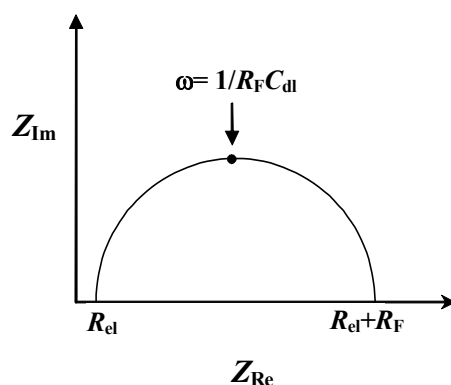
FIGURE 6.1. Niquist plot for a parallel *RC* circuit: impedance components at different frequencies *f* ($\omega = 2\pi f$).
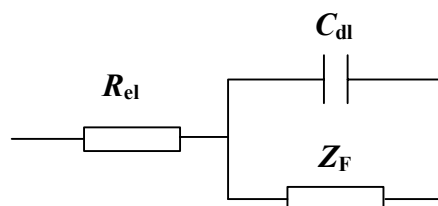
FIGURE 6.2. Equivalent circuit of a very simple electrochemical cell: the Randles circuit.

The double-layer capacitance is regarded as a pure capacitance represented in the circuit by a capacitor of capacitance C_{dl}. The faradaic process is represented by an impedance, Z_F. In one of the representations, this impedance is separated into a pure resistance due to charge transfer, R_F, and a general impedance called Warburg impedance, Z_W, which is related to the mass-transfer resistance. In contrast to R_{el} and C_{dl} which are nearly ideal (frequency-independent) circuit elements, the faradaic impedance usually changes with frequency.

The circuit considered here is based on the simplest electrode process. Many other circuits have been devised, for example, those including circuit components for adsorption of electroreactants, multistep charge transfer, or homogeneous chemistry. It is important to understand that equivalent circuits drawn for electrochemical cells are not unique. Moreover, it is only in the simpler cases that one can identify all individual circuit elements with processes that occur in the electrochemical cell. Still, impedance studies do provide a wealth of interesting information if interpreted with the necessary chemical and physical intuition.

6.1.1 AC Impedance spectroscopy in solid-state cells

The technique of electrochemical impedance spectroscopy (EIS) is one of the most commonly used techniques in electrochemistry, both aqueous and solid. Many studies in solid-state electrochemistry performed by impedance spectroscopy were undertaken with the aim of identifying the reaction kinetics and the process mechanisms.

The impedance spectrum obtained for the solid-electrolyte electrochemical cell:

Introduction

O_2, Pt/$(ZrO_2)0.91$-$(Y_2O_3)0.09$/Pt, O_2

is rather more complex than the spectra commonly seen in aqueous systems, since here the contribution of impedance of the solid electrolyte to the total cell impedance is significant (Fig. 6.3). Three semicircles are recognized in the Nyquist plot. They are identified by studying the effects produced when varying experimental parameters [2]:

a. geometrical factors of the sample;

b. composition of the solid electrolyte: nature and concentration of oxygen dopants;

c. microstructure of the electrolyte;

d. nature and texture of the electrode material: metal or semiconductor;

e. oxygen partial pressure;

f. current density.

Thus, the first semicircle of Fig. 6.3 was found to represent the bulk properties of the solid electrolyte, in particular the conductivity. R_1 represents the intergrain resistance.

The second semicircle represents the effect of the grain boundaries. The value (R_2 - R_1) corresponds to the contribution of the grain contacts to the total electrolyte resistance.

The third semicircle represents the electrode phenomena that in addition to the faradaic processes may include adsorption-desorption processes as well as mass-transfer processes; here R_2 is an overall electrolyte resistance and R_3 is a resistance attributable to the electrochemical process (faradaic resistance).
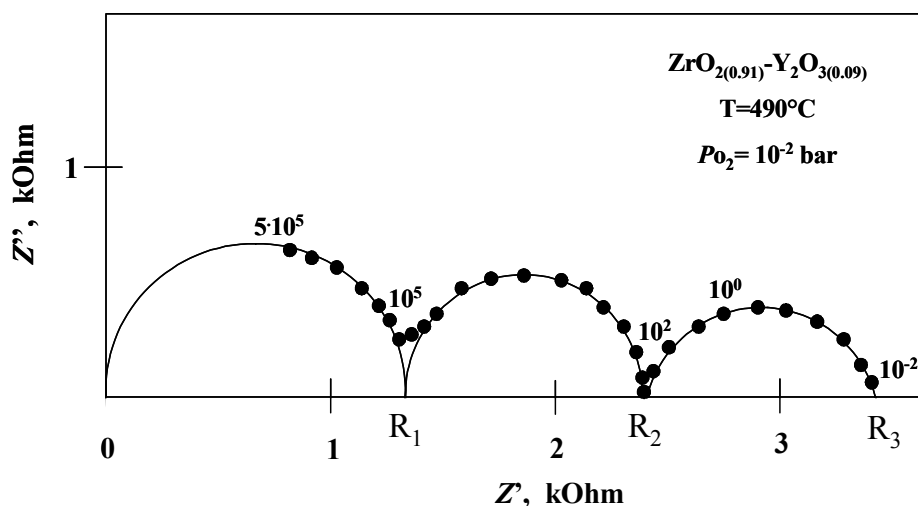

FIGURE 6.3. Complex impedance spectrum of the cell Pt/YSZ/Pt. Numbers on the semicircles are the excitation frequencies, *f*, in Hz.

The presence and shape of the three semicircles strongly depend on working temperature and cell configuration. The first two semicircular arcs correspond to parallel *R-C* circuit elements, while the third one is more complex. When the electrode process contains slow diffusion steps, a diffusion impedance will have to be added to the charge-transfer impedance. An adsorption process would contribute to the double-layer capacitance with an additional adsorption capacitance. Different equivalent circuits can be found in the literature depending on the rate-determining step (rds).

6.1.2 Ac impedance spectroscopy in electrochemical promotion of catalysis

Recently, impedance spectroscopy was used to investigate the origin of electrochemical promotion at a Pd catalyst electrode deposited on YSZ and exposed to CH_4/O_2 and C_2H_4/O_2 gas mixtures [3]. Other systems studied were Au, Pt, Rh electrodes interfaced with YSZ in different gas mixtures (pure O_2 and H_2 and C_2H_4-O_2 mixtures).

Figure 6.4 shows complex impedance spectra (Nyquist plots) recorded for the CH_4, O_2, Pd/ YSZ system. The impedance in the frequency range above 10^4 Hz was found to represent the impedance of the bulk electrolyte and grain boundaries. Three distinct features of the impedance spectra were discussed by the authors. (*i*) In the range of high frequencies (higher than 300 Hz), part of a small depressed semicircle is observed at absolute values of overpotential lower than 0.6 V. (*ii*) At frequencies lower than 300 Hz, the main feature under open-circuit conditions is an inclined straight line, which can be considered as part of a depressed semicircle. In fact, when raising the applied dc potential difference to high positive or negative values a depressed semicircle (semicircle 2) clearly develops. This semicircle becomes smaller with increasing and decreasing polarization (overpotential), indicating that it reflects processes at the Pd/YSZ interface. (*iii*) At high positive overpotentials (higher than 0.6 V) a third depressed semicircle (semicircle 3) appears in the lowest frequencies range.
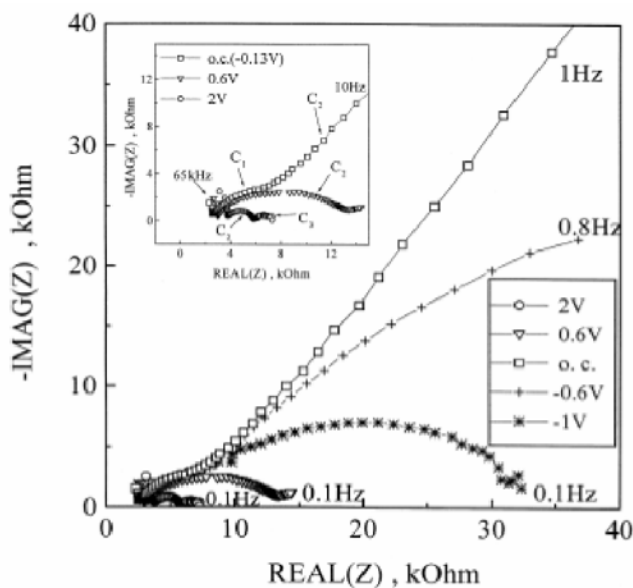
FIGURE 6.4. Complex impedance spectra (Nyquist plots) for the C_2H_4, O_2, Pd/YSZ system at different Pd catalyst potentials. Conditions: $T = 400\ °C$, $P_{O_2} = 1.9$ kPa, $P_{C_2H_4} = 2.6$ kPa.

C_1 most likely corresponds to a tpb covered with PdO, while C_2 corresponds to a tpb covered with reduced Pd. The third semicircle is interpreted as a "backspillover oxygen semicircle". It only appears when positive values of U_{WR} are imposed, *ie*, when O^{2-} ions are supplied to the catalyst surface.

For a more detailed analysis of the impedance spectra, each of the above semicircles was fitted to a single resistor–capacitor combination, and the corresponding capacitance values were determined.

From the values of C_3 and C_2 shown in Table 6.1, it can be seen that C_3 on an average is 2500 times higher than C_2. Interestingly, the ratio C_3/C_2 nicely compares with the ratio N_G/N_{tpb} (equal to 3570) of the catalyst's tpb exposed surface (measured via surface titration: $N = 3 \times 10^{-7}$ mol Pd) and the "surface" corresponding to the gas–metal–electrolyte three-phase boundary (tpb: $N_{tpb} = 8.4 \times 10^{11}$ mol Pd). Impedance spectroscopy thus allows one to estimate the three-phase-boundary length via:

$$\frac{N_{\text{tpb}}}{N_{\text{G}}} = \frac{C_3}{C_2} \tag{6.3}$$

From the total mass of the Pd electrode (0.3 mg) and its surface area, one has:

$$N_{\text{tpb}} = \frac{(l_{\text{tpb}}/2r_{\text{Pd}})}{N_{\text{AV}}} \tag{6.4}$$

where $r_{\text{Pd}} = 1.8 \ \overset{\circ}{A}$ is the atomic radius of Pd, N_{AV} is Avogadro's number, and l_{tpb} is the three-phase-boundary length computed via

$$l_{\text{tpb}} = \pi S/\bar{d} \tag{6.5}$$

where d is the average catalyst crystallite size, and S is the geometric surface area of the catalyst electrode ($S = 0.6 \ \text{cm}^2$).

TABLE 6.1. Ratios C_3/C_2 for methane and ethylene oxidation at Pd/YSZ (for comparison, $N_{\text{G}}/N_{\text{tpb}} = 3570$)

Methane oxidation		Ethylene oxidation	
U_{WR}, V	C_3/C_2	U_{WR}, V	C_3/C_2
1	2700	1.1	710
1.1	3190	1.4	920
1.23	2570	1.75	890
1.37	2060		
1.5	1810		

These observations provide strong indications that the appearance of the depressed semi-circle in the low-frequency range at high positive overpotentials is related to a process of charge separation extending all over the catalyst surface, which can be identified as a backspillover of charged species, in agreement with the model proposed to explain the origin of the effect of electrochemical promotion [4, 5]. This type of behavior was also observed for ethylene oxidation at the same catalyst, for which the C_3/C_2 ratios are shown in Table 6.1.

In very recent work [6], the impedance of Au/YSZ, Pt/YSZ, and Rh/YSZ has been studied in different gas mixtures and under electrochemical promotion conditions. For an interpretation of

the experimental results, the authors used several electrical equivalent circuits, such as R(RQ)(RQ), R(RC), and RG, where R is a resistance either of the solid electrolyte or electrode process, Q is a constant phase element, and G is a Gerischer impedance [7]. Under special conditions for a CEC (chemical-electrochemical-chemical)-type reaction [8], the complex expression reduces to a rather simple impedance relation:

$$Z_{(\omega)} = \frac{Z}{\sqrt{k + j\omega}} \qquad (6.6)$$

Here k represents the effective transfer rate of the chemical reaction. The form of this impedance dispersion is somewhat similar in shape to a finite-length Warburg impedance.

Although EIS provides important information about the properties of the system, it is usually more difficult than in the steady-state polarization measurements to obtain expressions describing the frequency-dependent behavior in terms of a physicochemical description. Therefore, in impedance spectroscopy an identification of the process kinetics may be procured, either by starting from experimental data, reducing them to an electrical equivalent circuit, and then deriving a reaction mechanism, or by proceeding in the reverse order, *viz*, by first assuming a reaction mechanism, then designing the corresponding theoretical equivalent circuit, and finally proceed to an experimental confirmation by means of impedance measurements.

The present chapter has two main goals: (i) experimentally substantiating the kinetic scheme proposed in the previous chapter for the oxygen exchange reaction on Rh electrodes in contact with YSZ and TiO$_2$/YSZ (section 3.1: Impedance measurements at equilibrium potential), (ii) confirming the often suggested mechanism of electrochemical promotion via impedance measurements in the O$_2$, Rh/YSZ and O$_2$, Rh/TiO$_2$/YSZ systems (section 6.3.2: Impedance measurements under polarisation). The approach to this task was divided into the following stages:

1. design of a theoretical impedance model for the O^{2-}/O$_2$ process and of a theoretical equivalent circuit for this process;

2. definition of an equivalent circuit that would correspond to the experimental data over a broad range of frequencies, and calculation of its parameters;

3. comparison of the expression for the impedance in terms of the equivalent circuit from (2) with that derived for the theoretical model from (1).

6.2 Theory

6.2.1 Theoretical impedance model for the O_2, Rh/electrolyte system at equilibrium

Consider the Rh electrode interfaced with YSZ or TiO_2/YSZ under open-circuit conditions in an O_2 atmosphere. In such a system at equilibrium, two processes are taking place: cathodic reduction of oxygen (Eqs. (5.10) to (5.12), Chapter 5) and anodic oxidation of oxygen ions (Eqs. (5.13) and (5.14), Chapter 5). It will be assumed that the electrochemical reaction sites (ERS) for cathodic and anodic processes are different. Impedance models can then be developed independently for each process, and similar to the impedance model proposed for the lithium electrode by Kuznetsov and co-workers [9].

Consider first the <u>cathodic process</u> of O_2 reduction:

$$O_2 \leftrightharpoons 2\,O_{(MG)} \tag{6.7}$$

$$O_{(MG)} \xrightarrow{\;V_d\;} O_{(ERS)} \tag{6.8}$$

$$O_{(ERS)} + 2e^- \xrightarrow{\;i_C\;} O^{2-} \tag{6.9}$$

where MG stands for metal/gas; V_d is the rate of atomic oxygen interfacial diffusion from MG to ERS boundaries; and i_C is the rate of electrochemical reduction of oxygen. Oxygen dissociatively adsorbs at the MG interface with a rate of adsorption B.

Assuming that the steps of oxygen adsorption and electron transfer are fast steps, then interfacial diffusion of atomic oxygen will be the rate-limiting step.

The charge density on the Rh electrode depends on electrode potential (U) and on the quantity of adsorbed $O_{(MG)}$ on the metal surface (Γ) [10]:

$$q = q(U, \Gamma) \tag{6.10}$$

Then the derivative of the complete differential of electrode charge density with respect to time is equal to the charging current passing through the electrode [11]:

$$i_{cc} = \frac{dq}{dt} = \frac{\partial q}{\partial U}\frac{dU}{dt} + \frac{\partial q}{\partial \Gamma}\frac{d\Gamma}{dt} \tag{6.11}$$

Taking advantage of the method of complex amplitudes [11-13], one then can write for the phasor (complex current amplitude) of the charging current (δi_{cc}):

$$\delta i_{cc} = \frac{d\delta q}{dt} = j\omega\frac{\partial q}{\partial U}\delta U + j\omega\frac{\partial q}{\partial \Gamma}\delta\Gamma = j\omega a_1\delta U + j\omega b_1\delta\Gamma \tag{6.12}$$

where δU is the phasor of electrode potential; $\delta\Gamma$ is the phasor of adsorption; the coefficients $a_1 = \frac{\partial q}{\partial U}$ and $b_1 = \frac{\partial q}{\partial \Gamma}$.

The relation between adsorbed $O_{(MG)}$, O_2 in the gas phase, and electrode potential is given by the adsorption isotherm:

$$\Gamma = \Gamma(C, U) \tag{6.13}$$

where C is the concentration of oxygen in the gas phase.

The balance of adsorbed oxygen atoms is determined by the magnitude of the diffusion flux:

$$\frac{d\Gamma}{dt} = -V_d \tag{6.14}$$

Applying the method of complex amplitudes to (6.14) one can make the transition to phase variables:

$$\frac{d\delta\Gamma}{dt} = i\omega\delta\Gamma = -\delta V_d \tag{6.15}$$

For the phasor of adsorption, the equation can be written as:

$$\delta\Gamma = \frac{\partial\Gamma}{\partial U}\delta U + \frac{\partial\Gamma}{\partial C}\delta C = a_2\delta U + k_2\delta C \tag{6.16}$$

The phasor of the diffusion flux is related to the phasor of the bulk concentration by the equation:

$$\delta V_d = (1+j)\omega^{1/2}\sqrt{D/2}\delta C \tag{6.17}$$

where D is the coefficient of atomic oxygen diffusion.

The faradaic current (i_{fc}) is determined by oxygen diffusion, and for the phasor of current in the case of semi-infinite diffusion one obtains:

$$\delta i_{fc} = F\delta V_d = F(1+j)\omega^{1/2}\sqrt{D/2}\,\delta C = (1+j)\omega^{1/2}k_3\delta C \qquad (6.18)$$

For the balance of adsorbed species at the Rh surface, one has:

$$F\frac{d\delta\Gamma}{Dt} = j\omega F\delta\Gamma = -\delta i_{fc} \qquad (6.19)$$

The total cathodic current consists of a charging current and a faradaic current:

$$i_C = i_{cc} + i_{fc} \qquad (6.20)$$

The phasor of the total cathodic current flowing at the two-phase boundary is given by the sum of phasors of the charging current and the current of the faradaic process:

$$\delta i_C = \delta i_{cc} + \delta i_{fc} \qquad (6.21)$$

For the <u>anodic process</u> of oxygen formation occurring at the equilibrium potential at Rh electrodes in contact with YSZ or TiO_2/YSZ, one can write (see Chapter 6):

$$O^{2-} - 2e^- \xrightarrow{\;i_A\;} O_{(ERS)} \qquad (6.22)$$

$$2\,O_{(ERS)} \leftrightharpoons O_{2(G)} \qquad (6.23)$$
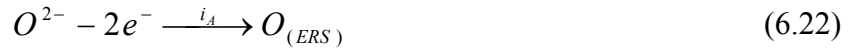
where i_A is the rate of electrochemical oxidation of oxygen ions.

In the anodic process, the rate-determining step is an electron-transfer step (Eq. (6.22)). Therefore, the relations for the magnitude of the phasors are:

$$\tilde{i}_{ca} = j\omega\frac{\partial q}{\partial U}\delta U \qquad (6.24)$$

$$\delta i_{fa} = \frac{\partial i_{fa}}{\partial U}\delta U \qquad (6.25)$$

$$\delta\tilde{i}_A = \delta\tilde{i}_{ca} + \delta\tilde{i}_{fa} \tag{6.26}$$

For the phasor of total current of the equilibrium process, one can write:

$$\delta i_{O^{2-}/O_2} = \delta i_C + \delta i_A \tag{6.27}$$

The complex conductivity of the oxygen electrode in the system with solid electrolyte is described by the following relation:

$$Y = \frac{\delta i_{O^{2-}/O_2}}{\delta U} \tag{6.28}$$

Insofar as the phasors of the anodic and cathodic current are mutually independent, the complex conductivity of an electrode can be represented as a sum of cathodic and anodic conductivities, which are determined separately from each other:

$$Y = \frac{\delta \tilde{i}_{O^{2-}/O_2}}{\delta U} = \frac{\delta \tilde{i}_C}{\delta U} + \frac{\delta \tilde{i}_A}{\delta U} = Y_C + Y_A \tag{6.29}$$

It is easy to find the expression for the admittance of the anodic process:

$$Y_A = j\omega\frac{\partial q}{\partial U} + \frac{\partial i_{fa}}{\partial U} = j\omega C_{da} + R_a^{-1} \tag{6.30}$$

where C_{da} is the double-layer capacitance of the anode.

An electric equivalent circuit for the admittance of the anodic process Eq. (6.30) can be formulated as the parallel combination of a double-layer capacitance and a resistance of the electrochemical reaction.

For the purposes of obtaining the solution for the cathodic process, it will be preferable to write the sets of Eqs. (6.12), (6.16), (6.18), (6.19) and (6.21) in a matrix form [11-13] (see Annex):

$$\delta U \cdot M = L \cdot N \tag{6.31}$$

where M is a matrix vector composed of the coefficients at δU, the transposed matrix M being:

$$M^T = \begin{bmatrix} 0 & j\omega a_1 & 0 & a_2 & 0 \end{bmatrix} \tag{6.32}$$

N is a matrix column composed of the left-hand sides of Equations (6.12), (6.16), (6.18), (6.19) and (6.21), the transposed matrix N being:

$$N^T = \begin{bmatrix} \delta i_C & \delta i_{cc} & \delta i_{fc} \delta \Gamma & \delta C \end{bmatrix} \tag{6.33}$$

and L is a square matrix of fifth order:

$$\begin{bmatrix} -1 & 1 & 1 & 0 & 0 \\ 0 & -1 & 0 & j\omega b_1 & 0 \\ 0 & 0 & -1 & 0 & (1+j)\omega^{1/2}k_3 \\ 0 & 0 & 0 & -1 & k_2 \\ 0 & 0 & -1 & j\omega F & 0 \end{bmatrix} \tag{6.34}$$

Now the admittance of the cathodic process can be represented as follows:

$$Y_C = \frac{\delta i_C}{\delta U} = \frac{\Delta' L}{\Delta L} \tag{6.35}$$

where ΔL is the determinant of matrix L; $\Delta'L$ is the determinant of a matrix obtained by substituting the first column in matrix L by the matrix vector M.

The equetion 6.31 can be represented as:

$$\delta U \begin{bmatrix} 0 \\ j\omega a_1 \\ 0 \\ a_2 \\ 0 \end{bmatrix} = \begin{bmatrix} -1 & 1 & 1 & 0 & 0 \\ 0 & -1 & 0 & j\omega b_1 & 0 \\ 0 & 0 & -1 & 0 & (1+j)\omega^{1/2}k_3 \\ 0 & 0 & 0 & -1 & k_2 \\ 0 & 0 & -1 & j\omega F & 0 \end{bmatrix} \begin{bmatrix} \delta i_C \\ \delta i_{cc} \\ \delta i_{fc} \\ \delta \Gamma \\ \delta C \end{bmatrix} \tag{6.36}$$

$$\Delta L = \begin{vmatrix} -1 & 1 & 1 & 0 & 0 \\ 0 & -1 & 0 & j\omega b_1 & 0 \\ 0 & 0 & -1 & 0 & (1+j)\omega^{1/2}k_3 \\ 0 & 0 & 0 & -1 & k_2 \\ 0 & 0 & -1 & j\omega F & 0 \end{vmatrix} = -1 \begin{vmatrix} -1 & 0 & j\omega b_1 & 0 \\ 0 & -1 & 0 & (1+j)\omega^{1/2}k_3 \\ 0 & 0 & -1 & k_2 \\ 0 & -1 & j\omega F & 0 \end{vmatrix} =$$

$$= \begin{vmatrix} -1 & 0 & (1+j)\omega^{1/2}k_3 \\ 0 & -1 & k_2 \\ -1 & j\omega F & 0 \end{vmatrix} = -1 \begin{vmatrix} -1 & k_2 \\ j\omega F & 0 \end{vmatrix} -1 \begin{vmatrix} 0 & (1+j)\omega^{1/2}k_3 \\ -1 & k_2 \end{vmatrix} = j\omega F k_2 + (1+j)^{1/2}k_3 \quad (6.37)$$

The determinant of a matrix (6.34) obtained by substituting the first column in matrix L by the matrix vector M is:

$$\Delta' L = \begin{vmatrix} 0 & 1 & 1 & 0 & 0 \\ -j\omega a_1 & -1 & 0 & j\omega b_1 & 0 \\ 0 & 0 & -1 & 0 & (1+j)\omega^{1/2}k_3 \\ -a_2 & 0 & 0 & -1 & k_2 \\ 0 & 0 & -1 & j\omega F & 0 \end{vmatrix} = \begin{vmatrix} -j\omega a_1 & 0 & j\omega b_1 & 0 \\ 0 & -1 & 0 & (1+j)\omega^{1/2}k_3 \\ -a_2 & 0 & -1 & k_2 \\ 0 & -1 & j\omega F & 0 \end{vmatrix} -$$

$$-\begin{vmatrix} 0 & 1 & 0 & 0 \\ 0 & -1 & 0 & (1+j)\omega^{1/2}k_3 \\ -a_2 & 0 & -1 & k_2 \\ 0 & -1 & j\omega F & 0 \end{vmatrix} = -j\omega a_1 \begin{vmatrix} -1 & 0 & (1+j)\omega^{1/2}k_3 \\ 0 & -1 & k_2 \\ -1 & j\omega F & 0 \end{vmatrix} -$$

$$-a_2 \begin{vmatrix} 0 & j\omega b_1 & 0 \\ -1 & 0 & (1+j)\omega^{1/2}k_3 \\ -1 & j\omega F & 0 \end{vmatrix} + a_2 \begin{vmatrix} 1 & 0 & 0 \\ -1 & 0 & (1+j)\omega^{1/2}k_3 \\ -1 & j\omega F & 0 \end{vmatrix} = -j\omega a_1 \cdot (-1)\begin{vmatrix} -1 & k_2 \\ j\omega F & 0 \end{vmatrix} +$$

$$+(-j\omega a_1) \cdot (-1)\begin{vmatrix} 0 & (1+j)\omega^{1/2}k_3 \\ -1 & k_2 \end{vmatrix} + (-a_2) \cdot (1+j)\omega^{1/2}k_3 \begin{vmatrix} 0 & j\omega b_1 \\ -1 & j\omega F \end{vmatrix} +$$

$$+ a_2 j\omega F \begin{vmatrix} 1 & 0 \\ -1 & (1+j)\omega^{1/2}k_3 \end{vmatrix} = j\omega a_1 j\omega F k_2 + j\omega a_1 (1+j)\omega^{1/2}k_3 +$$

$$+ a_2(1+j)\omega^{1/2}k_3 j\omega b_1 + a_2 j\omega F(1+j)\omega^{1/2}k_3 = j\omega a_1(j\omega Fk_2 + (1+j)\omega^{1/2}k_3) +$$

$$+ a_2(1+j)\omega^{1/2}(k_3 j\omega b_1 + j\omega Fk_3) \tag{6.38}$$

The expression for input conductivity of the cathodic process:

$$Y_C = \frac{\delta i_C}{\delta U} = \frac{\Delta'L}{\Delta L} = \frac{j\omega a_1(j\omega Fk_2 + (1+j)\omega^{1/2}k_3) + a_2(1+j)\omega^{1/2}(k_3 j\omega b_1 + j\omega Fk_3)}{j\omega Fk_2 + (1+j)^{1/2}k_3}$$

As a result, one has the expression for input conductivity (admittance) of the cathodic process:

$$Y_C = j\omega a_1 + \frac{(j-1)\omega^{3/2}a_2 k_3(b_1 + F)}{j\omega k_2 F + (1+j)\omega^{1/2}k_3} = j\omega C_{dc} + \frac{1}{(j\omega C_a)^{-1} + (1-j)\omega^{3/2}A} \tag{6.39}$$

where C_{dc} is the double-layer capacitance at the cathode;

$$C_a = \frac{Fk_2}{a_2 k_3(b_1 + F)}$$ is the adsorption capacitance;

$$A = \frac{1}{2a_2(b_1 + U)}$$ is the constant of Warburg impedance.

The electric equivalent circuit for admittance of the cathodic process Eq. (6.39) consists of the cathode's double-layer capacitance C_{dc} combined in parallel with a series combination of adsorption capacitance C_a and Warburg impedance Z_W.

Therefore, the admittance (impedance) of the rhodium/oxygen electrode in the system with solid electrolyte can be represented as follows:

$$Y = \frac{1}{Z} = j\omega(C_{da} + C_{dc}) + R_c^{-1} + ((j\omega C_a)^{-1} + (1-j)\omega^{-1/2}A)^{-1} \tag{6.40}$$

An electric equivalent circuit for the admittance (6.40) that includes the resistance of the electrolyte is presented in Fig. 6.5. It follows from Eq. (6.40) that due to the assumption of independent cathodic and anodic processes, only the double-layer capacitance cannot be divided into cathodic and anodic components. The other elements of the equivalent circuit corresponding to the parallel processes (Eqs. (6.7) to (6.9)) and (Eqs. (6.23) and (6.13)) can be determined experimentally.

The equivalent circuit derived theoretically (Fig. 6.5) for the Rh/oxygen electrode is known from the literature [14, 15], and was first proposed by Povorov *et al* for describing the corrosion of the lithium electrode in a lithium battery [15, 16]. Recently the same equivalent circuit has been derived theoretically, again for a lithium electrode, by Kuznetsov *et al* [9]. The authors have shown that this model is able to describe the corrosion processes of a lithium electrode when these occur at spatially separated surfaces.

For a comparison and confirmation of the theoretical equivalent circuit presented in Fig. 6.5 in terms of a circuit that corresponds to experimental results, the set of experimental data was fitted using a frequency response analysis (FRA) program (version 4.9, see Chapter 3).
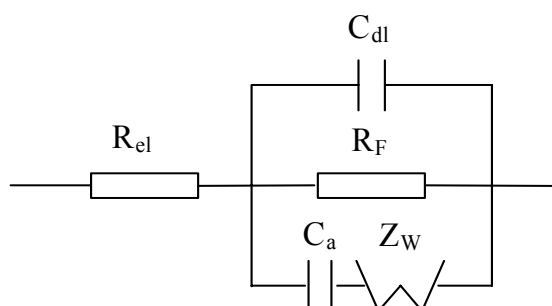
FIGURE 6.5. Theoretical electric equivalent circuit for admittance of the Rh electrode interfaced with solid electrolyte in oxygen atmosphere.

6.3 Results and discussion

6.3.1 Impedance measurements at equilibrium potential

Typical experimental impedance spectra obtained for Rh electrodes interfaced with YSZ and TiO_2/YSZ solid electrolytes at open circuit, constant oxygen partial pressure ($Po_2 = 0.5$ kPa), and constant temperature ($T = 450$ °C) are shown in Figure 6.6. For both electrochemical cells, these spectra consist of two semicircles: one at high frequencies (50 kHz - 2 kHz), which is a semicircle centered on the real axis, and the other at low frequencies (1 kHz - 0.1 kHz) having its center shifted below the real axis. The high-frequency semicircle is attributed to the bulk proper-

ties of the solid electrolyte [2, 17]. It changes when varying the working temperature, since the conductivity of the solid electrolyte changes with temperature but remains constant when applying a polarizing potential. The first semicircular arc corresponds to parallel R-C circuit elements, R being related to the electrolyte's resistance and C representing the geometric capacitance of the samples [2]. The second semicircle is related to the electrode process.

It is interesting to analyse the first semicircular arc, since it provides information about the properties of the solid electrolyte. There is a considerable difference in sizes of the first semicircle between the Rh/YSZ and Rh/TiO$_2$/YSZ system, and consequently in parameters R. This difference arises from the diverse nature of the YSZ and TiO$_2$ supports, and can be rationalized in terms of differences in grain size and grain boundary resistance between the two solids.
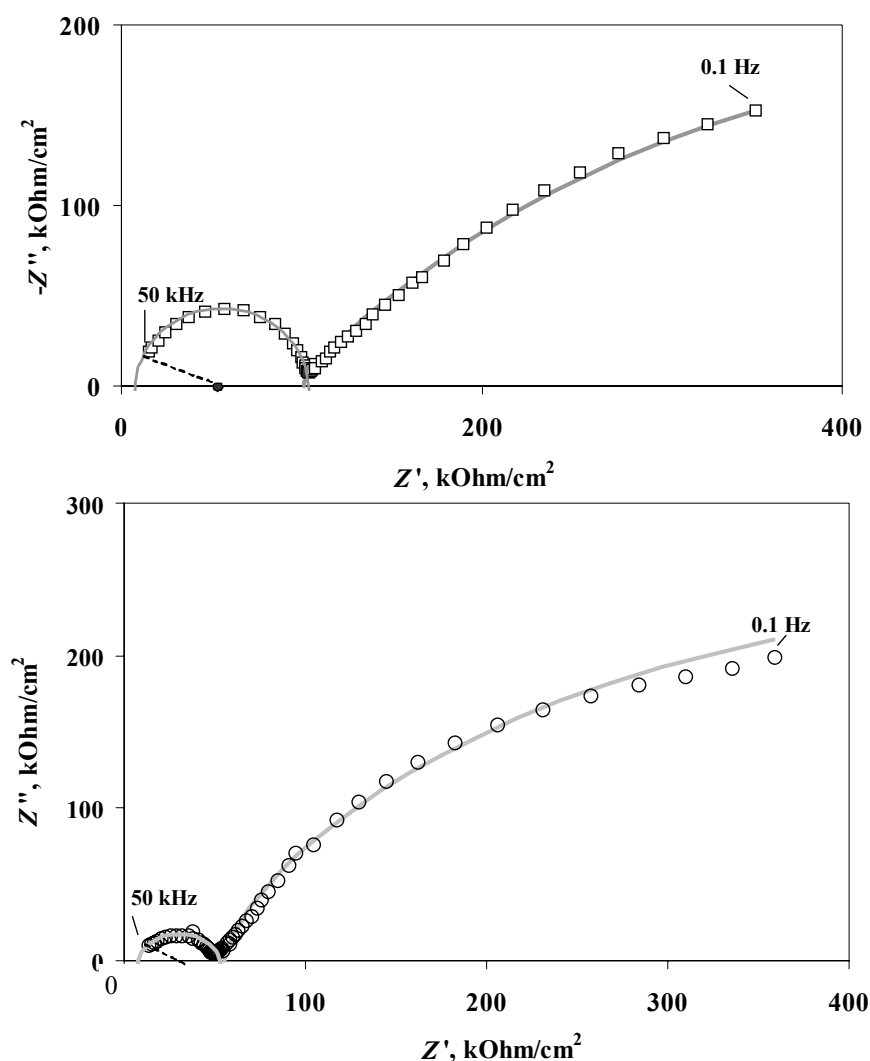
FIGURE 6.6. Experimental impedance spectra for Rh/YSZ and Rh/TiO₂/YSZ electrochemical cells (symbols) and theoretical spectra obtained with the R-C parallel elements for the first semicircle (50 kHz - 2 kHz) and the equivalent circuit (Fig. 6.5) for the second semicircle (gray line) in P_{O_2} = 0.5 kPa at T = 450 °C.

Figure 6.7 shows the experimental impedance spectra (symbols) and impedance spectra (solid lines) simulated with the theoretical equivalent circuit (Fig. 6.5), for a Rh electrode interfaced with YSZ solid electrolyte over the temperature range from 450 to 600 °C at a constant oxygen partial pressure of 0.5 kPa.

Here the simulations obtained for the first semicircular arc are not shown; this arc can again be represented by parallel *R-C* elements. One can see how the spectra change with temperature within a constant domain of frequencies (50 kHz - 0.1 Hz), reflecting an increase in rate of the electrode process with temperature. It is interesting to note that the semicircle of the electrode process can only be observed at temperatures > 400 °C. The first semicircle almost disappears at 600 °C. The results of simulation obtained when employing the equivalent circuit (Fig. 6.5) are in very good agreement with experimental data obtained in the Rh/YSZ system, and the reproducibility is satisfactory. The parameters extracted for the electric equivalent circuit for admittance of the Rh electrode in oxygen at different temperatures are listed in Table 6.2.

TABLE 6.2. Parameters of the electric equivalent circuit for admittance of the Rh electrode interfaced with YSZ in 0.5 kPa of oxygen

T, °C	R_{el}, kohm/cm^{2*}	C_{dl}, μF/cm^{2*}	R_F, kohm/cm^{2*}	C_a, μF/cm^{2*}	Z_W, kohm/cm^{2*}
450	106.0	1.57	814.3	130.1	2.94
500	37.4	1.0	146.4	133.0	1.58
550	18.1	1.2	67.2	143.4	0.83
600	11.4	1.39	21.5	130.8	0.72
E_a, kJ/mol	78.0	2.7	130	1.1	51.5

*geometric surface area of the electrode

FIGURE 6.7. Experimental impedance spectra (symbols) and theoretical spectra obtained with the equivalent circuit (Fig. 6.5) (solid lines) for a Rh electrode on YSZ. P_{O_2} = 0.5 kPa, T= 450 - 600 °C.

As in the Rh/YSZ system (Po_2 = 0.5 kPa), impedance measurements were also performed at different temperatures (T = 500 - 600 °C) in the Rh/TiO$_2$/YSZ electrochemical cell. Typical experimental spectra (symbols) and simulated results (solid lines) are shown for the Rh/TiO$_2$/YSZ electrode in Fig. 6.8. The spectra change with temperature.
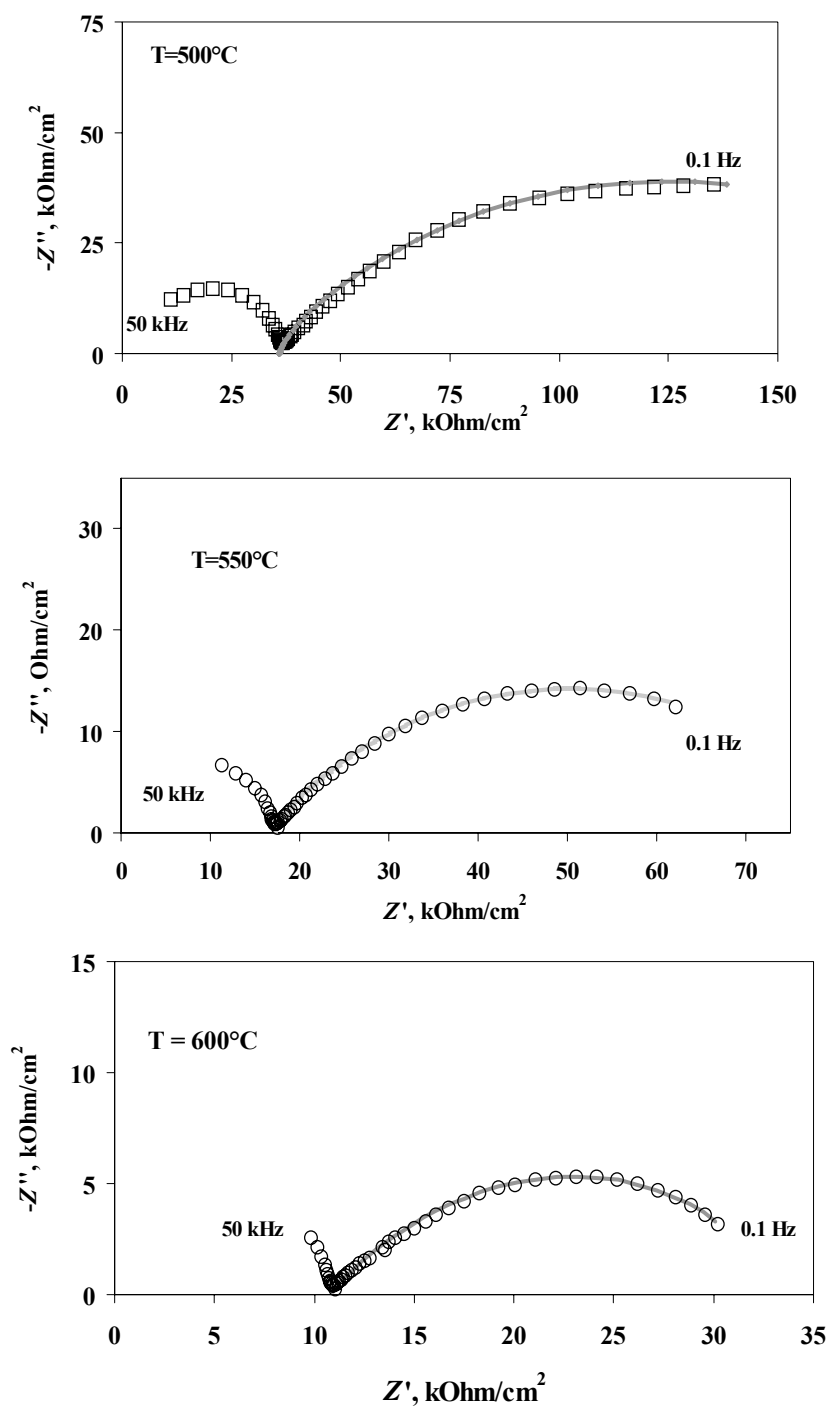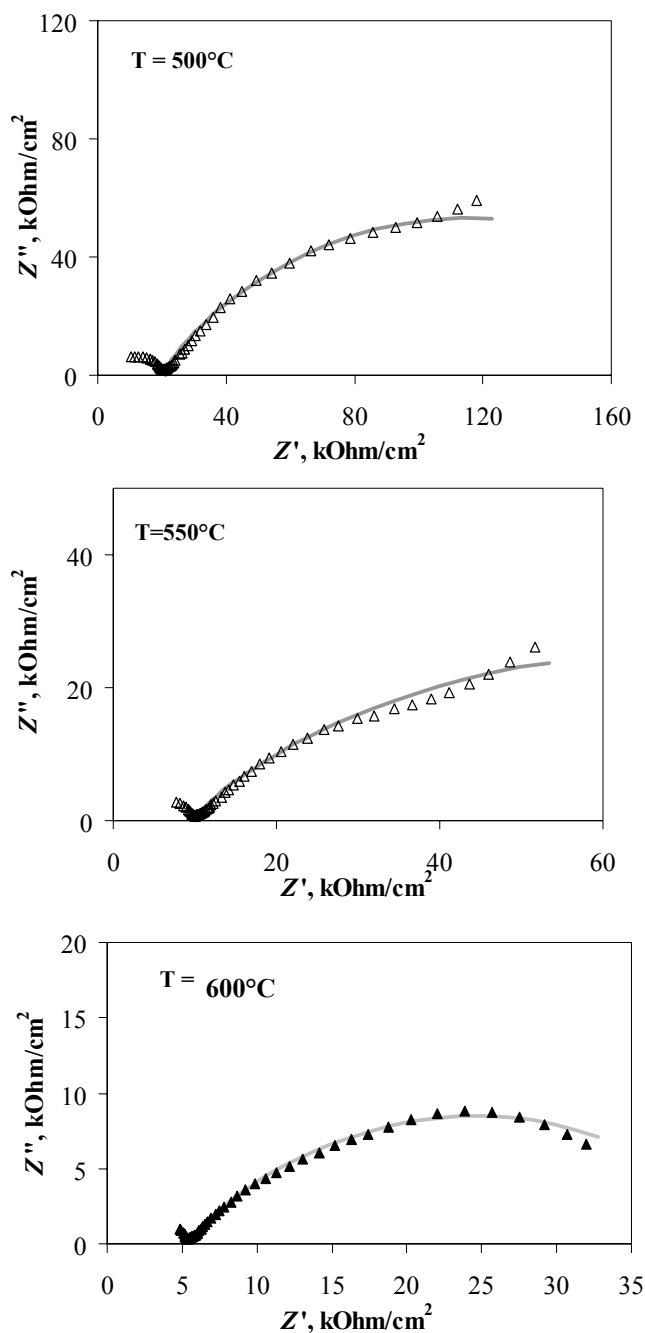

FIGURE 6.8. Experimental impedance spectra (symbols) and theoretical spectra obtained with the equivalent circuit (Fig. 6.5) (solid lines) for a Rh electrode on a TiO$_2$/YSZ support. Po_2 = 0.5 kPa, T = 450 - 600 °C.

Results and discussion

The theoretical results that were obtained with the equivalent circuit (Fig. 6.5) are in satisfactory agreement with the experimental spectra. The parameters of the electric equivalent circuit (Fig. 6.5) for admittance of the Rh electrode interfaced with TiO_2 are shown in Table 6.3.

TABLE 6.3. Parameters of the electric equivalent circuit for admittance of the Rh electrode interfaced with TiO_2/YSZ in 0.5 kPa oxygen

T, °C	R_{el}, kohm/cm^2	C_{dl}, μF/cm^2	R_F, kohm/cm^2	C_a, μF/cm^2	Z_W, kohm/cm^2
450	55.41	2.78	1200.4	123.6	80
500	22.40	2.49	447.38	125.3	31.3
550	10.93	2.22	167.14	122.8	14.4
600	5.22	2.31	35.45	130.5	9.35
E_a, kJ/mol	82.3	6.6	127.0	1.5	76.1

The following observations were made when analyzing and comparing the impedance parameters of the two electrochemical cells Rh/YSZ and Rh/TiO_2/YSZ:

Total electrolyte resistance R_{el} - determined as the intersection of the high frequency part of the second semicircle with real axis. It decreases with increasing temperature in both systems. The total resistance of Rh/TiO_2/YSZ is smaller than that of Rh/YSZ. The apparent activation energies of the electrolyte resistance are 78.0 kJ/mol and 82.3 kJ/mol for Rh/YSZ and Rh/TiO_2/YSZ, respectively (Tables 6.2 and 6.3).

Double-layer capacitance C_{dl} - related to the electric double layer at the Rh electrode. The values of C_{dl} at Rh/TiO_2 are higher by a factor of two than those at Rh/YSZ. No distinct temperature dependence could be observed; it appears that C_{dl} remains rather constant while the temperature increases.

Charge transfer resistance R_F - decreases with increasing temperature at both electrodes, Rh/YSZ and Rh/TiO_2, which implies increasing reaction rates of the anodic process. The value of R_F obtained by fitting of the experimental data is almost twice larger for Rh/TiO_2 than for Rh/YSZ, while the activation energies are quite similar at the two electrodes (Tables 6.2 and 6.3). Both the charge transfer resistance and the activation energy results are in good agreement with

values derived from polarization measurements at Rh electrodes interfaced with YSZ and TiO_2 (Chapter 5). On the basis of this parameter, the exchange current densities will be evaluated below.

Adsorption capacitance C_a - at the equilibrium potential, it largely corresponds to the process (Eq. (6.7)) of dissociative oxygen adsorption at the gas-exposed Rh electrode surface. An adsorption capacitance may also be created by O^{2-} species from the solid electrolyte adsorbing at the gas-exposed catalyst surface, where they are equilibrated electrostatically by their mirror charges in the metal. These oxygen ions at the surface are in equilibrium with oxygen ions in the solid electrolyte (see Chapter 2, Fig. 2.4). At both electrodes, the C_a values derived are much higher than the values of double-layer capacitance. At the same time, when comparing the C_a values themselves it is clear that they are almost identical in the Rh/YSZ and Rh/TiO_2 systems. It also appears that the adsorption capacitance is independent of temperature over the range from 450 to 600 °C.

Mass-transfer resistance Z_W (Warburg impedance) - in the model described above, this quantity is related to the process that is limited by interfacial diffusion of atomic oxygen from the gas-exposed surface area to the electrochemical reaction sites where the charge-transfer process takes place. As expected, this parameter decreases with increasing temperature. The difference between the two electrodes is significant. The high Warburg impedance found for Rh/TiO_2 may be related to the low ionic conductivity of titania. The activation energies of the Warburg impedance are shown in Tables 6.2 and 6.3.

From the description of faradaic impedance [1, 11, 12], it is clear that measurements are made while the working electrodes are at equilibrium at the mean dc potential. Since the amplitude of the sinusoidal perturbation is small, one can use the linearized i-η characteristics to describe the electrical response to the departure from equilibrium caused by this perturbation:

$$R_F = \frac{RT}{nFi_0} \tag{6.41}$$

so that it is easy to evaluate the exchange current densities i_0 from impedance spectra. The charge-transfer resistance (Tables 6.2 and 6.3, fourth columns) was used to calculate i_0. The i_0 values obtained for the Rh/YSZ and Rh/TiO_2/YSZ systems are given in Table 6.4. It can be seen that the exchange current densities are lower for Rh interfaced with TiO_2 at all temperatures

investigated. There is good agreement with the values calculated from steady-state polarization measurements using the low-field approximation of the Butler-Volmer equation (Table 5.1, Chapter 5).

TABLE 6.4. Exchange current densities at the Rh electrode on YSZ and TiO$_2$/YSZ evaluated from the impedance measurements at an oxygen partial pressure of 0.5 kPa

T, °C	Rh/YSZ i_0, μA/cm^2	Rh/TiO$_2$/YSZ i_0, μA/cm^2
450°	0.18	0.13
500	1.08	0.37
550	2.50	1.06
600	8.33	5.30

The charge transfer resistance, R_F, evaluated from experimental spectra at the equilibrium potential for Rh/YSZ is lower than that for Rh/TiO$_2$/YSZ. This is in agreement with the steady-state polarization measurements, and shows that Rh/TiO$_2$/YSZ is much more polarizable than Rh/YSZ. The exchange current densities extracted from impedance spectroscopy are similar to the i_0 obtained from steady-state polarization measurements. Arrhenius plots of exchange current densities evaluated, both from the impedance measurements and from the i-U_{WR} curves in the low-field approximation of the Butler-Volmer equation are shown for Rh/YSZ and Rh/TiO$_2$/YSZ electrodes in Fig. 6.9. It is seen that the agreement between values obtained with the two techniques is satisfactory. The exchange current densities are always much smaller at the Rh/TiO$_2$ interface. This is in good accord with the results of electrochemical promotion in the Rh/YSZ and Rh/TiO$_2$/YSZ systems, where at the same applied current a much higher potential was observed for Rh on TiO$_2$ than for Rh on YSZ (see Chapter 5).

The results obtained in the present chapter are in good agreement with the theoretical model proposed, and also with the steady-state polarization measurements described in the preceding chapter (Chapter 5). This means that at the equilibrium potential, the cathodic and anodic process occur in parallel at Rh/YSZ and Rh/TiO$_2$/YSZ, and may be described by the schemes of Eqs. (6.7 - 6.9) and (6.22, 6.23). The cathodic process is limited by a mass-transfer process con-

sisting of interfacial diffusion of atomic oxygen to electrochemically reactive sites, the anodic process is limited by the charge-transfer step.
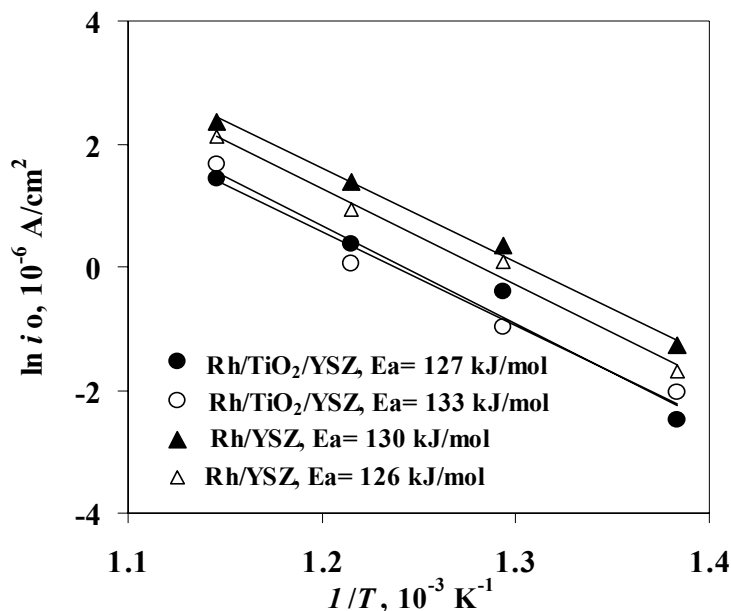

FIGURE 6.9. Arrhenius plots of the exchange current densities calculated for Rh/YSZ (▲: impedance measurements; △: low-field approximation) and Rh/TiO$_2$/YSZ (●: impedance measurements; ○: low-field approximation). Oxygen partial pressure: 0.5 kPa.

6.3.2 Impedance measurements under polarization

Useful information about the kinetics of the electrode process and about the characteristics of the system itself can be gained from impedance measurements under polarization. It is clear that at overpotentials of $|\eta| > 10$ mV, only either the anodic or the cathodic process will take place at the Rh electrode. Consequently, the theoretical equivalent circuit (Fig. 6.5) then corresponds, either to oxygen ion oxidation or to oxygen reduction.

Under positive polarization in the system Rh/solid electrolyte, the process of backspillover occurs in addition to oxygen evolution (Eqs. (6.22) and (6.23)). This mechanism is well known, and plays an important role in the electrochemical promotion of catalysis [18]. According to the theory of electrochemical promotion, applied positive potentials lead to the oxidation of oxygen ions at the three-phase boundary, and also to some charge injection into the metal surface exposed

to the gas phase. This positive charge appearing on the surface will cause migration of oxygen ions from the YSZ and formation of an overall neutral double layer at the metal/gas interface, an "effective electrochemical double layer". This mechanism includes a charge-transfer step, a mass-transfer step, and the formation of two double layers. Therefore, the equivalent circuit of Fig. 6.5 can be used for describing the Rh/solid electrolyte systems under positive polarization.

a) Charge transfer leading to the formation of atomic oxygen at the Rh-YSZ-O_2 interface, its recombination, and its desorption to the gas phase (Eqs. (6.22) and (6.23)), this step corresponds to the charge-transfer resistance (R_F) (Fig. 6.5);

b) diffusion of O^{2-} from YSZ to the gas-exposed metal surface, a process that may be described by a Warburg impedance (Z_W);

c) oxygen ion adsorption on the gas-exposed metal surface and formation of a double layer between metal and gas phase, this step may be described by an adsorption capacitance (C_a).

The steps b) and c) correspond to the backspillover mechanism [18].

Under <u>negative polarisation</u> the reduction of oxygen will include the following steps, similar to the situation at the equilibrium potential:

a) dissociative adsorption of atomic oxygen at the gas-exposed Rh surface, a process that may be described by an adsorption capacitance (C_a) (Fig. 6.5);

b) diffusion of oxygen atoms to the three-phase boundary (MEG) and further to the two-phase boundary Rh/solid electrolyte, a process that may be described by a Warburg impedance (Z_W);

c) charge transfer at the Rh/YSZ interface, a process that may be described by a charge-transfer resistance (R_F).

In both the anodic and the cathodic process, the electric double layer at the metal/solid-electrolyte interface is described by a double-layer capacitance C_{dl}.

Figure 6.10 shows experimental impedance spectra recorded under anodic and under cathodic polarization at a Rh electrode interfaced with YSZ, from which the electrolyte resistance that remains constant at any given temperature, and amounts to 11.4 kohm/cm^2 at 600 °C, has already been subtracted. The experimental spectra coincide with spectra following from the theoretical model and the theoretical equivalent circuit (Fig. 6.5) (solid lines in Figs. 6.10 A, B). Note that impedance measurements under polarization were carried out at different temperatures between 450 and 600 °C. For each temperature, good agreement between the experimental and

theoretical results was found, which implies that both the anodic and the cathodic process on Rh/ YSZ is readily described by the equivalent circuit proposed.
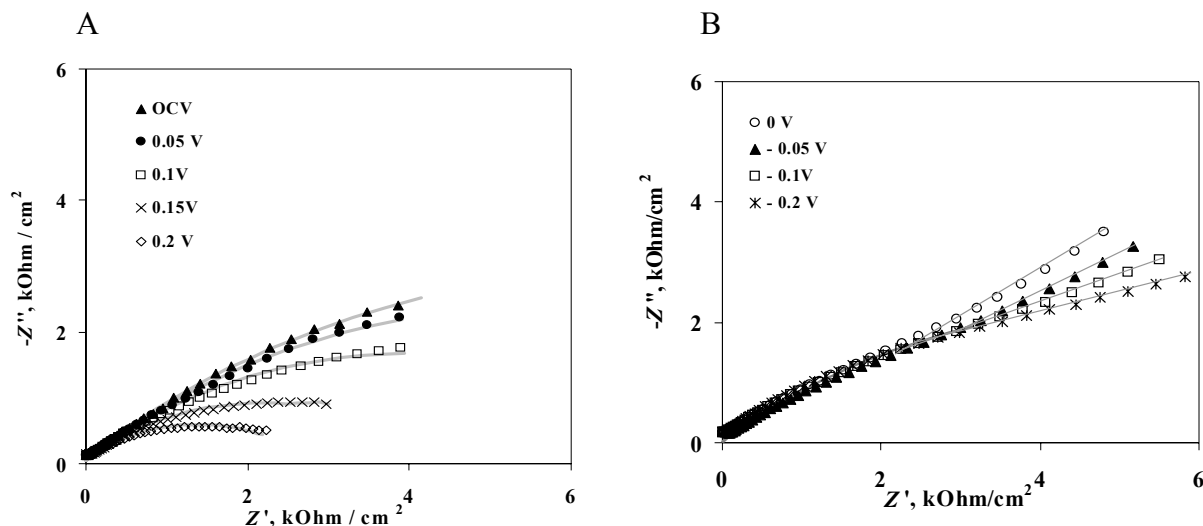

FIGURE 6.10. Impedance spectra obtained for a Rh electrode interfaced with YSZ at $T = 600$ °C, $Po_2 =$ 0.5 kPa at different positive (A) and negative (B) catalyst potentials. Symbols correspond to experiment, lines to theoretical prediction.

The parameters of impedance of the Rh electrode interfaced with YSZ that were calculated by using the theoretical equivalent circuit (Fig. 6.5) are summarized in Fig. 6.11. They are shown as functions of applied potential.

The parameters of the experimental electric equivalent circuits for admittance of the Rh electrode at different potentials are in good agreement with the mechanisms suggested to be valid under anodic and cathodic polarization (Fig. 6.11). It is interesting to comment on the behavior of double-layer and adsorption capacitance of the Rh electrode (Fig. 6.11, B). The double-layer capacitance slightly decreases with increasing positive and negative potential, while the adsorption capacitance significantly increases with increasing positive, and remains constant with increasing negative polarization.

In the work of Vayenas and co-workers [3, 18] exploring the origins of electrochemical promotion, the EIS technique had provided evidence for the formation of an "effective double layer" across the entire gas-exposed electrode surface (section 6.1.2). The capacitance of this metal/gas double layer was found to be much higher (order of magnitude: 200 $\mu F/cm^2$; in the present work, values between 100 and 300 $\mu F/cm^2$ were found) than that of the metal/solid-elec-

trolyte double layer (0.1 - 10 $\mu F/cm^2$ [3]; in the present work, C_{dl} values between 0.4 and 2 $\mu F/cm^2$ were found).

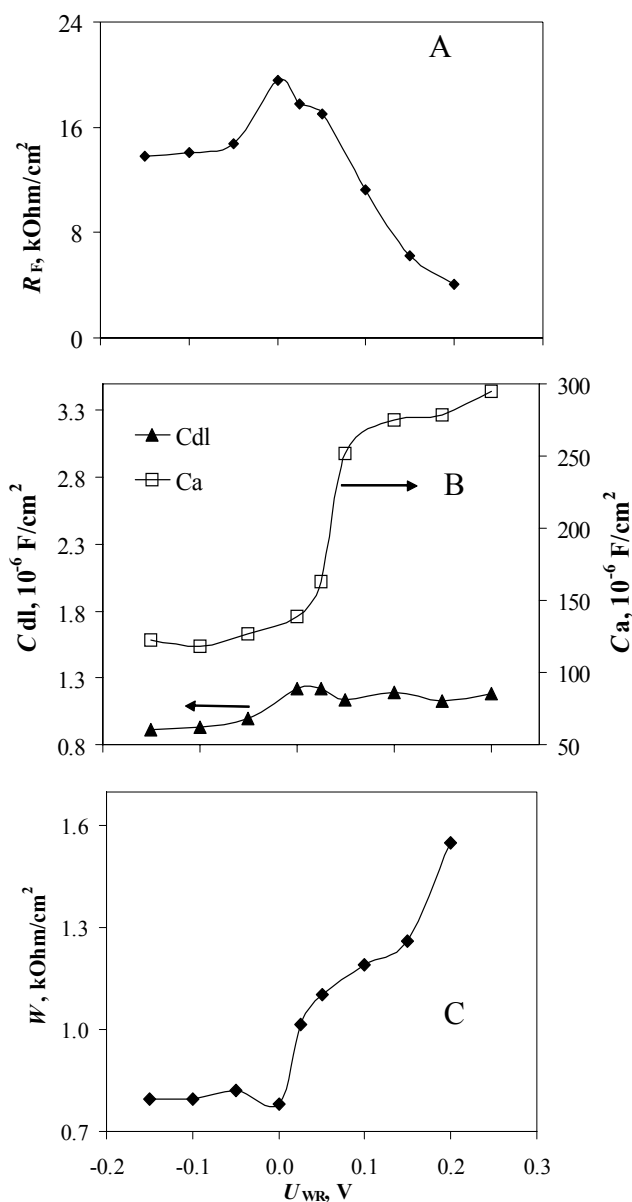**FIGURE 6.11. Parameters of the electric equivalent circuit for admittance of the Rh electrode in the system with YSZ. Po$_2$ = 0.5 kPa, T = 600 °C.**

The values of both capacitances are known to be related to the gas-exposed electrode surface area, N_G, and to the "surface area" of the three-phase boundary, N_{tpb}, by Eq. (6.3). For the case of Rh/YSZ, it can be written as:

$$\frac{N_{tpb}}{N_G} = \frac{C_{dl}}{C_a} \tag{6.42}$$

This relation [18] allows one to calculate the tpb length on the basis of impedance measurements. Typical values of N_{tpb} are of the order of 10^{-9}-10^{-10} mol metal/cm^2 electrolyte, *ie*, typically by a factor of 10^2 to 10^3 smaller than N_G. The parameter N_{tpb} expresses the number of moles of electrode metal in contact, both with the solid electrolyte and with the gas phase. More commonly the length of the tpb is normalized with respect to surface area, *S*, of the electrolyte. This normalized tpb length, denoted $N_{tpb,n}$, is N_{tpb}/S, its values are given in Table 6.5 for Rh/YSZ catalyst as a function of applied potential. These values correspond to a "length", l_{tpb}, of several km per cm^2 of solid electrolyte.

TABLE 6.5. Normalized tpb lengths, $N_{tpb,n}$, in the Rh/YSZ system as a function of the applied potential; $T = 600$ °C, $Po_2 = 0.5$ kPa

U_{WR}, V	$N_{tpb,n}$, 10^{-10} mol Rh/cm^2
-0.15	6.118
-0.10	5.99
-0.05	6.57
0.00	6.7
0.025	5.7
0.05	3.42
0.10	3.3
0.15	3.08
0.20	3.06

Results and discussion

Increasing potential leads to increasing mass-transfer resistance. This is understandable, since positive polarization enhances the electrode's charge density and necessitates more negative charges neutralizing this charge. Negative polarization remains without influence on the Warburg impedance, which confirms limitation of the process by mass transfer.

A schematic representation of the state of the Rh/YSZ and Rh/O$_2$ interfaces at open circuit and under positive polarization is shown in Fig. 6.12. Under these conditions the catalyst surface is populated by two types of oxygen: oxygen adsorbed from the gas phase O$_{(MG)}$ (Eq. (6.7), not shown in Fig. 6.12) and backspillover oxygen from the solid electrolyte (O^{2-}). The amount of O^{2-} on the catalyst surface will depend on the applied potential. At this point the question arises how O^{2-} can leave the catalyst surface. It can be suggested that O^{2-} is slowly oxidized to atomic oxygen which can leave the surface after its recombination to molecular oxygen.
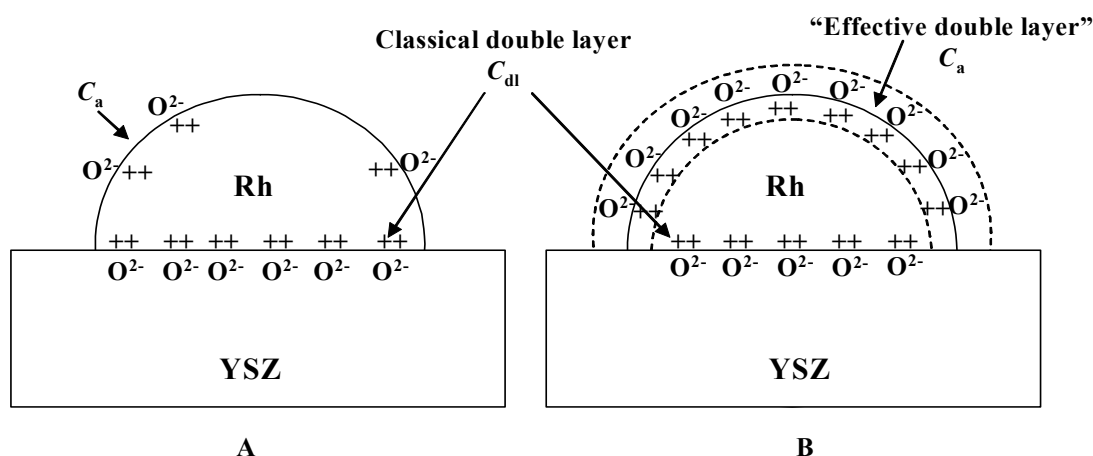
FIGURE 6.12. Schematic representations of the state of the Rh/YSZ and Rh/O$_2$ interfaces and of the corresponding capacitances. A: open-circuit conditions; B: positive polarization.

Impedance spectra recorded with the Rh/TiO$_2$/YSZ electrochemical cell under positive and negative polarization from which again the electrolyte resistance has already been eliminated are shown in Fig. 6.13. This figure only shows experimental spectra. An application of theory to this electrode was difficult, insofar as an extra semicircle here appears in the high-frequency region. Positive potentials lead to a dramatic decrease in size of the spectrum over the entire frequency

range. This is mainly attributed to a decrease in charge-transfer resistance, similar to what is seen at the Rh/YSZ electrode.

A   B

FIGURE 6.13. Impedance spectra of the Rh electrode interfaced with TiO$_2$/YSZ at T = 600 °C, Po_2 = 0.5 kPa at different positive (A) and negative (B) catalyst potentials.

Negative polarization leads to changes in shape of the spectra, only in the high-frequency region. The spectra no longer have the shape of a simple semicircle centered below the real axis, as was the case at open circuit in the present system, and at open and closed circuit in the Rh/YSZ system.
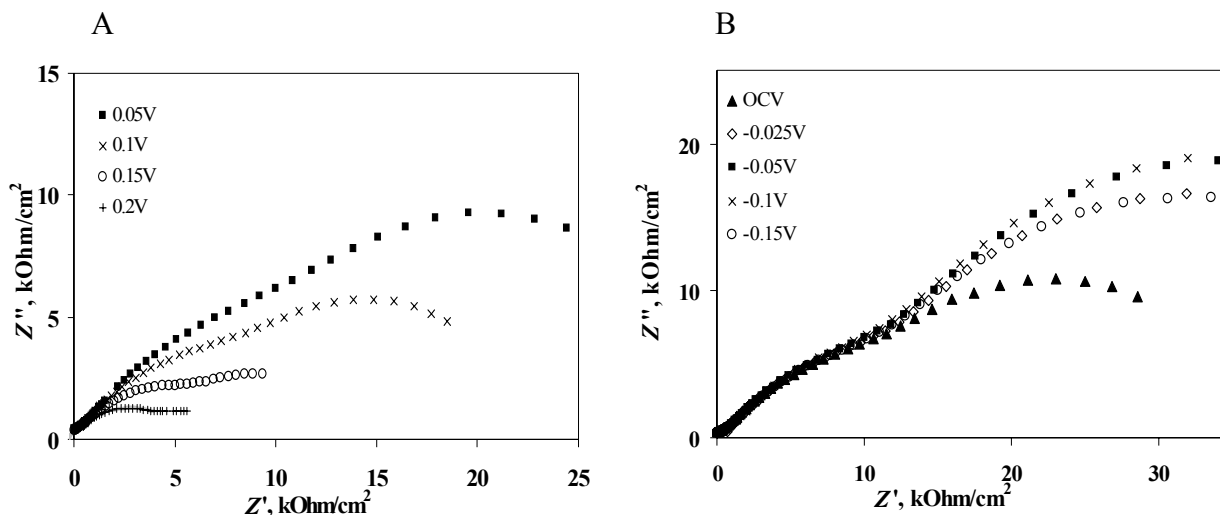
The good agreement between theoretical model and experiment that was observed for the Rh catalyst electrode interfaced with YSZ does not exist in the case of Rh/TiO$_2$/YSZ. At open circuit theory and experiment coincide, but at closed circuit theory is unable to describe the real process. This implies that the system becomes more complex when a potential is applied. The mixed ionic-electronic conductivity of TiO$_2$ which could be modified by current flow/applied potential leading to changes in electrode mechanism would appear plausible as an explanation. Another explanation would be the spread of the three-phase boundary across the electrolyte/gas interface (EG) that had already been mentioned earlier. According to literature data, if a solid electrolyte possesses both ionic and electronic conductivity, the electrochemical process can take place, not only at the metal/electrolyte boundary but also at the electrolyte/gas interface. A third explanation for appearance of the second, potential-dependent semicircle is related to the backsp-

illover of ionic oxygen species. Such a behavior had already been observed in the Pd/YSZ system (see section 6.1.2) at high positive U_{WR} [3]. The concentration of backspillover oxygen at the Rh surface interfaced with TiO$_2$/YSZ is much higher than its concentration at Rh/YSZ. This explanation is consistent, too, with the observation that electrochemical promotion of ethylene oxidation is more efficient in the Rh/TiO$_2$/YSZ system than in the Rh/YSZ system (see later in Chapter 8). The effect of polarization on the Rh/TiO$_2$/YSZ system will merit further detailed examination.

6.4 Conclusions

In the present chapter an impedance model of the Rh/oxygen electrode in contact with solid electrolytes has been designed. The model is based on steady-state polarization data that had been discussed in the preceding chapter (Chapter 5).

1. The impedance model set up for the oxygen exchange processes at Rh electrodes interfaced with YSZ and TiO$_2$/YSZ was confronted with experimental results. For this purpose, electrochemical impedance spectra were recorded at T = 450 - 600 °C in P_{O_2} = 0.5 kPa at open circuit and under polarization. Experimental results for the equilibrium process O^{2-}/O$_2$ at Rh/YSZ and Rh/TiO$_2$/YSZ are in good accord with theoretical impedance representations of the reaction mechanism.

2. At the equilibrium potential, two processes take place: oxygen evolution and oxygen reduction. In the cathodic process, dissociative adsorption at the gas-exposed metal surface, interfacial diffusion of atomic oxygen, and a two-electron transfer step are considered. The rate-limiting step is interfacial diffusion of atomic oxygen from the metal/gas (MG) interface to the electrochemically reactive sites. In the anodic process, the first stage is a two-electron transfer step, which is followed by oxygen recombination and desorption to the gas phase. The rate-determining step is charge transfer itself.

3. From both the impedance and the steady-state polarization results, it is clear that the exchange current densities are much lower at Rh/TiO$_2$/YSZ than at Rh/YSZ, which implies higher polarizability of the former system. In general, the behavior of the two systems is quite similar, and at the equilibrium potential and/or in the low-polarization region, they can be described by the same reaction mechanism.

4. The equivalent circuit proposed is also applicable to the processes of oxygen evolution and oxygen reduction in the Rh/YSZ system under polarization. Under anodic polarization the reaction mechanism may in addition to the charge-transfer step include migration of oxygen ions and formation of an "effective double layer" at the gas-exposed metal surface. This is manifest from high values of capacitance (>100 $\mu F/cm^2$), which increase with increasing positive U_{WR}. Under polarization, the impedance of the Rh/TiO$_2$/YSZ electrode becomes more complex than that of Rh/YSZ, and requires further investigations. The conclusions drawn from the impedance analysis under positive polarization are well supported by those obtained by Vayenas and co-workers [3].

6.5 References

1.   A. J. Bard and L. R. Faulkner, *Electrochemical methodes. Fundamentals and applications* John Wiley & Sons, Inc. (2001).

2.   C. Deportes, M. Duclot, P. Fabry, J. Fouletier, A. Hammou, M. Kleitz, E. Siebert, and J.-L. Souquet, *Electrochimie des solides* Press Universitair de Grenoble, Grenoble (1994).

3.   A. D. Frantzis, S. Bebelis, and C. G. Vayenas, *Solid State Ionics,* **136-137** (2000) 863.

4.   C. G. Vayenas, S. Bebelis, and S. Ladas, *Nature,* **323** (1990) 625.

5.   J. Pritchard, *Nature,* **343** (1990) 592.

6.   T. Badas, Thesis, University of Patras, Patras, (2003).

7.   H. Gerischer, *Z. Phys. Chem.,* **198** (1951) 216.

8.   M. S.-R. a. J. H. Sluyters, in *Electrochemical Chemistry,* Vol. 4 A. J. Bard, ed.), Marcel Dekker, New York, (1970), p. 68.

9.   A. A. Kuznetsov and V. V. Netesa, *Ukr. Chim. Journal,* **65** (1999) 126

10.   A. A. Kuznetsov, *Elektrokhimiya,* **29** (1993) 23

11.   B. M. Grafov and E. A. Ukshe, *Electrochemical AC circuits* Nauka, Moscow (1973).

12.   B. M. Grafov and E. A. Ukshe, *The kinetics of complex electrochemical reactions* Nauka, Moscow (1981).

13.   A. A. Kuznetsov, *Zashch. Met,* **25** (1989) 585.

References

14. L. S. Kanevskiy, M. B. Avdolyan, and T. L. Kulova, *Elektrokhimiya,* **31** (1995) 383.

15. Y. M. Povorov and I. V. Vorob'eva, *Elektrokhimiya,* **18** (1982) 1693.

16. Y. M. Povorov, L. A. Beketaeva, and I. V. Vorob'eva, *Elektrokhimiya,* **19** (1983) 586.

17. V. N. Chebotin and M. V. Perfilev, *Electrochemistry of solid electrolytes* Khimiia Publ. House, Moscou (1978).

18. C. G. Vayenas, S. Bebelis, C. Pliangos, S. Brosda, and D. Tsiplakides, *Electro-chemical activation of catalysis. Promotion, Electrochemical promotion, and metal-support interaction.* Kluwer Academic/Plenum Publishers, New York (2001).

CHAPTER 7 **Promotion of Rh catalysts:** Open-circuit ethylene oxidation

Ethylene oxidation on Rh catalysts exhibits a sudden transition from a region of high to a region of low reaction rates as the oxygen partial pressure increases above a certain critical value. This sudden transition is accompanied by the formation of a rhodium surface oxide that is responsible for deactivation of the catalyst. A model explaining this macroscopic deactivation of Rh catalysts was proposed and illustrated with results obtained at Rh(40 nm)/YSZ and Rh(40 nm)/TiO$_2$/YSZ catalysts. The Rh/YSZ catalysts have a finite catalytic activity towards ethylene oxidation, only in reducing feed compositions, while on Rh/TiO$_2$/YSZ catalysts high reaction rates of C$_2$H$_4$ oxidation can be maintained over a wide range of oxygen partial pressures. Deactivated Rh/TiO$_2$/YSZ catalysts are readily reactivated by changing the gas composition from oxidizing to reducing, while deactivated Rh/YSZ catalysts remain inactive under the same conditions. The greater ease of modification of the catalytic activity observed for Rh on an interlayer of TiO$_2$ correlates with a greater ease of reduction of this Rh surface oxide to metallic rhodium. The phenomenon may be inter-

preted, either by strong electronic-type metal-support interactions or by a self-driven wireless electrochemical promotion mechanism.

7.1 Introduction

The oxidation of ethylene to CO_2 on rhodium-based catalysts has been extensively investigated in the instance of Rh dispersed on different supports as well as of polycrystalline Rh films interfaced with ZrO_2 (8 mol% Y_2O_3) solid electrolyte [1-4]. It was demonstrated that the catalytic performance of the rhodium catalysts depends on their oxidation state [3-6], rhodium metal being much more active than rhodium oxide. Detailed investigations of the catalytic activity of Rh in its different oxidation states were performed in the group of electrochemical engineering at EPFL, by I. Bolzonella, in the instance of propylene combustion under open-circuit and electrochemical promotion conditions [7]. It was demonstrated that this reaction strongly depends on the oxidation state of Rh, and it was possible to distinguish three domains of catalyst operation in terms of the reaction rates, r, as functions of oxygen partial pressures, P. The domain of low reaction rates corresponds to catalyst surfaces in the oxide form. The second domain where the catalyst surface is between its oxidized and reduced state was called a transition domain. The third domain begins where the abrupt increase in reaction rate occurs. In this domain the rhodium catalyst surface is completely reduced. On the basis of these observations, a reaction model was proposed [7], and this model is described in detail in Chapter 2, section 2.3 of the present thesis. This model nicely explains the mechanism of propylene or ethylene oxidation on Rh catalysts, and it also explains the reasons for the dramatic decrease or increase in reaction rate. However, it does not define a mechanism for surface deactivation nor any parameters that would be responsible for it. Moreover, the model is unable to explain the hysteresis of reaction rates very often observed at the Rh catalysts.

In this chapter, first a simple phenomenological model describing and qualitatively discussing the sudden transition of the Rh catalyst from high to low activity will be presented [8]. By "phenomenological", it is intended to say that the model does not account for details of the microscopic processes occurring in the system, it merely describes the process globally and in a generic manner. Despite this restriction, the model is able to establish a link between the sudden transition from high to low reaction rates and the growth of a new surface structure. As an interesting consequence, the predicted hysteresis in the r-P characteristics is discussed.

The model will then be illustrated and tested using experimental results for ethylene oxidation on Rh/YSZ and Rh/TiO$_2$/YSZ catalysts. It will be shown that the catalytic activity and stability of Rh can be dramatically enhanced by interfacing it with a layer of TiO$_2$ deposited on the YSZ solid electrolyte used as support.

7.2 Theory

7.2.1 Generic model for a macroscopic deactivation of surface processes

During the oxidation of propylene [7] or ethylene [3, 4], rhodium catalysts exhibit the following behavior: the reaction rate r smoothly increases as a function of the external control parameter P until this reaches a critical value P^{crit}, at which point the reaction rate suddenly drops and goes toward zero with increasing P (Fig. 7.1). This drop marks the transition between ranges of high and low reaction rates. Thus, such systems exhibit what may be considered a generalized phase transition. In the oxidation of C$_2$H$_4$ on rhodium catalysts, the reaction rate r is the rate of production of CO$_2$, the external control parameter is the partial pressure of O$_2$ in the feed gas stream.

In parallel with the sudden drop in reaction rate r, the growth of a surface structure $\Sigma(p)$ not present prior to this transition is observed. The growth of this surface structure is responsible for the abrupt decrease in reaction rate r with increasing oxygen partial pressure P. The mechanism of formation of this structure is a microscopic one, whereas the deactivation effect is macroscopic. Apart from the example of ethylene oxidation, a broad sample of systems are known which exhibit surface processes resulting in a sudden transition from high to low reaction rates as a function of external parameters. Typical examples are certain electrolytic processes, several systems in heterogeneous catalysis (oxidation of CO and C$_2$H$_4$ on Pt) [9], cases of electrochemical promotion of catalysis [10], and metal passivation [11].
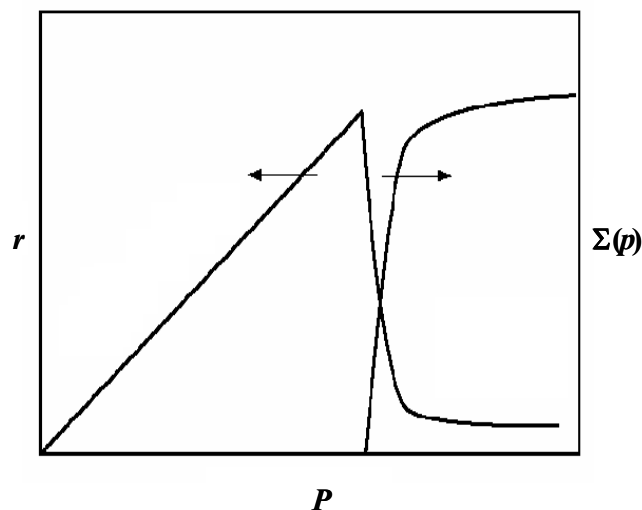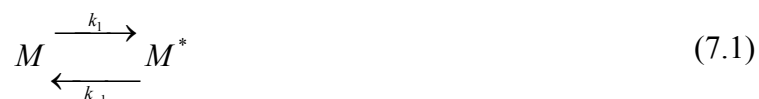
FIGURE 7.1. Generic *r-P* characteristics.

Definition of the model

Consider a surface on which a number L of sites exist. Each of these sites can be in one of two states: activated or nonactivated. The transformation between these two states is a microscopic process symbolized by the following reaction equation:

$$M \xrightarrow[\;k_{-1}\;]{\;k_1\;} M^*$$ (7.1)

where M is a nonactivated site and M^* is an activated site.

An activated site will contribute to the reaction rate r by producing a product C from a reactant R, and then return to the nonactivated state:

$$R + M^* \xrightarrow{\;k_2\;} M + C$$ (7.2)

The product C is supposed to leave the surface, and to interact no longer with the process considered. Transformation (7.2) can take place, only if the activated site M^* does not belong to the structure $\Sigma(p)$ deactivating the surface. In the following, sites belonging to the structure $\Sigma(p)$ will be called deactivated sites. The fraction p of activated sites changes as a function of time t:

Theory

$$\frac{dp}{dt} = k_1(1-p) - k_{-1}p - k_2\left[p - P(p)\right] \tag{7.3}$$

By introducing $\tau = k_2 t$ as the product of time t and reaction rate constant k_2, (1.3) can be rewritten as:

$$\frac{dp}{d\tau} = \tilde{k}_1(1-p) - \tilde{k}_{-1}p - \left[p - P(p)\right] \tag{7.4}$$

where $\tilde{k}_1 = k_1/k_2$ and $\tilde{k}_{-1} = k_{-1}/k_2$. The discussion can then be reduced to two parameters.

Macroscopic deactivation

The emergence and growth of the deactivating surface structure $\Sigma(p)$ is specific to the system considered. Very often a reaction (7.2) becomes more and more hindered by the presence of increasing numbers of nearest neighbors among the active sites M^*. The exact form of $\Sigma(p)$ will depend on the nature of the bond between the nearest neighbors. In order to keep the discussion sufficiently general, it is proposed to identify this macroscopic structure with the infinite cluster as defined in percolation theory [12]. Under these assumptions, fraction p varies with τ as:

$$\frac{dp}{d\tau} = \tilde{k}_1(1-p) - \tilde{k}_{-1}p - \sum_s sn_s(p) \tag{7.5}$$

where n_s is the normalized cluster number defined as:

$$n_s = \lim_{L \to \infty} \frac{N_{s-clusters}}{L} \tag{7.6}$$

A cluster is defined as a group of neighboring occupied sites, and s is the cluster size (given as the number of sites belonging to the cluster). In the following, the infinite cluster will be used as a prototype for the deactivating structure $\Sigma(p)$.

Starting from Equation (7.5), the *r-p* characteristics can be determined. Considering (7.2), the reaction rate r is given by:

$$r = k_2 \sum_s sn_s(p) \tag{7.7}$$

The $r - \tilde{k}_1$ and $r - \tilde{k}_{-1}$ characteristics

By definition, the $r - \tilde{k}_1$ characteristics express the stationary r flux as a function of $\tilde{k}_1$. Stationary solutions are directly calculated by combining (7.5) and (7.7), and adding $\dot{p} = 0$. For a discussion, these solutions can be represented graphically as shown in Figure 7.2, A. Depending on the parameters $\tilde{k}_i$ (i = 1, -1), either one stable solution or one unstable and two stable solutions exist for $r(\tilde{k}_1)$. Which of the stable solutions is reached by the system will depend on the initial conditions and, therefore, on its history. The system is said to exhibit bistable behavior. It follows that the $r - \tilde{k}_1$ characteristics exhibit hysteresis between a forward and reverse scan of $\tilde{k}_1$, as shown in Fig. 7.2, B. Forward scan means that the system starts with $\tilde{k}_1 = 0$ and $p(0) = 0$, then $\tilde{k}_1$ is progressively increased. Reverse scan means that the system starts with $\tilde{k}_1 = \infty$ and $p(0) = 1$, then $\tilde{k}_1$ is progressively decreased until $\tilde{k}_1 = 0$. The $r - \tilde{k}_{-1}$ characteristics can be discussed analogously. Just as in the $r - \tilde{k}_1$ characteristics, a hysteresis is present in the r-$\tilde{k}_{-1}$ characteristics (see Fig. 7.2, C) [8].

7.3 Experimental

A single-pellet cell configuration was used for the kinetic measurements, its detailed description can be found in Chapter 3, section 3.1, Fig. 3.1. Rhodium catalyst electrodes (thickness 40 nm) were deposited by sputtering. The procedure of catalyst preparation was presented in Chapter 3, section 3.2. The experimental setup used for ethylene oxidation under open-circuit conditions was described in detail in Chapter 3, section 3.3.1. The working temperature range was 310 to 400 °C, the ranges of $P_{C_2H_4}$ and P_{O_2} were 0 to 2.2 kPa. The gas flow rate was 200 mL/min.
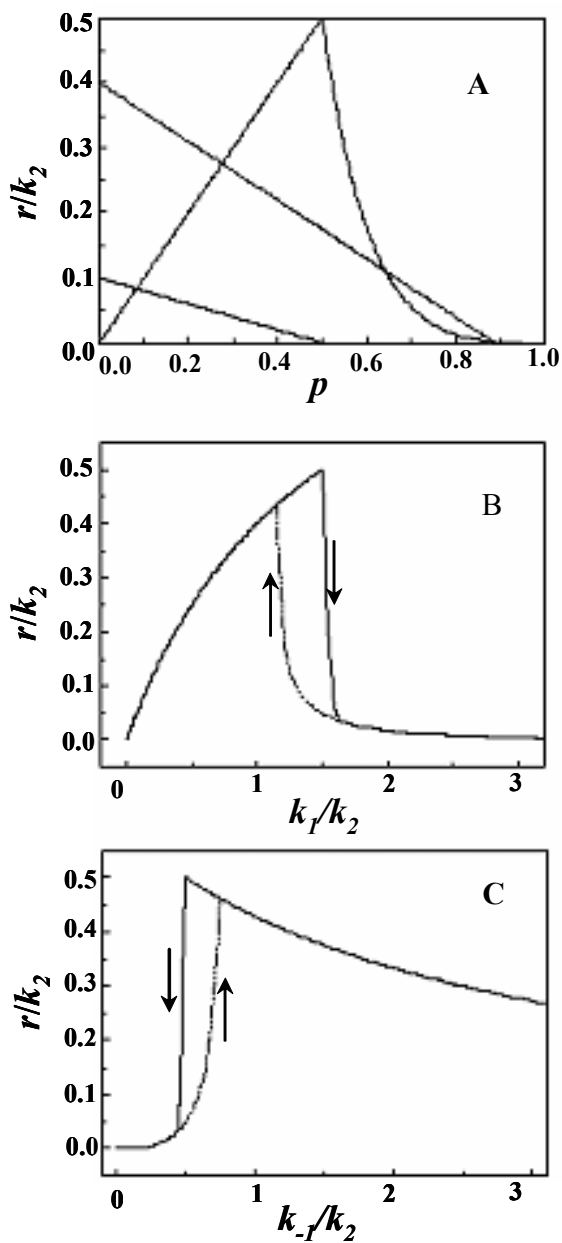
FIGURE 7.2. Solutions of Equation (7.5). A: graphical stationary solutions; B: $r - \tilde{k}_1$ characteristics; C: $r - \tilde{k}_{-1}$ characteristics.

7.4 Results

Figure 7.3 shows the effects of oxygen partial pressure on the rate of C_2H_4 oxidation and on the catalyst potential, U_{WR}, at constant $P_{C_2H_4} = 2$ kPa for the two catalysts under open-circuit conditions ($I = 0$). Both for the Rh/YSZ and for the Rh/TiO$_2$/YSZ catalyst, the catalytic rate first increases with increasing P_{O_2} but then, at a critical partial pressure denoted hereafter as $P_{O_2}^{crit}$, it decreases sharply. This sudden rate decrease is accompanied by an abrupt increase in the catalyst's open-circuit potential, and has been shown [3, 4] to be due to Rh_2O_3 surface oxide formation. The reaction rate over Rh/TiO$_2$/YSZ is higher than that over Rh/YSZ, an observation which can be attributed at least in part to the higher surface area of the Rh/TiO$_2$/YSZ catalyst (Chapter 4). It is worth noting that the value of $P_{O_2}^{crit}$ found for the Rh/YSZ catalyst is smaller by a factor of two. This should be due to surface properties of the catalyst rather than to a simple geometric factor. The catalyst's open-circuit potential varies between 50 mV and 150 mV for Rh/YSZ, and between -200 mV and -50 mV for Rh/TiO$_2$/YSZ.

It should be noted that in the case of Rh/YSZ, only freshly prepared catalysts were active towards ethylene oxidation in the range of working temperatures and C_2H_4 and O_2 partial pressures employed. Once deactivated in the oxidizing gas composition, the Rh/YSZ catalyst could not be reactivated by merely changing the gas composition under open-circuit conditions. It will be shown below that electrochemical promotion of catalysis is effective for reactivating the Rh/YSZ catalyst (Chapter 8). The behavior of the Rh/TiO$_2$/YSZ catalyst is different: when deactivated in an oxidizing gas composition (excess of O_2), this catalyst is readily reactivated by changing the gas composition back to reducing (excess of C_2H_4).
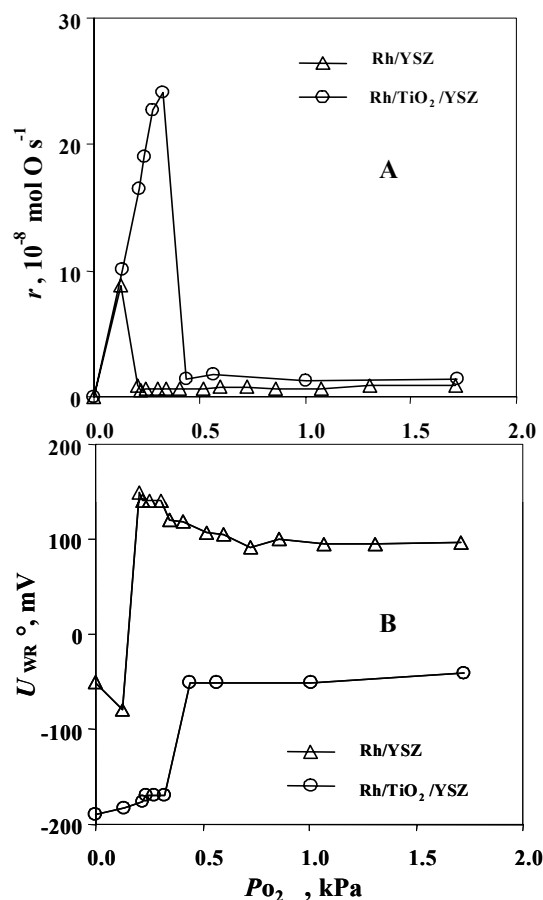
Results

FIGURE 7.3. Effects of oxygen partial pressure on the open-circuit catalytic rate (A) and on the open-circuit catalyst potential (B) observed at Rh/YSZ (triangles) and Rh/TiO$_2$/YSZ (circles) catalyst electrodes. Conditions: T = 310 °C, $P_{C_2H_4}$ = 2 kPa.

A typical example of deactivation/activation effects seen at 400 °C at Rh/TiO$_2$/YSZ is shown in Fig. 7.4 (to be compared with Figure 7.2, B). It illustrates the variation of the C$_2$H$_4$ oxidation rate, *r,* and of the corresponding catalyst potential, U_{WR}, with oxygen partial pressure at constant ethylene partial pressure ($P_{C_2H_4}$ = 2 kPa). The measurements were made under stationary conditions involving a cyclic change of P_{O_2} in the feed: starting from a minimum oxygen partial pressure (0 kPa), going up to the maximum value of P_{O_2} = 1.5 kPa and then back to the minimum value (zero). The typical waiting time after changing the inlet composition was 20 to 30 min.
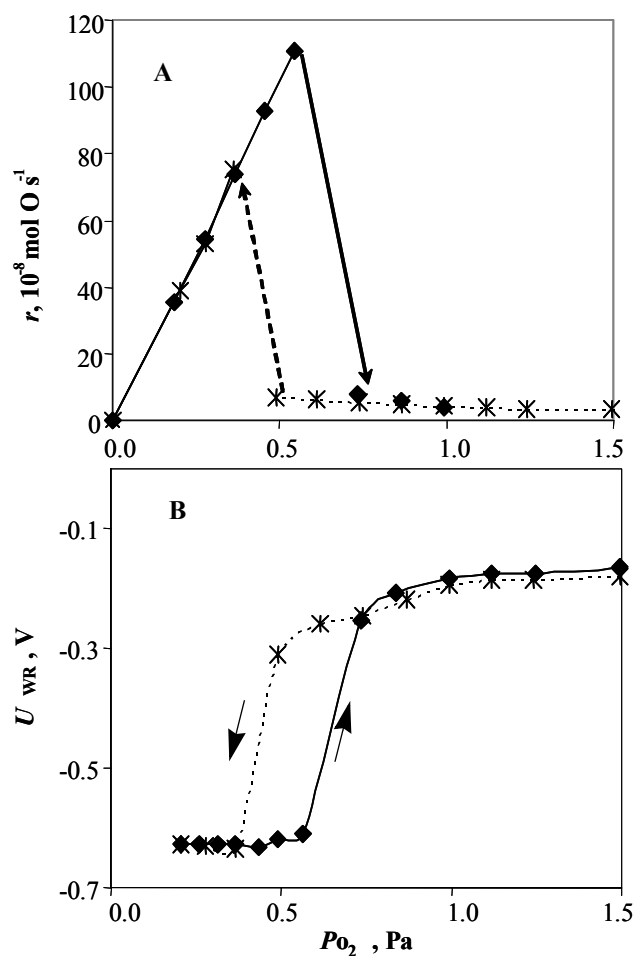
FIGURE 7.4. Effects of oxygen partial pressure on the open-circuit catalytic rate (A) and on the open-circuit catalyst potential (B) observed at Rh/TiO$_2$/YSZ catalyst films. Forward run (0 –> 1.5 kPa): diamonds; reverse run (1.5 –> 0 kPa): crosses. Conditions: $T = 400$ °C, $P_{C_2H_4} = 2$ kPa.

In the forward scan, the catalytic rate first increases with increasing P_{O_2} but then, at a critical partial pressure of $\vec{P}_{O_2}^{crit} = 0.75$ kPa, it decreases sharply. This sudden rate decrease is accompanied by an abrupt increase in the catalyst's open-circuit potential (Fig. 7.4, B), which is due to superficial Rh$_2$O$_3$ formation [4]. In the reverse scan, an oxygen partial pressure smaller than

$\overleftarrow{P}_{O_2}^{crit} = 0.5$ kPa is required for reactivation of the catalyst.

While increasing oxygen partial pressures favor the transition from activated sites M^* to the formation of a deactivated structure $\Sigma(p)$, increasing ethylene partial pressures to the contrary

disfavor this transition. The reaction rates and the catalyst's potential are shown as functions of the ethylene partial pressure at constant P_{O_2} = 0.2 kPa and 310 °C for the Rh/YSZ and Rh/TiO$_2$/ YSZ catalysts in Fig. 7.5. The open-circuit rate remains very low on Rh/YSZ over the entire range of P_{O_2} investigated. The corresponding catalyst potentials also remain positive, and practically constant. Both observations show that the Rh surface continues to be in the superficial Rh$_2$O$_3$ state [3, 4]. This is consistent with the observation that higher partial pressures of ethylene are required for reducing this rhodium surface oxide.
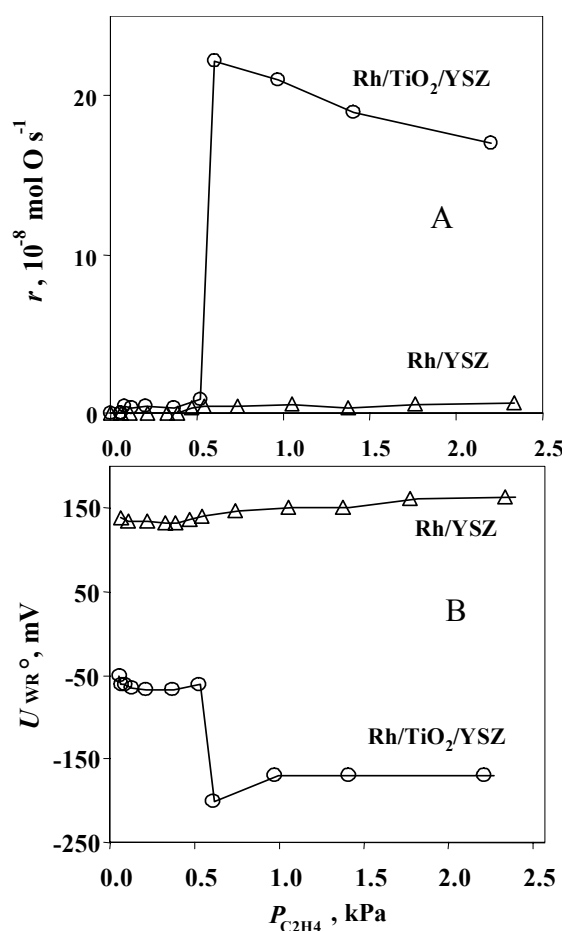

FIGURE 7.5. Effects of ethylene partial pressure on the open-circuit catalytic rate (A) and on the open-circuit catalyst potential (B) observed at Rh/YSZ (triangles) and Rh/TiO$_2$/YSZ (circles) catalyst electrodes. Conditions: T = 310 °C, P_{O_2} = 0.2 kPa.

Figure 7.6 shows reaction rates and the corresponding catalyst potentials recorded at Rh/TiO$_2$/YSZ catalyst in forward and reverse scans of $P_{C_2H_4}$ at constant oxygen partial pressure (P_{O_2} = 0.2 kPa) (to be compared with Figure 7.2, C). The measurements were made under stationary conditions, as mentioned above, involving a cyclic change of $P_{C_2H_4}$ in the feed: starting from the maximum ethylene pressure ($P_{C_2H_4}$ = 2.2 kPa), going down to the minimum value (0 kPa) in the forward scan, then back from this minimum to the maximum value in the reverse scan. The critical partial pressures were found to be $\overleftarrow{P}_{C_2H_4}^{crit}$ = 0.5 kPa and $\overrightarrow{P}_{C_2H_4}^{crit}$ = 0.9 kPa.

It is interesting to note that the hysteresis phenomenon observed during ethylene oxidation on Rh/TiO$_2$/YSZ is very similar to that observed during partial methane oxidation on Rh/TiO$_2$/YSZ (these results will be presented in Chapter 9) [13, 14].
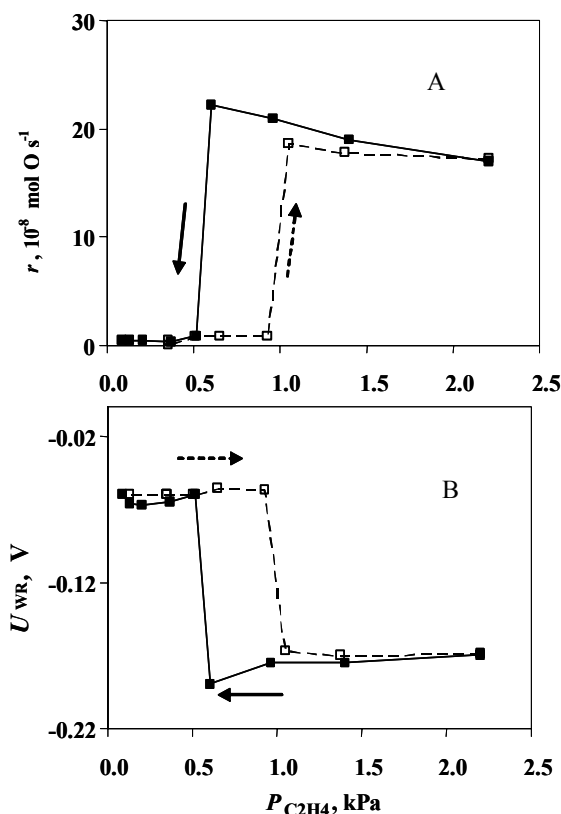

FIGURE 7.6. Effects of ethylene partial pressure on the reaction rate of ethylene oxidation (A) and on the corresponding catalyst potential (B) observed at Rh/TiO$_2$/YSZ catalyst films. Forward run (2.2 –> 0 kPa): full symbols; reverse run (0 –> 2.2 kPa): open symbols. Conditions: T = 310 °C, P_{O_2} = 0.2 kPa.

7.5 Discussion

According to the model proposed for the macroscopic deactivation of ethylene oxidation, the Rh surface has different sites (see Eq. (7.1)):

$$Rh \underset{k_{-1}}{\overset{k_1}{\rightleftarrows}} Rh - O_{ads} \tag{7.8}$$

where Rh is a nonactivated site while $Rh-O_{ads}$ is an activated site that should not belong to the deactivated structure $\Sigma(p)$. This means that activated and nonactivated sites both correspond to the metallic Rh surface. In the present case the deactivated structure is rhodium oxide (Rh_2O_3).

The rate-limiting step of ethylene oxidation can be written according to Eq. (7.2):

$$C_2H_4 + Rh - O_{ads} \xrightarrow{k_2} Rh + I_n \tag{7.9}$$
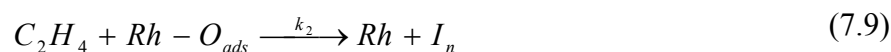
where I_n are intermediates that are converted to final products (CO_2 and H_2O) in a fast step. In reality, C_2H_4 is also adsorbed on the Rh surface. For simplification of the model, it is assumed that any C_2H_4 molecule becoming adsorbed immediately takes part in the process (Eq. (7.9)).

Figure 7.7 is a qualitative representation of the Rh surface, here subdivided into L squares, during ethylene oxidation and during its deactivation due to growth of a surface structure $\Sigma(p)$. As mentioned above, the deactivated structure is Rh_2O_3, its growth occurring at a critical partial pressure of oxygen or ethylene. The results obtained nicely correlate with the model proposed. As predicted by the model, the catalyst exhibits transitions between a deactivated and an activated surface which occur with hysteresis between the forward and reverse scan of the external parameters (Figs. 7.4 and 7.6). However, the model is only applicable to freshly prepared Rh/YSZ catalysts, since it is only at the beginning of the experiment that Rh/YSZ catalysts display catalytic activity towards CO_2 formation, as well as the appropriate activated and nonactivated sites. During an experiment they become deactivated (oxidized), and it is impossible to reactivate them by merely changing the gas composition.

The behavior of $Rh/TiO_2/YSZ$ is completely different, this catalyst when deactivated in an excess of oxygen is readily reactivated by exposure to a reducing gas composition [8].
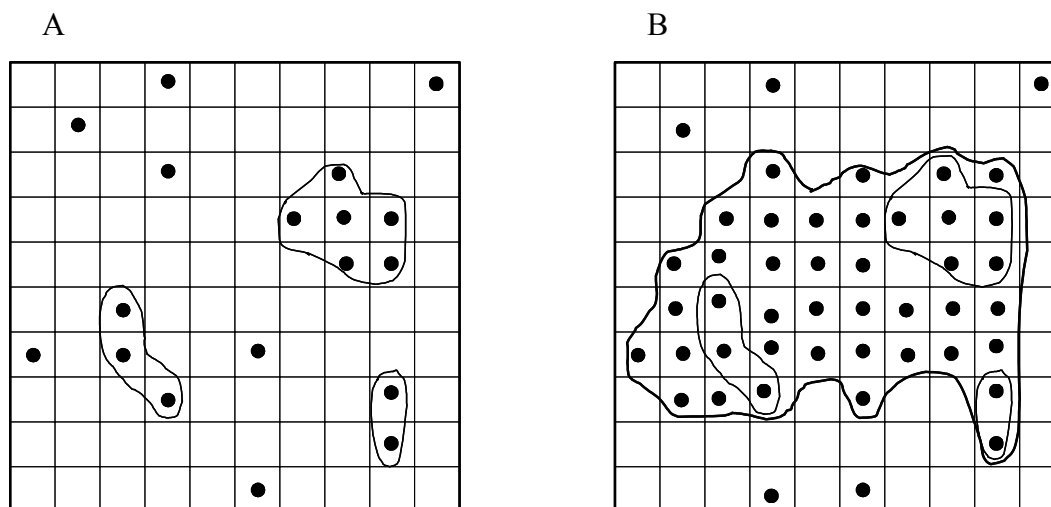
FIGURE 7.7. The Rh catalyst surface subdivided into *L* squares, during ethylene oxidation according to the percolation model [12]. Squares containing symbols ● are activated sites (Rh-O_{ads}); empty squares are nonactivated sites (Rh). The sites are occupied with a mean occupation probability *p*. Part A: neighboring activated sites build clusters n_s; Part B: growth of a deactivated surface structure $\Sigma(p)$ (Rh_2O_3).

Under the working conditions, the $Rh/TiO_2/YSZ$ catalyst can exist in two well-defined states, one characterized by high reaction rates and low catalyst potentials, the other by low reaction rates and high catalyst potentials. The state of the catalyst depends on the external parameters P_{O_2} and $P_{C_2H_4}$. The region of low reaction rates corresponds to rhodium oxide poisoning the reaction. In the region of high reaction rates the catalyst is in its reduced state. At intermediate gas compositions the Rh supported on TiO_2/YSZ can exist in either of two distinct states: active or inactive, depending on the gas composition to which the catalyst had been exposed just previously. The hysteresis in the plots of reaction rate and catalyst potential is related to the formation and decomposition of rhodium surface oxide.

The TiO_2 interlayer is responsible for the fact that higher values of the catalytic activity and stability are observed for $Rh/TiO_2/YSZ$, as compared to the values observed for Rh/YSZ. The effect of TiO_2 can be explained, either by strong metal-support interactions (SMSI) [15] or by a model based on the theory of electrochemical promotion of catalysis (EPOC) [10]. Strong metal-support interactions are, either of an electronic type or of a geometric type, the latter also being known as the decoration model. In the present case, where the Rh catalyst is not highly dispersed

Discussion

but, rather, exists as a film deposited on titania, an electronic effect could be effective only in the presence of long-range interactions. Possible modifications in electronic structure of a metal by long-range effects are changes in d-band population, changes in the density of states at the Fermi level, and a shift of the Fermi level due to the different work functions of metal and support. In the case of Rh, the first two effects are less important because of the high density of unoccupied d states above the Fermi level, whereas depending on the nature of the support, Fermi level shifts may be very important. In fact, the metal-semiconductor boundary-layer theory states that, at thermodynamic equilibrium, the Fermi energy levels of electrons in the two solids in contact are equal. Upon contact of two solids having different Fermi levels (work functions), charge must be transported from one material to the other until the Fermi levels at the interface are equilibrated. Obviously, the solid having the lower work function gets positively charged, the other gets negatively charged. The work function of stoichiometric, unreduced TiO_2 is 5.5 eV, that of Rh is 5.1 eV, hence upon contact, negative charge is transported from the Rh catalyst to the TiO_2 support. The resulting increase in the catalyst's work function leads to a lowering of the catalyst-oxygen bond strength and, consequently, to a decrease in the stability of rhodium oxide. Modifications of the catalytic activity of Rh on TiO_2 supports had already been reported for highly dispersed Rh catalysts [16, 17]. In the present work, similar results have now been obtained for a Rh film catalyst deposited on TiO_2. This demonstrates that electronic-type SMSI may be long-range interactions affecting the entire metal catalyst.

An alternative explanation for the effect of the TiO_2 support on the stability of rhodium oxide against reduction to metallic Rh is based on the theory of electrochemical promotion of catalysis (EPOC). In the model of electrochemical promotion, this phenomenon is regarded as catalysis in the presence of an electrically controlled double layer formed by an ion backspillover mechanism at the gas-exposed catalyst surface. As in the case of electronic-type SMSI discussed above, the thermodynamic driving force for electron transport is the difference in Fermi levels of the two solids in contact. Since TiO_2 is a semiconductor exhibiting mixed (electron and O^{2-} ion) conduction, the positive charge built up on Rh by the electronic effect will induce migration of O^{2-} ions to the catalyst/support interface, the driving force being the difference in electrochemical potentials of oxide ions in the two oppositely charged solids. The O^{2-} ions accompanied by their mirror charges in the metal may then spread out across the entire gas-exposed catalyst surface by the backspillover mechanism, thus forming an overall neutral electric double layer. This popula-

tion of the surface with dipoles increases the surface potential, the concomitant increase in work function affecting the binding strength of chemisorbed species. More precisely, the adsorption energy of electron donors will increase while that of electron acceptors (*eg*, atomic O) and also the stability of the Rh oxide against reduction are lowered.

The close analogy between electrochemical promotion of catalysis (EPOC) and strong metal-support interactions (SMSI) is obvious, and these two phenomena may in fact be considered as functionally identical, and only operationally different [1].

7.6 Conclusions

A phenomenological model was presented that is able to explain the macroscopic deactivation of Rh catalysts during ethylene oxidation. In this model, processes controlled by an external parameter P, either P_{O_2} or $P_{C_2H_4}$, are considered. Macroscopic deactivation occurring at a certain critical value of P is explained in terms of growth of a structure inhibiting the surface reaction. In C_2H_4 oxidation at Rh, this structure corresponds to a Rh surface oxide (Rh_2O_3); the growth of this structure is nicely confirmed by the observed values of catalyst potential.

Catalysts $Rh/TiO_2/YSZ$ are much more stable against oxidation, and catalytically more active than Rh/YSZ. This promotion of the C_2H_4 oxidation process on $Rh/TiO_2/YSZ$, which is much more pronounced than on Rh/YSZ, may be interpreted, either by strong electronic-type metal-support interactions or by a self-driven wireless electrochemical promotion mechanism. In both cases, the ultimate cause of promotion resides in different work functions of catalyst and support. Equilibration of the Fermi levels causes weakening of the Rh-O chemisorptive bond, and makes reduction of the oxidized surface sites easier.

7.7 References

1. J. Nicole, D. Tsiplakides, C. Pliangos, X. E. Verykios, C. Comninellis, and C. G. Vayenas, *J. Catal.,* **204** (2001) 23.

2. X. E. Verykios, in *Catalysis and Electrocatalysis at nanoparticle surface* A. Wieckowski, E. R. Savinova, and C. G. Vayenas, eds., Marcel Dekker, Inc., New York - Basel, (2003), p. 745

References

3. C. Pliangos, I. V. Yentekakis, V. G. Papadakis, C. G. Vayenas, and X. E. Verykios, *Applied Catalysis B: Environmental,* **14** (1997) 161.

4. C. Pliangos, I. V. Yentekakis, X. E. Verykios, and C. G. Vayenas, *J. Catal.,* **154** (1995) 124.

5. S. H. Oh and J. E. Carpenter, *J. Catal.,* **80** (1983) 472.

6. G. L. Kellog, *Surface Sci.,* **171** (1986) 359.

7. I. Bolzonella, *Electrochemical promotion of rhodium catalyst. Application to nitrogen monoxide reduction.* Thesis No 2743, EPFL, Lausanne, (2003).

8. R. Wüthrich, E. A. Baranova, H. Bleuler, and C. Comninellis, *Electrochem. Commun.,* **6** (2004) 1199.

9. M. M. Slin'ko and N. I. Jaeger, in *Studies in Surface Science and Catalysis*, Vol. 86 B. Delmon and J. T. Yates, eds., Elsevier, Amsterdam, (1994).

10. C. G. Vayenas, S. Bebelis, C. Pliangos, S. Brosda, and D. Tsiplakides, *Electrochemical activation of catalysis. Promotion, Electrochemical promotion, and metal-support interaction.* Kluwer Academic/Plenum Publishers, New York (2001).

11. G. L. Griffin, *J. Electrochem. Soc.,* **131** (1984) 18.

12. D. Stauffer and A. Aharony, *Inroduction to Percolation Theory* Taylor & Francis, London (1998).

13. E. A. Baranova, G. Fóti, and C. Comninellis, *Electrochem. Commun.,* **6** (2004) 170.

14. E. A. Baranova, G. Fóti, and C. Comninellis, *Electrochem. Commun.,* **6** (2004) 389.

15. S. J. Tauster, S. C. Fung, and R. L. Garten, *JACS,* **100** (1978) 170.

16. F. Solymosi, I. Tombacz, and M. Kocsis, *J. Catal.,* **75** (1982) 78.

17. P. Meriaudeau, O. H. Ellestad, M. Dufaux, and C. Naccache, *J. Catal.,* **75** (1982) 243.

CHAPTER 8 **Electrochemical promotion of Rh catalysts:** Closed-circuit ethylene oxidation

Electrochemical promotion of catalysis (EPOC) was investigated in the instance of a model reaction, the oxidation of ethylene on sputtered Rh film catalysts (40 nm thick) deposited on YSZ and on YSZ covered with a thin layer of TiO_2. It was found that the two catalysts differ in their behavior under polarization (closed circuit).

Small anodic currents applied to the Rh/YSZ catalyst cause periodic oscillations of the catalytic rate and potential having a frequency that can be controlled electrochemically. The oscillations of reaction rate are synchronous with those of catalyst potential, but always in the opposite direction. These oscillations can be interpreted in terms of the formation and decomposition of rhodium surface oxide: minimum rates correspond to an oxidized Rh surface (Rh oxide), maximum rates to reduced Rh catalyst (Rh metal). This phenomenon is fully reversible but can only be observed under closed-circuit conditions.

Currents applied to $Rh/TiO_2/YSZ$ lead to a pronounced nonoscillatory electrochemical promotion of the catalyst. Its catalytic activity for C_2H_4 oxidation can be reversibly enhanced by up to a factor of 80 via an anodic current or potential applied to the catalyst, the increase in oxidation rates being up

to 2000 times larger than the rate of supply of O^{2-} to the Rh catalyst electrode.

The electrochemical promotion behavior observed at the two catalytic systems has its origin in an anodically controlled migration (backspillover) of O^{2-} species from YSZ to the Rh/gas interface and in the concomitant destabilization of surface Rh_2O_3 formation via repulsive lateral interactions.

8.1 Introduction

One factor that limits the commercial utilization of electrochemical promotion is the low degree of metal dispersion (typically 10^{-3} to 10^{-5}) found in the thick, porous films (typically 0.2 to 10 μm, most often produced by decomposition of a paste) used in practically all prior electrochemical promotion studies [1]. Metal dispersion expresses the percentage of metal catalyst or electrode exposed to the gaseous reactants. For most commercial supported catalysts, degrees of metal dispersion of 10 to 100 % are required [2]. The low degrees of dispersion typically used in prior EPOC studies may be acceptable for certain active catalyst phase materials but can be prohibitive for many noble-metal applications [1].

This problem can in many cases be overcome by dispersing the active phase on an electronically conductive material [1]. In a related approach, an industrial promoted catalyst is interfaced with a solid electrolyte. In this case the bulk of the commercial catalyst must be conductive. The feasibility of this concept was already demonstrated in the synthesis of NH_3 on Fe-based, promoted commercial catalysts (BASF S6-10 RED) [3]. This commercial catalyst is electronically conducting, since it is not supported on an insulating support (such as SiO_2, Al_2O_3), and it was found that this catalyst film when deposited on the H^+-conducting oxide electrolyte ($Ca_{0.9}ZrIn_{0.1}O_{3-\alpha}$) was sufficiently conductive to also act as an electrode of the solid electrolyte cell. Another case was SO_2 oxidation on V_2O_5-$K_2S_2O_7$-based catalysts (Haldor-Topsoe VK-58) [4]. A third approach to the problem is the induction of electrochemical promotion without an intermediate conductive phase. In this case the active catalyst phase is highly dispersed on a solid electrolyte. This approach was not yet fully demonstrated.

A first step toward EPOC with highly dispersed catalysts is the utilization of very thin, porous metal films deposited by sputtering on a solid electrolyte. In the present chapter, the electrochemical modification of catalytic activity of 40-nm Rh films on solid-electrolyte supports was investigated for the first time in an oxidation reaction. The electrolytes were YSZ as well as YSZ covered by a thin layer of TiO_2 (4 µm). Ethylene oxidation served as a model reaction. The use of similar 40-nm Rh and Pt films for a successful electrochemical promotion of NO reduction in the presence of propene was reported very recently [5].

8.2 Experimental

The experimental setup, cell configuration, and catalyst electrode preparation used for studying the electrochemical promotion of ethylene oxidation have been described in detail in Chapter 3, section 3.2; and section 3.1.1, Figure 3.1. The temperature range was 310 - 400 °C, the ranges of $P_{C_2H_4}$ and P_{O_2} were 0 to 2.2 kPa. The gas flow rate was 200 to 500 mL/min.

8.3 Results

8.3.1 Electrochemical promotion of Rh/YSZ catalysts. Oscillatory behavior

It was shown in the preceding chapter that only a freshly prepared Rh catalyst can alternate between two states: active and inactive. After its exposure to working conditions, the catalyst becomes deactivated, its reactivation requires a much higher C_2H_4 partial pressure than used during the experiments. It has been found, however, that catalyst reactivation is readily achieved by applying a current or potential, *ie*, by electrochemical promotion of catalysis (EPOC).

Figure 8.1 shows a galvanostatic transient (constant imposed current) of C_2H_4 oxidation recorded on a Rh catalyst film deposited on YSZ, together with the corresponding transient of catalyst potential. Application of an anodic current of 50 µA leads to a pronounced rate increase and to induction of an oscillatory state of C_2H_4 oxidation rate and catalyst potential. The effect is fully reversible, the catalyst returning to its initial steady state upon interruption of the current. The oscillations of catalyst potential are synchronous with those of the rate of CO_2 production, but in the opposite direction, *ie*, increasing rates correspond to decreasing catalyst potentials, just as in

the case of C_2H_4 and CO oxidation on Pt [6]. The rate enhancement ratio, ρ, is as high as 52 in the maximum of C_2H_4 oxidation rate (Fig. 8.1). At the rate maximum, $\Lambda = 1024$, which says that each O^{2-} supplied to the catalyst causes 1024 chemisorbed oxygen atoms to react with C_2H_4 to CO_2 and H_2O. Note that the catalyst potential remains below 0.9 V during the oscillations.
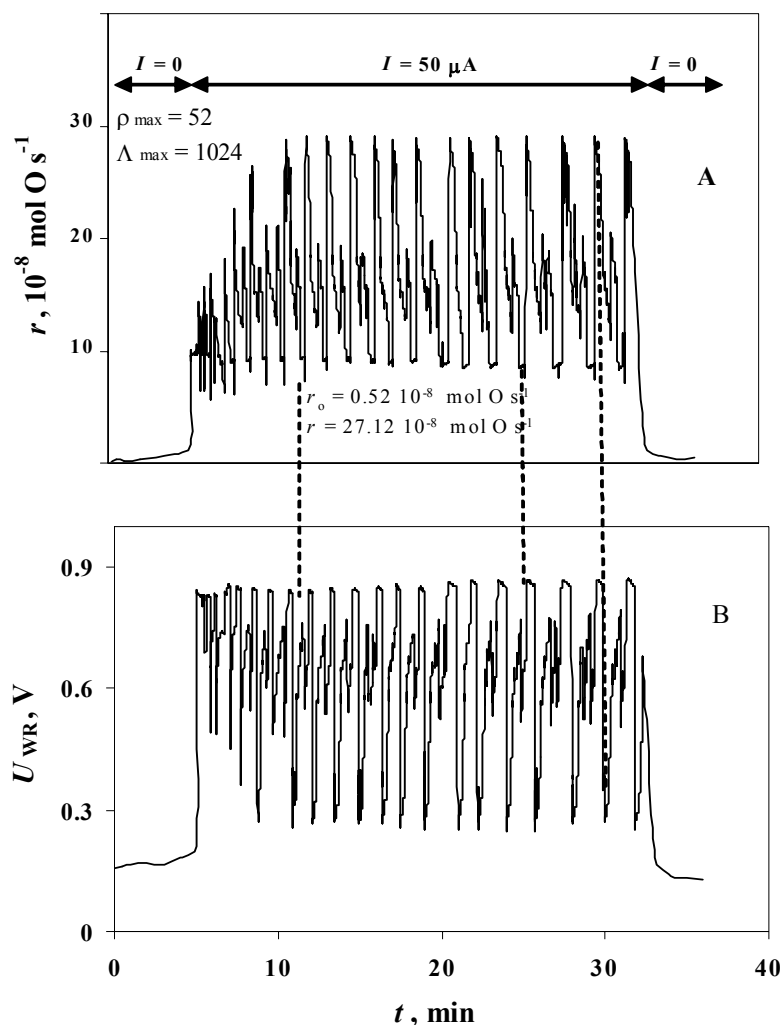

FIGURE 8.1. Response of the catalytic rate (Part A) and of catalyst potential (Part B) of the Rh/YSZ catalyst electrode to an applied anodic current step of +50 μA. T = 350 °C. Gas composition: $P_{O_2} = 0.41$ kPa, $P_{C_2H_4} = 2$ kPa. Flow rate: 200 mL/min.

Figure 8.2, Parts A and B show the effects of oxygen partial pressure, P_{O_2}, on the rate of C_2H_4 oxidation and in the catalyst's potential at constant $P_{C_2H_4}$ and $T = 350\ °C$ which are produced while an anodic (positive) current is applied to the catalyst. The open-circuit behavior ($I = 0$, $U_{WR} = U°_{WR}$) is shown for comparison. The open-circuit catalytic rate is rather low due to surface oxide formation. The OCP remains practically unchanged at a value of 0.25 V, implying that the catalyst continues to exist in the same oxidation state. At intermediate P_{O_2} values, the applied anodic currents induce rate and potential oscillations exhibiting a maximum at $P_{O_2} = 0.6\ kPa$, where the ρ-value is 52. At high P_{O_2} values (oxidized surface), imposed anodic currents have a very small effect.
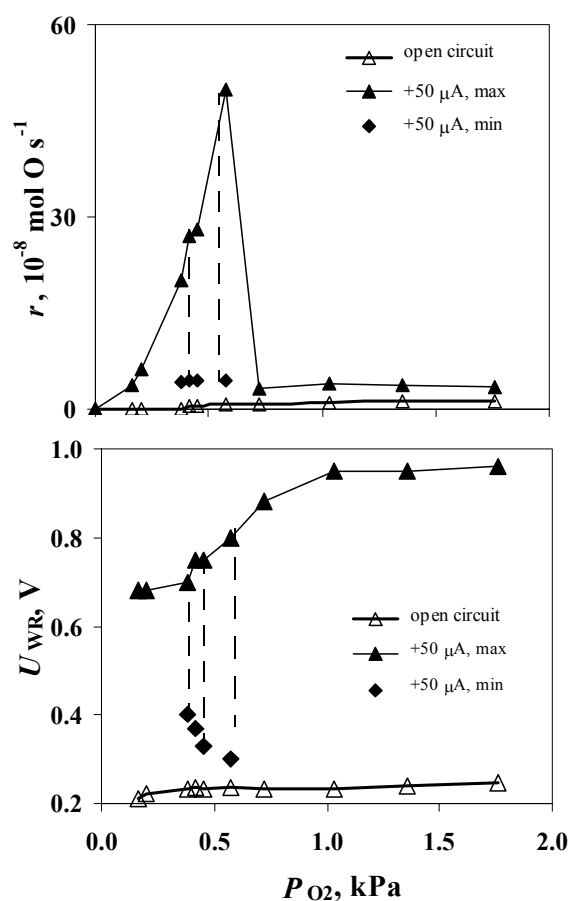

FIGURE 8.2. Effects of P_{O_2} and of the applied current on the rate of C_2H_4 oxidation on Rh/YSZ and on the catalyst's potential. $I = +50\ \mu A$, $T = 310\ °C$, $P_{C_2H_4} = 2\ kPa$. Flow rate: 200 mL/min. Triangles and diamonds connected by vertical dashed lines show the upper and lower limits of oscillations.

Effect of the $P_{C_2H_4}/P_{O_2}$ ratio on the rate and potential oscillations. - A typical example of rate and catalyst potential oscillations seen at a constant oxygen partial pressure of 0.5 kPa and different values of $P_{C_2H_4}$ (so that different $P_{C_2H_4}/P_{O_2}$ ratios are realized) is shown in Fig. 8.3, Parts A to D. Under open-circuit conditions, the catalyst is in its original, stable steady state exhibiting a low reaction rate and no oscillations. However, when a current is applied the reaction rate increases and the system exhibits oscillatory behavior. After an interruption of the current the catalyst returns to its initial steady state. Higher ethylene partial pressures lead to a higher oscillation frequency and lower oscillation amplitude. When the ratio $P_{C_2H_4}/P_{O_2}$ attains a value of about two, the oscillations die away, and the catalyst attains a stable active state characterized by a high ethylene oxidation reaction rate (Fig. 8.3, Parts A to D). The oscillations of catalyst potential are synchronous with those of the reaction rate, but in the opposite direction, *ie*, increasing rates correspond to decreasing catalyst potentials, as already shown in Fig. 8.1. It can be seen in Fig. 8.3 that rate and catalyst potential oscillate between values corresponding to a reduced Rh surface and values corresponding to an oxidized (surface Rh_2O_3) Rh surface.

Results

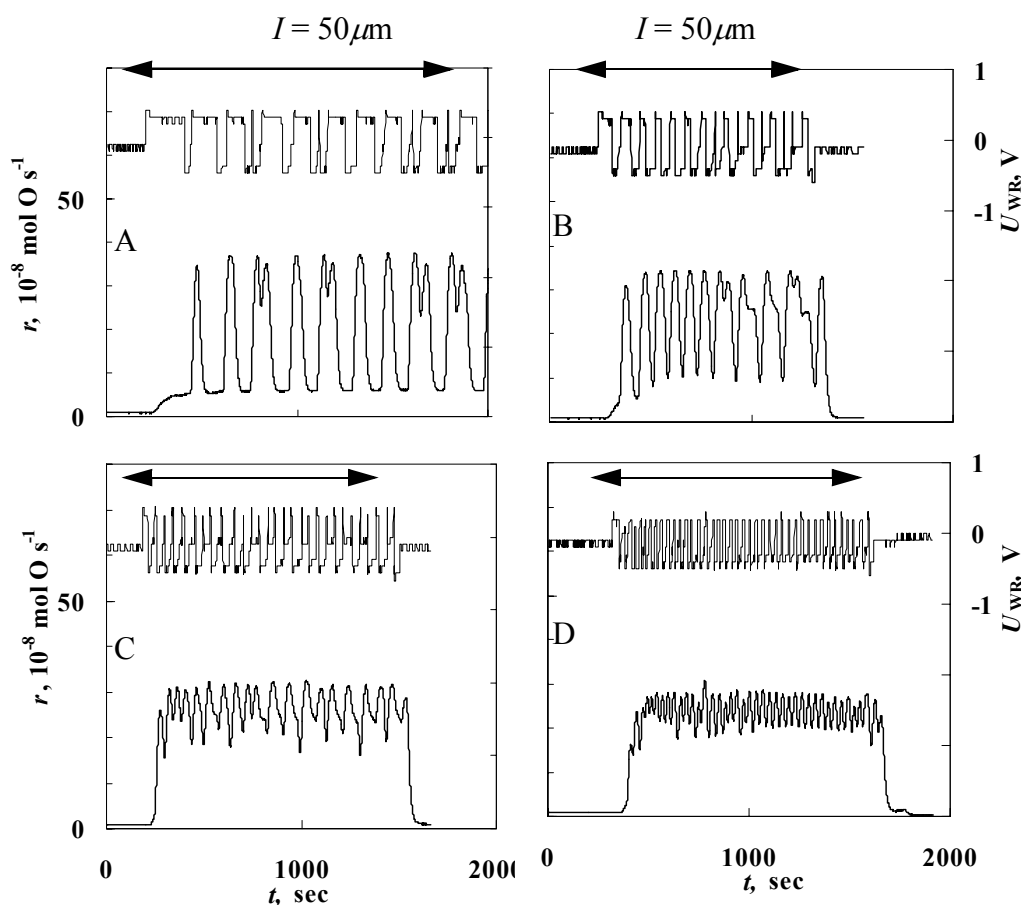**FIGURE 8.3. Response of the ethylene oxidation rate on Rh(40 nm)/YSZ at T = 390 °C and of the corresponding catalyst potential to an applied anodic current step of +50 µA. Gas composition: $P_{C_2H_4}$ variable, P_{O_2} = 0.5 kPa. Flow rate: 200 mL/min. Part A: $P_{C_2H_4}/P_{O_2}$ = 1.10; Part B: $P_{C_2H_4}/P_{O_2}$ = 1.24; Part C: $P_{C_2H_4}/P_{O_2}$ = 1.51; Part D: $P_{C_2H_4}/P_{O_2}$ = 1.80.**

Figure 8.4 shows the rates of C_2H_4 oxidation as a function of the ratio of partial pressures $P_{C_2H_4}/P_{O_2}$ gathered from the experimental results reported in Figs. 8.3, Parts A to D. Three curves can be distinguished in the figure: one that corresponds to the reaction rates under open-circuit conditions, where the rates are low; and two others that correspond to the upper and lower limit of oscillating reaction rates of ethylene oxidation observed while applying an anodic current. The larger the $P_{C_2H_4}/P_{O_2}$ ratio, the smaller will be the amplitudes of the oscillations. When the oscillations have died out at a $P_{C_2H_4}/P_{O_2}$ ratio of about two, the catalyst attains a high steady-

state activity at closed circuit. Hence, under given working conditions a transition domain where rate and potential exhibit oscillations can be identified. Within this domain, both of the rhodium species (Rh and Rh_2O_3) are present on the catalyst at the same time.

A rate enhancement ratio, ρ, as high as 61 was found for the maximum value of the C_2H_4 oxidation rate at $P_{C_2H_4}/P_{O_2}$ = 1.10 (Fig. 8.3, Part A and Fig. 8.4, point A), where Λ = 1398, *ie*, each O^{2-} supplied to the catalyst causes 1398 chemisorbed oxygen atoms to react with C_2H_4 to CO_2 and H_2O.
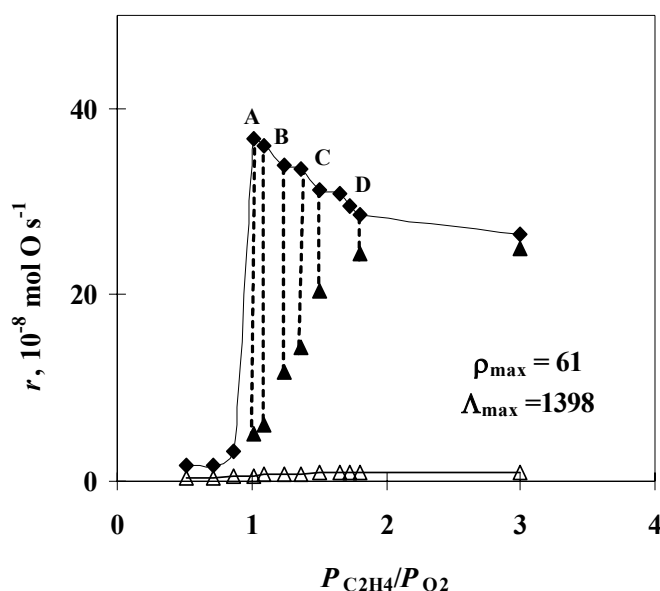
FIGURE 8.4. The C_2H_4 oxidation rates on Rh/YSZ as functions of the $P_{C_2H_4}/P_{O_2}$ ratio under open-circuit conditions (open symbols) and at closed circuit (I = 50 μA) (filled symbols) at T = 390 °C. Gas composition: $P_{C_2H_4}$ variable, P_{O_2} = 0.5 kPa. Flow rate: 200 mL/min. Diamonds and triangles connected by vertical dashed lines show the upper and lower limits of rate oscillations. Points A - D correspond to the Fig. 8.3, Parts A to D.

The effects of the $P_{C_2H_4}/P_{O_2}$ ratio on the oscillatory behavior of the Rh catalysts was also studied at other temperatures: 310, 350, and 420 °C. It was found that the reaction rates always exhibited oscillations when an anodic current was applied, but at higher temperatures the transi-

tion domain of the $P_{C_2H_4}/P_{O_2}$ values within which the reaction rate and catalyst potential will oscillate becomes narrower.

The oscillations always follow the same trends, namely, increasing ethylene partial pressures lead to increasing oscillation frequency and decreasing oscillation amplitude. The oscillation frequencies observed under closed-circuit conditions (I = 50 μA) at different working temperatures are summarized in Figure 8.5 as functions of the $P_{C_2H_4}/P_{O_2}$ ratio.
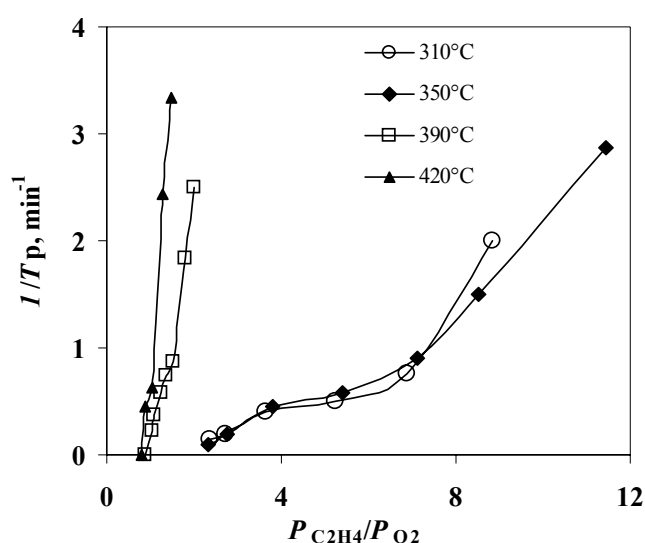
FIGURE 8.5. Frequencies of the rate and potential oscillations seen when applying an anodic current (I = +50 μA), as functions of the ratio of partial pressures, $P_{C_2H_4}/P_{O_2}$, at different temperatures. Gas composition: $P_{C_2H_4}$ variable, P_{O_2} constant. At 310 °C and 350 °C: P_{O_2} = 0.2 kPa; at 390 °C and 420 °C: P_{O_2} = 0.5 kPa.

Effects of temperature and gas flow rate on the rate and potential oscillation. - The effect of temperature on the oscillation behavior was investigated at constant oxygen and ethylene partial pressures while applying a constant positive current of 50 μA (Fig. 8.6). Note that here, too, the oscillations of catalyst potential (U_{WR}) are synchronous with those of reaction rate, but in the opposite direction, similar to Figs. 8.2 and 8.3. At 350 °C in the region of partial pressures of the reactant where oscillations occur, the reaction rate oscillates with a high amplitude, while the fre-

quency of the oscillations is very low (Fig. 8.6). Increasing the temperature at a given gas compo-

sition leads to higher amplitudes and frequencies of the oscillations. This implies that the surface

processes provoking the oscillations are accelerated with increasing temperature.
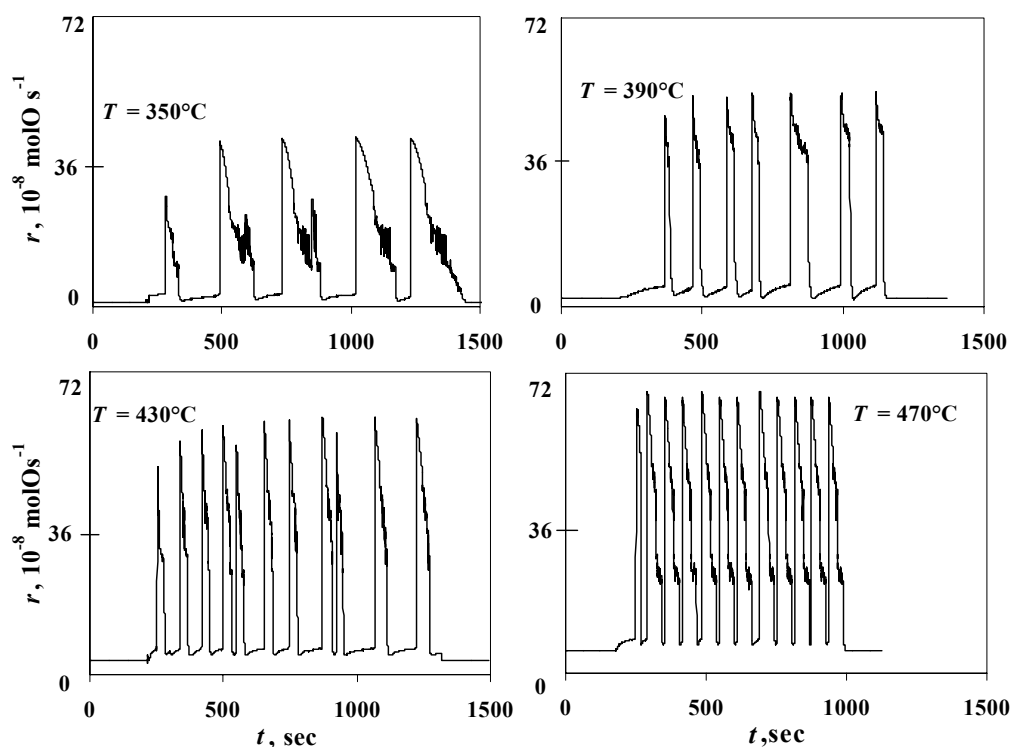
FIGURE 8.6. Response of the ethylene oxidation rates on Rh(40 nm)/YSZ at different temperatures to an applied anodic current step of +50 μA . Gas composition: $P_{C_2H_4}$ = 2 kPa, P_{O_2} = 0.69 kPa. Flow rate: 200 mL/ min.

The effects of gas flow rate on the oscillation behavior of Rh/YSZ catalysts has been inves-

tigated at constant temperature ($T = 350$ °C) and gas composition. Higher gas flow rates lead to

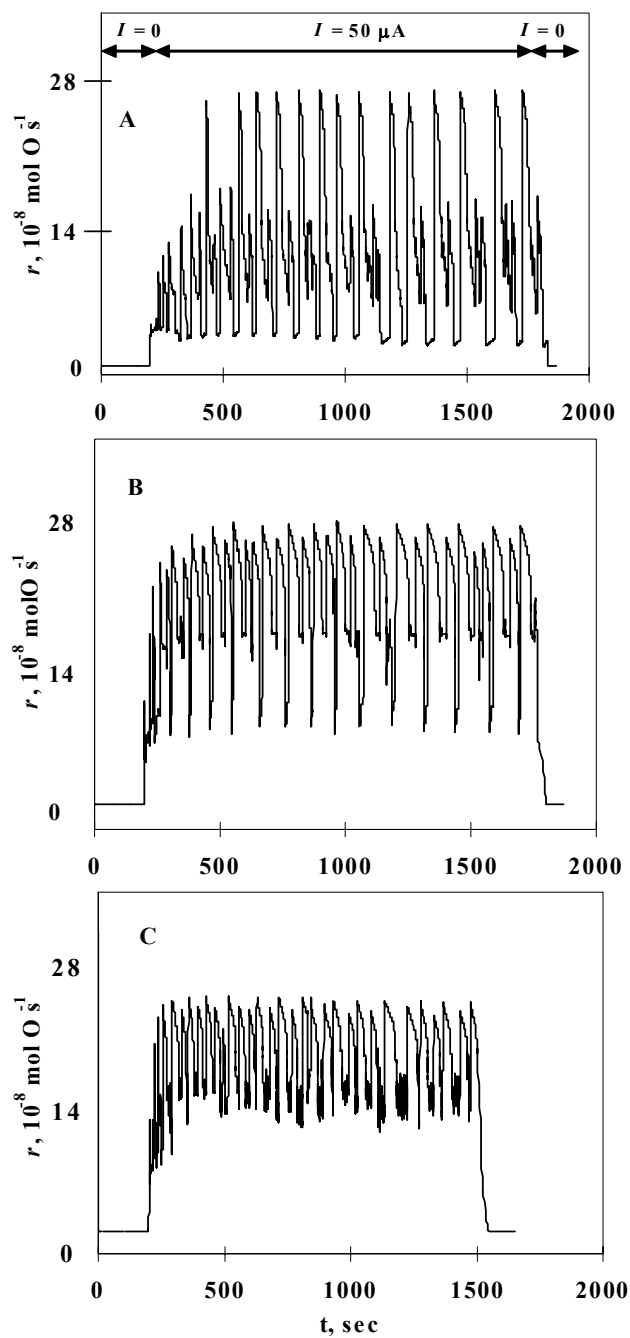catalyst stabilization, that is, decreasing oscillation amplitude and increasing oscillation fre-

quency.

FIGURE 8.7. Response of the ethylene oxidation rates on Rh(40 nm)/YSZ at different gas flow rates to an applied anodic current step of +50 μA. Part A: 200 mL/min; Part B: 400 mL/min; Part C: 600 mL/min. Gas compositions: $P_{C_2H_4} = 2$ **kPa,** $P_{O_2} = 0.4$ **kPa.** $T = 350$ **°C.**

Figure 8.8 shows the frequencies of the reaction rate oscillations seen at Rh/YSZ catalysts while applying an anodic current, as functions of gas flow rate and working temperature.
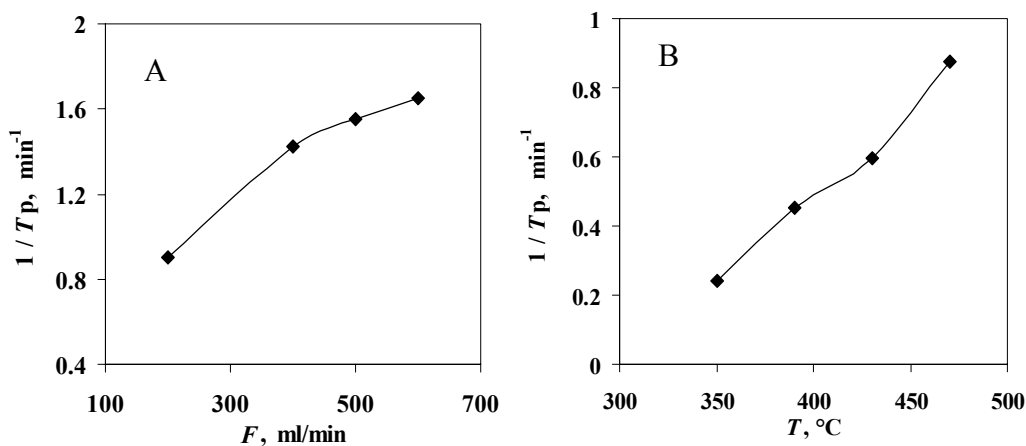
FIGURE 8.8. The frequencies of the reaction rate oscillations seen when applying an anodic current (I = +50 μA). Part A: Effect of gas flow rate at constant gas composition: $P_{C_2H_4}$ = 2 kPa, P_{O_2} = 0.4 kPa, T = 350 °C. Part B: Effect of temperature at constant gas composition: $P_{C_2H_4}$ = 2 kPa, P_{O_2} = 0.69 kPa. Flow rate: 200 mL/min.

8.3.2 Electrochemical promotion of Rh/TiO$_2$/YSZ catalysts

The transient behavior of Rh/TiO$_2$/YSZ catalysts seen at constant gas composition when applying an anodic current is shown in Figure 8.9. The behavior of Rh catalysts interfaced with TiO$_2$ is different from that of Rh/YSZ under these conditions. At the same temperatures and imposed currents, this catalyst attains a stationary state, both in terms of the rate of C$_2$H$_4$ oxidation and in terms of catalyst potential (Fig. 8.9). The catalytic rate increases by a factor of 78 (a 7800-% rate increase, ρ = 78), the apparent faradaic efficiency Λ = 1790. Note that the catalyst potential stabilizes at a value of 1.4 V. Thus, compared with the Rh/YSZ catalyst electrode, the Rh/TiO$_2$/YSZ electrode is much more polarizable.
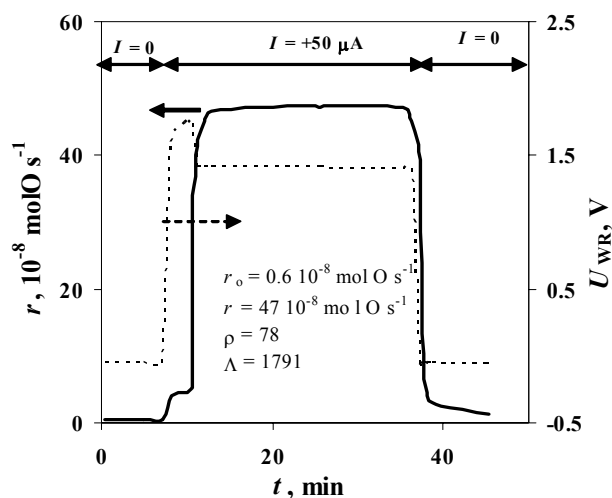
FIGURE 8.9. Response of the catalytic rate (solid curve) and of catalyst potential (dotted curve) of the Rh/TiO$_2$/YSZ catalyst electrode to an applied anodic current step of +50 μA. T = 350 °C. Gas composition: P_{O_2} = 0.4 kPa, $P_{C_2H_4}$ = 0.64 kPa. Flow rate: 200 mL/min.

Figure 8.10, Parts A and B show the effect of oxygen partial pressure, P_{O_2}, on the rate of C$_2$H$_4$ oxidation and on catalyst potential under conditions of an applied positive current, recorded at constant $P_{C_2H_4}$ for Rh/TiO$_2$/YSZ catalyst at 350 °C. For comparison, a plot of r vs P_{O_2} for open-circuit conditions is also reproduced. At intermediate values of P_{O_2}, applied anodic currents lead to a pronounced (up to eightyfold) increase in reaction rate over the open-circuit value (ρ = 80), which is due to a significant increase in the critical oxygen partial pressure ($P_{O_2}^{crit}$). At higher values of P_{O_2} (oxidized surface), imposed anodic currents have a very small effect.
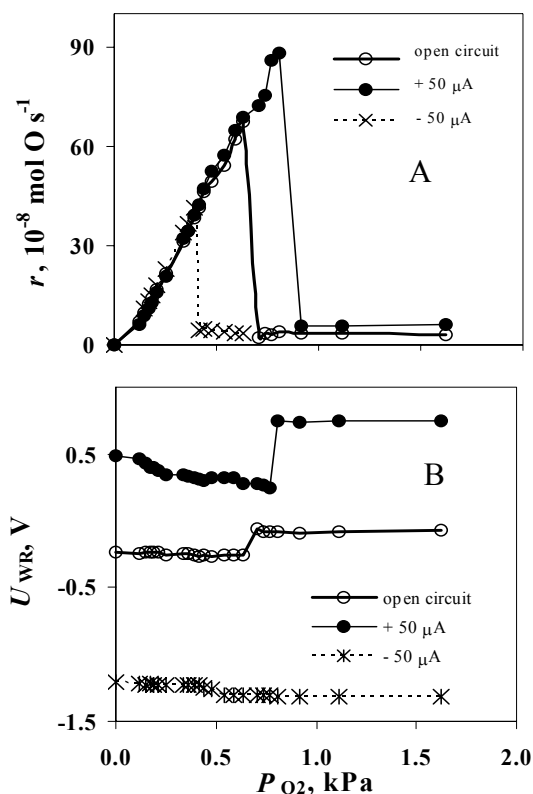
FIGURE 8.10. Effects of P_{O_2} and of the applied current on the rate of C_2H_4 oxidation at Rh/TiO$_2$/YSZ (Part A) and on the corresponding catalyst potentials (Part B). I = ±50 µA, T = 350 °C, $P_{C_2H_4}$ = 2 kPa. Flow rate: 200 mL/min.

Application of a cathodic (negative) current leads to a decrease in the catalytic reaction rate and in the critical P_{O_2} value. Therefore, ethylene oxidation on Rh can be regarded as a purely electrophobic reaction [1, 7], *ie*, as a catalytic reaction occurring with a rate that increases with increasing potential (U_{WR}) or work function (Φ) at any given gas composition [1, 8]. Positive currents supply O^{2-} to the catalyst, and thus destabilize the Rh surface oxide through repulsive lateral interactions between the spillover O^{2-} species and the oxygen atoms of the surface Rh$_2$O$_3$. The spillover O^{2-} ions cause, both a weakening of the Rh=O chemisorptive bonds and a strengthening of the Rh-C$_2$H$_4$ chemisorptive bonds, this effect becoming stronger with increasing U_{WR}. According to the model developed for macroscopic deactivation of the Rh catalysts (Chapter 7), and for this Rh catalyst at fixed ethylene partial pressure, this will cause $\tilde{k}_1$ to increase with

increasing anodic current and, symmetrically, $\tilde{k}_1$ to decrease with increasing cathodic current. It follows that positive currents cause a shift of the critical partial pressure to higher values.

Figure 8.11 shows the effects of ethylene partial pressure and applied positive currents on the rates of C_2H_4 oxidation. For comparison, rates observed at open circuit are reported. The reaction rate curves have a sigmoid shape. The branch of low rates and high potentials corresponds to an oxidized surface, while the branch of high rates and low potentials corresponds to a reduced surface of the Rh catalyst. This arises from the reduction of the Rh surface oxide that occurs above a critical $P_{C_2H_4}^{crit}$, also manifest in the values of catalyst potential (Fig. 8.11, Part B). A rate increase up to 74 times was observed with applied positive currents.
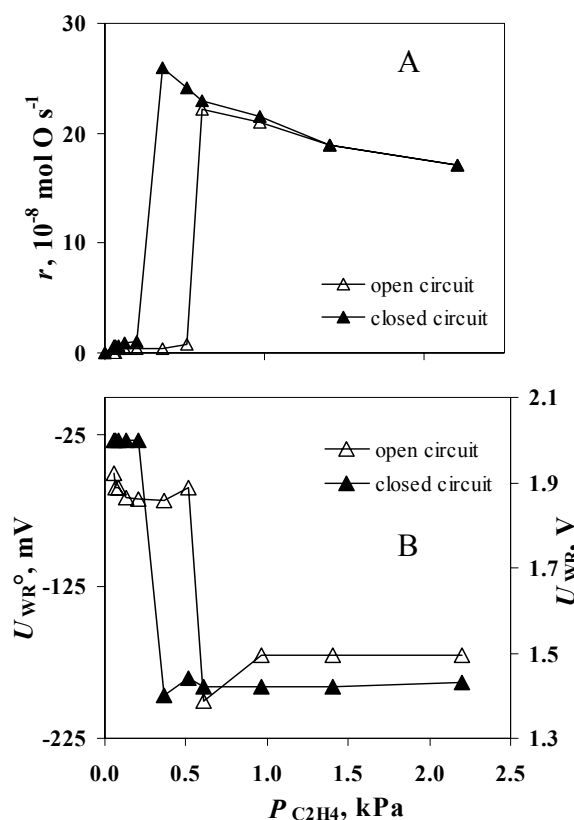
FIGURE 8.11. Effects of $P_{C_2H_4}$ and of applied currents on the rate of C_2H_4 oxidation (Part A) and on the catalyst potential (Part B) observed at Rh/TiO$_2$/YSZ catalysts. $I = 50$ μA, $T = 310$ °C, $P_{O_2} = 0.2$ kPa.

In Figure 8.12, reaction rates recorded on the Rh/TiO$_2$/YSZ catalyst at 350 °C at two oxygen partial pressures (0.2 and 0.4 kPa) are compared under conditions of open and closed-circuit operation. At open circuit, increasing P_{O_2} leads to increasing reaction rates, but also to a shift in the critical partial pressure of ethylene from 0.4 kPa to 1.4 kPa. Application of a positive current causes a pronounced decrease of $P_{C_2H_4}^{crit}$, clearly demonstrating that increasing catalyst potentials are indicative of decreasing stability of the Rh surface oxide. Increasing temperature at constant P_{O_2} leads to a decrease of the critical $P_{C_2H_4}^{crit}$ value, both at open circuit (Fig. 8.13, Part A) and when applying a positive current (Fig. 8.13, Part B).

FIGURE 8.12. Effects of $P_{C_2H_4}$ and of applied currents on the rates of C$_2$H$_4$ oxidation on Rh/TiO$_2$/YSZ at two partial pressures of oxygen. Open symbols: open circuit, filled symbols: I = + 50 µA. T = 350 °C. Flow rate: 200 mL/min.

The data shown in Figure 8.14 which were obtained potentiostatically illustrate the relation between catalyst potential and the rate enhancement ratio ρ in reducing and oxidizing gas compositions. In both cases the reaction exhibits electrophobic behavior. However, due to the electrochemically induced decomposition of Rh$_2$O$_3$ surface oxide the effect is more pronounced under oxidizing conditions. Note that even under reducing conditions, the catalytic rate will become negligibly small when a negative potential is applied, which is due to cathodically assisted formation of Rh surface oxide already seen in Fig. 8.10.
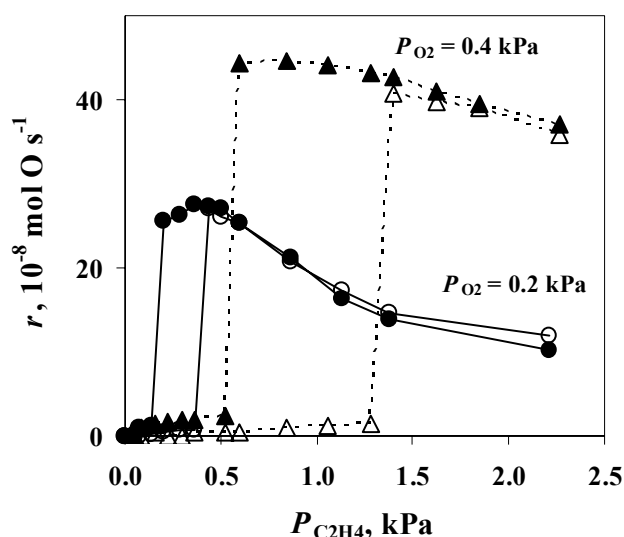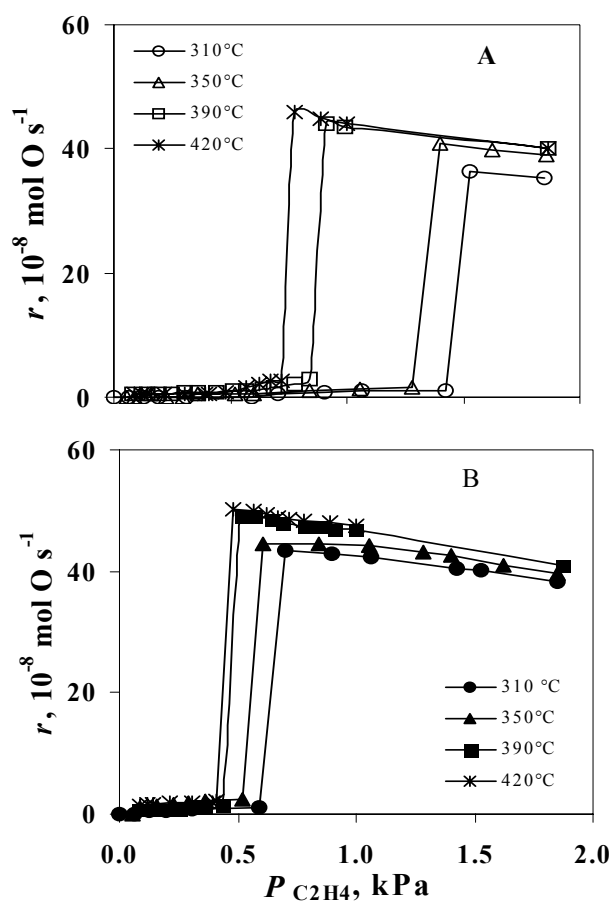
FIGURE 8.13. Effects of $P_{C_2H_4}$ and of applied currents on the rates of C_2H_4 oxidation on Rh/TiO$_2$/YSZ at different temperatures. Part A: open circuit, Part B: $I = + 50$ µA. $P_{O_2} = 0.5$ kPa. Flow rate: 200 mL/min

.
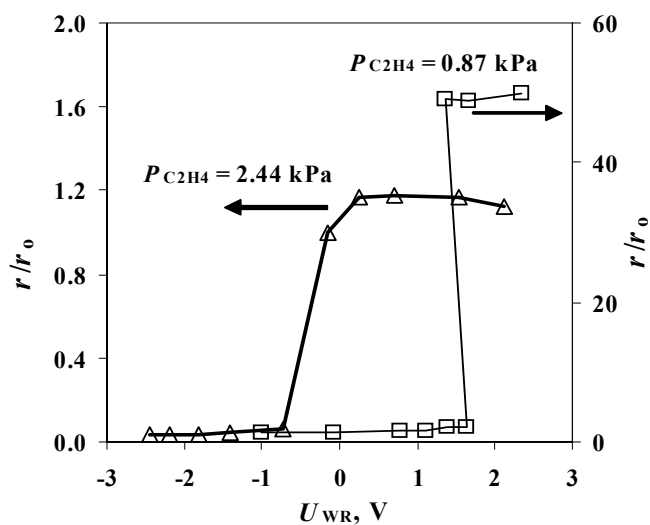
FIGURE 8.14. Effects of catalyst potential on ratios r/r_0 (= ρ) at the Rh/TiO$_2$/YSZ catalyst electrode in reducing (triangles) and oxidizing (squares) gas compositions. T = 310 °C, P_{O_2} = 0.4 kPa. Flow rate: 200 mL/ min.

8.4 Discussion

The results obtained clearly demonstrate that Rh nanofilm catalysts can be efficiently promoted by application of positive currents or potentials. This is in very good agreement with the theory of electrochemical promotion, and shows that ethylene oxidation on Rh catalysts is an electrophobic reaction ($\partial r / \partial U_{WR} > 0$).

The results obtained for ethylene oxidation over 40-nm Rh catalyst films supported on YSZ clearly show that the nature of the Rh catalyst significantly changes when applying a positive current. In fact, anodic polarization gives rise to oscillations in the reaction rate and corresponding catalyst potential (Fig. 8.1). At open circuit, the rate exhibits a stable, nonoscillatory behavior characterized by low rates of CO$_2$ formation at given gas compositions and temperatures. Low catalytic activities observed on Rh are related to its fully oxidized state. Positive currents supply O^{2-} ions to the catalyst/support interface, and these oxygen ions according to the mechanism of electrochemical promotion will act as promoters [1]. The promoting O^{2-} species are sacrificial promoters, *ie*, they are consumed in the catalytic reaction occurring on the catalyst

Discussion

---

surface, and spent O^{2-} are continuously replenished via reduction of gaseous O_2 at the countere-lectrode [1].

In several heterogeneous catalytic systems operating close to the limits of surface oxide stability, oscillatory behavior has been found repeatedly [9 and reference therein, 10, 11]. In most cases these oscillations of reaction rate are observed in a transition region between the two steady states characterized by high and low reaction rates [9]. The catalyst's bistability can arise, either from multiple steady states on the catalyst surface or from multiplicity in the reactor dynamics. In [9], it was shown that additives or impurities that may constitute catalyst promoters as well as catalyst poisons can play a significant role in the induction of oscillatory behavior of a catalyst. In fact, additives present in the gas phase or on the catalyst surface will merely behave as additional adsorbates on the catalyst surface. They will block sites, can affect the activity of the catalyst and induce oscillations [12-15]. The impurities can be responsible for the appearance of oscillations if in the region of bistability, they are acting so as to drive the system from one state to the other.

The induction of oscillatory states in the rate of C_2H_4 oxidation on Rh (40 nm)/YSZ via anodic polarization is an effect similar to that observed during CO oxidation on electropromoted polycrystalline Pt films (5 μm) deposited on YSZ [11]. In this work [11] the oscillations were induced by electrochemically controlled backspillover of oxygen ions from the solid electrolyte to the catalyst surface. The authors observed that reaction rate oscillations can be induced by positive, and stopped by negative currents [1]. The effect of the positive current was interpreted in terms of changes in the surface coverage by chemisorbed oxygen, CO, and PtO_2. In the case of positive currents, O^{2-} ions are continuously supplied to the Pt surface, which implies that the backspillover species, which in some way are "impurities", should be present on the catalyst surface in order to switch on the rate oscillations [9].

The mechanism by which the self-sustained oscillations are generated at Rh/YSZ can be explained as follows. According to the present results, the Rh surface oxide is stable at given temperatures and gas compositions. When by anodic polarization and the concomitant O^{2-} supply to the catalyst, a weakening of oxygen bonds to the rhodium surface is caused, the oxygen that had previously been associated with Rh_2O_3 becomes available for the reaction with C_2H_4, and this causes an abrupt decrease in the $P_{C_2H_4}/P_{O_2}$ ratio over the catalyst. When this ratio falls below some critical ratio $(P_{C_2H_4}/P_{O_2})^{crit}$, formation of surface Rh_2O_3 will resume. However, this

causes an increase in the $P_{C_2H_4}/P_{O_2}$ ratio due to extra consumption of gaseous O_2, so the oxide becomes unstable again, and the cycle is repeated.

The results obtained for C_2H_4 oxidation over Rh nanofilm catalysts can be summarized as follows: (*i*) Rate oscillations can be triggered by applied positive currents, only in the domain where the catalyst exhibits bistability. At low $P_{C_2H_4}/P_{O_2}$ ratios the applied currents do not lead to rate oscillations. Under more strongly reducing conditions (high $P_{C_2H_4}$), applied currents lead to a dramatic increase in reaction rate. In this domain, the oscillations have a very small amplitude and almost die away. (*ii*) The frequency of the oscillations increases with increasing $P_{C_2H_4}/P_{O_2}$ ratios, temperatures, and gas flow rates. (*iii*) The catalyst potential and the rate of CO_2 production exhibit synchronous oscillations while a decrease in catalyst potential always corresponds to an increase in reaction rate.

Nonoscillatory electrochemical promotion of $Rh/TiO_2/YSZ$ is tied to the presence of the TiO_2 interlayer. Several of its advantages for EPOC were already cited above: it raises the catalyst's surface area and degree of dispersion (see the SEM analysis, section 4.1, Chapter 4), and it depresses the exchange current density at the metal/gas interface (see Chapters 5 and 6). This is also manifest in all figures of the present chapter in the overpotentials created at the $Rh/TiO_2/YSZ$ interface, which at a given current are always larger than those created at the Rh/YSZ interface. The third advantage of TiO_2 is an enhanced stability of the reduced and highly active Rh phase, which as shown in Chapter 7 is due to effects of SMSI established between Rh and TiO_2. Over and above the metal-support-promoted state of $Rh/TiO_2/YSZ$, the catalytic activity is boosted further by applied positive currents.

This is supported by Figure 8.15, where the temperature dependence of the critical $(P_{O_2}/P_{C_2H_4})^{crit}$ ratios for surface Rh_2O_3 formation observed in prior work with thick Rh films (10 μm) [16, 17] (the triangles in Fig. 8.15 for thick films on YSZ, electropromoted or at open-circuit) are compared with those observed in the present work (thin films without and with TiO_2 interlayers, circles and squares in Figure 8.15). It can be seen that TiO_2 sublayers generally lead to higher $(P_{O_2}/P_{C_2H_4})^{crit}$ ratios, *ie*, destabilize the formation of Rh_2O_3. As already discussed in detail, anodic polarization (electropromoted films) leads to even higher $(P_{O_2}/P_{C_2H_4})^{crit}$ ratios,

Discussion

while for thin Rh films without a TiO$_2$ interlayer the $(P_{O_2}/P_{C_2H_4})^{crit}$ ratio is lowest, *ie*, thin Rh films without a TiO$_2$ interlayer are more readily oxidized than thick films. On the other hand, the electropromoted states of thick films without TiO$_2$ and thin films with TiO$_2$ are very similar (the two sets of data at the top of Fig. 8.15), which is consistent with the functional similarity of electrochemical promotion and metal-support interactions discussed in Chapter 2, section 2.2.3.
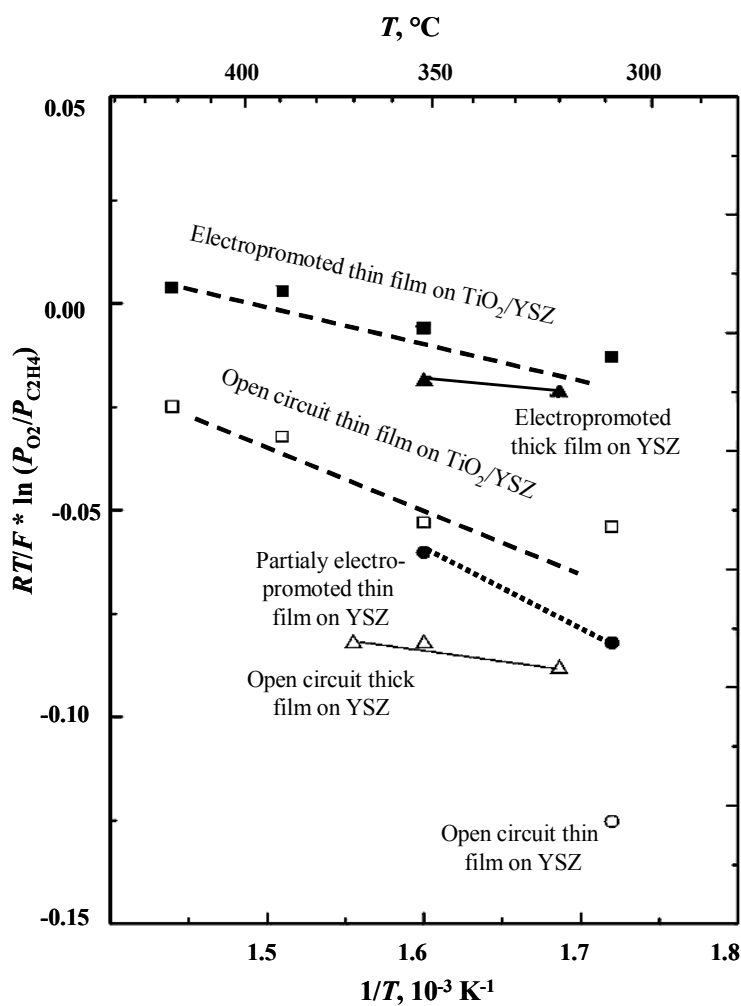
FIGURE 8.15. Temperature dependence of the critical ratios $(P_{O_2}/P_{C_2H_4})^{crit}$ **for Rh surface oxide formation on thick films [16, 17] and thin sputtered Rh samples with and without a TiO$_2$ interlayer. (□) Thin sputtered Rh film on TiO$_2$/YSZ, open circuit; (■) thin sputtered Rh film on TiO$_2$/YSZ, closed circuit; (○) thin sputtered Rh film on YSZ, open circuit; (●) thin sputtered Rh film on YSZ, closed circuit; (▲) thick Rh film on YSZ, closed circuit. Data for thick Rh films on YSZ taken from [16, 17].**

That the polarizability of Rh/TiO$_2$/YSZ catalyst electrodes is much higher than that of Rh/YSZ catalyst elelctrodes, is in good agreement with the polarization and impedance measurements (Chapters 5 and 6). It was found that the i_0 values at the Rh/TiO$_2$ interface were about twice lower than those at the Rh/YSZ interface. The smaller exchange current density characteristic of the Rh/TiO$_2$/YSZ interface leads to a higher faradaic efficiency, Λ, since it is well established that the magnitude of Λ can be estimated from the approximate expression

$$\Lambda \approx 2Fr_0/I_0 \qquad (8.1)$$

where r_0 is the open-circuit catalytic rate and i_0 is the exchange current density of the metal/solid electrolyte interface.

As seen in Table 8.1, the correlation between the obtained in the present chapter faradaic efficiencies and the exchange current densities of Rh/YSZ and Rh/TiO$_2$/YSZ is good. Even if the value of Λ calculated from i_0 and Eq. (8.1) is higher than the value obtained experimentally, the ratios of Λ and i_0 for the two catalysts are about the same, and close to two.

TABLE 8.1. Faradaic efficiencies and exchange current densities in the Rh/YSZ and Rh/TiO$_2$/YSZ systems at $T = 350$ °C and $P_{O_2} \approx 0.5$ kPa

Catalyst electrode	Λ (Figs. 8.1 and 8.9)	i_0, A
Rh/YSZ	1024	$2.2*10^{-8}$
Rh/TiO$_2$/YSZ	1791	$1.2*10^{-8}$

The pronounced electrophobic behavior (ρ-values of up to 80) observed at both of the thin Rh films (Rh/YSZ and Rh/TiO$_2$/YSZ), which is semiquantitatively similar to that observed at thick Rh/YSZ films, mainly depends on destabilization of surface Rh$_2$O$_3$ via repulsive lateral interactions with the electromigrating backspillover O^{2-} ions poisoning the catalytic reaction [16, 17]. This point, *ie*, that anodic polarization of a metal film can destabilize a surface oxide, is somehow surprising, but is well documented and analyzed in the literature on electrochemical promotion [1]. It is known, for example, that the chemisorptive bond energy of oxygen decreases (linearly and with a slope close to -1) with applied anodic potential [1, 18]. This experimental result has been confirmed by rigorous quantum-mechanical calculations [19], which have shown

that Stark-type electrostatic interactions in the double layer present at the metal-gas interface are the main cause of electrochemical (and also of chemical) promotion.

It should be pointed out, though, that the difference between Rh/YSZ films (where rate oscillations occur) and Rh/TiO$_2$/YSZ films (where rate oscillations do not occur over the parameter range investigated) can be traced to the fact that in the latter case, due to the much lower exchange current density at the Rh/TiO$_2$/YSZ films and identical applied current densities, the resulting potential is much higher than in the case of Rh/YSZ. This higher potential then destabilizes the Rh surface oxide much more efficiently, and thus the surface remains reduced over a wider range of gas compositions.

The results obtained in the present chapter demonstrate that it will be technically feasible to induce electrochemical promotion at very thin (40 nm) catalyst films. The degree of Rh metal dispersion in these films is of the order of 10 %, as shown both in the present study and in similar studies of NO reduction by propene in the presence of O$_2$ on films similarly deposited [5]. This is a very significant improvement with respect to metal dispersion relative to practically all prior electrochemical promotion studies [1], an improvement which practically closes the gap of noble-metal dispersion, and thus of noble-metal cost, between electrochemically promoted films and commercial, nanodispersed noble-metal catalysts (where metal dispersion typically amounts to 10 - 100 % [20, 21]). Thus, the main obstacle to a commercial utilization of electrochemical promotion has in principle been removed by these results.

8.5 Conclusions

The feasibility of electrochemical promotion of thin Rh films (40 nm) prepared by sputtering has been demonstrated for the first time. The pronounced electrophobic electrochemical promotion of C$_2$H$_4$ oxidation observed on the thin Rh films is similar to that observed with thick Rh films. The electrochemical promotion of thin films having degrees of metal dispersion of the order of 10 % is of considerable technological importance.

Small anodic currents applied to the Rh/YSZ catalyst cause periodic catalytic rate and potential oscillations with a frequency that can be controlled electrochemically. The oscillations can be interpreted in terms of the formation and decomposition of rhodium surface oxide: minimum rates correspond to an oxidized Rh surface (Rh oxide), maximum rates to reduced Rh cata-

lyst (Rh metal). The phenomenon observed is fully reversible, and only occurs under closed-circuit conditions.

Catalysts Rh/TiO$_2$/YSZ exhibit pronounced nonoscillatory electrochemical promotion, their catalytic activity for C$_2$H$_4$ oxidation can be reversibly enhanced by up to a factor of 80 by applying a positive anodic current or potential. The increase in oxidation rate is up to 2000 times larger than the rate of supply of O^{2-} to the Rh catalyst electrode.

The electrochemical promotion behavior observed in the two catalytic systems is due to anodically controlled migration (backspillover) of O^{2-} species from YSZ to the Rh/gas interface and to the concomitant destabilization of surface Rh$_2$O$_3$ formation via repulsive lateral interactions.

8.6 References

1. C. G. Vayenas, S. Bebelis, C. Pliangos, S. Brosda, and D. Tsiplakides, *Electrochemical activation of catalysis. Promotion, Electrochemical promotion, and metal-support interaction.* Kluwer Academic/Plenum Publishers, New York (2001).

2. A. Wieckowski, E. R. Savinova, and C. G. Vayenas, *Catalysis and Electrocatalysis at Nanoparticles* Marcel Dekker, Inc., New York (2003).

3. C. G. Yiokari, G. E. Pitselis, D. G. Polydoros, A. Katsaounis, and C. G. Vayenas, *J. Phys. Chem.,* **104** (2000) 10600.

4. I. M. Petrushina, V. A. Bandur, F. Cappeln, and N. J. Bjerrum, *J. Electrochem. Soc,* **147(8)** (2000) 3010.

5. S. Balamenou, D. Tsiplakides, A. Katsaounis, S. Thiemann-Handler, B. Cramer, G. Fóti, C. Comninellis, and C. G. Vayenas, *Applied Catalysis B: Environmental,* **52** (2004) 181.

6. C. G. Vayenas, C. Georgakis, J. N. Michaels, and J. Tormo, *J. Catal.,* **67** (1981) 348

7. C. G. Vayenas, S. Bebelis, and S. Ladas, *Nature,* **323** (1990) 625.

8. C. G. Vayenas, S. Bebelis, S. G. Neophytides, and I. V. Yentekakis, *Nature,* **343** (1990) 625.

9. M. M. Slin'ko and N. I. Jaeger, in *Studies in Surface Science and Catalysis*, Vol. 86 B. Delmon and J. T. Yates, eds., Elsevier, Amsterdam, (1994).

References

10.   C. G. Vayenas, B. Lee, and J. N. Michaels, *J. Catal.,* **66** (1980) 37

11.   I. V. Yentekakis and C. G. Vayenas, *J. Catal.,* **111** (1988) 170

12.   A. K. Galwey, P. Gray, J. F. Griffiths, and S. M. Hasko, *Nature,* **313** (1985) 668.

13.   T. Lamb, R. P. Scott, P. Watts, B. Holland, S. Gentry, and A. Jones, *J.Chem.Soc. Chem.Commun.,* **23** (1977) 882.

14.   R. C. Yeates, J. E. Turner, A. J. Gellman, and G. A. Somoriai, *Surface Sci.,* **149** (1985) 175.

15.   K. E. Keck and B. Kasemo, *Surface Sci.,* **167** (1986) 313.

16.   C. Pliangos, I. V. Yentekakis, V. G. Papadakis, C. G. Vayenas, and X. E. Verykios, *Applied Catalysis B: Environmental,* **14** (1997) 161.

17.   C. Pliangos, I. V. Yentekakis, X. E. Verykios, and C. G. Vayenas, *J. Catal.,* **154** (1995) 124.

18.   C. G. Vayenas, S. Brosda, and C. Pliangos, *J. Catal.,* **203** (2001) 329.

19.   C. Sanchez and E. Leiva, in *Handbook of Fuel Cells: Fundamentals, Thechnology and applications*, Vol. 2 W. Vielstich, H. A. Gasteiger, and A. Lamm, eds., John Wiley & Sons, Ltd, England, (2003).

20.   L. L. Hegedus, R. Aris, A. T. Bell, M. Boudart, N. Y. Chen, B. C. Gates, W. O. Haag, G. A. Somorjari, and J. Wei, *Catalyst design: Progress and Perspectives.* John & sons, New York (1987).

21.   G. Ertl, H. Knötzinger, and J. Weitkamp, *Hand Book of Catalysis* VCH, Weinheim (1997).

CHAPTER 9 **Promotion of Rh catalysts:** Partial methane oxidation at open and closed circuit

The catalytic activity of Rh for the partial oxidation of methane to syngas can be markedly influenced by interfacing polycrystalline Rh films with a dispersed TiO_2 interlayer deposited on the YSZ supports. High CO selectivities (close to 97 %) can be attained at 550 °C over a wide range of CH_4/O_2 ratios. The modification of catalytic activity and selectivity towards CO and H_2 production observed at Rh interfaced with an interlayer of TiO_2 is related to the lower stability of Rh surface oxide against reduction to metallic Rh. This phenomenon may be interpreted, either by strong electronic-type metal-support interactions or by a self-driven wireless electrochemical promotion mechanism. The Rh/TiO_2/YSZ catalyst exhibits the particular characteristic of having two distinct stable states, an inactive (oxidized) and an active (metallic) state, in the partial oxidation of methane to syngas. At a gas composition close to stoichiometric ($CH_4 : O_2 = 2 : 1$) and 550 °C, the inactive Rh/TiO_2/YSZ catalyst was successfully activated by applying currents, either positive or negative. The phenomenon observed is an example of "permanent electrochemical promotion" providing a permanent rate enhancement ratio of 11 and a CO selectivity of 45 %. The activation by

negative currents is explained by electrochemical reduction of rhodium surface oxide, while in the instance of applied positive currents the rhodium surface oxide breaks down due to a weakening of the Rh-O bond strength which occurs due to the accumulation of backspillover oxygen at the gas-exposed catalyst surface.

9.1 Introduction

Over the last decade, many efforts have been made to improve the catalytic partial oxidation of CH_4 with oxygen, and achieve syngas formation according to Eq. (9.1) [1, 2]:

$$CH_4 + \frac{1}{2}O_2 \rightarrow CO + 2H_2 \qquad (9.1)$$

This process has some advantages over conventional steam reforming, namely: it is more energy-efficient and can produce the H_2/CO mole ratio of two (instead of three in steam reforming) that is desired for methanol or Fischer-Tropsch synthesis. However, this reaction has not yet been developed on an industrial scale due to problems related to catalyst deactivation, mainly by carbon deposition and/or oxidation of the catalyst to the corresponding oxide.

Prettre *et al* [3] were among the first to report the formation of syngas by partial oxidation of CH_4 with supported Ni catalysts over the temperature range from 973 to 1173 K. The reaction was reported to occur in two steps. In the first step, methane is converted to CO_2 and water until all oxygen has been converted according to Eq. (9.2):

$$CH_4 + 2O_2 \rightarrow CO_2 + 2H_2O \qquad (9.2)$$

In the second step, syngas is produced via secondary reactions such as the carbon dioxide reaction Eq. (9.3) and the steam-reforming reaction Eq. (9.4):

$$CH_4 + CO_2 \rightarrow 2CO + 2H_2 \qquad (9.3)$$

$$CH_4 + H_2O \rightarrow CO + 3H_2 \qquad (9.4)$$

It is generally agreed that the type of catalyst used may strongly influence the reaction pathway. It has in fact been reported that on Rh catalysts the partial oxidation of methane to CO

and H_2 occurs in a single step (Eq. (9.1)) without the formation of intermediate CO_2 [4], just as had been the case on Ni catalysts [3].

More recent studies have demonstrated that Rh is one of the most promising catalysts for the partial oxidation of methane, because it offers the highest selectivity toward H_2 production [4]. However, problems related to Rh catalyst deactivation, mainly due to carbon deposition and/ or Rh oxidation to Rh_2O_3, have not yet been completely resolved.

It is the aim of the work reported in this chapter to investigate a modification of catalytic activity and improved stability against deactivation of Rh catalysts for the partial oxidation of methane that is achieved by interfacing the Rh catalyst with TiO_2 particles supported on YSZ solid electrolyte ($Rh/TiO_2/YSZ$). In the first part of this chapter the promoting effects of TiO_2 will be studied under open-circuit conditions, where the YSZ support is not considered to play any role in the observed phenomena but is used to enable potential measurements. The results will be discussed in terms of strong metal-support interactions (SMSI) [5] and of electrochemical promotion of catalysis (NEMCA) [6].

In the second part of this chapter, investigations of the same systems under closed-circuit conditions are described. It was the aim of this part to explore the possibilities of a current-assisted activation of $Rh/TiO_2/YSZ$ catalysts for a selective oxidation of methane with oxygen to CO and H_2.

9.2 Experimental

The ring-type electrochemical cell used in the present work has been described in detail earlier (Chapter 3, section 3.2). The catalyst film was deposited on the inner surface, the gold counterelectrode on the outer surface of an YSZ ring. The catalyst was prepared by paste deposition (see Chapter 3, section 3.2.3). The experimental setup was described in Chapter 3, section 3.3.5. Currents or potentials were applied in a direct polarization mode where the catalyst served as the working electrode, and the gold film served as the counterelectrode.

The selectivity, S(CO), of methane oxidation to CO was calculated with the following equation:

$$S(CO) = \frac{r_{CO}}{r_{CO} + r_{CO_2}} \qquad (9.5)$$

where r_{CO} and r_{CO2} are the rates of CO and CO_2 product formation.

9.3 Results

9.3.1 Promotion of Rh catalysts by a TiO_2 interlayer [7]

The catalytic activity of Rh/YSZ and Rh/TiO_2/YSZ catalysts was investigated by a cyclic variation of the mole ratios of CH_4 and O_2 in the feed, which started from the maximum ratio of 39 : 1, went down to a minimum value of 1 : 2 in the forward run, and then returned from this minimum to the maximum value of 39 : 1 in the reverse run [7]. All measurements were made under stationary conditions; the typical waiting time after any change in inlet composition was 20 to 30 min. A typical example of the results obtained at 550 °C is reported in Figure 9.1. This figure shows that a freshly prepared Rh/YSZ catalyst is active toward partial CH_4 oxidation at a methane/oxygen mole ratio of 39 : 1 (Fig. 9.1, left-hand parts). However, in the forward run (from the ratio of 39 : 1 to a ratio of 1 : 2) the catalytic activity of Rh/YSZ towards CO production decreases rapidly, and falls to almost zero at a CH_4/O_2 mole ratio of about three. In the reverse run, when the CH_4/O_2 ratio increases from 1 : 2 to 39 : 1, the specific reaction rate of CO formation remains almost zero while the rate of CO_2 formation slightly increases with increasing CH_4/O_2 mole ratios.

A completely different behavior was observed during partial methane oxidation with the Rh catalysts interfaced with TiO_2 (Fig. 9.1, right-hand parts). In this case both the forward and reverse runs are characterized by high catalytic activity towards CO and H_2 formation. In the forward run on Rh/TiO_2/YSZ, the specific rate of CO_2 production increases with decreasing CH_4/O_2 mole ratios, and reaches a maximum value when $CH_4 : O_2 = 1 : 1$, while at this gas composition the production of CO has almost completely ceased. Also, the reverse run on Rh/TiO_2/YSZ is characterized by a smaller rate of CO_2 formation and a higher catalytic activity towards CO formation than observed in the forward run.
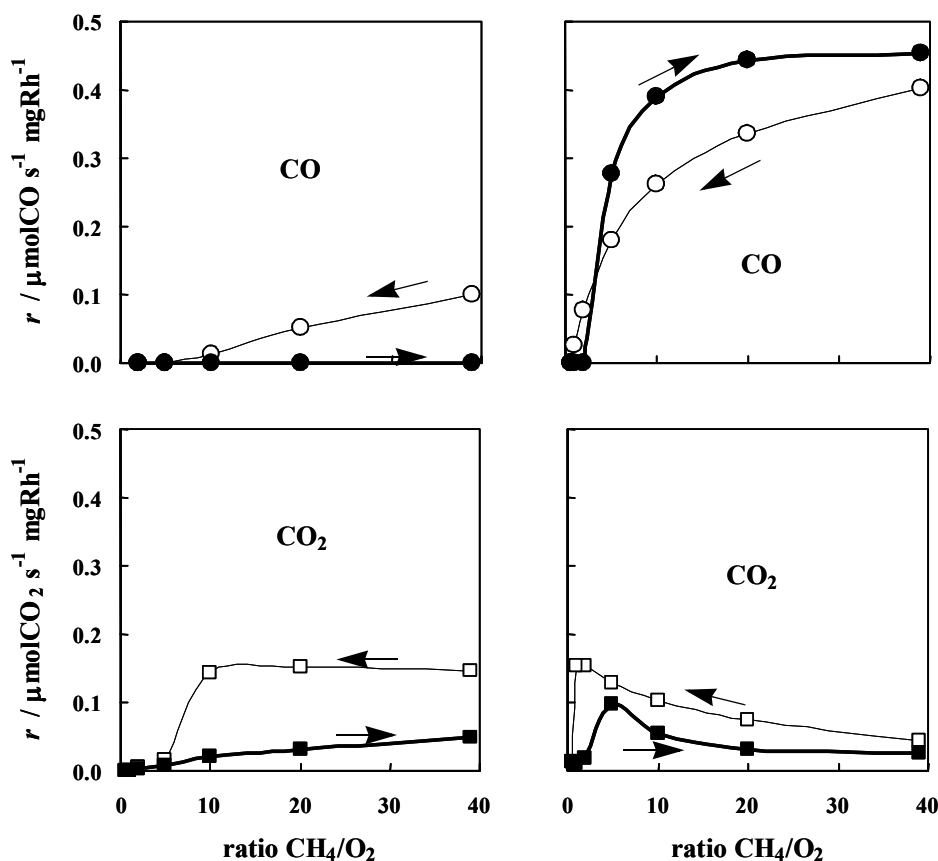
FIGURE 9.1. Oxidation of methane over Rh/YSZ (left-hand parts) and Rh/TiO$_2$/YSZ (right-hand parts) catalysts at $T = 550$ °C. Specific formation rates, r, of CO (circles) and CO$_2$ (squares) as functions of the CH$_4$/O$_2$ mole ratio. Feed composition: CH$_4$ variable, 0.5 kPa of O$_2$. Open symbols and light lines: forward scan; full symbols and heavy lines: reverse scan.

Figure 9.2 shows the selectivities toward CO formation as functions of the CH$_4$/O$_2$ mole ratios for Rh/YSZ and Rh/TiO$_2$/YSZ. The Rh films supported on a TiO$_2$ interlayer always display a much higher selectivity towards CO formation than the Rh/YSZ catalysts. However, the most interesting effect of the TiO$_2$ support resides in the fact that Rh/TiO$_2$/YSZ catalysts deactivated in an oxidizing feed (CH$_4$: O$_2$ < 2 : 1) are readily reactivated by exposure to a reducing gas compo-sition. The feed composition cycles can be repeated many times without any indication of activity losses. This is not so with the Rh/YSZ catalysts, which cannot be reactivated by exposure to a

reducing gas composition. In fact, here the reverse runs always were characterized by zero CO production, and hence zero CO selectivity (Fig. 9.2).
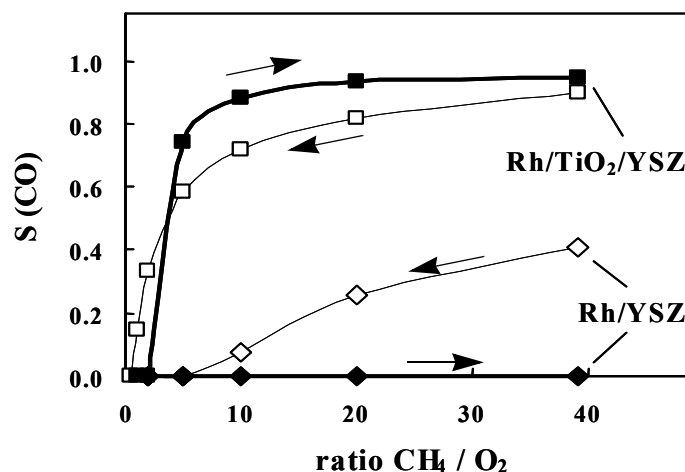
FIGURE 9.2. Oxidation of methane over Rh/YSZ (diamonds) and Rh/TiO$_2$/YSZ (squares) catalysts at T **= 550 °C. Selectivities of CO formation,** S(CO) **(Eq. (9.5)), as functions of the CH$_4$/O$_2$ mole ratio. Feed composition, symbols, and lines as in Fig. 9.1.**

Figure 9.3 shows the influence of temperature on the CO selectivities exhibited by Rh/TiO$_2$/YSZ catalysts while the feed composition was cycled between high and low methane/oxygen mole ratios. It can be seen that independently of the reaction temperature, in the forward runs the catalysts become deactivated at a CH$_4$/O$_2$ mole ratio close to unity. However, in the reverse runs, catalyst reactivation strongly depends on the reaction temperature: the higher the temperature, the lower is the CH$_4$/O$_2$ mole ratio at which the catalyst is reactivated. It should be noted that at temperatures below 400 °C a reactivation could not be observed.
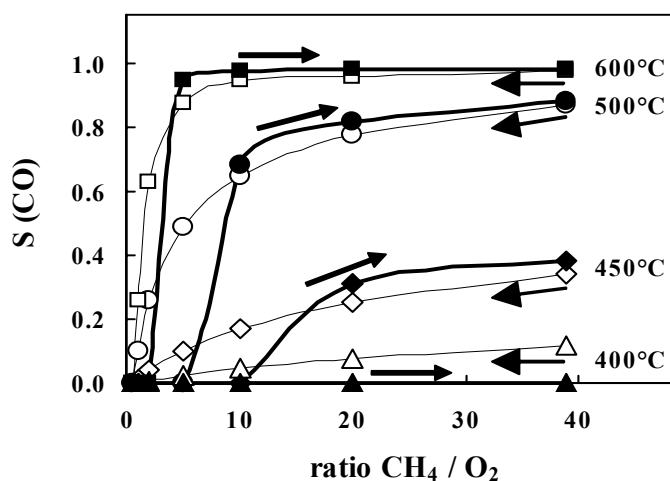
FIGURE 9.3. Selectivities of CO formation, *S*(CO) (Eq. (9.5)), during methane oxidation over Rh/TiO$_2$/ YSZ catalysts at different temperatures, as functions of the CH$_4$/O$_2$ mole ratio. Feed composition, symbols, and lines as in Fig. 9.1.

Figure 9.4 shows the oxygen conversions X(O$_2$) and the mole ratios of products H$_2$ and CO obtained at 550 °C over Rh/TiO$_2$/YSZ catalysts while cycling the methane/oxygen mole ratio. In the gas mixture produced, the H$_2$/CO ratios gradually increased with decreasing CH$_4$/O$_2$ mole ratio in the feed. Figure 9.4 shows that oxygen conversion is almost complete at CH$_4$/O$_2$ mole ratios higher than five (the region where the rhodium catalyst is active), but it is lower than 10 % at CH$_4$/O$_2$ mole ratios below two (the region where the rhodium catalyst is inactive).
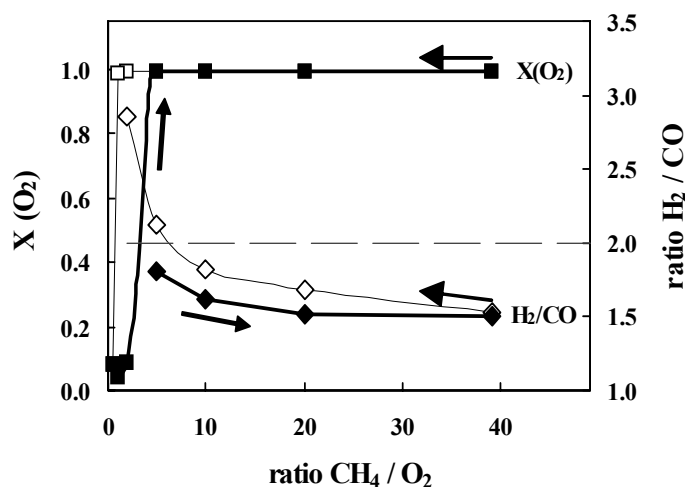
FIGURE 9.4. Oxygen conversion, X(O$_2$), and the mole ratios of H$_2$ and CO produced during methane oxidation over Rh/TiO$_2$/YSZ catalysts at T = 550 °C, as functions of the CH$_4$/O$_2$ mole ratio in the feed. Feed composition, symbols, and lines as in Fig. 9.1. The horizontal dashed line shows the mole ratio of H$_2$ and CO produced in the direct partial oxidation of methane with oxygen.

Figure 9.5 shows the potentials (U_{WR}) measured at the Rh films (working electrode) on the Rh/TiO$_2$/YSZ catalysts against the gold reference electrode while cycling the CH$_4$/O$_2$ inlet mole ratio at 550 °C. In the forward run, an abrupt increase in catalyst potential is observed at a CH$_4$/O$_2$ mole ratio close to unity, but the corresponding decrease in U_{WR} in the reverse run is much less abrupt. These trends of U_{WR} reflect the changes in catalytic activity and selectivity of the Rh films, both in the forward and in the reverse run (Fig. 9.2). The observed changes in catalyst potential are certainly related to modifications of the catalyst surface (rhodium oxide at low CH$_4$/O$_2$ mole ratios, metallic rhodium at high CH$_4$/O$_2$ mole ratios).

Results
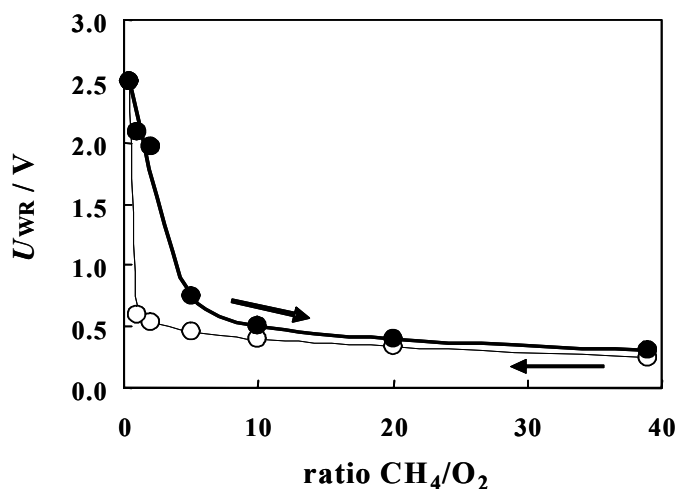
FIGURE 9.5. Potentials of the Rh/TiO$_2$/YSZ catalysts, U_{WR}, during methane oxidation at T = 550 °C as functions of the CH$_4$/O$_2$ mole ratio. Ring-type electrochemical cell with gold reference electrode. Feed composition, symbols, and lines as in Fig. 9.1.

9.3.2 Current-assisted activation of Rh/TiO$_2$/YSZ catalysts [8]

The most interesting feature of the Rh/TiO$_2$/YSZ catalysts that was revealed above is the fact that Rh films deactivated in oxidizing feeds (CH$_4$: O$_2$ < 2 : 1) are readily reactivated by exposure to a reducing gas composition. Figure 9.6 (which is similar to Fig. 9.3) shows the effects produced by varying feed compositions at two reaction temperatures, 550 °C and 600 °C, in the CO selectivity of Rh/TiO$_2$/YSZ catalysts while the gas compositions were cycled from high to low methane/oxygen mole ratios in the forward run, and back from the low mole ratio of 1 : 2 to the maximum value in the reverse run. All measurements were made under stationary conditions (waiting times of 20 to 30 min after any change in inlet composition). The figure shows that in the forward run (open symbols and light lines), the catalyst became deactivated at a CH$_4$/O$_2$ mole ratio of less than unity at both reaction temperatures. In the reverse run (full symbols and heavy lines), a CH$_4$/O$_2$ mole ratio of more than two was needed for reactivation of the catalyst, the actual values being a function of temperature. The higher the temperature, the lower will be the CH$_4$/O$_2$ mole ratio needed for reactivation of an inactive catalyst.
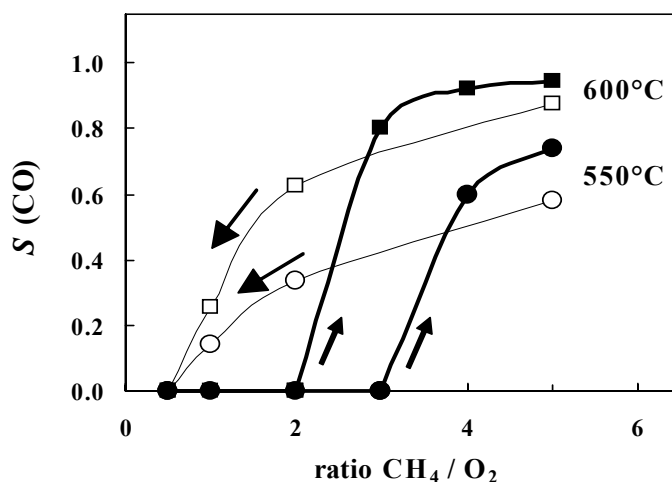
FIGURE 9.6. Selectivities of CO formation, S(CO) (Eq. (9.5)), during methane oxidation over Rh/TiO$_2$/ YSZ catalysts at different temperatures, 550 °C (circles) and 600 °C (squares), as functions of the CH$_4$/O$_2$ mole ratio. Feed composition: CH$_4$ variable, 0.5 kPa of O$_2$. The measurements were made under stationary conditions, see text. Open symbols and light lines: forward scan; full symbols and heavy lines: reverse scan. Inactive state: zero CO selectivity; active state: finite CO selectivity.

Within a range of feed compositions close to stoichiometric with respect to partial methane oxidation according to Eq. (9.1), the rhodium catalyst could exist in two distinct states: active and inactive, depending on the temperature and gas composition to which the catalyst had been exposed in advance (see Fig. 9.6). The Rh/TiO$_2$/YSZ catalysts treated with a reducing gas composition prior to the catalytic measurements were in the active state. To the contrary, after an exposure to oxidizing conditions, they were deactivated. The hysteresis observed in the reaction rates and selectivities of partial methane oxidation has been attributed to the formation and decomposition of rhodium surface oxide. Although a deactivated catalyst is not able to undergo spontaneous reactivation, this change can be assisted by different means. One possibility is a change in feed composition in the direction of higher CH$_4$/O$_2$ mole ratios, as reported above [7] and illustrated in Fig. 9.6 (a zoom of Fig. 9.1). An alternative way of reactivating the rhodium catalysts, by applying an appropriate current or potential at invariant feed composition, has been attempted in the present work.

The effects of applied currents on catalyst activity were studied at 550 °C and CH$_4$/O$_2$ mole ratios of 1 : 1 and 2 : 1 where, unless assisted otherwise, the oxidized Rh/TiO$_2$/YSZ cata-

lysts will remain inactive, which implies zero CO production and very low CO_2 production. Figure 9.7 illustrates the reactivation of a $Rh/TiO_2/YSZ$ catalyst achieved when applying a negative current while using stoichiometric gas feeds of $CH_4 : O_2 = 2 : 1$ (1 and 0.5 kPa, respectively). It shows in Part A the applied current density, i; in Part B the cell potential, U_{WC}; in Part C the specific reaction rates of CO_2 formation, r_{CO2}; and in Part D the specific reaction rates of CO production, r_{CO}, all as functions of time. At the outset the oxidized catalyst was inactive, and exhibited a very low rate of CO_2 formation and zero CO production under open-circuit conditions ($i = 0$). Upon applying a negative (cathodic) current, the rate of CO_2 formation gradually increased during the first few minutes until a critical state was reached where the CO_2 production suddenly increased, the catalyst's potential dropped, and a significant rate of CO production appeared which was attended by complete O_2 conversion (active catalyst state). No activation was observed within several hours when the applied negative current density was lower than 0.7 mA/cm^2 (curves (a) in Fig. 9.7). With an applied current density of 0.7 mA/cm^2, reactivation occurred after 33 minutes (curves (b) in Fig. 9.7), while at current densities in the range of 0.75 to 0.85 mA/cm^2 it occurred within a reasonably short time of 3 to 6 minutes (curves (c) in Fig. 9.7). Thus, the higher the current density, the shorter will be the time required for reactivation of the catalyst.

The same experiments were repeated with applied positive (anodic) currents, and gave similar results that are shown in Fig. 9.8 summarizing the observations in terms of *i-U* curves.

At an oxidizing feed ratio of $CH_4 : O_2 = 1 : 1$, an analogous behavior was recorded when negative or positive currents were applied but, in this case, currents an order of magnitude higher were required for reactivation than at a 2 : 1 feed ratio.

The observed differences in the specific rates of CO_2 and CO formation between open and closed-circuit operation cannot be attributed to the phenomenon of reversible electrochemical promotion, since no relaxation of the CO_2 and CO production could be observed after an interruption of the current in the active state (curves (b) and (c) in Fig. 9.7).
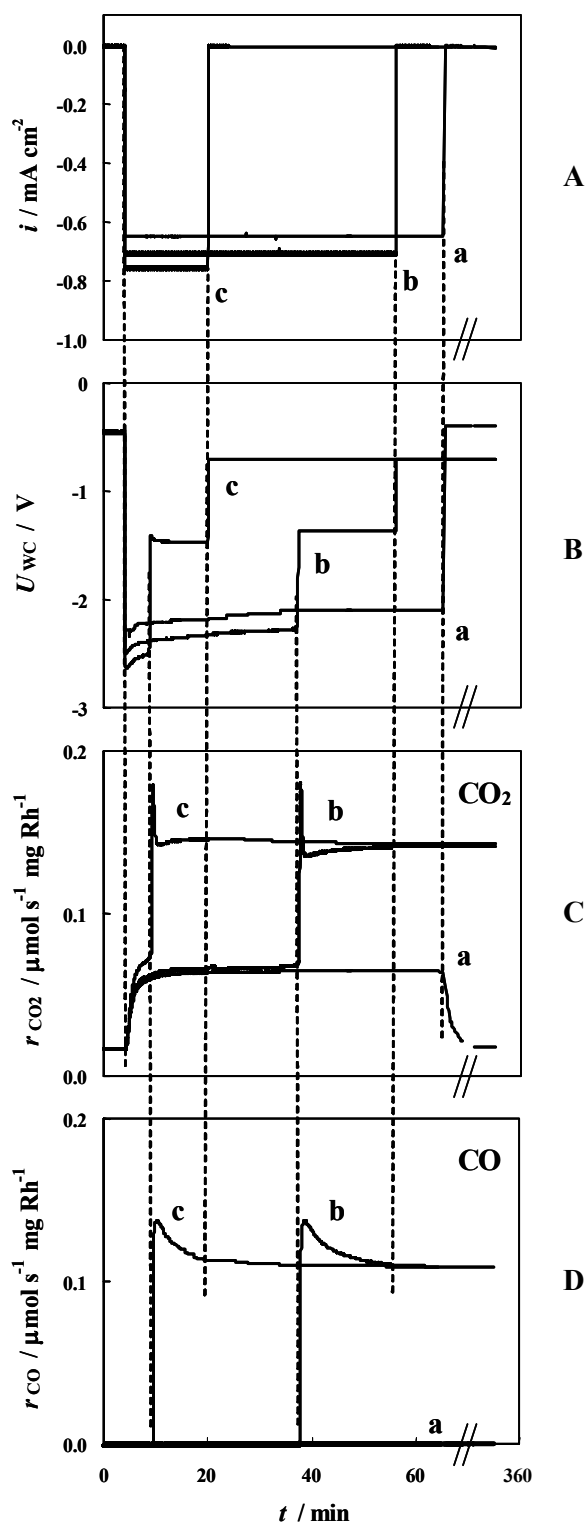
FIGURE 9.7. Activation of Rh/TiO$_2$/YSZ catalysts in a ring-type electrochemical cell by application of negative currents at stoichiometric feed compositions of CH$_4$(1 kPa)/O$_2$(0.5 kPa) at T = 550 °C. Three separate experiments performed with different current densities of (a) 0.65, (b) 0.70, and (c) 0.75 mAcm^{-2} are shown. In all experiments, the catalyst had in advance been deactivated with an oxidizing feed of CH$_4$(0.5 kPa)/O$_2$(1 kPa) at the same temperature. Shown as functions of time are: In Part A the applied current density, i; in Part B the cell potential, U_{WC}; in Part C the specific reaction rates of CO$_2$ formation, r_{CO2}; and in Part D the specific reaction rates of CO production, r_{CO}.

Similarly to the case where activation/deactivation was induced by changing feed composition (Fig. 9.6), the catalyst exhibited two distinct (and stable) open-circuit behaviors: prior to application of the current, it was inactive (stable inactive state), but once reactivated due to an applied current, the catalyst indefinitely maintained the high activity acquired, even after an interruption of the current.

The phenomena are reminiscent of the effects of permanent electrochemical promotion reported for IrO_2 and Rh catalysts [9-12]. After successful reactivation (curves (b) and (c) in Fig. 9.7), an interruption of the current only affects the cell potential, which is shifted to an open-circuit value (reduced catalyst) that is more negative than its value at the inactive (oxidized) catalyst, either prior to reactivation or after an unsuccessful attempt of reactivation with a current that was too low (curve (a) in Fig. 9.7, Part B). This pattern of behavior is equally valid for negative and positive activation currents, and leads to identical shifts of the open-circuit potential regardless of the sign of the applied current.

Figure 9.8 summarizes in terms of *i-U* curves the results obtained for the reactivation of oxidized $Rh/TiO_2/YSZ$ catalysts by application of a negative or positive current at a CH_4/O_2 mole ratio of 2 : 1 (stoichiometric feed). Two steady-state *i-U* curves are shown, one for rhodium oxide (inactive state) and one for Rh metal (active state), the former of course ending at the minimum current densities required to achieve reactivation. In fact, the system jumped from one curve to the other when the critical reactivation current was attained under given conditions, the jumps indicating decomposition of the rhodium surface oxide to Rh metal. Figure 9.8 nicely illustrates that positive and negative currents were equally efficient for reactivation, except that the negative current required to reactivate an inactive $Rh/TiO_2/YSZ$ catalyst was smaller than the corresponding positive current. Since the changes in catalytic activity of the $Rh/TiO_2/YSZ$ catalysts have been attributed to oxidation and reduction of the rhodium films, it is concluded that the reduction of rhodium surface oxide is stimulated, both by positive and by negative currents.
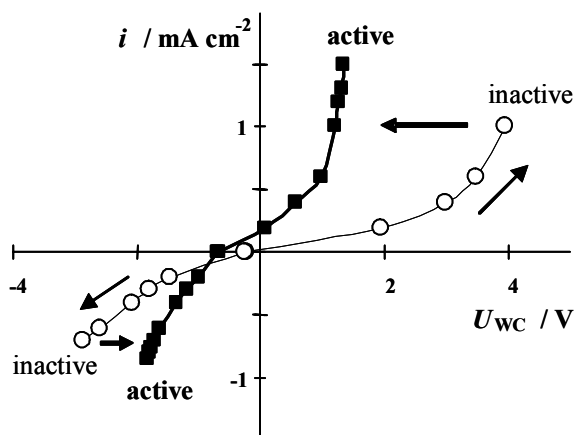
FIGURE 9.8. Steady-state polarization curves recorded in a ring-type $Rh/TiO_2/YSZ$ electrochemical cell, and the minimum current densities required to reactivate an inactive (oxidized) catalyst in less than 10 minutes at the stoichiometric CH_4(1 kPa)/O_2(0.5 kPa) feed composition at $T = 550$ °C. Open symbols and light lines: inactive state; full symbols and heavy lines: active state. Conditions of deactivation as in Fig. 9.7.

9.4 Discussion

The role of the TiO_2 support in the catalytic activity of Rh-based catalysts toward the partial oxidation of methane is certainly related to the stability against reduction of the rhodium oxide formed during exposure of the catalyst to an oxidizing atmosphere ($CH_4/O_2 < 2$), as in the case of ethylene oxidation on $Rh/TiO_2/YSZ$. In fact, it was demonstrated by the experimental results that with TiO_2 as a support, the Rh catalyst remains active even after exposure to feeds with a low CH_4/O_2 mole ratio (where rhodium oxide formation is favored). This is not the case in the absence of TiO_2, where the Rh catalysts remain inactive after exposure to oxidizing conditions ($CH_4/O_2 < 2$), even at high CH_4/O_2 mole ratios (Figs. 9.1, 9.2). An interpretation of these observations may be attempted, as in the case of C_2H_4 oxidation, either in terms of strong metal-support interactions (SMSI) [5] or by a model based on the theory of electrochemical promotion of catalysis (EPOC) [6] (Chapter 2).

The observed modifications of activity and selectivity of the Rh catalysts supported on TiO_2 might also be due to a partial reduction of TiO_2 (formation of TiO_x) by hydrogen produced during the reaction (Eq. (9.1)). In fact, TiO_2 can be reduced by hydrogen at relatively moderate temperatures (T > 400 °C) [5]. When one atom of oxygen is lost from the surface, two electrons

Discussion

are left in the oxygen vacancy to maintain electrical neutrality. One electron is trapped by a neighboring Ti^{4+} that becomes Ti^{3+}, while the other electron remains essentially free. This increases the free electron concentration at the surface, and hence causes a decrease in work function [13, 14]. TiO_x is a degenerate semiconductor having a very high carrier concentration; the high electrical resisitivity of TiO_2 (10^{10} ohm.cm) dramatically decreases upon partial reduction to values of 10 and 10^{-2} ohm.cm at $x = 1.9995$ and $x = 1.75$, respectively [15]. At the surface of dispersed TiO_2 supports partly covered with Rh catalyst, a spatially nonuniform surface oxidation is expected to occur resulting in the coexistence of regions where TiO_2 remains unreduced, and others with variable values of x depending on accessibility of the TiO_2 surface to hydrogen gas [16]. At the temperatures used in our experiments, the suboxide (TiO_x) species may well diffuse towards the metal and decorate its surface; this was actually demonstrated by XPS analysis (Chapter 4). Nevertheless, apart from the highly different electrical properties of TiO_2 and TiO_x, the essential role of the TiO_x entities that have migrated to the metal surface remains that of rendering part of this surface inaccessible to chemisorption and to catalytic action [17]. It is believed, therefore, that the geometric decoration model of SMSI cannot adequately interpret the present experimental findings.

The close analogy between electrochemical promotion of catalysis (EPOC) and strong metal-support interactions (SMSI) was already demonstrated in an earlier chapter (Chapter 6), and these phenomena may be considered as functionally identical, and only operationally different [18]. In the present case, when no potential or current is applied, even the operational difference should vanish under steady-state reaction conditions. The partly reduced oxide TiO_x and the Rh metal form local galvanic cells $TiO_x|TiO_2|Rh$ in which TiO_2 serves as the electrolyte. In these cells, as shown in Fig. 9.9, the promoting O^{2-} species are slowly consumed in the catalytic reaction occurring at the catalyst surface (the O^{2-} are a sacrificial promoter) while spent O^{2-} are continuously replenished via reduction of gaseous O_2 at the TiO_2/gas (or TiO_x/gas) interface; this is a self-driven electroless or wireless EPOC mechanism.
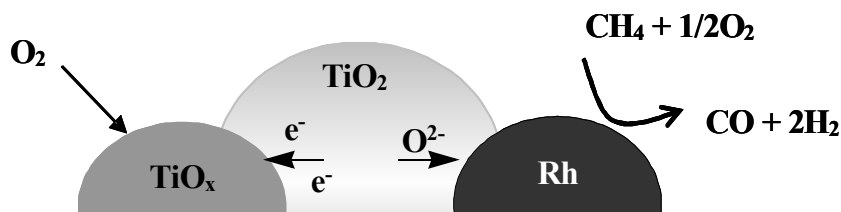
FIGURE 9.9. Self-driven electrochemical promotion of partial CH$_4$ oxidation on Rh interfaced with TiO$_2$, with internal short-circuiting.

A plausible and easy explanation of the reactivation of Rh catalysts supported on TiO$_2$ which is observed when applying a relatively high current could be by the effect of local heating. In fact, the actual temperature of the catalyst was not known, only that of the reacting gas mixture close to the catalyst was measured. The local temperature of the catalyst might be significantly different from the temperature measured in the gas phase, all the more because the low flow rates created a CSTR-like environment around the catalyst that was unfavorable for efficient heat transfer from the catalyst toward the gas. A very conservative estimate of the temperature difference between catalyst and gas, the former being heated by the applied current, was attempted using a heat transfer coefficient of 5 Wm^{-2}K^{-1}, which is typical for natural convection in gases. This would give a high estimate of catalyst temperature, because the actual heat transfer, although poor, was certainly better than that by natural convection.

Considering the heating power in the inactive (more highly resistive) catalyst at the moment of reactivation (see Fig. 9.8), and assuming bulk heating, hence a uniform temperature within the coating, temperature differences between catalyst and gas as low as 2 and 6 degrees were calculated for negative and positive applied currents at a stoichiometric feed composition and $T = 550$ °C. Such a weak local heating cannot be responsible for the observed reactivation, since at the given gas composition at open circuit, the catalyst remained inactive even at 600 °C (see Fig. 9.6). It can now be concluded that local heating by the applied current cannot be the sole cause of reactivation. This conclusion is further reinforced by the asymmetry of the phenomenon, the positive currents required to achieve reactivation being higher than the negative currents required under the same conditions. Although the semiconductor character of the interlayer may

Discussion

also contribute to the asymmetry, the asymmetric current requirements suggest above all that different mechanisms of catalyst regeneration prevail when applying positive and negative currents.

The rectivation of inactive (oxidized) rhodium catalysts by negative currents can be explained most simply by electrochemical reduction of the rhodium oxide:

$$Rh^{3+} + 3e^- \rightarrow Rh^0 \tag{9.6}$$

In fact, even the minimum amount of charge passed through the catalyst during activation (about 4 mA over a time of three minutes in stoichiometric feed) would be enough to reduce roughly 10 % of the total amount of rhodium deposited, if present as an oxide, while the fraction of rhodium atoms exposed to the gas (and hence catalytically active) is actually as low as 1 % or less in Rh paste catalysts.

The reactivation by positive currents in turn can be explained by the theory of electrochemical promotion of catalysis. Positive currents supply O^{2-} ions to the catalyst/support interface. These ions are released at the three-phase boundary (tpb), then spread out across the entire gas-exposed catalyst surface by a mechanism of backspillover. During their migration these ions are accompanied by their mirror charges in the catalyst, thus forming an overall neutral double layer of dipoles at the catalytically active surface. The population of the surface with dipoles raises the surface potential, the concomitant increase in work function lowers the bond strength of chemisorbed oxygen as well as the stability of the rhodium surface oxide against chemical reduction.

The current-assisted activation of the Rh/TiO$_2$/YSZ catalysts produced dramatic enhancements of both the catalytic activity and the selectivity toward partial CH_4 oxidation; the high catalytic reaction rates thus acquired remained unchanged after an interruption of the current. This effect of activation may be quantified by the "permanent" rate enhancement ratio, γ, defined as the ratio of the open-circuit reaction rates prior to (r_0) and after (r') application of the current (Chapter 2, section 1.2):

$$\gamma = \frac{r'}{r_0} \tag{9.7}$$

The reaction rates are suitably expressed in terms of reacted oxygen (mol O s^{-1}) calculated from the specific rates of CO and CO_2 formation according to the stoichiometry of reactions (9.1)

and (9.2), respectively. At the stoichiometric gas composition ($CH_4 : O_2 = 2 : 1$) a "permanent" rate enhancement ratio, γ, as high as 11 was obtained. However, the most interesting feature of current-assisted activation is the increase in selectivity of the Rh catalysts. Prior to application of the current the selectivity for partial methane oxidation was zero (no CO formation at all) while during current flow as well as after interruption of the current, the selectivity of the Rh catalysts was as high as 45 % at the stoichiometric gas composition at 550 °C.

9.5 Conclusions

In this chapter, the partial oxidation of methane over Rh catalysts supported on YSZ containing a thin interlayer of TiO_2 was investigated. Under working conditions the rhodium catalyst exists in two well distinguished surface states: active and inactive. According to measured catalyst potentials, these two states correspond to rhodium metal (active state) and rhodium oxide (inactive state).

The remarkable increase in catalytic activity and selectivity towards CO and H_2 production that occurs when Rh is in contact with TiO_2 is related to the drop in stability of the Rh surface oxide against reduction to metallic Rh. This phenomenon may be interpreted, either by strong electronic-type metal-support interactions or by a self-driven wireless electrochemical promotion mechanism. In both cases, the ultimate cause of promotion are different work functions of catalyst and support. Equilibration of the Fermi levels causes weakening of the Rh-O chemisorptive bonds, and facilitates reduction of oxidized surface sites.

At gas compositions close to stoichiometric ($CH_4 : O_2 = 2 : 1$) at temperatures in the range of 500 to 600 °C, Rh catalysts have two stable states: inactive (Rh oxide) and active (Rh metal), depending on the gas composition to which the catalyst had been exposed in adance. It was found that positive and negative currents both can produce reactivation manifesting itself in a large increase of both the catalytic reaction rate and the selectivity for partial methane oxidation. This phenomenon is a typical example of permanent electrochemical promotion, since after interruption of the current the reactivated catalyst remained active indefinitely. At the stoichiometric feed composition at 550 °C a γ-value ("permanent" rate enhancement ratio) of 11 and a CO selectivity of 45 % were obtained.

The results suggest that the mechanisms of reactivation by positive and negative currents are different. It is believed that negative currents sustain the electrochemical reduction of rhodium

oxide, while positive currents cause breakup of rhodium surface oxide due to weakening of the rhodium-oxygen bond strength by accumulated backspillover oxygen at the gas-exposed catalyst surface, just as seen in the reversible electrochemical promotion of catalysis with anodic currents.

9.6 References

1.   M. A. Pena, J. P. Gomez, and J. L. G. Fierro, *Appl. Catal. A,* **144** (1996) 7.

2.   S. C. Tsang, J. B. Claridge, and M. L. H. Green, *Catal. Today,* **23** (1995) 3.

3.   M. Prettre, C. Eichner, and M. Perrin, *J. Chem. Soc. Faraday Trans.,* **43** (1946) 335.

4.   D. A. Hickman, E. A. Haupfear, and L. D. Schmidt, *Catal. Lett.,* **17** (1993) 223.

5.   S. J. Tauster, S. C. Fung, and R. L. Garten, *JACS,* **100** (1978) 170.

6.   C. G. Vayenas, S. Bebelis, C. Pliangos, S. Brosda, and D. Tsiplakides, *Electrochemical activation of catalysis. Promotion, Electrochemical promotion, and metal-support interaction.* Kluwer Academic/Plenum Publishers, New York (2001).

7.   E. A. Baranova, G. Fóti, and C. Comninellis, *Electrochem. Commun.,* **6** (2004) 170.

8.   E. A. Baranova, G. Fóti, and C. Comninellis, *Electrochem. Commun.,* **6** (2004) 389.

9.   J. Nicole and C. Comninellis, *J. Appl. Electrochem.,* **28** (1998) 223.

10.   C. Pliangos, C. Raptis, T. Badas, and C. G. Vayenas, *Solid State Ionics,* **136-137** (2000) 767.

11.   E. Varkaraki, J. Nicole, E. Plattner, and C. Comninellis, *J. Appl. Electrochem.,* **25** (1995) 978.

12.   G. Fóti, O. Lavanchy, and C. Comninellis, *J. Appl. Electrochem.,* **30** (2000) 1223.

13.   Y. W. Chung, W. J. Lo, and G. A. Somorjai, *Surface Sci.,* **64** (1977) 588.

14.   T. Ioannides and X. E. Verykios, *J. Catal.,* **161** (1996) 560.

15.   *Gmelin's Handbook Part 24* Weinheim (1951).

16.   F. Pesty, H. P. Steinruck, and T. E. Madey, *Surface Sci.,* **339** (1995) 83

17.   G. L. Haller and D. E. Resasco, *Advances in Catalysis,* **36** (1989) 173.

18.   J. Nicole, D. Tsiplakides, C. Pliangos, X. E. Verykios, C. Comninellis, and C. G. Vayenas, *J. Catal.,* **204** (2001) 23.

CHAPTER 10 **General discussion**

The main results obtained in the present work are discussed and the principal conclusions drawn. This work continues the complex investigations started several years ago in the "NEMCA group" of Prof. Comninellis, EPFL. It is focused on the electrochemical promotion of catalysis (EPOC) and on its connection with the phenomenon of metal-support interactions (MSI). Both EPOC and MSI are interfacial phenomena, therefore, one of the major challenges in the field of electrochemical promotion is that of elucidating the mechanism by which the promoting effect propagates from one interface (catalyst/electrolyte) to the other (catalyst/gas). Due to the interdisciplinary nature of electrochemical promotion, which involves concepts from at least five different fields (catalysis, surface science, electrochemistry, solid state ionics, chemical reaction engineering), the present study uses different techniques and approaches in order to reach the goals contemplated. For the experimental work, two Rh catalysts were chosen where Rh was deposited by sputtering in a thickness of 40 nm, either directly on YSZ or on YSZ covered with a TiO_2 layer (4 μm).

In the first chapter of results (Chapter 4: *Characterization of Rh catalyst electrode*s), data characterizing the Rh catalyst electrodes sputtered on YSZ (Rh/YSZ) and on a layer of TiO_2 deposited on YSZ support (Rh/TiO$_2$/YSZ) were presented. Several types of analysis were employed in order to elucidate the morphological properties (SEM, AFM) of the Rh catalysts and their chemical surface composition (XPS). It follows from SEM and AFM analyses that TiO_2 forms a nanostructured layer completely covering the YSZ substrate. The thin layer of Rh catalyst sputtered on YSZ or TiO$_2$ forms continuous layers and replicates the support morphology. In both systems, Rh/YSZ and Rh/TiO$_2$/YSZ, the catalyst films have a nanoparticle-size grain structure. After exposure of the catalysts to working conditions (high temperature, applied currents/potentials, mixtures of C_2H_4 and O_2) during 200 hours, it was confirmed that the catalyst films have good stability and adhesion to the substrate surface.

The oxidation state of the Rh surface undergoes considerable changes during exposure, both to oxidizing or to reducing gas compositions. After reduction as well as after oxidation, Rh supported on TiO$_2$ was found to be in a more highly reduced state than Rh on YSZ. After reduing treatment, the Rh/TiO$_2$/YSZ sample contains a larger amount of weakly bonded oxygen, which can be attributed to oxygen "backspillover" from the TiO$_2$. This oxygen may migrate in some form of TiO_x, since after reduction some quantity of Ti was found on the Rh surface but disappeared after oxidation of the catalyst. The driving force for this migration is the difference in work functions of Rh catalyst and TiO$_2$ support. The migration occurring more particularly after a reducing treatment leading to electronic-type SMSI.

These characteristics of the two catalysts were often recalled in later chapters in order to explain the electrochemical and catalytic behavior of the Rh/YSZ and the Rh/TiO$_2$/YSZ catalysts.

In Chapter 5 (*Electrochemical characterization of the Rh catalysts: Polarization measurements*), studies of oxygen kinetics (O$_2$/O^{2-} couple) performed for the first time on Rh thin-film electrodes interfaced with a pure ionic conductor (ZrO$_2$ + Y$_2$O$_3$ solid electrolyte) and with a mixed electronic-ionic conductor (TiO$_2$) supported on YSZ are reported. The temperature range examined was between 450 and 600 °C, the oxygen partial pressures ranged from 0.5 to 20 kPa. Exchange current measurements at different T and P_{O_2} provided important information as to the kinetics and mechanism of the O$_2$/O^{2-} electrode reaction at the interface. The exchange current

densities found at Rh/TiO$_2$(4 μm)/YSZ are less than half those found at Rh/YSZ, and decrease further with increasing titania thickness.

From the experimental results obtained at low and high polarization, and after an analysis of literature data, a mechanism was proposed for the O$_2$/O^{2-} exchange process. In the cathodic process, the first step is fast dissociative adsorption of oxygen at the gas-exposed Rh surface. The second step is atomic oxygen diffusion from the gas-exposed catalyst surface to the electrochemical reaction sites (ERS), where a fast two-electron transfer reaction then takes place:

$$O_2 \leftrightarrows 2\ O_{(MG)} \text{ fast step} \tag{10.1}$$

$$O_{(MG)} \xrightarrow{\textit{diffusion}} O_{(ERS)} \text{ slow step} \tag{10.2}$$

$$O_{(ERS)} + 2e^- \rightarrow O^{2-} \qquad \text{fast step} \tag{10.3}$$

The cathodic process is limited by interfacial diffusion of oxygen atoms from the gas-exposed metal surface to ERS. These can be located, either at the Rh/solid electrolyte two-phase boundary or at the Rh/solid electrolyte/gas three-phase boundary. It is obvious that so long as the rate of surface diffusion is lower than the rate of charge transfer, current will flow predominantly near the three-phase boundary region.

The anodic process includes two steps: two-electron transfer at ERS and oxygen desorption. The most probable location of the electrochemically reactive sites is the three-phase boundary, where the atomic oxygen produced recombines to molecules and untergoes exchange with the gas phase.

$$O^{2-} - 2e^- \rightarrow O_{(ERS)} \qquad \text{slow step} \tag{10.4}$$

$$2\ O_{(ERS)} \leftrightarrows O_{2(G)} \text{ fast step} \tag{10.5}$$

The mechanism (Equations (10.1) to (10.5)) proposed could be confirmed in the next chapter (Chapter 6: *Electrochemical characterization of Rh catalysts: Impedance measurements*) by impedance spectroscopy. First, a theoretical impedance model of the O$_2$/O^{2-} process at the equilibrium potential was developed. Then the impedance model was confronted with the experimental data. For this purpose, electrochemical impedance spectra were recorded at T = 450 - 600 °C

and Po_2 = 0.5 kPa under open-circuit conditions. The experimental results for the equilibrium process O_2/O^{2-} at Rh/YSZ and Rh/TiO$_2$/YSZ are in good accord with theoretical impedance representations of the reaction mechanism. The good correlation between theory and experiment constitutes support for validity of the reaction mechanism proposed in the preceding chapter.

The exchange current densities i_0 extracted from the impedance measurements are similar to the values obtained for i_0 from steady-state polarization measurements, and are much lower for Rh/TiO$_2$/YSZ than for Rh/YSZ, indicating that the former catalyst is more highly polarizable. The agreement between the exchange current values obtained from steady-state polarization and impedance techniques is satisfactory. The difference in exchange currents found between the two catalysts is in good accord with the results of electrochemical promotion found for Rh/YSZ and Rh/TiO$_2$/YSZ, where with the same applied current, a higher catalyst potential was observed for Rh interfaced with TiO$_2$ than for Rh/YSZ (see Chapter 8).

Verifying the mechanism of electrochemical promotion was the topic of the second part of Chapter 6. To this end impedance measurements at Rh/YSZ and Rh/TiO$_2$/YSZ were performed under polarization. At overpotentials of $|\eta| > 10$ mV, only the anodic or the cathodic process will take place at the Rh electrode.

Under positive polarization a process of backspillover occurs in addition to oxygen evolution (Eqs. (10.4) and (10.5)) in the system Rh/solid electrolyte. Applied positive potentials lead to oxidation of oxygen ions at the three-phase boundary as well as to some charge injection into the metal surface that is exposed to the gas phase. This positive surface charge will induce migration of oxygen ions from the YSZ and formation of an overall neutral double layer, an "effective electrochemical double layer", at the metal/gas interface. Under negative polarization, oxygen is reduced at Rh/YSZ, a process that includes dissociative adsorption of atomic oxygen at the gas-exposed Rh surface, followed by its diffusion to the three-phase boundary (MEG) and further to the Rh/solid electrolyte two-phase boundary where charge transfer then takes place.

Interesting observations were made concerning the behaviour of the double-layer and adsorption capacitances at the Rh/YSZ electrode (Fig. 10.1). The double-layer capacitance remains almost constant when a positive or negative potential is applied, while the adsorption capacitance significantly increases upon positive polarization, but remains constant upon negative polarization. These results are evidence for formation of an "effective double layer" across the entire gas-exposed electrode surface. The capacitance of this metal/gas double layer had values

much higher (100 - 300 $\mu F/cm^2$ in order of magnitude) than that of the metal/solid electrolyte double layer (0.4 - 2 $\mu F/cm^2$).

The values of the two capacitances are related to N_G, the gas-exposed surface area of the electrode, and to N_{tpb}, the "surface area" of the three-phase boundary, by Eq. (6.39) of Chapter 6. From impedance data it is then possible to calculate the length of the tpb. The values obtained for N_{tpb} are of the order of 10^{-10} mol Rh/cm^2 electrolyte for Rh/YSZ, roughly a factor of 10^2 smaller than N_G for which a value of $N_G = 1.6 \cdot 10^{-8}$ mol was found in Chapter 3, section 2.2, and correspond to a "length", l_{tpb}, of several km per cm^2 of the solid electrolyte.
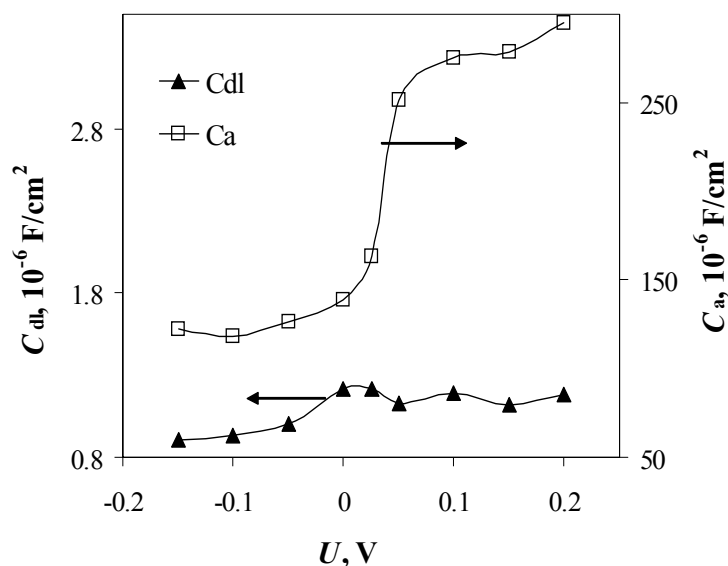
FIGURE 10.1. Values of double-layer and adsorption capacitances at Rh/YSZ calculated with the equivalent circuit of Fig. 6.5, Chapter 6. Po$_2$ = 0.5 kPa, T = 600 °C.

From impedance measurements at Rh/TiO$_2$/YSZ, it was seen that strong polarization led to changes in the reaction mechanism. Rhodium electrodes interfaced with TiO$_2$ yield more complex spectra when polarized; the associated electrode processes merit further detailed examination.

Effects of metal-support interactions have been investigated, both at thin (40 nm) and at thick (several μm) Rh catalyst films supported on YSZ and TiO$_2$/YSZ, using two model reac-

tions: ethylene oxidation (*Chapter 7: Promotion of Rh catalysts: Open-circuit ethylene oxidation*) and partial methane oxidation (*Chapter 9: Promotion of Rh catalysts: Partial methane oxidation at open and closed circuit*). In these reactions, a sudden transition from a region of high to a region of low reaction rates is observed to occur at these Rh catalysts with increasing oxygen partial pressure. This sudden transition is accompanied by the formation of rhodium surface oxide responsible for deactivation of the catalyst. A phenomenological model was proposed (*Chapter 7: Promotion of Rh catalysts: Open-circuit ethylene oxidation*) with the aim of explaining this deactivation of Rh catalysts during ethylene and methane oxidation. This model is quite similar to the model proposed by Bolzonella *et al* (see Chapter 2, section 1.3), but in addition takes into account the external parameters that are responsible for surface deactivation, and is able to explain the hysteresis of reaction rates often observed at Rh catalysts.

Two kinds of sites, activated (Rh-O_{ad}) or nonactivated (Rh), are assumed to exist on Rh metal. Their mutual transformation is a microscopic process described by the following reaction:

$$M \underset{k_{-1}}{\overset{k_1}{\rightleftarrows}} M^*$$ (10.6)

where M is a nonactivated site and M^* is an activated site.

The activated site may contribute to the reaction rate r by generating a product C while using up a reactant R, and then returns to its nonactivated state:

$$R + M^* \overset{k_2}{\longrightarrow} M + C$$ (10.7)

Product C is supposed to leave the surface, and thus no longer to interact with the process considered. The reactive transformation (10.7) can only occur when the activated site M^* (Rh-O_{ad}) does not belong to the structure $\Sigma(p)$ deactivating the surface (Rh_2O_3). The sites belonging to the structure $\Sigma(p)$ are called deactivated sites. The fraction p of activated sites is a function of time written as:

$$\frac{dp}{dt} = k_1(1-p) - k_{-1}p - k_2[p - P(p)]$$ (10.8)

This model is able to reproduce the hysteresis effects seen between forward and reverse scans of an external parameter such as the partial pressures of reactants.

The Rh/YSZ catalyst has a finite catalytic activity towards ethylene and partial methane oxidation, only in reduced feeds having an excess of C_2H_4 or CH_4. Once deactivated in an oxidizing gas mixture, this catalyst could not be reactivated by mere exposure to a reducing gas mixture. According to the values of catalyst potential, deactivation is due to the formation of Rh surface oxide poisoning the reactions.

A completely different behavior was exhibited by the Rh catalyst interfaced with TiO_2 during ethylene and partial methane oxidation. Under working conditions, this rhodium catalyst exists in two well distinguished surface states: active and inactive, both being stable under the appropriate conditions. It could be demonstrated that a reactivation of deactivated (oxidized) Rh/TiO_2/YSZ catalysts is possible via a mere shift of the feed composition from lean to rich. According to the values of catalyst potential, the two states correspond to rhodium metal (active state) and rhodium oxide (inactive state).

Thus, when Rh is in contact with TiO_2 a remarkable increase in catalytic activity and selectivity of the Rh catalyst is seen with respect to CO and H_2 production. These improvements are due to a lower stability of TiO_2-supported Rh surface oxide against reduction to metallic Rh. This promotion effect may be interpreted, either in terms of strong electronic-type metal-support interactions or by a self-driven wireless (electroless) electrochemical promotion mechanism. In both cases, the ultimate cause of promotion are different work functions of catalyst and support. Equilibration of the Fermi levels causes a weakening of the Rh-O chemisorptive bonds and facilitates the reduction of oxidized surface sites.

These considations reveal the close analogy that exists between electrochemical promotion of catalysis (EPOC) and strong metal-support interactions (SMSI), two phenomena that may be considered as being functionally identical, and only operationally different. In partial methane oxidation, when TiO_2 can be reduced by hydrogen produced during the reaction, even the operational difference vanishes under steady-state reaction conditions. The partly reduced titanium oxide (TiO_x) and the Rh metal form local galvanic cells TiO_x|TiO_2|Rh in which TiO_2 functions as the electrolyte. In these cells, as shown in Fig. 10.2, the promoting O^{2-} species are slowly consumed in the catalytic reaction occurring at the catalyst surface (the O^{2-} are sacrificial promoters) while spent O^{2-} are continuously replenished via reduction of gaseous O_2 at the TiO_2/gas (or TiO_x/gas) interface: a self-driven wireless EPOC mechanism.
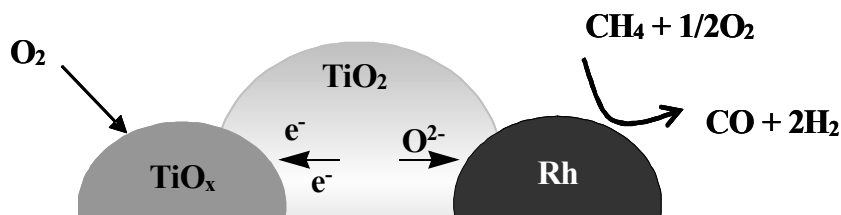
FIGURE 10.2. Self-driven electrochemical promotion of partial CH$_4$ oxidation on Rh interfaced with TiO$_2$, with internal short-circuiting.

Electrochemical promotion of catalysis has been investigated on the basis of the same model reaction of ethylene oxidation (*Chapter 8: Electrochemical promotion: Closed-circuit ethylene oxidation*) and partial methane oxidation (*Chapter 9: Promotion of Rh catalysts: Partial methane oxidation at open and closed circuit*). The electrochemical promotion of thin (40-nm) Rh films prepared by sputtering has been demonstrated for the first time. The pronounced electrophobic electrochemical promotion of C$_2$H$_4$ oxidation on Rh observed on these films is similar to that observed with thick Rh films.

When small anodic currents are applied to the Rh/YSZ catalyst, periodic oscillations of the catalytic rate and catalyst potential occurring with a frequency that can be controlled electrochemically are excited (Fig. 10.3). These oscillations can be interpreted in terms of the formation and decomposition of rhodium surface oxide: minimum rates correspond to an oxidized Rh surface (Rh oxide), maximum rates to reduced Rh catalyst (Rh metal). This phenomenon is fully reversible, and only observed under closed-circuit conditions. At the maximum of the oscillations, a rate enhancement ratio of $\rho = 52$ and a faradaic efficiency of $\Lambda = 1024$ were found.

The results obtained for C$_2$H$_4$ oxidation over Rh nanofilm catalysts can be summarized as follows: (*i*) Rate oscillations can be triggered by applied positive currents, only in the domain where the catalyst exhibits bistability. At low $P_{C_2H_4}/P_{O_2}$ ratios the applied currents do not lead to rate oscillations. Under more strongly reducing conditions (high $P_{C_2H_4}$), applied currents lead to a dramatic increase in reaction rate. In this domain, the oscillations have a very small amplitude

and almost die away. (*ii*) The frequency of the oscillations increases with increasing $P_{C_2H_4}/P_{O_2}$ ratios, temperatures, and gas flow rates. (*iii*) The catalyst potential and the rate of CO_2 production exhibit synchronous oscillations while a decrease in catalyst potential always corresponds to an increase in reaction rate. (*iv*) The Rh surface oxide is stable at given temperatures and gas compositions. When by anodic polarization and the concomitant O^{2-} supply to the catalyst, a weakening of oxygen bonds to the rhodium surface is caused, the oxygen that had previously been associated with Rh_2O_3 becomes available for the reaction with C_2H_4, and this causes an abrupt decrease in the $P_{C_2H_4}/P_{O_2}$ ratio over the catalyst. When this ratio falls below some critical ratio $(P_{C_2H_4}/P_{O_2})^{crit}$, formation of surface Rh_2O_3 will resume. However, this causes an increase in the $P_{C_2H_4}/P_{O_2}$ ratio due to extra consumption of gaseous O_2, so the oxide becomes unstable again, and the cycle is repeated.

FIGURE 10.3. Response of the catalytic rate (Part A) and of catalyst potential (Part B) of the Rh/YSZ catalyst electrode to an applied anodic current step of +50 µA. $T = 350$ °C. Gas composition: $P_{O_2} = 0.41$ kPa, $P_{C_2H_4} = 2$ kPa. Flow rate: 200 mL/min.

Catalysts Rh/TiO$_2$/YSZ exhibit pronounced nonoscillatory electrochemical promotion; their catalytic activity for C$_2$H$_4$ oxidation can be reversibly enhanced by up to a factor of 80 by applying a positive anodic current or potential (Fig. 10.4). The increase in oxidation rate is up to 2000 times larger than the rate of supply of O^{2-} to the Rh catalyst electrode.
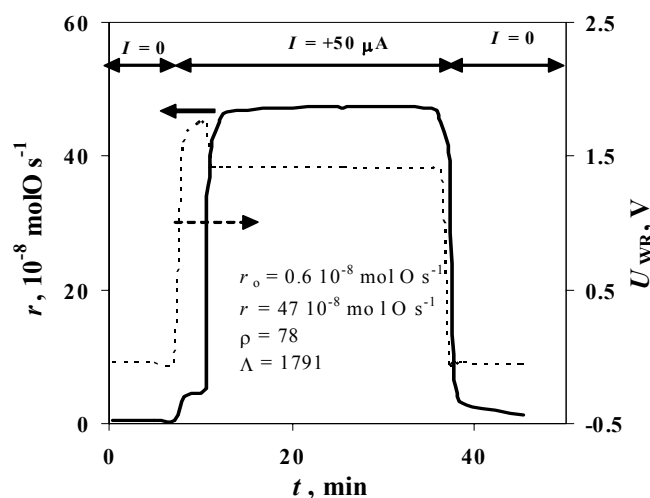
FIGURE 10.4. Response of the catalytic rate (solid line) and of catalyst potential (dotted line) of the Rh/TiO$_2$/YSZ catalyst electrode to an applied anodic current step of +50 μA. T = 350 °C. Gas composition: P_{O_2} = 0.4 kPa and $P_{C_2H_4}$ = 0.64 kPa. Flow rate: 200 mL/min.

That the polarizability of Rh/TiO$_2$/YSZ catalyst electrodes is much higher than that of Rh/YSZ catalyst elelctrodes, is in good agreement with the polarization and impedance measurements (Chapters 5 and 6). It was found that the i_0 values at the Rh/TiO$_2$ interface were about twice lower than those at the Rh/YSZ interface. The smaller exchange current density characteristic of the Rh/TiO$_2$/YSZ interface leads to a higher faradaic efficiency, Λ (Table 10.1).

TABLE 10.1. Faradaic efficiencies and exchange current densities in the Rh/YSZ and Rh/TiO$_2$/YSZ systems at T = 350 °C and $P_{O_2} \approx 0.5$ kPa

Catalyst electrode	Λ (Figs. 10.3 and 10.4)	I_0, A
Rh/YSZ	1024	$2.2*10^{-8}$
Rh/TiO$_2$/YSZ	1791	$1.2*10^{-8}$

The pronounced electrophobic behavior (ρ-values of up to 80) observed at both of the thin Rh films (Rh/YSZ and Rh/TiO$_2$/YSZ), which is semiquantitatively similar to that observed at thick Rh/YSZ films, mainly depends on destabilization of surface Rh$_2$O$_3$ via repulsive lateral interactions with the electromigrating backspillover O^{2-} ions poisoning the catalytic reaction.

At thick Rh catalyst films interfaced with TiO_2/YSZ, an interesting behavior was observed during partial methane oxidation (*Chapter 9: Promotion of Rh catalysts: Partial methane oxidation at open and closed circuit*). In addition to the strong metal-support interactions, this catalyst exhibits a pronounced "permanent" electrochemical promotion (Chapter 2, section 1.2), *ie*, under certain working conditions the catalyst can be activated, both by applying a positive or a negative current. At gas compositions close to stoichiometric ($CH_4 : O_2 = 2 : 1$) and temperatures between 500 and 600 °C, these Rh catalysts can exist in either of two stable states: inactive (Rh oxide) and active (Rh metal), depending on the gas composition to which the catalyst had been exposed in advance. It was found that positive as well as negative currents may lead to activation manifesting itself in a large increase of the catalytic reaction rate and in the selectivity for partial methane oxidation. This phenomenon is a typical example of permanent electrochemical promotion, inasmuch as after an interruption of the current the reactivated catalyst will remain active indefinitely. With a stoichiometric feed composition at 550 °C a "permanent" rate enhancement ratio of $\gamma = 11$ and a CO selectivity of 45 % were obtained.

The results suggest that the mechanisms of reactivation by positive and negative currents are different. It is believed that negative currents sustain the electrochemical reduction of rhodium oxide, while positive currents cause breakup of the rhodium surface oxide due to weakening of the rhodium-oxygen bond strength by accumulated backspillover oxygen at the gas-exposed catalyst surface, just as seen in the reversible electrochemical promotion of catalysis with anodic currents.

List of symbols

1. List of acronyms

DIMSI	dopant-induced metal-support interaction
EIS	electrochemical impedance spectroscopy
EP	electrochemical promotion
EP_r	reversible electrochemical promotion
EP_i	irreversible electrochemical promotion
EPOC	electrochemical promotion of catalysis
ME	metal/electrolyte interface
MEG	metal/electrolyte/gas interface
MG	metal/gas interface
MSI	metal-support interaction
NEMCA	non-faradaic electrochemical modification of catalytic activity
rds	rate determining step
SEM	scanning electron microscopy
tpb	three-phase boundary
TPD	temperature programmed desorption

SMSI	strong metal-support interaction	
XPS	x-ray photoelectron spectroscopy	
YSZ	yttria-stabilized zirconia	

2. Roman symbols

Symbol	Meaning	Units
A	constant of Warburg impedance	ohm $s^{0.5}$
C	concentration	mol m^{-3}
C_a	adsorption capacitance	F cm^{-2}
C_{dl}	double layer capacitance	F cm^{-2}
C_{da}	double layer capacitance at anode	F cm^{-2}
C_{dc}	double layer capacitance at cathode	F cm^{-2}
D	diffusion coefficient	$m^2\,s^{-1}$
D_C	catalyst dispersion	-
E_a	apparent activation energy	kJ mol^{-1}
E_F	Fermi level	eV
E_C	electrostatic energy	eV
$\dot{E}$	phasor of the electrode potential	V
e	elementary charge	$1.602\ 10^{-19}$ C
F	Faraday constant	96485 C mol^{-1}
I	current	A
I_0	exchange current	A
$\dot{I}$	phasor of applied current	A
i	current density	A cm^{-2}
i_0	echange current density	A cm^{-2}
I_n	intermediate species	-

Roman symbols

j	imaginary number	$j = \sqrt{-1}$
k_1	rate constant of formation of activated sites	s^{-1}
k_{-1}	rate constant of formation of non-activated sites	s^{-1}
k_2	reaction rate constant	s^{-1}
l_{tpb}	three-phase boundary length	$m\ cm^{-2}$
M	non-activated sites of Rh surface	-
M^*	activated sites of Rh surface	-
m	mass	g
N_{AV}	Avogadro's number	$6.02 \cdot 10^{23} mol^{-1}$
N_G	surface area of catalyst in mol	mol
N_{tpb}	length of three-phase boundaries in mol	mol
n	number of electrons taking part in the overall reaction	-
$O_o{}^x$	oxygen atom on a normal oxygen site	-
P	partial pressure	Pa
PIj	promotion index	-
p	fraction of activated sites at Rh surface	-
q	surface charge	C
R	gas constant	$8.314 JK^{-1} mol^{-1}$
R_a	surface roughness parameter	μm
R_{el}	resistance of electrolyte	$ohm\ cm^{-2}$
R_F	charge transfer resistance	$ohm\ cm^{-2}$
r	catalytic reaction rate under closed-circuit	$mol\ O\ s^{-1}$
r_0	catalytic reaction rate under open-circuit	$mol\ O\ s^{-1}$
Δr	reaction rate difference	$mol\ O\ s^{-1}$
r_F	rate of formation of promoting species	$atoms\ s^{-1}$
r_u	unpromoted catalytic rate per unit mass of the active catalyst	$mol\ O\ s^{-1}\ g^{-1}$
r'	reaction rate of O consumption after EPOC	$mol\ O\ s^{-1}$
T	temperature	°C, K

t	time	s
S	geometric electrode surface area	cm^2
S(CO)	selectivity of CO production	-
U	potential	V
U_{WR}	potential difference between working and reference electrode	V
U_{WC}	potential difference between working and counter electrode	V
ΔU_{WR}	change in catalyst potential	V
V_d	rate of atomic oxygen interfacial diffusion	$atom\ s^{-1}$
$V_{ö}$	oxygen vacancy in the lattice	-
X	convertion	-
x_i	mole fraction	-
Y	admittance of electrode	$ohm^{-1}\ cm^{-2}$
Z_{Im}	imaginary part of impedance Z	ohm
Z_{Re}	real part of impedance Z	ohm
Z_t	total impedance of electrochemical cell	ohm
Z_W	Warburg impedance	$ohm\ cm^{-2}$
Z'	real part of impedance Z	$ohm\ cm^{-2}$
Z"	imaginary part of impedance Z	$ohm\ cm^{-2}$

3. Greek symbols

Symbol	Meaning	Units
α_a	anodic transfer coefficient	-
α_c	cathodic transfer coefficient	-
Γ	adsorption of oxygen atoms	$mol\ cm^{-2}$
γ	permanent rate enhancement factor	-

Greek symbols

η	overpotential	V
θ	surface coverage	-
Λ	enhancement factor (Faradaic efficiency)	-
$\bar{\mu}_e$	electrochemical potential	eV
μ_e	chemical potential	eV
ρ	rate enhancement factor	-
Σ(*p*)	deactivated surface structure	-
τ	time constant	s
Φ	work function	eV
ΔΦ	change in work function	eV
ϕ	inner potential	V
χ	surface potential	V
Ψ	outer potential	V
ω	angular speed	rad^{-1}

Subscripts

A	relative to anode
C	relative to cathode
c	related to catalyst
cc	relative to charge current of cathodic process
ca	relative to charge current of anodic process
fa	relative to faradaic current of anodic process
fc	relative to faradaic current of cathodic process
G	gas
M	metal
ME	metal/electrolyte interface
MEG	metal/electrolyte/gas interface
MG	metal/gas interface
MSI	metal-support interaction
S	semiconductor

List of symbols

SB   Schottky barrier

Superscripts

0   index for standard conditions

crit   critical partial pressure of gas

m   exponent in relation of exchange current and oxygen partial pressure (Eq. 2.48)

Curriculum Vitae

Olena Baranova   Ukrainian

av. Maria Belgia 1   29 July 1976
1006 Lausanne

Education

2002 - 2005	**Institute of Chemical Sciences and Engineering, EPFL, Lausanne, Switzerland,** Docteur ès sciences
1999 - 2002	**Department of Physical Chemistry, Ukrainian State Chemical Technology University, Ukraine,** Candidate of Chemical Science, specialty: Electrochemistry
1993 - 1999	**Ukrainian State Chemical Technology University, Ukraine,** M.Sc. in Chemical Technology and Engineering

Professional experience

from 2002 -	**Institute of Chemical Sciences and Engineering, EPFL,** Assistant
	Participation in two EU projects: 1. Natural Gas Fuelled Solid Oxide Fuel Cells (SOFCs) for cogeneration of electricity and chemicals.
	2. SMART NOx abatement systems for next-generation environmental technologies
1999 - 2002	**Department of Physical Chemistry, Ukrainian State University of Chemical Engineering, Ukraine,** Research assistant

Internship

May-June 2003	**Department of Chemical Engineering, University of Patras, Greece**
March-July 2001	**Group of electrochemical engineering, EPFL, Switzerland**
July-Nov. 1999	**UkrESTO, Ltd, Dnepropetrovsk, Ukraine**

Language

Russian - Mother tongue	**English** - Fluent
Ukrainian - Mother tongue	**German** - Beginner
French - Excellent	

Publications

1. E.A. Baranova, A. Thursfield, S. Brosda, G. Fóti, Ch. Comninellis, C.G. Vayenas. Electrochemically induced oscillations of C2H4 oxidation over thin sputtered Rh catalyst films. *J. Cat.* (2005) submitted.

2. E.A. Baranova, A. Thursfield, S. Brosda, G. Fóti, Ch. Comninellis, C.G. Vayenas. Electrochemical promotion of ethylene oxidation over Rh catalyst thin films sputtered on YSZ and TiO_2/YSZ supports. *J. Electrochem. Soc.* **152** (2) E40-E49 (2005).

3. R.Wüthrich , E.A. Baranova , H. Bleuler, Ch. Comninellis. A phenomenological model for macroscopic deactivation of surface processes. *Electrochem Commun.* **6**. 1199-1205 (2004).

4. E.A. Baranova, G. Fóti, Ch. Comninellis. Promotion of Rh catalyst interfaced with TiO_2. *Electrochem Commun.* **6**. 170-175 (2004).

5. E.A. Baranova**,** G. Fóti, Ch. Comninellis. Current-assisted activation of Rh/TiO_2/YSZ catalyst. *Electrochem Commun.* **6**. 389-394 (2004).

Oral Presentations

1. E.A. Baranova, G. Fóti, Ch. Comninellis. Reactor Development for Practical Utilization of Electrochemical Promotion of Catalysis. International Conference on Solid State Ionics. 17-22 July, 2005, Baden-Baden, Germany.

2. E.A. Baranova, G. Fóti, Ch. Comninellis. Electrochemical promotion and metal-support interaction. The 1st Workshop in Electrochemical Promotion. 7 octobre 2003, Lausanne, Switzerland.

3. E.A. Baranova, G. Fóti, Ch. Comninellis. EPOC with Rh/YSZ and Rh/TiO_2/YSZ catalysts. The 2nd Workshop in Electrochemical Promotion. 24 June 2004, Lyon, France.

4. E.A. Baranova, G. Fóti, Ch. Comninellis. Promotion of Rh nanofilm catalyst interfaced with TiO_2 particles. 55th Annual Meeting of ISE, 19-24 September 2004 Thesssaloniki, Greece

Posters

1. E.A. Baranova, G. Fóti, Ch. Comninellis. Electrochemical Promotion of Rh Catalysts. International Conference on Solid State Ionics. 17-22 July 2005, Baden-Baden, Germany.

2. E.A. Baranova Electrochemical promotion of sputter-coated Rh catalysts on TiO_2/YSZ and YSZ supports. LGRC Summer Poster Session. 17 June 2003, Lausanne, Switzerland

3. E.A. Baranova Electrochemical promotion and metal-support interaction: Ethylene oxidation over Rh catalyst supported on YSZ and TiO_2/YSZ. Séminaire hors-ville en chimie inorganique et génie chimique. Octobre 2003, Champéry, Switzerland.